13

Modelling the Influence of the Froth Phase on Recovery in Batch and Continuous Flotation Cells

Z.T. Mathe NHD BSc (Chemical Engineering)

Thesis Submitted in Fulfillment of the
Requirements for the Degree of
Doctor of Philosophy

Mineral Processing Research Unit
Department of Chemical Engineering
University of Cape Town

September 2000

The basic requirement of a mathematical model is precision rather than elegance, although a solution that has both qualities will generally be more acceptable than one that is in a clumsy form with many parameters

-E.T. Woodburn

SYNOPSIS

The ever increasing costs of erecting new flotation circuits or expanding and modifying existing ones require very accurate methods of sizing flotation cells capable of achieving desired recovery and grade of concentrate. In addition, the depletion of high grade ores has necessitated better control and optimisation of existing flotation circuits to reduce operating costs. Design and optimisation of flotation systems is usually based on data derived from bench-scale flotation cells such as batch flotation cells. However, the relevance of parameters derived from these type of cells in predicting flotation performance in continuously operated cells is not well understood. Moreover, the design and optimisation of flotation cells, especially with respect to the capacity of the cell to handle various types of froth structures, still depends primarily on art and experience. Despite this problem, the use of batch cells has continued to play a vital role in present day flotation research in many mining companies and research institutions. For instance, batch data is used (i) to generate grade-recovery curves for studying the influence of changing physical and chemical parameters, and (ii) to extract pulp kinetic parameters such as flotation rate constants, floatability parameters, and the mass fractions of different floating classes. Due to several differences between batch and continuous systems, the information derived from these type of cells is often not well correlated. It is believed that the poor link between batch and continuous flotation systems is mainly due to the use of flotation models that do not account for the influence of the froth phase. This is further complicated by the lack of understanding of the practical significance of froth models proposed in the literature. In light of this it was felt that the literature on froth investigations should be compiled, presented, critically analysed and evaluated in a systematic manner to assist in design, research investigations and analysis of existing flotation cells and circuits. Froth models in the literature were evaluated based on their usefulness in predicting or describing the influence of the froth phase in flotation, particularly with regard to their practical use in linking batch and continuous performance.

It was found that models proposed in the literature do not adequately describe the influence of the froth phase in a practically useful manner. Hence, a new froth recovery model was developed in this thesis. The proposed froth recovery model assumes that floatable particles report to the concentrate launder attached to bubbles, and those floatable particles detached from bubbles within the froth phase also have a chance of either reporting to the concentrate via entrainment or dropback to the pulp phase. Firstly, the following equation was proposed to describe the recovery of floatable particles, either for size class i or mineral type i, within the froth phase:

$$R_{f(i)} = \exp(-\beta\, FRT) + [1 - \exp(-\beta\, FRT)] \cdot \frac{1}{1+\omega_i\, FRT}$$

where β is a derived parameter arguably related to the rate at which bubbles are coalescing and breaking-up at the surface, FRT is the froth retention time parameter, described by the effective volume of the froth per volumetric flow rate of the concentrate, and ω_i is the settling rate to the pulp phase of detached particles of component i, either size class or mineral type, within the froth phase.

To determine model parameters, a large data set was required. This is due to the semi-empirical nature of the proposed froth model. In this regard, the use of data obtained from continuously operated cells was therefore not suitable for deriving model parameters. It was thought that this could only be achieved by using data obtained from a batch flotation cell. A batch flotation cell has a distinct advantage of being suitable for generating, rapidly, large amount of data. However, the non-steady behaviour of froths found in this type of cell require a robust methodology for extracting the necessary parameters. In turn this methodology was developed in this thesis. The main hypothesis of this methodology is that batch flotation performance, in terms of recovery, can be adequately approximated by treating a batch test as if it consists of a series of tests carried out in continuously operated flotation cells. Each flotation time interval is regarded as a single stage. Treating batch data in this manner allows for the derivation of desired kinetic parameters to describe flotation performance.

The model parameters were evaluated using laboratory flotation procedures, floating single mineral species, and plant data, floating platinum bearing Merensky reef ore from the North West province of South Africa in a 60 ℓ flotation cell. Batch and continuous tests, using quartz as a probe mineral, were carried out at various froth heights and air flow rates using a 3.5 ℓ flotation cell. Chemistry was kept constant. Samples were analysed by size. Parameters that describe pulp and froth performances were then derived from the observed data. A correlation between the drainage parameter and particle size was observed, which was shown to be well described by the following expression:

$$\omega_i = a + b\, d_{p(i)}^2$$

In the above equation, the parameter, a, was considered to represent the water drainage rate under the froth conditions arising in the flotation cell (frother type and concentration, solids characteristics, etc), while the parameter b represents a proportionality constant for particle drainage rate as a function of size. The b parameter was subsequently found to be well described by the following equation:

$$b = g\,(\rho_s - \rho_f)/18\,\eta\,h$$

where g is the gravitational acceleration, ρ_s is the density of the solid, ρ_f is the density of the fluid, η is the apparent fluid viscosity and h is the froth height through which particles have to settle.

Subsequently, the model for describing the overall froth recovery of floatable particles was modified as follows:

$$R_{f(i)} = \exp(-\beta * FRT) + [1 - \exp(-\beta * FRT)] * [\frac{1}{1+(a+b*dp(i)^2)*FRT}]$$

It was further hypothesised that the rate at which water drains within the froth phase has a direct influence on the rate at which bubbles coalesce. To simplify and reduce the number of parameters required to describe froth performance, a and β parameters were therefore assumed to be equal. The final form of the R_f equation was therefore given by the following expression:

$$R_{f(i)} = \exp(-\beta * FRT) + [1 - \exp(-\beta * FRT)] * [\frac{1}{1+(\beta+\frac{g(\rho_s - \rho_f)}{18\,\eta\,h} dp_{(i)}^{\,2})*FRT}]$$

In the case of the quartz system, parameters derived from batch data were then used to predict continuous flotation performance. An excellent correlation between predicted and measured concentrate mass flow rates was observed when froth and pulp parameters derived using batch data were used to predict continuous performance. The correlation coefficient was found to be 0.95.

To test the general applicability of the froth modelling methodology and froth recovery model proposed in this thesis, it was decided to use batch data from the literature, generated by Feteris (1983) using an artificial galena/silica system. A good correlation between the measured total masses of galena recovered to the concentrate and predicted masses was observed. These results showed that the refined froth recovery model can be used successfully to describe the influence of the froth phase on the overall flotation recovery in a binary system. Thus far, however, the analysis was limited to particle size classification of single floating mineral species. It was therefore considered necessary to extend and test the proposed froth recovery model and the methodology for extracting kinetic parameters from batch data using a more realistic, and complex, ore flotation system.

Batch and continuous data, obtained by floating Merensky ore on plant site using a 60 ℓ flotation cell, were employed. Froth modelling analysis was performed by mineral and liberation. The correlation between the measured mineral masses and predicted masses obtained from this work was encouraging, given the complexity of the ore that was used. Modelling results from the Merensky ore system seem to suggest that the froth recovery of the various sulphide minerals was the same, at least for the fully liberated fractions. Application of the proposed methodology to other mineral and liberation classes has not yet been refined.

In this thesis, it was only possible to quantify the influence of the froth phase on flotation in batch and continuous systems for the minerals that are fully liberated and report to the concentrate launder predominantly via a true flotation mechanism.

Undoubtedly, this research work is regarded as a major contribution to the current use of batch flotation data. Besides using batch data for generating grade-recovery curves, it can now be also used to study the influence of operating parameters on froth recovery. In addition, the derived froth parameters can be used as initial estimates for feasibility studies and during flotation circuit/cell simulation. It must be pointed out, however, that the nature of batch froths (i.e. non-steady-state behaviour) might introduce some limitations where the froth characteristics are changing rapidly with flotation time. This is because the froth stability parameter, β, in the proposed R_f equation represents an average value for the entire batch test. Scale-up of bench-scale data will have a much better chance to succeed if the laboratory and commercial operations are carried out in the same type of system (i.e. continuous mode). The foregoing comments do not imply that the proposed methodology for linking batch data to continuous performance has no value. Such method can provide an important initial evaluation of projected pilot or industrial plant flotation performance and costs.

ACKNOWLEDGEMENTS

Firstly, I am indebted to the people who supervised various stages of this project. This study was initiated under the supervision of Prof. J-P Franzidis, who is now with the JK Mineral Research Centre in Brisbane, Australia. In the later stages, I worked very closely with Mr M.C. Harris and Prof C.T. O'Connor. Their practical approach to the subject, coupled with underlying mechanistic fundamentals, was always fascinating. I will always be grateful for their invaluable assistance and guidance throughout my postgraduate studies.

The financial assistance of the National Research Foundation towards this research is hereby acknowledged. Opinions expressed in this work, or conclusions arrived at, are those of the author and are not necessarily to be attributed to the National Research Foundation.

The author wishes to also express his sincere gratitude to the following people and organisations:

To the staff and students of the University of Cape Town Mineral Processing Research Unit;

To Impala Platinum Limited for financial support and authorising plant testwork;

To my family, especially my mother, for their love, support and encouragement;

To Ketselisitsoe for ukuba isizathu sokuthi ngihlale eKapa isikhathi esingaka.

Finally, I would like to thank the almighty God for giving me the strength to survive the stress related to doing a higher degree.

LIST OF PUBLICATIONS

The following publications have emanated from the work carried out in this thesis:

Mathe, Z.T., Harris, M.C., O'Connor, C.T. and Franzidis, J-P., 1998. Review of froth modelling in steady state flotation systems, *Minerals Engineering*, 11(5): 397-421.

Mathe, Z.T., Harris, M.C. and O'Connor, C.T., 1999. **A** review of methods to model the froth phase in non-steady flotation systems, *Minerals Engineering*, 13(2): 127-140.

Mathe, Z.T., Harris, M.C. and O'Connor, C.T., 2000. Modelling the influence of the froth phase on recovery in batch and continuous flotation cells, *Proceedings of the XXI International Mineral Processing Congress*, Rome. Ed. by P. Massacci , Vol. B, pp B8a33-B8a39.

TABLE OF CONTENTS

LIST OF FIGURES

CHAPTER 1

CHAPTER 2

CHAPTER 3

LIST OF TABLES

CHAPTER 1

CHAPTER 3

CHAPTER 4

NOMENCLATURE

A - empirical parameter in the collection efficiency equation [-]
A_c - cross-sectional area of a flotation cell [cm^2]
B - film drainage constant
C - concentration of floatable material in the pulp at any time t [g/ℓ]
c - concentration of suspended material
J_g - superficial gas velocity
d_b - bubble size [cm]
D_c - column diameter [cm]
d_p - particle size [µm]
E_k - collection efficiency [-]
Ent_i - entrainment factor (based on recovery of particles within the froth phase) of species i [-]
e_i - global (froth and pulp) entrainment factor of species i [-]
$f_i(k)$ - stochastic distribution of rate constants of species i [-]
g - gravitational acceleration [m/s^2]
h - froth height [cm]
H_c - length of the column collection zone [cm]
j_w - superficial wash water rate [cm/s]
J_g - superficial airflow rate [cm/s]
J_t - superficial tailings rate
k - overall flotation rate constant [1/min]
k_c - collection zone flotation rate constant [1/min]
k_i - flotation rate constant of species i [1/min]
K - equilibrium effects parameter
K' - froth transfer rate constant [1/min]
K'' - dropback rate constant [1/min]
k_{fi} - detachment rate constant [1/min]
$m_{fi}(z)$ - mass of component i attached to bubbles at any froth height
$m_{fi}(0)$ - mass of component I attached to bubbles at zero froth height
m - empirical parameter in the collection efficiency equation
P - floatability parameter [-]
P_f - froth probability function [-]
Q_a - specific aeration rate
Q_{conc} - concentrate volumetric flowrate [cm^3/min]
R - overall flotation recovery [-]
R_a - overall flotation recovery in a countercurrent flotation mode [-]
R_c - collection zone flotation recovery [-]
R_s - secondary collection zone flotation recovery [-]
R_f - froth recovery [-]
R_i - cumulative recovery of species i [-]
R_b - overall flotation recovery in cocurrent mode [-]
R_w - recovery of water [-]
R_{fe} - froth recovery of entrained material [-]
R_{ce} - collection zone recovery of entrained material [-]
R_e - global recovery of entrained particles [-]

R_o - overall flotation recovery of floatable particles [-]
R_{wc} - recovery of water within the collection zone [-]
R_∞ - mineral recovery at infinitely large time in a batch test [-]
S - contact area
S_b - bubble surface area flux [cm^2 air/cm^2 cell.min]
u - vertical bubble velocity
V_f - froth volume [cm^3]

Greek symbols

ε_g - gas hold-up [-]
α - derived froth parameter related to the amount of non-draining mineral
σ - froth transmission factor
η - apparent fluid viscosity [$N.s/m^2$]
γ - column drainage coefficient
ϖ - froth throughput coefficient
κ - froth removal coefficient
β - derived froth stability parameter [1/min]
ρ_p - particle density [Kg/m^3]
ρ_L - liquid density [Kg/m^3]
ψ - angle between the particle and the vertical axis of the bubble
r_p - particle radius
ω_i - settling rate constant of component i [1/min]
τ_c - pulp residence time [min]
τ_f - mean froth residence time [min]
χ - multiplier, associated with kinetic effects
$\propto$ - fraction of the aeration air within the cell effective in transporting solids over the concentrate weir
τ - mean retention time [min]
ξ - empirical parameter [1/min]
λ - empirical parameter of component i [1/min]
ς - empirical constant

GLOSSARY OF TERMS

Entrainment: Non-selective recovery of particles suspended in the froth slurry into the concentrate launder

Floatability: Propensity of the mineral to form a stable attachment to a bubble

Froth Stability: Refers to the persistence of the froth

Froth Mobility: Refers to the speed at which bubbles loaded with particles flow over the concentrate weir

Froth Recovery: Fraction of particles that arrive at the pulp-froth interface (either attached to bubbles or entrained) which eventually reports to the concentrate launder

Hydrophobic: Refers to the tendency of the mineral/s to be water repellent

Hydrophilic: Refers to the mineral/s that have an affinity for water

Mineral Liberation: Refers to the degree of release of the mineral occurring as free particles in the ore in relation to the total content

Overall Recovery: Fraction of mineral species in the feed which eventually reports to the concentrate launder

COMMON ABBREVIATIONS

CALC	Calculated
Chalco	Chalcopyrite
Conc	Concentrate
DFI	Dynamic Frothability Index
DTP	Dithiophosphate
Ent	Entrainment
Fe-S	Iron-Sulphides
FRT	Froth Retention Time
HCL	Hydrochloric acid
HPYC	Hexadecyl pyridiniumchloride
JKMRC	Julius Kruttschnitt Mineral Research Centre
LED	Light-emitting diodes
MIBC	Methyl Isobutyl Carbinol
NaOH	Sodium Hydroxide
Pent	Pentlandite
PGM	Platinum Group Metal
PVC	Polyvinyl Chloride
QEM-SEM	Quantitative Evaluation of Minerals by Scanning Electron Microscopy
RTD	Residence Time Distribution
SIBX	Sodium Isobutyl Xanthate
STDEV	Standard Deviation
UCLA	University of California Los Angeles
UCT	University of Cape Town
UMIST	University of Manchester Institute of Science and Technology

CHAPTER 1

Introduction

CHAPTER 1: INTRODUCTION

1.1 BACKGROUND

The most widely used and economical technique to separate valuable minerals from gangue or unwanted material in the minerals and mining industries is the flotation process. The froth flotation process involves the capture of small mineral particles by small bubbles and their collection in the form of a froth. Various chemical reagents which are added to a mixture of solids present in water-based suspension (pulp) influence the flotation response of different minerals during flotation. This is a consequence of mineral surface conditions created by these reagents, which favour attachment of certain solids to the air bubbles. Such chemical reagents are classified as collectors, frothers, and modifiers (activators and depressants). Collectors and modifiers are reagents that coat or react with mineral surfaces and render them hydrophobic or hydrophilic. Frothers, on the other hand, are surface active reagents that stabilize air-induced flotation froths. Together with air flow rate and flotation cell design criteria, frothers also determine the size and distribution of bubbles arising in the flotation cell. The flux of rising bubbles determines the amount of particles transferred from the pulp phase into the pulp-froth interface. Upon arrival of particle-bubble aggregates at the pulp-froth interface, the froth phase hydrodynamics and froth stability determine the ultimate recovery of both attached and suspended mineral particles into the concentrate launder. Hence, the flotation process is governed by principles of fluid mechanics (pulp and froth phase hydrodynamics), surface chemistry and physics.

To model and study the principles and processes involved in the flotation process accurately, a well controlled environment is required. This is usually achieved by conducting testwork in laboratory scale flotation cells. As a result, much effort has gone into the investigation of the effect of operating conditions on flotation performance using batch flotation cells. However, the relevance of data obtained from flotation cells of this type in deriving kinetic parameters for use in describing industrial flotation performance has been questioned. This is mainly because of the non-steady-state behaviour of the mineral recovery in batch flotation cells. The prevalent current trend in flotation research is to use pilot-scale continuously operated flotation cells. It is widely accepted, however, that laboratory batch flotation cells have several great advantages over continuously operated cells.

At the moment, laboratory batch flotation cells are the most economical devices for testing new ores and for studying the effect of chemical reagents and many other flotation variables on flotation response. This is mainly because batch flotation tests can be rapidly carried out and are

an inexpensive way of assessing mineral flotation response at various operating conditions. The main current uses of batch data are depicted in Figure 1.1.

Firstly, batch tests are used to generate recovery-grade curves. These curves are used as a basis for optimising reagents suites in industrial flotation circuits. However, the differences between batch and continuous cell designs make it very unlikely that the recovery-grade curves derived using a batch cell would be directly applicable to continuous systems. Furthermore, batch tests are used to obtain water recovery versus gangue recovery curves. The recovery of water is associated with entrainment (Engelbrecht and Woodburn, 1975). As such the water recovery is used to indicate whether the mineral is recovered by either entrainment mechanism or true flotation (Smith and Warren, 1989).

Secondly, images of froths found in batch tests are used to analyse the surface froth characteristics. This is performed in order to gain more information about the differences in flotation behaviour under different conditions and to infer the influence of the froth phase on the overall flotation performance. An extensive review of this method is provided in Mathe *et al* (2000). Parameters measured by this technique are bubble size, froth stability and froth mobility.

Thirdly, evaluation of the effects of altering flotation variables is easily accomplished by fitting batch data to first-order kinetic rate equations. This is the traditional use of batch tests in modelling. The kinetic modelling of flotation processes is important from both a design and an operation perspective, providing a basis for the simulation of industrial flotation circuits (King, 1975,1978; Woodburn and Wallin, 1984; Loveday and Raghubir, 1995; Agar *et al*, 1998). In the past, scale-up of batch data to industrial flotation performance has been largely based on determining flotation rate constants using batch cells and multiplying these constants by arbitrary numbers to predict continuous performance. The problem of scale-up, however, is further complicated by various flotation conditions such as power input, the size and mixing characteristics of the cell, hydrodynamics of the pulp and froth phases, transportation of particles and bubbles from the froth phase into the concentrate launder, and the chemical environment in which the ore is being treated. These factors differ significantly from one cell to another, especially when bench-scale and industrial cells are considered. More recent research has shown that it is possible to decouple some of these factors. For example, Gorain *et al* (1996) have shown that it is possible to decouple pulp hydrodynamic factors and mineral floatability based on the bubble surface area flux (S_b*) produced in the cell. S_b has been shown to be readily amenable to

* $S_b = 6\ J_g/d_b$, where J_g is the superficial gas velocity and d_b is the mean bubble size

both measurement (Tucker *et al*, 1994) and prediction (Gorain *et al*, 1999). However, very little progress has been made in trying to quantify the influence of the froth phase in terms of particle recovery in the froth zone, often termed R_f.

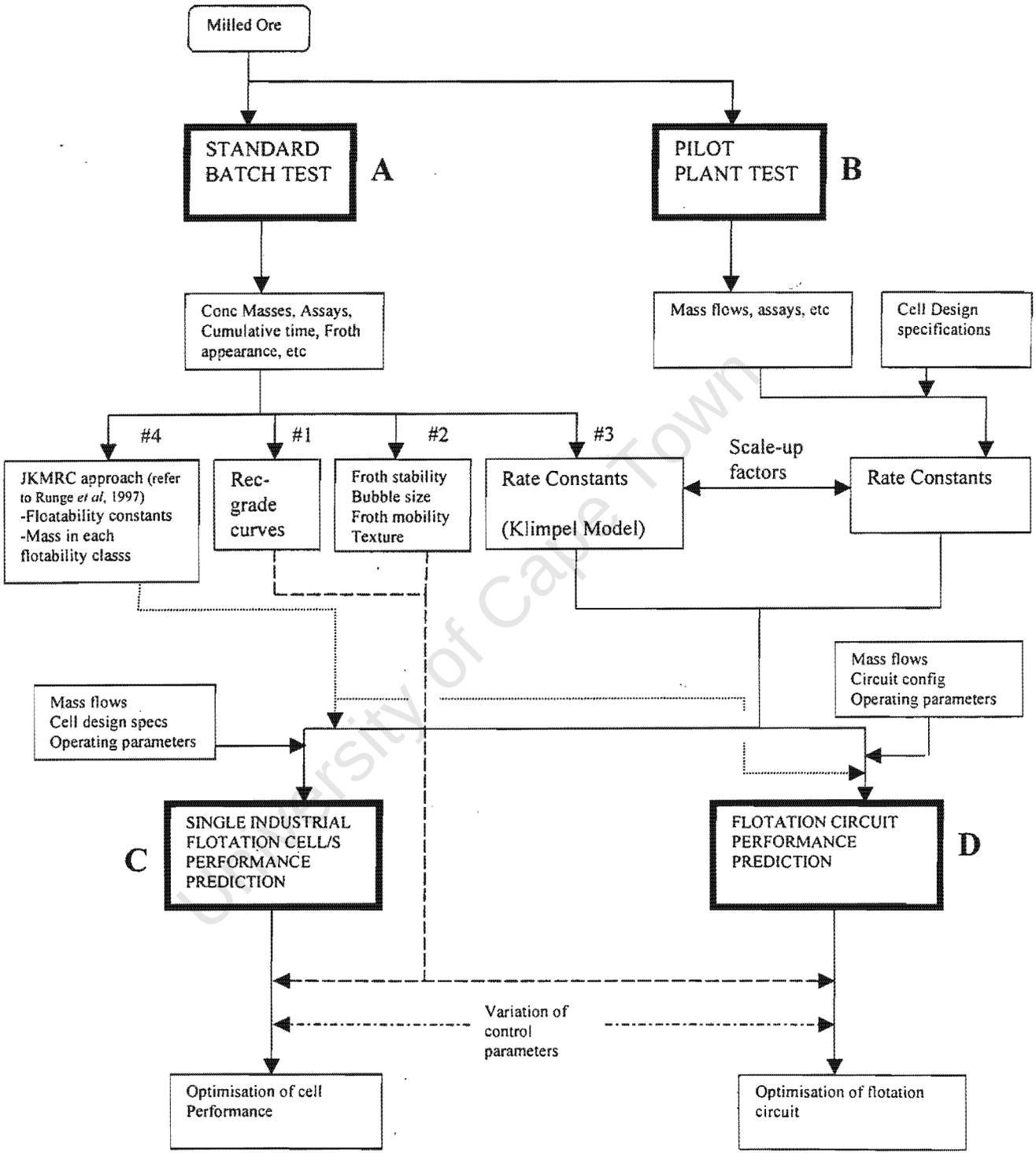

Figure 1.1 Flotation Performance Analysis: Available options

Recently, parameters, such as mineral floatability and the fraction of floatable classes, used in the modelling and simulation of flotation circuits (JKMRC approach) to describe pulp processes have been derived from tests conducted in batch flotation cells (Harris, 1998; Runge *et al*, 1997). In most cases, however, the methods used to derive these parameters do not adequately account for the effects associated with the froth phase and a 100% recovery of minerals within the froth phase is usually assumed in batch flotation tests. This is because batch flotation tests are often conducted at shallow froth conditions in order to minimise the influence of the froth phase. As a result, very little quantitative information is taken into account with respect to the influence of the froth phase in batch flotation systems. Generally, as the flotation cell volume increases, the effect of the froth increases, and the relevance of batch derived parameters based only on pulp kinetics becomes more questionable. It is believed that this problem emanates from the lack of fundamental models for describing the influence of the froth phase in various flotation systems. Developing such a model requires an in-depth understanding of the processes occurring within the froth phase.

The complexity of the froth phase has made it almost impossible to develop a global model that can be used to quantify the influence of physical and chemical parameters on froth performance. This problem is further complicated by other interactive factors involved in the froth phase, such as the influence of froth height, particle size, froth stability, drainage of water and minerals, bubble loading, froth mobility and removal. Linking all the factors and processes governing the froth behaviour when mathematically describing the influence of the froth on flotation performance is a daunting task. In fact, in none of the research work reported in the literature are these factors all modelled together. Given this situation, the influence of the froth zone on the overall flotation process is often accounted for by use of empirically derived parameters and functions when designing, simulating and optimising flotation cells. This approach makes it difficult to identify the intrinsic parameters that need to be extracted or estimated using bench-scale flotation systems such as batch cells. As a result there is as yet no true link between batch operating and continuous operating flotation systems. In addition, very little is known about the extent to which the froth models proposed in the literature can be applicable to this problem. A significant proportion of the review presented in this chapter is therefore focused on froth modelling. The main aim is to critically analyse and evaluate froth investigations and establish their practical significance and usefulness.

1.2 SCOPE OF THIS THESIS

This chapter began by providing a background and establishing the motivation for the thesis. In

the next section, a review of the flotation process, in general, is provided. This includes a critical analysis and evaluation of proposed froth models found in the literature. The analysis of froth models is focused mainly on the mathematical description of the processes involved in the froth phase. The emphasis of this section is on assessing the usefulness of the proposed froth models, particularly the parameters used, in the description and prediction of the recovery of different minerals within the froth phase in various flotation systems. The key findings from this review are summarised in section 1.4 below. This section concludes with several hypotheses, based on the literature review, on how the key questions raised in section 1.3 and research objectives (section 1.5) can be addressed.

A practical froth recovery model and a methodology for analysing batch data and linking this to continuous froth performance are proposed in Chapter 2. The laboratory experimental testwork conducted to test and evaluate the proposed models and methodology are discussed in Chapter 3, in which a detailed description of the equipment, ore, chemicals and procedures used are given. In addition, experimental and modelling results are presented and discussed with respect to their physical significance on the froth performance and modelling. This is based on experimental data collected from a flotation cell operated in both batch and continuous modes. Although the analysis presented here includes pulp phase processes, the emphasis is on the prediction of the mineral recovery within the froth phase. An additional set of laboratory data, obtained from the literature, was also used in Chapter 3 to demonstrate the general applicability of the proposed method for extracting model parameters using batch data. This set of data, obtained from floating a mixture of galena and silica using a batch cell, was reported by Feteris (1983).

To further test and evaluate the potential use of the proposed froth recovery models and a methodology for linking batch to continuous data, a case study based on a data set obtained from flotation tests conducted on a plant site, floating a complex platinum ore in a 60 ℓ flotation cell, is presented in Chapter 4. Flotation tests were conducted in both batch and continuous modes. This work highlights the difficulties that can be encountered when trying to apply fundamental models to operating plant data. Nevertheless, the analysis presented in this chapter demonstrates the applicability and limitations of the proposed froth models.

To put the work presented in this thesis into perspective, Chapter 5 summarises the findings and presents conclusions drawn from the present study. This chapter concludes with some recommendations for future work.

1.3 REVIEW AND CRITICAL ANALYSIS OF LITERATURE

The aim of this section is to discuss the general description of the flotation process, with an emphasis on different methodologies and techniques of quantifying the influence of the froth phase. The fundamental questions to be addressed by this review are:

- How is the overall flotation performance described, mathematically, in batch and continuous flotation cells, and how is the influence of the froth phase accounted for?
- Can the influence of the froth phase in terms of particle recovery, often termed R_f, be measured, described or predicted in batch and continuous systems?
- Is there a froth model in the literature that can be used to adequately describe froth performance in batch and continuous flotation systems?
- Can data obtained from a batch flotation test be used to extract meaningful froth kinetic parameters which are transferable to continuous cells?
- How can these froth kinetic parameters be extracted from batch data?
- How can the variation of the froth and pulp phase flotation performances with flotation time be accounted for in a non-steady state flotation system?

This section starts by reviewing the approach used to describe the flotation process in the past. Thereafter it discusses the current approach of decoupling the major factors involved in the process. The emphasis here is mainly on the determination and usage of the froth recovery factor, R_f, in describing froth behaviour. A summary of the key findings is then provided. Finally, hypotheses are formulated on how the problem of using parameters derived from batch data to describe froth behaviour in continuous operations (*viz*, linking batch data to continuous performance) can be addressed.

1.3.1 General Description of the Flotation Process

The best way of describing the flotation process, in general, in a meaningful sense is by looking at the major steps involved in the process (Fig. 1.2). The steps involved include:

a. *chemical conditioning*;
b. *particle-bubble collision and attachment*;
c. *selective transfer of material from the collection zone to the froth zone*;
d. *non-selective transfer of material from the collection zone to froth zone by entrainment*;
e. *return of material from the froth phase to the pulp phase through liquid drainage*;
f. *reattachment of mineral particles to bubbles rising in the froth zone*;
g. *removal of the mineral particles at the surface of the froth.*

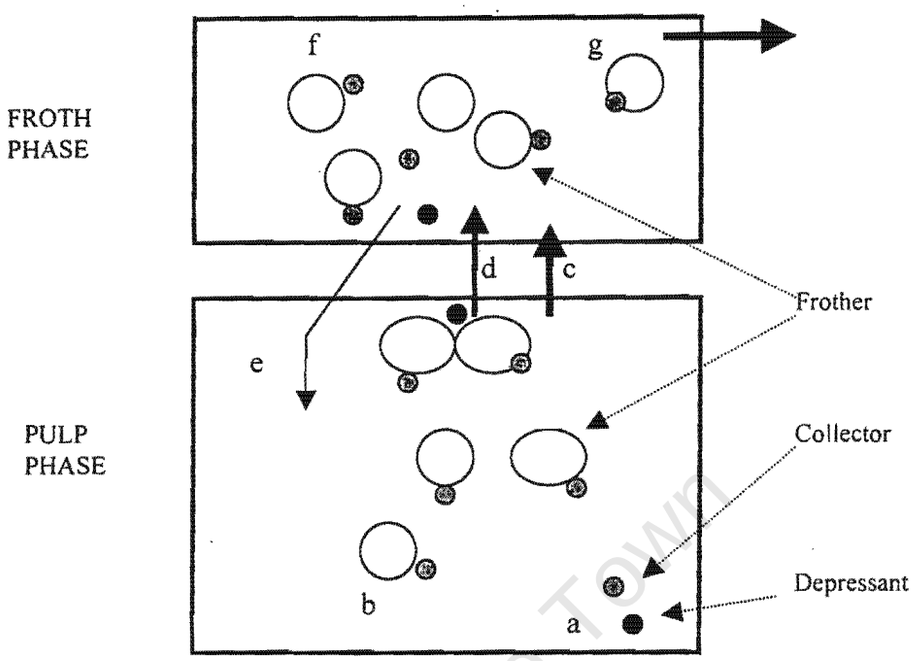

Figure 1.2 Steps involved in flotation

● **unwanted material** ◎ **desired mineral**

The consequence of these steps is reflected in the froth stability and the quality of the final product (grade and recovery). Clearly, this indicates that the flotation process is a very complicated physico-chemical system which cannot be explained by one simple theory or concept. However, looking at the main transfer processes involved simplifies the process. To avoid the complexity involved in describing these processes, several researchers have adopted the approach of describing flotation as a single rate process. This approach is now discussed.

1.3.2 Flotation as a Single Kinetic Rate Process

1.3.2.1 Batch Flotation

The flotation response of floatable minerals in a batch system can be described by the following equation (Arbiter and Harris, 1962):

$$\frac{dC}{dt} = -k\,C \qquad (1.1)$$

where C represents the concentration of floatable material in the pulp at any time t, and k is the flotation rate constant. Integrating the above equation gives:

$$\ln \frac{C(t)}{C(0)} = -kt \tag{1.2}$$

In terms of recovery, equation (1.2) becomes:

$$R = 1 - \exp(-kt) \tag{1.3}$$

where $R = \frac{C(t)}{C(0)}$

It has been widely observed that mineral recovery seldom reaches 100 percent, even at very long flotation times. As a consequence, equation (1.3) is generally used in the following form:

$$R = R_{\infty}\,(1 - e^{-kt}) \tag{1.4}$$

where R_∞ is the mineral recovery at infinitely large time in a batch test.

Equation (1.2) does not always yield a straight line when applied to mineral flotation data, and therefore a postulation has been made that the solid species i floats as if there is a stochastic distribution of rate constants, in which case the cumulative recovery of solid species is given by (Woodburn *et al*, 1994):

$$R_i = 1 - \int_0^{\infty} e^{-k_i t} f_i(k)\,dk \tag{1.5}$$

where $f_i(k)$ is a stochastic distribution of rate constants of species i and k_i is the flotation rate constant of species i.

Klimpel (1980) described $f_i(k)$ in terms of a uniform distribution of flotation rate constants (i.e. rectangular), up to a maximum of k_i, which leads to equation (1.5) becoming:

$$R_i = R_{\infty}\left[1 - \frac{1}{k_i} t\,(1 - e^{-k_i t})\right] \tag{1.6}$$

where R_i is the cumulative recovery of species i at any time t.

Equation (1.6) has been shown to fit batch data, obtained at shallow froths, very well (Fichera and Chudacek, 1992). Some of the alternative models to account for the variation of the flotation rate due to inherent characteristics of the ore (such as particle size distribution, shape, liberation and degree of chemical adsorption) use discrete values of flotation rates. These models have been reviewed by Fichera and Chudacek (1992), and will not be reviewed here again. The most important conclusion from their review was that the double distributed (size, floatability) models yield an adequate description of batch pulp flotation kinetics.

1.3.2.2 Steady State

For a continuous mechanical flotation cell (i.e. continuous inflow of feed, removal of concentrate and removal of tailings), it can be shown that the mineral recovery, assuming first-order kinetics and no overloading of bubbles, is given by the following equation (Arbiter and Harris, 1962):

$$R = \frac{k\,\tau}{k\,\tau+1} \tag{1.7}$$

where R is the fractional recovery, τ is the retention time in the slurry, equal to the slurry volume divided by the tails flow rate, and k is the overall (i.e. pulp and froth) flotation rate constant.

In the case of column flotation cells exhibiting plug flow transport, the recovery is given by the following equation (Finch and Dobby, 1990):

$$R = 1 - \exp(-k\,\tau) \tag{1.8}$$

Plug flow conditions, however, are most prevalent in laboratory/pilot-scale flotation cells (Finch and Dobby, 1990). Industrial flotation columns operate under conditions between those of plug flow and perfectly mixed flow. Tuteja *et al* (1994) have suggested that the model proposed in Yoon *et al* (1993), which assumes negligible influence of the froth phase and takes into account the axial mixing process in the pulp phase, sufficiently describes plant columns flotation recovery:

$$R = 1 - \frac{4a\exp(\frac{P_e}{2})}{(1+a^2)\exp(\frac{a P_e}{2} - (1-a^2)\exp(-\frac{a P_e}{2})} \quad (1.9)$$

where

$$a = \sqrt{1 + (4k\tau / P_e)} \quad (1.10)$$

and

$$P_e = 0.6\left(\frac{H_c}{D_c}\right)^{0.63}\left(\frac{J_t}{J_g(1-\varepsilon_g)}\right)^{0.5} \quad (1.11)$$

where D_c is the column diameter, H_c is the length of the column collection zone, J_t is the superficial tailings rate, ε_g is the air hold-up, and J_g is the superficial air flow rate.

For plug-flow conditions, P_e tends to infinity. Equation (1.9) then simplifies to equation (1.8). For a perfectly mixed cell, P_e becomes very large. Equation (1.9) then simplifies to equation (1.7).

The equations described above are mostly used for studying global (i.e. pulp and froth) flotation kinetics. The use of steady-state flotation cells, such as industrial flotation cells, in studying flotation kinetics requires many parameters which are difficult and costly to measure or derive. Flotation kinetics is easily studied in bench-scale flotation cells. For many years now, scale-up or comparison of bench-scale batch data to continuous flotation performance has been based on determining global flotation rate constants. The determined flotation rates are then used to calculate scale-up factors. This is the approach widely used by many chemical engineers for purposes of designing and optimising chemical reactors. The application of this approach to flotation processes is now reviewed.

1.3.3 Comparison between Batch and Continuous Performance

Comparison or scale-up of bench-scale flotation performance, particularly from batch data, to industrial scale flotation cells is a difficult and very important subject which has been studied by many authors. There are many aspects to this problem, ranging from chemical environment,

flotation cell size and hydrodynamic conditions within the froth and pulp phases, to metallurgical problems associated with different milling conditions. To address this problem, most of the proposed methods in the literature rely on the use of flotation rate constants. "Fudge" factors are used to account for the influence of the froth phase. Most notable is the work published by Woodburn *et al* (1976), Woodburn and Wallin (1984), King (1978), Loveday and Raghubir (1995) and Bourassa *et al* (1988). Generally, the methods employed by these authors rely on the use of global flotation rate constants, extracted from batch data, to predict flotation performance. Batch derived rate constants are multiplied by arbitrary numbers, mostly based on experience, for use in describing industrial flotation performance.

To account for the influence of the froth phase in flotation circuit modelling, King (1978) proposed the use of a froth transmission factor, σ. He defined this factor as the ratio of solids flow rate across the cell lip to that across the pulp-froth interface. All parameters for the plant model were based on estimates from batch tests. The measurement of σ, however, proved to be difficult. As a result, the ratio of water flow rate over the lip to the water flow rate in a cell (i.e. the conditions at the very start of a batch test) was used as a measure of the froth production capacity. In his model σ was used for the estimation of the kinetic flotation rate constants for different minerals. Calculated froth transmission coefficients decreased from 1 to 0 with an increase in flotation time.

Furthermore, Ross and Deventer (1987) proposed the use of froth discharge per unit volume of air that enters the froth to account for the influence of the froth phase. They also assumed that this parameter stays constant for both the laboratory and the plant flotation cell under similar operating conditions. In this case the froth discharge parameter was used to determine the bubble velocity at any height within the industrial flotation cell. In turn the bubble velocity was used in the calculation of the total concentration of the various species in the froth.

Lastly, Woodburn and Wallin (1984) proposed a model in which a first-order rate constant can be decoupled into kinetic effects on the basis of aeration rate (modelled by a multiplier χ**) and the equilibrium effects (modelled by K) that represents the inherent distribution of a solid species between an air interface and the continuous pulp phase. In this case, again, a laboratory batch test was used to estimate the flotation circuit model parameters (χ and K). Although partitioning the network calculations into aeration effects, froth stability and flotation characteristics of the solid species is sound, the absence of any scalable parameters makes this approach of limited use. It is often impossible to study the effect of operating conditions and froth phase variables on

** $\chi = \propto Q_a$, where Q_a is the "specific" aeration rate and $\propto$ is the fraction of the aeration air within the cell effective in transporting solids over the concentrate weir

parameters such as froth stability, unless these parameters are expressed in terms of measurable flotation variables.

The above approaches are fairly easy to use, and have been shown to have some usefulness when designing and optimising flotation circuits. However, the inherent shortcomings can sometimes lead to very high costs during plant commissioning if the circuit is overdesigned or underdesigned. Once the flotation circuit is designed and built, optimisation is achieved through very expensive trial and error plant campaigns. The main source of these costs emanates from the poor understanding of the link between batch and continuous flotation systems.

Batch flotation tests are usually carried out at very shallow froth. As such the derived flotation rate constants relate primarily to the pulp performance. A review of froth modelling in batch flotation cells (Mathe *et al*, 2000) showed that very little work has been done to improve understanding of the influence of the froth in this system. This is further complicated by the lack of quantitative froth models for describing industrial froth behaviour. Currently, there is no model for predicting froth performance, accurately, in any system. It is strongly believed, and has been acknowledged by many researchers, that the limitations and failure of these methods which make use of single, discrete or distributed flotation rate constants extracted from batch data to predict flotation performance in continuous cells are due to the fact that they do not account for the influence of the froth phase. The flotation process is treated as a single rheological system. It is widely acknowledged, however, that two distinct particulate zones exist in the flotation process, viz, froth and pulp. This is evident in the recent research on flotation which has focused on decoupling the influence of the pulp phase performance on the overall flotation recovery from that of the froth phase (Contini *et al*, 1988; Falutsu and Dobby, 1989; Finch and Dobby, 1990; Savassi, 1998). In turn the factors that influence froth and pulp phase recoveries have been further decoupled. This approach is now discussed.

1.3.4 Decoupled Flotation Process

This approach involves formulation of material balance equations around each of the two zones. For instance, Falutsu and Dobby (1989), Contini *et al* (1988) and Finch and Dobby (1990) proposed the following equation to describe the overall flotation recovery of floatable particles, R_o, in a countercurrent flow system:

$$R_O = \frac{R_C R_f}{1 - R_C + R_C R_f} \tag{1.12}$$

where R_c is the collection / pulp zone recovery of floatable particles.

Equation (1.12) assumes that the dropback of material from the froth to the pulp phase can be treated as a recycle (see Fig. 1.3).

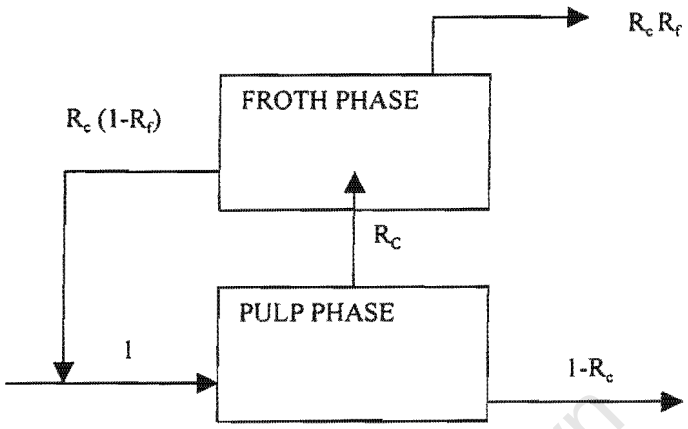

Figure 1.3 Decoupled flotation process (after Finch and Dobby, 1990)

To describe particle recovery in the pulp zone, particle removal is assumed to follow first-order kinetics. For plug-flow conditions within the pulp zone, the overall recovery equation reduces to the following three-parameter expression:

$$R_O = \frac{R_f - \exp(-k_c \tau_c) R_f}{R_f + \exp(-k_c \tau_c)(1 - R_f)} \qquad (1.13)$$

where τ_c is the mean retention time within the collection zone and k_c is the collection zone flotation rate constant.

For completely mixed conditions within the pulp zone, the overall recovery is given by:

$$R_O = \frac{k_c \tau_c R_f}{1 + k_c \tau_c R_f} \qquad (1.14)$$

An inadequate understanding of the froth phase has precluded the use of a more elaborate and useful froth model. A detailed analysis of the froth recovery studies reported in the literature is

provided in section 1.3.6 below.

Recently, Savassi (1998) proposed an equation that recognises that true flotation and entrainment of non-floating particles occurs simultaneously:

$$R_{o,i} = \frac{R_c R_f (1-R_w) + Ent_i R_w (1-R_c)}{(1-R_w)(1-R_c+R_c R_f) + Ent_i R_w (1-R_c)} \qquad (1.15)$$

where R_w is the recovery of water, and Ent_i is the entrainment factor of particles found in size class i.

The transfer processes that lead to equation (1.15) are depicted in Figure 1.4 below. In the development of equation (1.15), it appears as if the recovery of particles within the collection zone by entrainment mechanism is not accounted for. It is assumed that entrainment of particles occurs only within the froth phase. There is no mention of how these particles are transferred from the collection zone into the quiescent zone. Nevertheless, the above equation appears to represent a very important and significant step toward developing a comprehensive flotation model for predicting the overall recovery of minerals. The next challenging step, however, will be to describe each recovery in terms of measurable flotation parameters. So far, the focus has been on describing the collection zone recovery, R_c, and the froth recovery, R_f. Entrainment has been studied primarily from an empirical perspective by a variety of researchers (Savassi, 1998; Bisshop and White, 1976; Ross and Deventer, 1988; Kirjavainen, 1996; Johnson, 1972), However, no model exists for predicting water recovery, R_w. The progress with regard to R_c and R_f is discussed next.

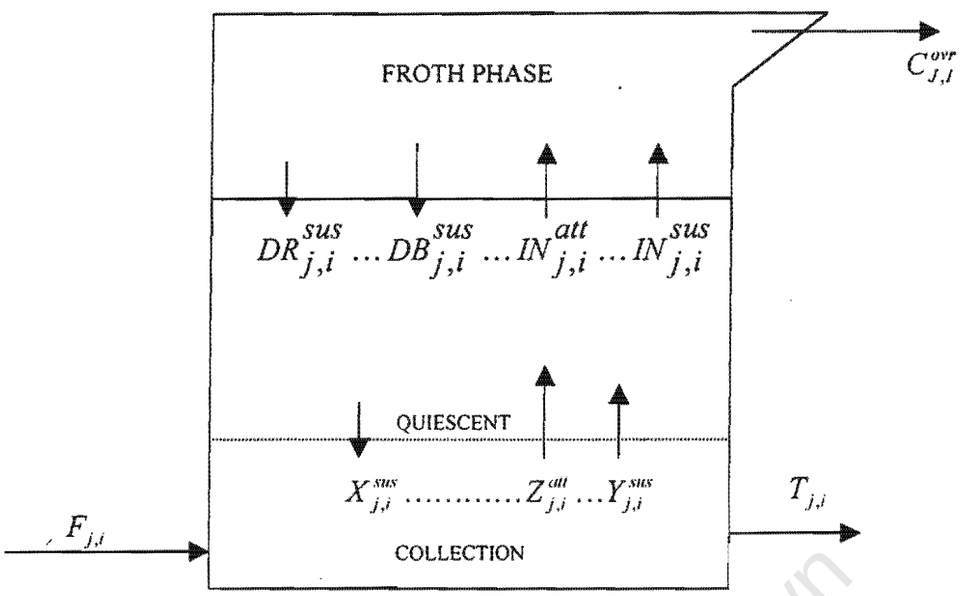

Figure 1.4 Mass transfer of solids in a continuous flotation cell (Savassi, 1998)

$F_{j,i}$: Total mass of particles entering the cell in the feed per unit time; $X_{j,i}^{sus}$: Mass of suspended particles transferred from the quiescent zone to the collection zone of the cell per unit time; $Z_{j,i}^{att}$: Mass of attached particles transferred from the collection zone to the quiescent zone per unit time; $Y_{j,i}^{sus}$:Mass of suspended particles transferred from the collection zone to the quiescent zone of the cell per unit time; $IN_{j,i}^{att}$: Mass of attached particles transferred from the quiescent zone to the froth region of the cell per unit time; $DR_{j,i}^{sus}$: Mass of entrained particles which are effectively drained from the froth region to the quiescent zone of the cell per unit time; $DB_{j,i}^{sus}$: Mass of particles which detach from air bubbles within the froth and are drained to the quiescent zone of the cell per unit time; $IN_{j,i}^{sus}$: Mass of suspended particles transferred from the quiescent zone to the froth region of the cell per unit time; $T_{j,i}$: Mass of particles leaving the cell in the tailings per unit time; $C_{j,l}^{ovr}$: Mass of particles which report to the concentrate of the cell via entrainment and true flotation per unit time

1.3.5 Decoupling hydrodynamic and particle floatability parameters describing R_c

Pulp phase flotation performance as discussed above is described by the flotation rate constant and the residence time. Residence time is a measurable parameter, and the flotation rate constant can be derived from experimental data. The problem with the flotation rate parameter is that it is a function of many flotation variables such as size of the particle, degree of liberation, chemical adsorption per unit area and the hydrodynamics of the system in which the ore is being treated. Many researchers have attempted to describe the influence of these variables on the flotation rate constant. Most notably, Jameson *et al* (1977) proposed the following equation:

$$k = \frac{3}{2} * E_k * \frac{J_g}{d_b} \qquad (1.16)$$

where J_g is the superficial gas velocity, d_b is the bubble size and E_k is the collection efficiency.

Yoon and Luttrell (1989) defined collection efficiency, E_k, as:

$$E_k = A(d_p / d_b)^m \qquad (1.17)$$

where d_p is the particle size, A and m are empirical parameters.

Equation (1.16) assumes that the particles are spherical. Finch and Dobby (1990) and Gorain (1998) demonstrated that this equation can be simplified by lumping the hydrodynamic variables together. Subsequently the following equation has been proposed:

$$k = P S_b \qquad (1.18)$$

where P is the so called floatability parameter and S_b is the bubble surface area flux.

Deglon *et al* (1999) pointed out that the relationship between k and S_b implies that the flotation rate constant should be inversely proportional to the bubble size to the power of 1 which is not consistent with the flotation literature which predicts a power of between 1.5 and 3. The factors used in equation (1.18) are now discussed in more detail.

1.3.5.1 Floatability parameter, P

According to Harris (1998), floatability is the propensity of the mineral to form a stable attachment to a bubble. Amongst many flotation variables, floatability is believed to be influenced mainly by the size of the particle, degree of liberation, chemical adsorption per unit area and the hydrodynamics of the system in which the ore is being treated. Mathematically, the effect of these variables on floatability has not been described. However, several endeavours are currently under way to achieve this objective (Vianna, 1999).

It is necessary to mention at this stage that the floatability parameter/s can be measured if the

influence of the froth layer is minimised (i.e. by floating at shallow froth). In fact, this is the approach which has been adopted currently to extract floatability parameters from batch data for use in plant simulations (Harris, 1998; Runge *et al*, 1997).

1.3.5.2 Hydrodynamic factor, S_b

The bubble surface area flux, S_b, has been identified and proved to be an important criterion for characterising flotation cell hydrodynamics (Deglon, 1998; Gorain, 1998). The S_b parameter can be determined by measuring the bubble size and superficial gas velocity. Bubble size can be directly measured using primarily the capillary tube technique (Tucker *et al*, 1994) or the drift flux analysis technique (Dobby *et al*, 1988). Recently, a fundamental framework for the prediction of bubble size from design specifications has been proposed (Deglon *et al*, 1999). Gorain *et al* (1999) have also proposed an empirical S_b model based on operating parameters. Clearly, there is a great potential for a fundamental S_b predictor to be developed in the near future. Furthermore, there is no reason why the above methods cannot be extended to develop an S_b predictor for the froth.

1.3.6 Froth Recovery, R_f

When a significant layer of froth is present, the linearity of equation (1.18) is lost (Gorain *et al*, 1996). This is obviously a consequence of the influence of the froth recovery. In spite of the new approaches to froth modelling brought about by the introduction of column cells, the froth recovery factor still remains an incompletely understood concept. It is believed that this incomplete understanding of the froth recovery (especially in conventional cells) is mainly due to processes occurring within the froth phase such as bubble coalescence and particle dropback. To date, no froth model has been proposed which can be used to accurately quantify and predict the influence of the froth phase in flotation. Prediction of the froth phase behaviour is seen as a very important factor in the continued economic use of the froth flotation process in the mining and minerals processing industry. Well controlled and optimised flotation circuits reduce operating costs significantly. Furthermore, it is strongly believed, and has been ackowledged by many researchers, that the limitations and failure of methods proposed in the literature, for deriving kinetic parameters from batch data, to predict flotation performance in continuous flotation cells are due to the fact that they do not account for the influence of the froth phase. It is imperative, therefore, that a robust froth model is identified or developed. As this topic forms the main thrust of this work, the froth recovery factor will now be discussed in more detail.

The following sections provide a critical analysis of the froth investigations found in the

literature. Firstly, a discussion on direct measurement of froth recovery is provided. This is followed by a discussion on indirect measurement of the froth recovery. Finally, an analysis and evaluation of proposed froth models, which are mostly descriptive, is provided. The proposed froth models are evaluated on the basis of theoretical validity, assumptions involved and their practical use to model different froth systems.

1.3.6.1 Direct measurement of froth recovery

Recently, the introduction of column flotation cells provided flotation researchers with a better way of sampling and analysing froth at different froth heights. Several researchers have now studied the mineral recovery within the froth phase, often referred to as froth recovery. For instance, direct measurement of froth dropback in a laboratory flotation column was performed by Falutsu and Dobby (1989). A modified laboratory column which isolates the froth zone from the collection zone was developed for this work (Fig. 1.5). Pure silica with a d_{80} particle size of approximately 35 μm was used for this testwork. Results indicated that froth recovery is (i) particle size dependent in favour of finer particles; (ii) dependent on froth bias velocity, decreasing as froth bias velocity increases (i.e. more wash water is added); (iii) not strongly dependent on froth height. This led to the conclusion that *dropback does not occur within the froth zone but rather solids are detached at the pulp/froth interface.* If one were to assume that for this particular system drainage/detachment of particles took place due to bubble coalescence as a result of fewer minerals in the froth, it is possible that reattachment took place within the froth zone, which kept the froth density more or less the same. In addition, the reported strong dependency of froth recovery on superficial bias velocity suggests that moderate bias velocities enhance froth mobility and cleaning action, leading to maximum froth performance. High bias velocity leads to significant downward motion of the water, causing detachment of hydrophobic particles.

The problem with this technique of directly measuring the froth dropback is that the two zones (i.e. collection and froth) are modelled separately. The dropback is recycled back to the feed line or discarded. This creates no interaction of the froth zone and collection zone. Also, the geometry of the column is different from that of a regular column flotation cell. It is, however, a very useful approach with respect to providing more understanding of the role played by froth dropback on froth behaviour.

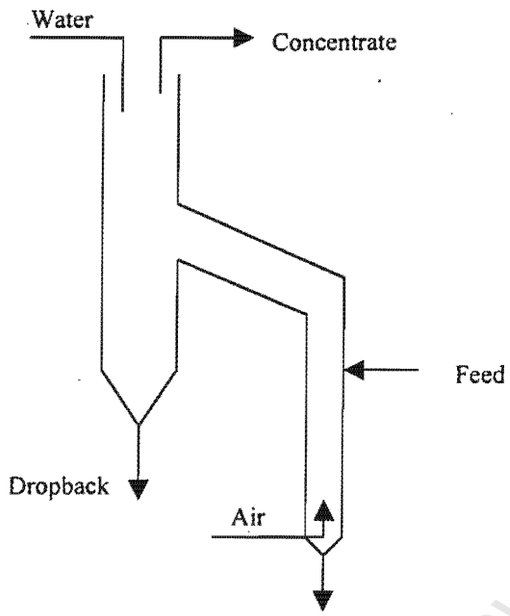

Figure 1.5 Modified laboratory column (after Falutsu and Dobby, 1989)

Another work on the determination of froth recovery in a flotation column, performed by Contini *et al* (1988), produced consistent observations with the direct measurement of froth dropback technique discussed above. This method involved operating a laboratory flotation column in cocurrent and countercurrent modes. The difference between the two modes was mainly that particles which dropped out of the froth in cocurrent mode were immediately lost to tailings, whereas in countercurrent mode, these particles were subject to recollection. Each operating mode was divided into three zones: froth zone, secondary collection zone, and primary collection zone. Expressions for the overall recovery as a function of the flotation rate constant, based on a first-order kinetic model describing the particle removal in the primary and secondary collection zones, and froth recovery were developed for each operating mode. For the countercurrent flotation mode, the following recovery equation was proposed:

$$R_a = \frac{R_c R_f}{1-(1-R_f)(R_c+R_s-R_c R_s)} \qquad (1.19)$$

where R_s is the recovery of particles within the secondary collection zone and R_c is the recovery of particles within the primary collection zone.

For the cocurrent flotation mode, the following overall recovery equation was proposed:

$$R_b = \frac{R_c R_f}{(1-R_f)(1-R_s)+R_f} \qquad (1.20)$$

The two expressions were then solved simultaneously for rate constant, k, and froth recovery, R_f. To simplify the analysis, it was assumed that the flotation rate constants in the two operating modes were the same. This is a very questionable assumption since the particle-bubble collision is expected to be very different between the two operating modes. Furthermore, it was assumed that the froth recovery in the cocurrent mode is the same as in countercurrent mode. This assumption was based on two conditions: (i) solids content of the froth is the same for both modes; and (ii) there is no froth overloading. It is questionable whether the first condition is truly satisfied. Owing to hydrodynamics, the solids content in a froth zone is probably greater in the cocurrent system compared to the countercurrent system. Nevertheless, results obtained from this method using silica in a 2.5 cm diameter column showed a strong resemblance to those obtained by Falutsu and Dobby (1989) in plots of froth recovery as a function of particle size, as may be seen in Figures 1.6 and 1.7.

Recently, Vera (1995) used Contini's approach to test the effect of operating conditions such as air flow rate and froth depth on the collection rate constant and froth recovery. This work was performed on site (at Hellyer Mill, Tasmania, Australia), and conducted with a zinc cleaner feed stream. The results confirmed the conclusions by Falutsu and Dobby (1989), that the froth recovery is not a strong function of froth height. However, when the secondary collection zone length was varied, it was determined that froth recovery was very much affected by froth depth.

In a continuously operated pilot-scale flotation plant consisting of 6 roughing cells (Wemco No. 2 open cells, 80 ℓ capacity each, and two single-unit cleaning stages), Cutting *et al* (1986; 1989) investigated the froth structure of a bulk sulphide ore float (approximately 50% sulphides by weight). The testing technique involved extracting froth samples at different points in the froth column, using a multi-point sampling lance, for analysis of pulp density, grade, etc. Results indicated perfect mixing at lower levels of the froth and plug-flow behaviour in the upper levels of the froth. Froth concentration data in the form of contours mapped on the plane of sampling showed a general grade enhancement with increase in froth height, accompanied by a general decrease in total froth concentration. Estimated mobility structure highlighted the loss in grade enhancement as a result of high aeration rates. Most importantly, the results from this testwork indicated significant changes in relative mineral concentration with froth height (Figure 1.8). This seems to imply that froth recovery varies with mineral type, and is very much influenced by

pattern of drainage, mixing and mobility of the froth.

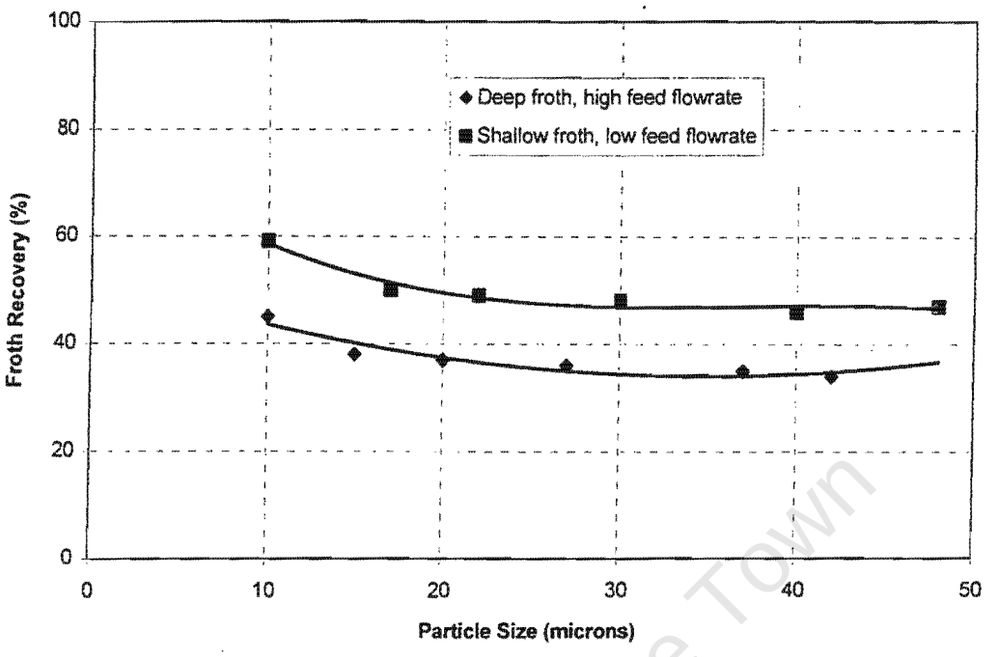

Figure 1.6 **Froth recovery versus particle size (Falutsu and Dobby, 1989)**

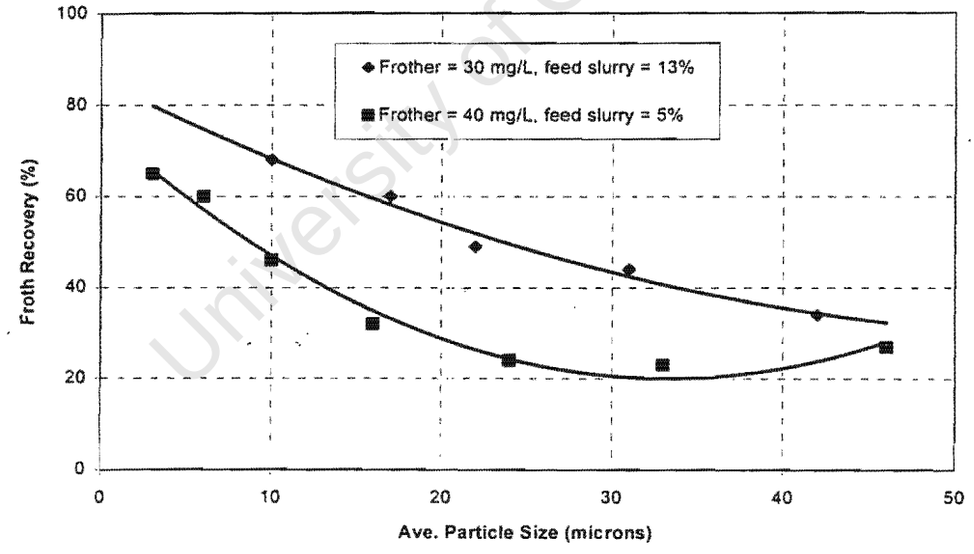

Figure 1.7 **Froth recovery versus particle size (Contini *et al*, 1988)**

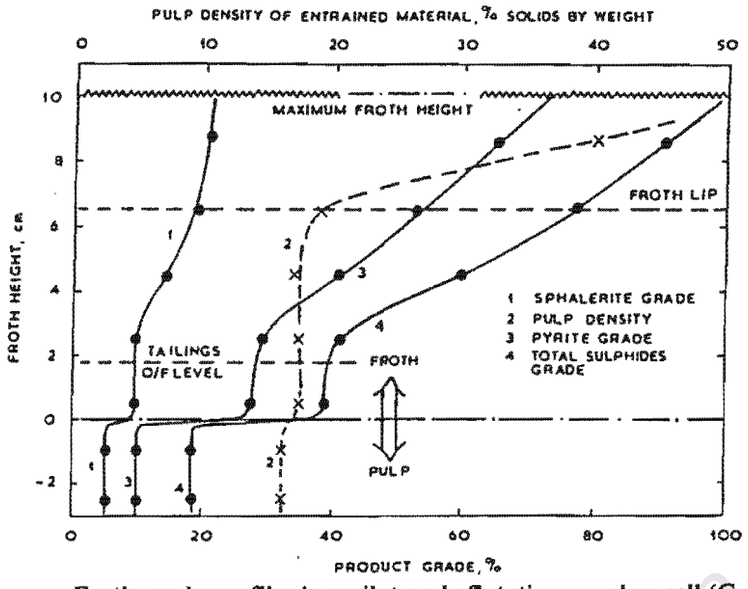

Figure 1.8 **Froth grade profiles in a pilot-scale flotation rougher cell (Cutting, 1989)**

The pilot-scale work, reported above, led to subsequent work on large-scale production cells based on generalized froth mobility and known drainage effects. Three regions in the flotation cell froth were identified: (i) the cell backplate; (ii) the central mechanism; and (iii) the discharge paddles zone. Froth concentration profiles in the three regions (Figure 1.9) established significant differences in the distribution of solids in three particle size ranges investigated. In addition, the distribution of cleaner cell discharges, in weight percent, indicated more particles of the size -38 μm than the particle size of +106 μm particles. This confirms that larger particles drain selectively, and fine particles are entrained by water more frequently. The implication of the above findings is that froth recovery is a function of particle size and it varies with lateral locations in the flotation cell.

Two sets of plant testwork were carried out to investigate froth structure in column flotation cells (Falutsu and Dobby, 1992): one at Cominco's Sullivan concentrator in Kimberley, B.C.; the second one at the Strathcona concentrator of Falconbridge Ltd. in Sudbury. The objective of the work was to investigate the performance in the froth in terms of grade profiles. The measurements were made in a plant which treats ore that contains 6.5% Zn (as sphalerite), 4.5% Pb (as galena) and 10% Fe (as pyrrhotite). In the first test, a probe supported by two parallel bars was used to sample froth at different froth height locations. Water was added to the probe to eliminate entrainment of gangue material. The samples were withdrawn using a peristaltic pump. See the schematic representation in Figure 1.10.

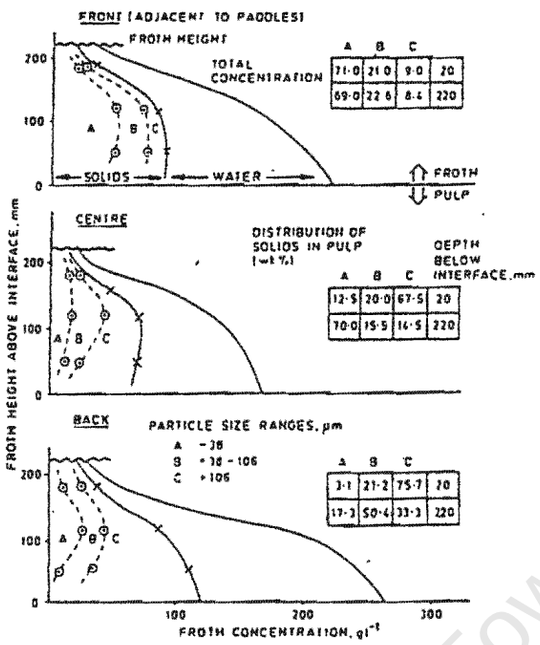

Figure 1.9 **Froth characteristics in a plane perpendicular to froth discharge lip (Cutting, 1989)**

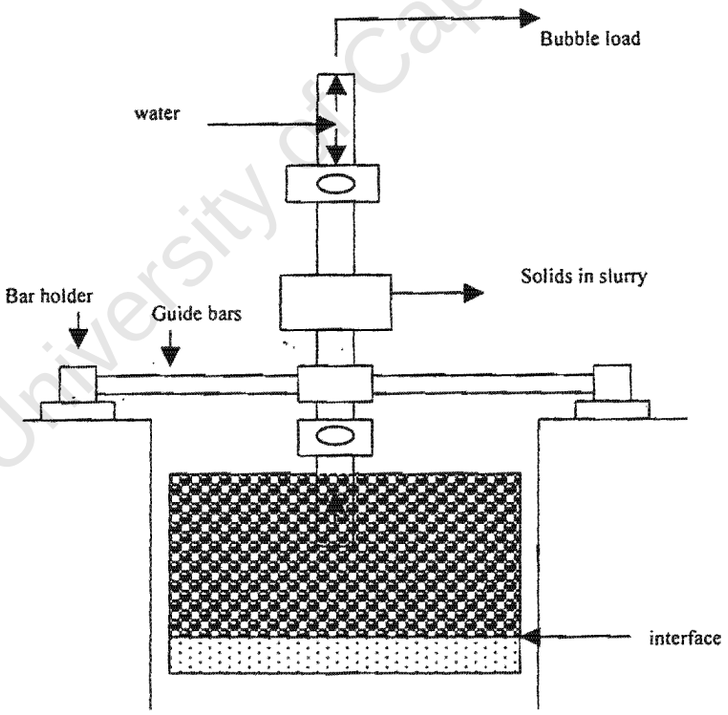

Figure 1.10 **Plant froth sampling apparatus (adapted from Falutsu and Dobby, 1992)**

The second test was carried out in a copper-nickel flotation column - copper being the final product. Froth was sampled isokinetically as shown in Figure 1.11. The assumption was that no recollection of hydrophobic particles occurred inside the probe. Tests were conducted to verify the trends observed in the first set of tests obtained using the method discussed above. Water was also added to eliminate entrainment.

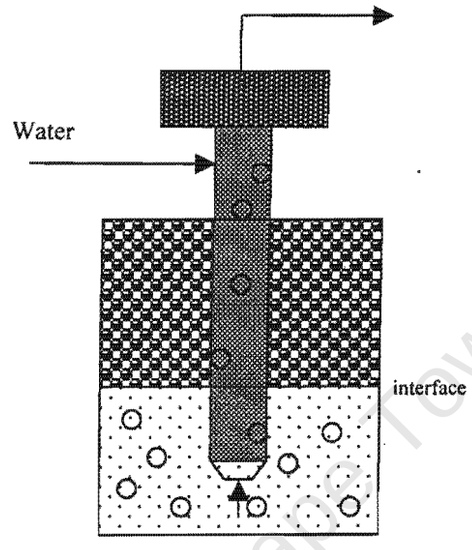

Figure 1.11 Isokinetic sampling apparatus (adapted from Falutsu and Dobby, 1992)

The question of bubble coalescence may be advanced in both these case studies. This is in addition to sub-processes known to occur in the froth zone itself. The use of a pump can completely change the froth structure inside the probe. As a result, bubble coalescence would be expected to occur at an accelerated rate, thereby increasing the drainage of hydrophobic minerals. Therefore, the final sample might end up not even close to approximating the true state of the froth at the point of sampling.

A better way to sample froth would be to scoop froth to a sealed container at a particular height before removing the sample out of the froth. In this way, the froth sample will reflect the true status of the froth (including water and solids contents) at a specific froth height. However, this is not an easy thing to do. Ross (1988) used a froth sampling lance (Figure 1.12) which accommodates the suggestion advanced above. This method was used to determine profiles of mineral species concentration and water in the froth. It was demonstrated that with careful adjustment, this sampling device could produce excellent froth measurement results. For instance, to ensure accurate measurements of water content in the froth, the trap door (B) could be

designed such that the door stays completely closed by pulling string (E). The sealing of the door in the present design depends on the pressure inside the tube, which might not always be sufficient. The problem with this technique, however, is that one cannot estimate the contribution of floatable material and entrained material to grade profiles, separately.

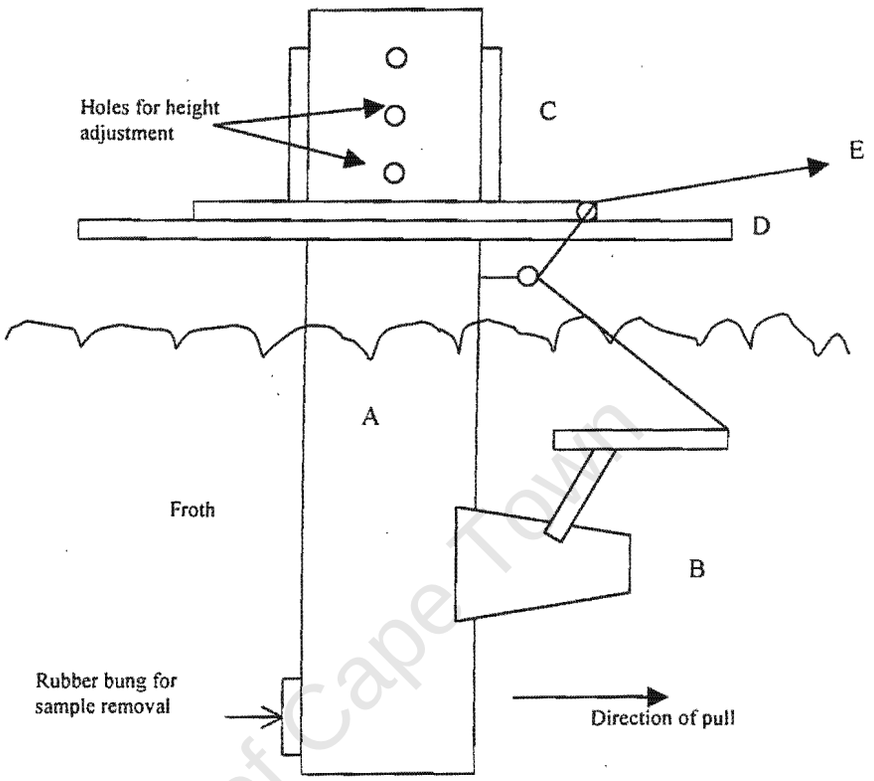

Figure 1.12 Froth sampling device (Ross, 1988)
A = sampling column; B = trap door; C = support walls; D = support bar; E = pulling string

Recently Savassi (1998) attempted to measure froth recovery of attached particles by modifying Falutsu and Dobby (1992) techniques. He further designed a device for measuring entrained particles (Figure 1.13). These devices were used to sample froth on site in the rougher bank of the Lead/Zinc concentrator at Mount Isa Mine. Results obtained from this work indicated that the froth recovery of attached particles of galena tend to decrease down the bank. At the moment, this method of measuring froth recovery of attached particles is restricted to flotation rougher cells, which obviously indicates the need for further development of reliable froth measuring devices.

According to Savassi (1998), in froth systems where the grade of the particles attached to air bubbles is close to that of the solids suspended in the pulp, and in froth systems where the bubble load is low (e.g. cleaners and scavengers), the proposed method of measuring froth recovery is

not likely to produce accurate measurements. This is because the accuracy of the froth analyser depends on there being a significant difference between the grade of attached and suspended particles in the pulp. Generally, the grade of the attached particles in the rougher cells is an order of magnitude greater than that of the particles suspended in the pulp. Hence, the proposed froth analyser is limited to rougher cells.

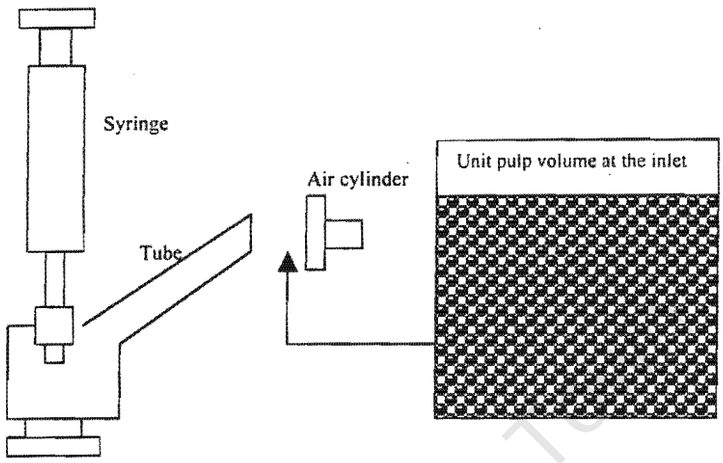

Figure 1.13 Entrainment analyser (Savassi, 1998)

1.3.6.2 Indirect measurement of froth recovery

In this second approach the froth performance is evaluated in terms of froth recovery factor, R_f, which Finch and Dobby (1990) mathematically described as follows:

$$R_f = k / k_c \tag{1.21}$$

where k_c is the collection zone flotation rate constant and k is the global flotation rate constant.

Several other approaches have been proposed to indirectly determine froth recovery using kinetic parameters. Most notably Laplante *et al* (1989) defined froth recovery as follows:

$$R_f = \frac{K'}{K'+K''} \tag{1.22}$$

where K´ is the froth transfer rate constant and K" is the dropback rate constant.

Feteris *et al* (1987) also defined froth recovery in terms of a probability function, P_f, as follows:

$$P_f = \frac{k}{k_c} \tag{1.23}$$

This probability is related to the probability of occurrences of a sequence of events occurring within the froth phase. A considerable knowledge regarding the influence on flotation performance of the froth phase in batch systems has been based on the measurement of the overall flotation rate constant at different froth heights which allows for the determination of the probability of a particle-bubble aggregate surviving the cleaning action of the froth. From the work by Feteris *et al* (1987) on galena ore (assaying as 81.8 % Pb, 0.82% Zn and 1.1% Fe, and 450 g of high grade white quartz) in a batch cell, a linear relationship between P_f and the depth of the froth phase was observed.

Several workers have investigated the variation of the overall flotation rate constant as a function of froth depth (Mular and Musara, 1991; Laplante *et al*, 1983a and 1983b). These workers reported that the overall flotation rate constant decreases linearly with an increase in froth depth. This relationship can obviously be used to analyse the effect of many flotation variables. For instance, Mular and Musara (1991) used the relationship to study the influence of pulp density on the collection zone flotation rate constant. Laplante *et al* (1989) later showed a curved relationship between k and the froth depth. The latter observation may be a more accurate representation of the relationship that describes the behaviour of the overall flotation kinetics with respect to the froth depth. It is expected that the froth recovery factor should sharply increase as particles spend less time in the froth phase. This indicates the importance of the froth residence time on froth behaviour. Nevertheless, when transformed to froth recovery, the k versus froth depth relationship can be used to study the influence of many flotation variables on froth performance. For instance, Vera *et al* (1999) used the approach to study the influence of frother dose, collector dose, impeller speed, feed percent solids and air flow rate on froth recovery. However, the R_f versus froth depth relationship can be used neither to determine directly the dominant processes within the froth phase, nor to develop a scale-up criterion for the froth phase. This can only be achieved if the froth recovery is described in terms of measurable parameters that do not depend on the geometry of the flotation cell.

1.3.6.3 Descriptive froth recovery models

Results obtained from the direct measurement of froth recovery studies all clearly show that froth recovery is a strong function of physical operating parameters such as particle size and density. Therefore, any attempt to describe the behaviour of particles that remain attached to bubbles in the froth and those that are detached must take into consideration the effect of particle size and density of the minerals. Physical operating conditions such as air flow rate and wash water addition, in the case of column flotation cells, should also be considered. In principle, the froth recovery model should incorporate the description of froth sub-processes such as bubble coalescence, particle detachment and entrainment or dropback of detached particles. The problem that arises with respect to these processes is that they are not amenable to any direct measuring technique. As such, a mathematical model which uses meaningful parameters is required. Proposed froth models found in the literature are shown in Table 1.1, and will be reviewed in chronological order.

Table 1.1 Proposed froth recovery models

Model	System used	Assumptions	Reference
$R_{f,i} = \exp(-k_{fi} * (h/J_g))$	General	No entrainment of floatable particles	Moys (1978)
$R_f = \frac{(q\exp(h(p-q))-pE)(1-E)}{(\exp(h(p-q))-E)(q-pE)}$	Pilot scale & industrial columns	No entrainment	Cutting *et al* (1982)
$R_{f,i} = \frac{\kappa}{1+k_{fi} * (h/J_g)}$	Industrial	No entrainment of floatable particles	Moys (1984)
$R_f = \exp(-\beta * FRT)$	General	No entrainment of floatable particles	Gorain *et al* (1998)
$R_f = 95\exp(-0.0144 * \frac{h(1+3J_w)}{J_g^3})$	Industrial column flotation cell (copper ore)	No entrainment	Yianatos *et al* (1998)
$R_f = (1-\alpha)\exp(-\beta * FRT)$	Industrial data	Non-selective detachment of particles	Harris (1998)

From the early studies on modelling of froth behaviour, researchers recognised that particle size and mineral type or density play a crucial role in determining the recovery of particles within the froth. Moys (1978) described the variation of mass of floatable component i (either size or mineral type) with froth height, assuming first-order kinetics, as follows:

$$m_{fi}(z) = m_{fi}(0)\exp(-k_{fi} * h / J_g) \qquad (1.24)$$

where k_{fi} is the detachment rate constant, m_{fi} (z) is the mass flow rate of species i attached to bubbles at any froth height, $m_{fi}(0)$ is the mass flow rate of species i attached to bubbles into the froth, h is the froth height and J_g is the superficial gas velocity.

From the above equation, it follows that froth recovery of floatable species i is given by the following expression:

$$R_{f,i} = \exp(-k_{fi} * h / J_g) \qquad (1.25)$$

The problem with this model is that k_{fi} is not amenable to any measurable technique. It can only be obtained by curve fitting to experimental data. In addition, the possibility of recovery of detached floatable particles via entrainment is not considered.

Cutting *et al* (1982) derived a quadratic equation to describe concentration gradient of suspended material per volume of froth with froth height:

$$-\frac{dc}{dh} = Bc - \gamma c^2 + \varpi \qquad (1.26)$$

where c is the concentration of suspended material, h is the froth height, B is the film drain coefficient, γ is the column drainage coefficient and ϖ is the froth throughput coefficient. Integration and solving of equation (1.26) lead to the following expression of froth recovery:

$$R_f = \frac{(q\exp(h(p-q)) - pE)(1-E)}{(\exp(h(p-q)) - E)(q-pE)} \qquad (1.27)$$

where p and q are the root of the quadratic in equation (1.26) and $E = (C_l - q) / (C_l - p)$, where C_l is the concentration at the bottom of froth.

The parameters used in equation (1.27) could be independently measured using an equilibrium flotation cell. An equilibrium cell is a laboratory flotation cell in which the sides are built up so that continuous froth removal is not possible (Watson and Grainger-Allen, 1974).

Moys (1984) improved his earlier model by incorporating the effect of froth removal:

$$R_{f,i} = \frac{\kappa}{1+k_{fi}^{*}(h/J_g)} \tag{1.28}$$

where κ is the froth removal efficiency.

Ross (1991a) further derived equations and modified existing ones, particularly those of Moys (1978), to describe the influence of the variation of froth properties with increasing height above the pulp-froth interface on the drainage rates of particles from the froth. Transforming his equations to froth recovery, as defined in this thesis, lead to very long and complex expressions. In addition, the parameters in these expressions need to be derived or measured using specially designed flotation cells, such as an equilibrium flotation cell. It must be pointed out, however, that these expressions appear to be sufficiently detailed for use in investigating the interactions between the sub-processes and operating variables, and their use in simulating froth recovery in large-scale flotation cells offers significant potential for future evaluation.

More recently Gorain *et al* (1998) used froth recovery values derived from plant data to show that a relationship exists between froth recovery and froth residence time. It is not yet possible, however, to measure the true froth residence time, as a result froth residence time was inferred from the use of a descriptive froth retention time parameter (FRT). FRT is given by:

$$FRT = V_f(1-\varepsilon_g) / Q_{conc} \tag{1.29}$$

where V_f is the froth volume, Q_{conc} is the concentrate flow rate and ε_g is the gas hold-up in the froth.

The relationship between froth recovery and froth retention time observed by Gorain *et al* (1998) appeared to be exponential, which obviously agrees with the proposed models above. Hence, they proposed to describe froth recovery as follows:

$$R_f = \exp(-\beta^{*} FRT) \tag{1.30}$$

where β is a derived froth stability parameter and FRT is the froth retention time.

Recently Yianatos *et al* (1998) proposed an empirical froth recovery equation based on data collected using a column flotation cell:

$$R_f = 95\exp(-0.0144 * \frac{h(1+3j_w)}{j^3_g}) \quad (1.31)$$

where j_w is the superficial wash water rate (cm/s), and h is the froth height (cm).

This model, in which froth recovery factor is described in terms of operating parameters, is clearly of considerable interest. The main problem with this model is that it was developed from column flotation data where entrainment is considered negligible. Therefore, its application to other systems, such as in conventional mechanical flotation cells, is limited.

The model proposed by Harris (1998) has some practical significance. Previous work on the effect of froth in flotation (Gorain *et al*, 1998) indicated that froth recovery seems to decrease exponentially with an increase in froth residence time. Following on this development, the following relationship to describe froth recovery has since been proposed:

$$R_f = (1-\alpha)\ exp\ (-\beta * FRT) + \alpha \quad (1.32)$$

where α is a derived froth parameter related to the amount of non-draining mineral, and β is a derived froth stability parameter.

Equation (1.32) assumes that froth recovery is non-selective (i.e. all minerals within the froth phase have the same froth recovery). However, the froth recovery of minerals is expected to vary with particle density, size and hydrophobicity. Nevertheless, its usefulness has been demonstrated by the modelling of froths found in industrial flotation cells (as shown in Figures 1.14 and 1.15).

The approach which has been adopted by many researchers is to propose models based on experimental observations and extract the required kinetic parameters by fitting performance equations to overall recovery data. Such data would generally be obtained either from specially designed laboratory flotation cells or directly from a plant. The nature of most of the proposed froth models is such that they are limited to describing flotation data (i.e. empirical). For this reason, the usefulness of batch data in extracting useful froth kinetic parameters for use in describing froth recovery is not yet clear. It is believed that this problem arises from the lack of

froth models which use parameters that have a physical meaning.

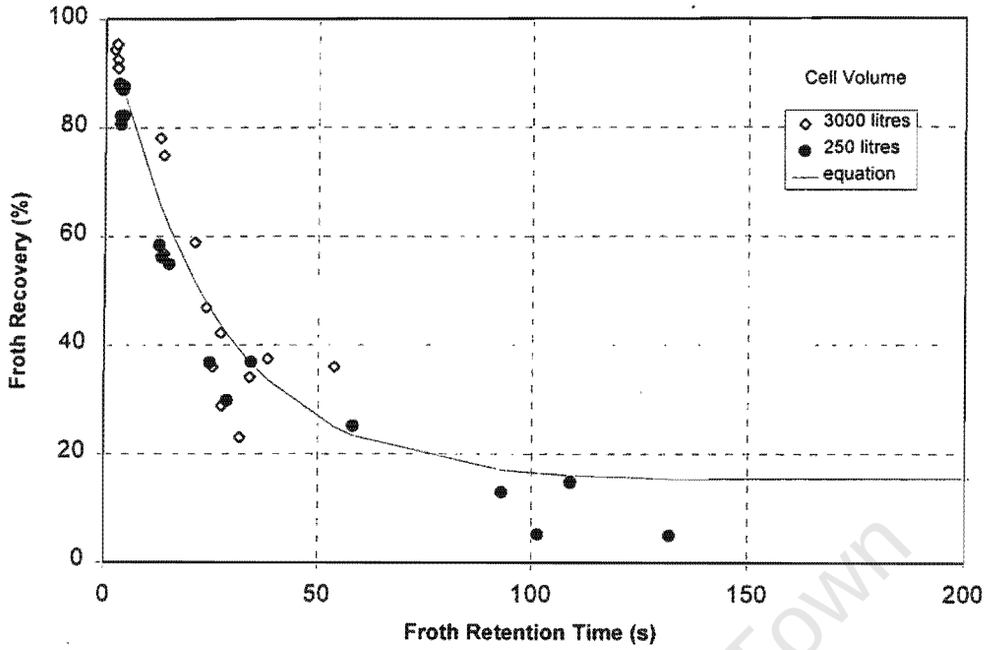

Figure 1.14 Effect of Froth Retention Time on R_f (Harris, 1998) (Copper ore, rougher application, Mt. Isa Mines, Australia)

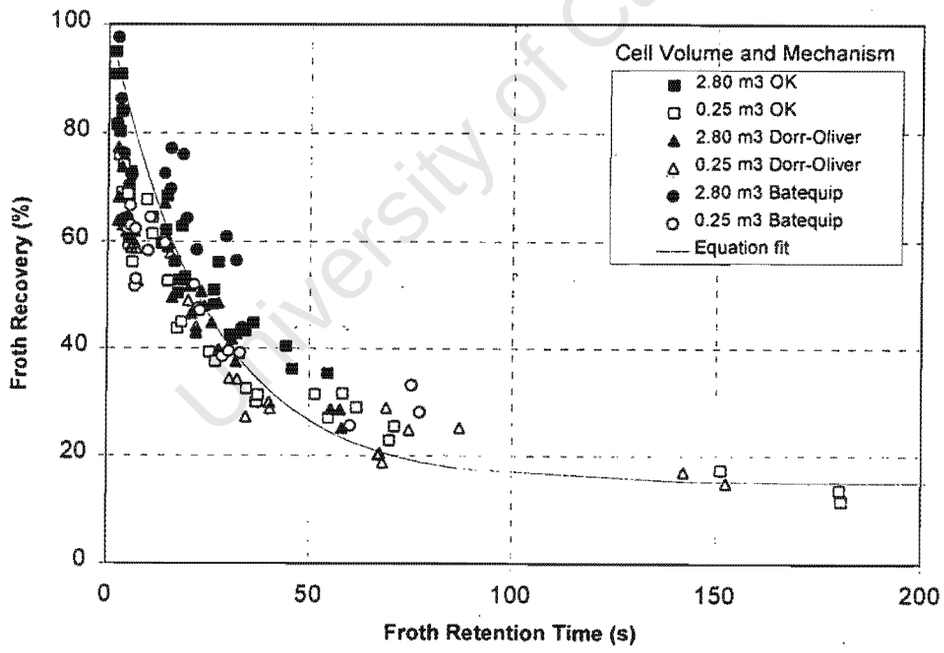

Figure 1.15 Effect of Froth Retention Time on R_f (Harris, 1998) (Zinc ore, cleaner application, Scuddles Mine, Australia)

The models that incorporate the effect of size and mineral type are clearly more descriptive than the simple two or three parameter models. The most important factor to note is that all these models indicate that froth recovery decreases exponentially with an increase in froth residence time. However, none of the above models explicitly describes the influence of bubble coalescence, particle detachment and drainage. Until this is addressed the use of the above models will be limited to describing existing data. In addition, all the models discussed above do not incorporate explicitly the effect of chemistry on froth recovery, or on pulp processes for that matter. The implications of this omission are discussed next.

1.3.7 Influence of Chemistry on Froth Performance

Perhaps, the greatest drawback of all the froth models cited above has been the exclusion of any chemistry effect. The influence of chemistry on froth performance, and on flotation in general, is a very complex and important subject on its own. Several researchers have investigated the influence of chemistry on flotation (e.g. research groups at the University of British Columbia, UCLA, UMIST, Ian Wark Institute and the University of Cape Town). To attempt to present a review of all the work conducted by these researchers will be beyond the scope of this thesis. For more information on this topic, the reader is referred to the publications by Klassen and Mokrousov (1963), King (1982), Laskowski and Ralston (1992) and Crozier (1992). For the purposes of this discussion, the analysis of the influence of chemistry on froth performance will be limited to the influence of frothers and the measurement of froth stability.

It is well known that bubble coalescence is associated with froth stability. Therefore, factors that affect bubble coalescence are expected to influence froth stability. Froth stability is another term that is not clearly understood and defined in the literature. Subrahmanyan and Forssberg (1988) defined the stability of a froth as the time of its persistence. Other authors (Moys, 1984; Woodburn *et al*, 1994) have defined froth stability as a fraction of air supplied to the cell which overflows in concentrate froth as unbroken bubbles. The stability of froths is influenced by many flotation variables and no theory in the literature explicitly describes the mechanism by which these variables influence froth stability. These factors include chemical and physical effects, particularly those of frothers. Frothers stabilize the bubble-particle aggregate by decreasing the surface tension of the air-liquid interface. Surface tension gradient drives the frother molecules from a low surface tension to a high value region. The rate at which this process (i.e. the movement of frother molecules from a low surface tension to a high value region) takes place differs from one type of frother to another and also depends on the frother concentration. As a result, the concentration of frother in the pulp phase has a major influence on the rate of bubble

coalescence within the froth phase, especially when deep froths are involved. This affects the bubble size distribution and bubble flux within the froth phase, which in turn determine the drainage rate and net flux of water and particles through the froth. Together with the cell dimensions, the flux of water and solids determine the retention time of particles within the froth phase.

Due to the absence of froth models that incorporate chemistry, the link between chemistry effects and froth recovery is difficult to quantify. So far, the influence of chemistry on froth has been studied only from a very fundamental perspective, such as investigation of froth stability in simple two-phase systems or by studying the global effects. Sun (1952) used two methods to measure the froth stability in a froth meter, viz, compressed air frothing and sucked air frothing. In the compressed air frothing method, the air was passed through a frother solution contained in a graduated glass cylinder. A fritted glass disk, which had an average pore diameter of 85 to 145 microns, was used to produce froth. In the sucked air frothing method, the same apparatus used in the compressed air method were employed with the exception of the use of a vacuum system to generate bubbles. These methods were used to investigate the frothing characteristics of pine oils. A frothability index (FI), defined as the ratio of a foam volume formed on a solution to a foam volume formed on a solution of a reference substance, was used to characterise the foam. n-Hexyl alcohol was chosen as the reference substance. The conclusion from this investigation was that the froth stability is governed by rate and time of aeration, height of liquid column, type of frother (i.e. chemical composition of the frother), solution pH, temperature and frother concentration in solution. It is questionable, however, whether the use of the frothability index (FI), as defined above, in characterising froth stability is relevant to three-phase froths.

Livshits and Dudenkov (1965) proposed the use of mechanical and pneumatic methods to measure froth stability. The mechanical method involves subjecting a known volume of aqueous frother solution to vigorous shaking in a glass cylinder for a given time. The change in froth volume and time of persistence of the froth after shaking is regarded as the degree of froth stability. Dippenaar (1978) used a method similar to the mechanical method proposed by Livshits and Dudenkov (1965) to study the effect of particle size and hydrophobicity on froth stability. In the pneumatic method, air is blown into the aqueous frother solution through a porous glass filter at a constant rate and pressure. A similar method was proposed by Bikerman (1938). The degree of dynamic stability is the maximum volume and the characteristics of static stability by its rate of decay. Johansson and Pugh (1992) used the pneumatic method to study the influence of particle size and hydrophobicity on the stability of mineralised froths. Their results showed that fine particles (26 to 44 μm) with an intermediate degree of hydrophobicity (i.e. contact angle of 65°) stabilise the froth, and more hydrophobic particles destabilises the froth.

To quantify frothing properties of frothers, Malysa *et al* (1981) proposed a method which uses a another frothability index (FI) described in terms of retention time (i.e. the average lifetime of a bubble in the frother solution and foam). Malysa *et al* (1987) further proposed that FI could be multiplied by a given concentration of frother in a solution to obtain dynamic frothability index (DFI). DFI is considered as a material constant because it characterises solely the frothing properties of the reagent itself. On the basis of Malysa *et al*'s dynamic frothability index, Sweet *et al* (1997) determined the effect of various normal and branched-chain alcohol type frothers on bubble size and frothability of aqueous solutions. They compared results between the frother concentrations at which the bubble size is substantially reduced (to 0.6 of its original value) and the dynamic frothability index. However, such comparison suffers from the limitations connected with linking the dynamic frothability index to froth recovery. Although the relevance of this work is obvious, the quantitative significance of it on froth recovery is not clear at the moment.

The other common approach of studying the influence of frothers on flotation is by comparing recovery-time curves obtained from batch floats. For instance, Hosten and Tezcan (1990) used this method to compare performance of three frothers (MIBC, pine oil and polypropylene glycol). The influence of frothers on froth performance is usually masked by the use of global recoveries. For this reason, very little insight has been gained on how frothers affect froth performance.

A recent attempt to quantify, directly, the influence of frother on froth recovery has been reported by Vera *et al* (1999). In this work a laboratory flotation cell, 16 ℓ , was used to float a copper rougher ore at different frother doses. The froth recovery was determined, indirectly, using the straight line relationship that exists between the overall flotation rate constant and the froth depth, discussed in section 1.3.6.2 above. The results indicated that an increase in frother dose leads to an increase in froth recovery. Beyond an optimum frother dose level, however, an increase in frother concentrations has a negative effect on froth recovery (Figure 1.16). This observation certainly shows that it will require a very complex froth recovery model to accommodate the effect of changing chemistry.

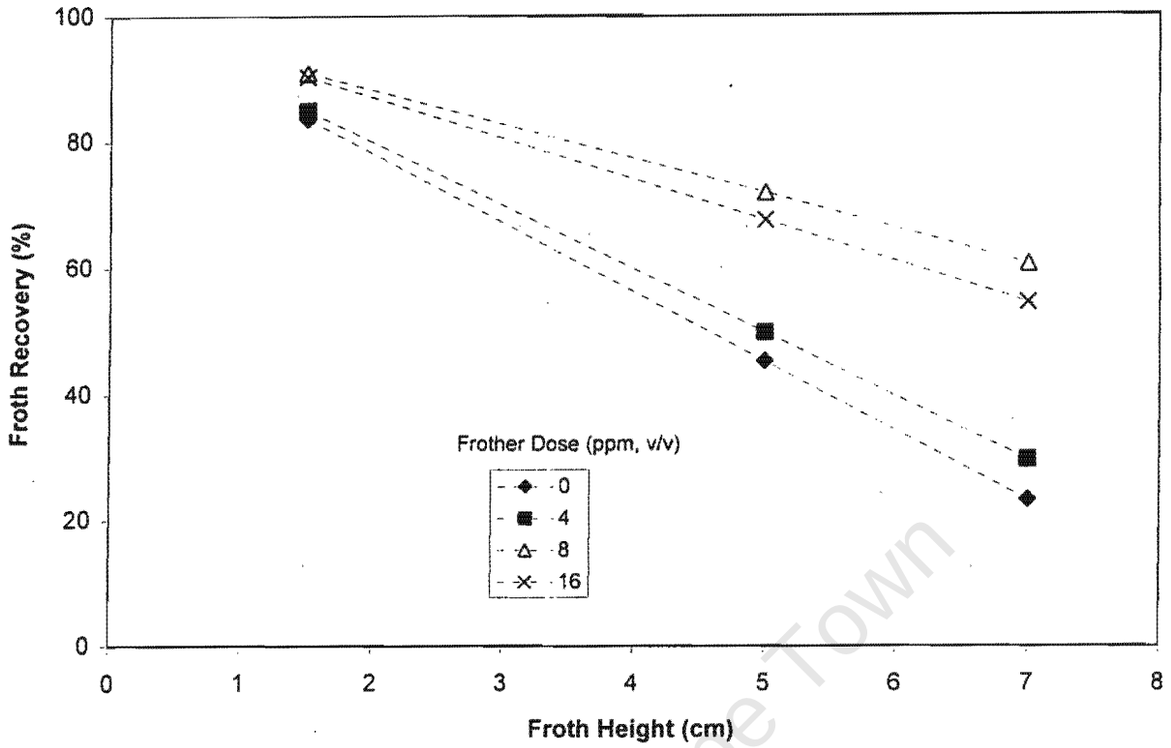

Figure 1.16 **Effect of frother concentration on froth recovery (data obtained from Vera *et al*, 1999)**

1.4 SUMMARY

1.4.1 Flotation Process in General

Pulp phase processes seem to be well described by first-order kinetic equations. The decoupling of ore floatability and pulp hydrodynamics (in terms of floatability, P, and bubble surface area flux, S_b) is regarded as one of the key achievements in the mathematical modelling of the flotation process. More work, however, needs to be done to establish the influence of physical and chemical factors on the floatability parameter. The bubble surface area flux, on the other hand, can be easily measured, and recently there has been some work geared toward predicting it from operating parameters (Gorain *et al*, 1999).

Key papers in froth investigations have been looked at from the perspective of determining their significance in froth modelling. Just as the process of froth flotation is often labeled as complex and difficult to understand, the froth models presented above are not different from the process itself. A considerable amount of fundamental knowledge about the behaviour of froth has been

established by the models and investigations presented so far. Good and reliable qualitative information about froth characteristics is now available. Froth sampling and measurement, particularly in conventional cells, seem to be another obstacle to the development of a realistic froth model.

This review has also shown that the influence of the froth phase on flotation performance can be accounted for by using a froth recovery factor. Froth recovery is determined by using either direct or indirect measurement methods or models derived from experimental data. It is therefore appropriate, here, to summarise the significance of the froth recovery studies, reviewed above, in determining the influence of the froth on different flotation systems. Firstly, direct and indirect methods are summarised. Secondly, descriptive mathematical expressions are summarised.

1.4.2 Froth Recovery

1.4.2.1 Direct and indirect measurement of Rf

Attempts have been made to directly measure froth recovery in laboratory flotation columns. This however requires specially designed flotation cells. Under these circumstances, the froth recovery measurement in bench-scale cells might not be directly useful in predicting froth performance in industrial cells. Nevertheless the results obtained by Falutsu and Dobby and by Contini have demonstrated that froth recovery is particle size dependent. From these studies, there is an indication that froth recovery for a particular ore can be measured using specially designed bench-scale flotation cells.

Moving from bench-scale to industrial cells, however, introduces another important factor which plays a key role in determining froth recovery, namely, froth characteristics and distance travelled by froth before overflowing into the concentrate launder. The indirect method of determining froth recovery has some very serious limitations in this respect.

Indirect method of determining froth recovery relies on the use factors such as the transfer rate constant of material from the pulp to the froth phase, dropback rate constant of detached particles from the froth back to the pulp, and the transfer rate constant of material from the froth into the concentrate launder. Some of these transfer rates are not physically measurable. Moreover, the measurable ones are expected to differ from one flotation cell to another, especially when bench-scale and industrial flotation cells are considered. As such, froth recovery measured in this manner is system specific. In addition, these parameters are expected to vary with flotation time in a batch system.

1.4.2.2 Mathematical Modelling

Direct or indirect measurement of the froth recovery, as discussed above, uses very questionable techniques. The alternative to this is to predict froth recovery based on empirical observations or fundamental principles. Froth models based on fundamental principles are very difficult to formulate, mainly due to the complex nature of the processes involved in the froth phase. As a result, the models presented in this review are based only on experimental observations and intuition. For instance, the models proposed by Harris (1998) and Yianatos *et al* (1998), which indicate that froth recovery decreases exponentially with an increase in froth retention time, are merely based on experimental observation and have no fundamental basis. Intuitively, however, one would expect coarse particles to dropback to the pulp phase more than the fine particles once detached from bubbles, which is the basis of Moys's models. The usefulness of these models, particularly Harris's model, has been demonstrated by their applicability to a wide range of data obtained from different plants operating under different conditions. However, their use at the moment is limited to describing existing plant flotation circuits or data. This situation makes it difficult to use bench-scale flotation cells, such as batch cells, to extract meaningful froth and pulp parameters.

1.4.3 Prediction of Flotation Plant Performance from Laboratory Data

From this review it is clear that the scale-up of flotation cells from the laboratory to an industrial scale is complicated mainly by the presence of the froth. Batch tests are the most widely used tool at present for performing mineral processing research work. Although, many researchers are currently looking at the use of pilot-scale type flotation cells, and cell banks of a variety of sizes, the use of batch cells generally still represents an integral part of these investigations. Most reported batch flotation investigations are carried out at shallow froth conditions. As such, the parameters extracted from batch tests pertain generally only to the processes occurring within the pulp phase. This is understandable since there are no practical froth models that use meaningful parameters that could be derived from batch systems. In addition, the non-steady state behaviour of batch froths creates another complication as froth recovery is expected to depend on flotation time in a batch system. This creates the complexity of using a non-steady state system (batch cell) to derive model parameters for a steady state system (continuous plant). Nevertheless, it is important to establish whether batch data can be utilised more efficiently. The issue of the influence of froth in this system is obviously the main obstacle.

1.5 SPECIFIC OBJECTIVES OF THE PRESENT STUDY

The main aims of the work presented in this thesis therefore are:

- to develop a realistic, practical and robust model to predict the extent to which particles in the froth phase of a flotation cell report to the launder;
- to develop a practical methodology for deriving the necessary model parameters using a non-steady state flotation cell, viz, a batch cell;
- to determine and evaluate parameters used in the proposed froth recovery model;
- to investigate the extent to which the model parameters derived from batch systems can be used to describe the behaviour in a continuous flotation system.

1.6 FORMULATION OF HYPOTHESES

The following hypotheses are the basis of the proposed froth recovery models and methodology for linking batch and continuous flotation data:

(i) It is possible to relate batch froth performance to continuous froth only if the key factors influencing the froth behaviour in both systems are taken into account. In this regard, it is proposed that a froth recovery model that takes into account the froth retention time could well be the way in which to relate batch and continuous froth behaviour.

(ii) The froth phase performance, in an environment in which the pulp chemistry is constant, can be adequately described by a froth model that incorporates true flotation of particles attached to bubbles, the behaviour of detached particles and transportation of minerals via the entrainment mechanism. The assumptions involved in the development of this model are discussed in Chap. 2.

(iv) Due to the non-steady-state behaviour of froths found in batch systems, the link between batch froths and continuous froth performance can be achieved by analysing data obtained from batch floats as if batch data are made up of a series of continuous flotation cells.

CHAPTER 2

Development of a Froth Recovery Model and a Methodology for Extracting Model Parameters from Batch Data

CHAPTER 2. DEVELOPMENT OF A FROTH RECOVERY MODEL AND A METHODOLOGY FOR EXTRACTING MODEL PARAMETERS FROM BATCH DATA

2.1 INTRODUCTION

To address the objectives outlined in Chapter 1 the following methodology has been adopted in the present chapter. Firstly, a qualitative description of the processes occurring in the froth phase, mainly bubble coalescence, detachment of hydrophobic particles, drainage and entrainment of detached particles is presented. The purpose of this section on qualitative description of the froth phase processes is to highlight and give a real picture of all the major froth sub-processes that a realistic froth model needs to quantify. Thereafter a clearer definition of froth recovery is formulated. Secondly, this section is then followed by a general discussion on the topic of mathematical modelling and the approach adopted in this study. Thirdly, quantitative descriptions of the froth phase processes are presented and used to describe froth recovery. The proposed froth recovery model uses a parameter called the froth retention time (FRT), which has been identified as the key parameter in the study of froth phase behaviour. Fourthly, a methodology for extracting parameters used in the proposed froth recovery model is presented.

2.2 QUALITATIVE DESCRIPTION OF FROTH PHASE PROCESSES

Several processes occurring in the froth phase determine the ultimate recovery of minerals into the concentrate launder. It is believed that most of the processes associated with selectivity, both with respect to mineral type and particle size, occurs at the pulp-froth interface. Such processes include detachment of loosely attached particles and draining back to the pulp phase of entrained particles. Although the process of particle detachment at the pulp-froth interface is not considered in this work, its qualitative description is included for the sake of completeness.

It is expected that the forces of bubble-particle attachment would play a very important role in terms of selective detachment of different minerals with varying hydrophobicity. The mechanism of particle detachment at the pulp-froth interface is believed to be caused mainly by sudden change in bubble rise velocity which leads to particles attached to bubbles detaching back to the pulp phase. Therefore, the probability of detachment of particles at the pulp-froth interface depends on the strength of attachment forces to resist detachment forces. Attachment forces are determined by the degree of hydrophobicity of attached particles and

the buoyancy force (i.e. the push exerted by the fraction of the particle volume immersed in the liquid). Detachment forces, on the other hand, may include capillary forces, drag force and gravitational forces (Rubinstein, 1995).

The attached particles that survive the disturbances occurring at the interface are then transported through to the froth where they further experience disturbances from the draining slurry. Draining slurry cause films between bubbles to thin, leading to bubble coalescence. It is known also that chemical reagents, such as frothers, have a major influence on bubble coalescence. Frothers promote the bubble-particle aggregate stability by decreasing the surface tension of the air-liquid interface. Surface tension gradient drives the frother molecules from a low surface tension to a high value region. The rate at which this process takes place differs from one type of frother to another and also depends on the frother concentration. As a result, the concentration of frother in the liquid film surrounding a bubble has a major influence on the rate of bubble coalescence within the froth phase, especially when deep froths are involved. This affects the bubble size distribution and bubble flux within the froth phase, which in turn determine the drainage rate and net flux of water and particles through the froth. Together with the cell dimensions, the flux of bubbles, water and solids determine the retention time of particles within the froth phase.

Furthermore, bubble coalescence (or froth stability) depends on the characteristics of the minerals within the froth. For instance, fine particles tend to stabilise froths (Dippenaar, 1978). Highly hydrophobic particles also penetrate the air-liquid interface to a much greater extent and rupture the film (Johansson and Pugh, 1992). This action leads to dropback of floatable particles, which may be non-selective.

Besides playing a major role in the stability of the froth, mineral properties contribute significantly to the amount of material rejected, or physically detached from bubbles, back to the collection zone in flotation processes. Particle size, particle density and hydrophobicity or contact angle may determine the overall froth recovery of individual minerals within the froth phase. Coarse and heavy particles that are loosely attached to bubbles have a high probability of dropping to the slurry within the froth phase due to gravity. Studies carried out in laboratory column cells have indicated a decrease in froth recovery of particles that arrive at the pulp-froth interface attached to bubbles with an increase in particle size (Contini *et al*, 1988; Falutsu and Dobby, 1989). This could be caused by gravity effects which results in coarse particles having high detachment rates. According to Bascur and Herbst (1982), the shear force exerted by the fluid draining past the particles would be greater in the case of larger particles.

Detached particles within the froth phase, either physically detached or contributed by bubbles breaking-up and coalescing, may be either entrained into the concentrate launder, drain back to the pulp phase or reattach to rising bubbles. Entrainment of detached particles into the concentrate launder is most likely to occur if particles are released near the top of the froth. For particles released within the froth, the chance of them being either entrained into the concentrate launder or returned to the pulp phase depends on their mineral properties (e.g. size, density, etc) and froth residence time. Generally, detached fine particles are expected to yield high froth recovery values, except in systems where the drainage of water is very high. It is well known that fine particles tend to follow water flows; as a result, it is possible to have situations where the froth recovery of fine particles is lower than the recovery of intermediate particles. This is expected to happen by a film drainage mechanism, where water and fine particles drain around the air bubbles. However, when high air flow rates are involved, which result in higher values of net upward water flow rates, the above statement might not be necessarily true.

As mentioned above, there is also a possibility for the detached particles to be reattached to bubbles rising in the froth zone. However, there is no concrete evidence in the literature to establish that reattachment of particles within the froth does take place. Klassen and Mokrousov (1963) estimated contact times (i.e. the time of contact for the case of particle sliding along the bubble) around 10 to 100 times greater in the froth compared to contact times in the pulp. This increases the possibility of attachment of particles detached in the froth phase. On the other hand, the lower impact velocity between a particle and a bubble in the froth phase may not be sufficient to allow the majority of particles to form an attachment.

Finally, there is an issue of hydraulic entrainment of non-floating (i.e. the gangue material) and very fine particles from the pulp phase into the froth phase. These particles enter the base of the froth suspended in the water between the bubbles (Moys, 1978) or by being trapped in the bubble wakes (Yianatos *et al*, 1986) or by being mechanically pushed up by ascending swarms of bubbles (Smith and Warren, 1989). Depending on the conditions within the froth phase, some of these particles have a chance of being washed back to the pulp phase or recovered into the concentrate launder. It is not known whether these particles will behave the same as detached floatable particles. The manner in which this issue is dealt with in this study will be discussed in section 2.5.2.

2.3 DEFINITION OF FROTH RECOVERY

In light of the above description of the processes involved in the froth phase, definitions of the froth recovery of particles that arrive at the pulp-froth interface attached to bubbles and froth

recovery of particles that arrive at the pulp-froth interface via entrainment are suggested. Froth recovery of floatable particles, R_f, is the fraction of particles that arrive at the pulp-froth interface attached to bubbles which eventually reports to the concentrate launder. This fraction includes detached floatable particles which report to the concentrate via entrainment. Secondly, the froth recovery of non-floating particles (i.e. the gangue material), R_{fn}, is the fraction of particles that arrive at the pulp-froth interface trapped between bubbles or mechanically pushed into the froth phase which reports to the concentrate launder. The approach adopted in describing froth recovery, mathematically, is now discussed.

2.4 MODELLING APPROACH ADOPTED

Mathematical modelling is the process of describing and approximating actual physical systems using mathematical techniques. This provides an alternative approach of predicting the effect of major variables on the process performance that would otherwise be difficult to study experimentally. A real process, in this case flotation, is mathematically abstracted or represented for purposes of understanding and predicting its behaviour. This approach also has the advantage of reducing experimental effort and costs of collecting raw data. In the flotation process most of the major process parameters, particularly those associated with the froth phase, are not yet measurable. This situation necessitates modelling of the froth phase even more. For a mathematical model to be useful, however, it must be robust and be based on realistic assumptions. The model can be checked against experimental data and then reconsidered in order to be effective and more useful in describing the physical process.

Generally, three types of modelling approaches are usually performed. Firstly, a model describing the physical process can be based on fundamental engineering principles and physical laws governing the system. In many processes, such as in the flotation process, lack of process knowledge and appropriate instruments for measuring the necessary data precludes the derivation of a fundamental, mechanistic, model. The second approach involves development of an empirical model from dynamic process data. This method is the most straight-forward and easy to use in deriving equations for describing the performance of the system. However, the parameters obtained, usually by fitting equations to experimental data using linear regression techniques, do not always have an obvious physical significance. The third approach, often referred to as a hybrid or semi-empirical approach, involves developing a model by combining the fundamental and empirical modelling approaches. In this study, the last two approaches are adopted, which allows the advantages of each modelling approach to be exploited. Quantitative description of the froth recovery is now considered.

2.5 QUANTITATIVE FROTH RECOVERY MODELS

As mentioned in section 2.3 above, particle recovery in the froth zone can be considered to occur via two mechanisms: recovery of intrinsically floatable particles (either attached to bubbles or by entrainment once detached from bubbles in the froth), and entrainment of intrinsically non-floating particles with water. Both these mechanisms are important in determining the overall performance, viz. recovery and grade, that can be achieved in a flotation cell. In general, four major sub-processes influence the froth recovery of floatable particles within the froth phase. These processes include bubble coalescence and break-up, detachment of particles, drainage and entrainment of detached particles. It is very difficult to account for the influence of all the operating parameters that affect these processes in one model. Froth residence time, however, has been identified as the most important froth parameter. It is worth discussing this parameter before deriving a froth recovery model.

The froth residence time refers to the time spent by particles within the froth phase before reporting to the concentrate launder. It is mainly determined by cell geometry, froth height, froth removal technique and water recovery. High froth residence time increase the exposure of loosely attached particles to froth disturbances such as water drainage between bubbles. This situation can induce an increase in the dropback of particles, particularly coarse particles. Several factors can lead to high froth residence time, such as solids overloading (as in highly mineralised froths), insufficient air flow rate and frother concentration (which affects water recovery and froth stability), and very deep froth heights. These factors result in less mobile froths, susceptible to froth disturbances induced by drainage and mechanical shocks. Drainage of water and particles, in turn, lead to undefined froth flow patterns.

The residence time distribution of particles within the froth is thus a characteristic of the mixing that occurs in the froth. In any froth phase system, the distribution of residence times can significantly affect its performance. Many particles leave the froth phase after spending a period of time somewhere in the vicinity of the mean residence time. However, this is not easily measurable at the moment. As a result, a descriptive parameter known as froth retention time (FRT) has been proposed as an approximation of true froth residence time. It must be emphasised though that it is not known how accurate this parameter, FRT, represents the actual residence time one would measure within the froth in a flotation cell. The following definition of FRT has been generally reported in the literature (Bisshop and White, 1976; Lynch *et al*, 1981; Gorain *et al*, 1998):

$$FRT = (1-\varepsilon_g)\, V_f/Q_{conc} \qquad (2.1)$$

where V_f is the froth volume (cross-sectional area of a cell, A_c, x froth height, h), Q_{conc} is the concentrate volumetric slurry flow rate, ε_g is the average gas hold-up within the froth (typically considered to be around 90% in bench-scale flotation cells (Goodall, 1992)).

It is acknowledged that the gas hold-up varies with air flow rate and froth height. However, it is not yet possible to accurately measure this parameter in conventional flotation cells. For the purposes of this study an auxillary equation deduced from work performed by Goodall (1992) is used to estimate gas hold-up at different air flow rates. Goodall (1992) measured gas hold-up in a batch cell by directly sampling the froth at different heights whilst floating a synthetic ore containing 10% pyrite and 90% quartz. He then quantified the amount of water, solids and air from the sampled froth. Gas hold-up measured at different air flow rates, whilst keeping all other parameters constant, is shown in Figure 2.1 below. The solids content of the pulp was 5%, which is comparable to the pulp density used in the current study. It is assumed that froth height has a minimal effect on this parameter in bench-scale mechanical flotation cells.

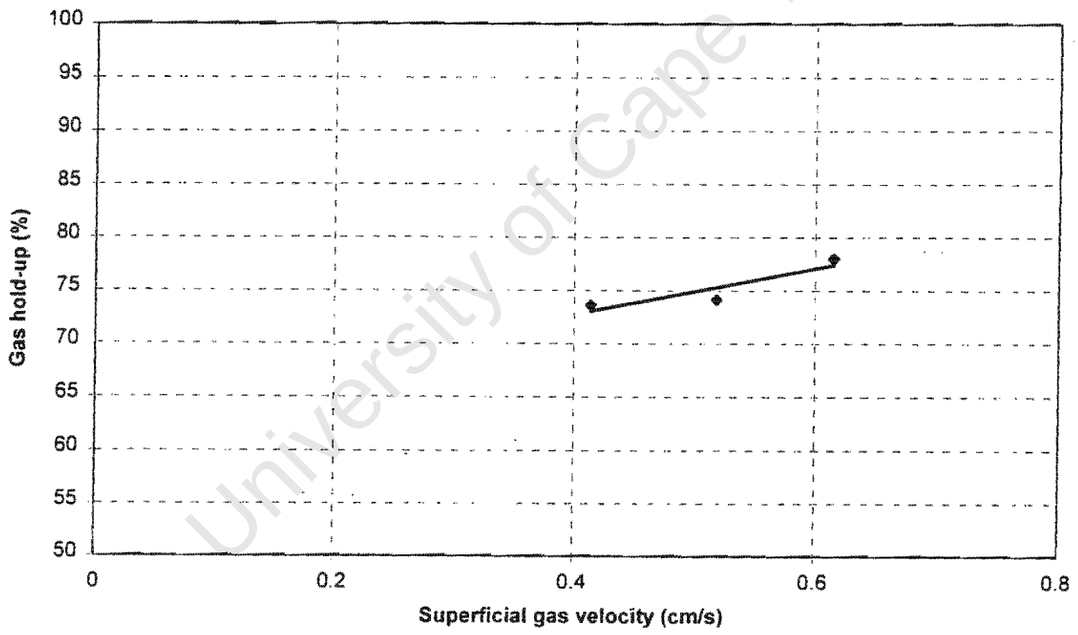

Figure 2.1 **Gas hold-up measurements at different air flow rates (Goodall, 1992)**

For the purposes of this study, a correlation was derived that relates gas hold-up, in percentage, to superficial gas velocity for the data shown in Figure 2.1:

$$\varepsilon_g = 64 + m_g J_g \qquad (2.2)$$

where m_g is the slope of the relationship, which was found to be 22, and J_g is the superficial gas velocity (cm/s).

The other description that has been used in the literature for estimating froth residence time is (Moys, 1989; Gorain, 1998):

$$\tau_f = h/J_g \tag{2.3}$$

where h is the froth height.

The above description essentially represents the air residence time within the froth, assuming that air is flowing freely through the froth layer. However, in real froths the gas flow rate is retarded by the presence of slurry within the froth. As a result, the above equation may be overestimating the true gas residence time. In addition, it is questionable to what extent the residence time of the gas will provide an indication of the residence time of the solids and water in the froth. It is believed that the froth retention time based on the concentrate slurry flow rate is the main driving force which determines the residence time of gas or bubbles and slurry within the froth. As such, the froth retention time (FRT) parameter is used throughout this study to estimate the mean froth residence time. It must be pointed out, however, that equation (2.3) is more useful than equation (2.1) from a prediction perspective, and therefore represents a useful relationship to be used in the absence of more information. The development of a froth recovery model of floatable particles is now considered.

2.5.1 Froth Recovery of Floatable Particles, R_f

The model presented here has been developed on the basis of five postulates. These are presented in turn in this section, with relevant discussion where required.

1) Floatable particles arrive at the pulp-froth interface attached to bubbles.

2) Within the froth phase, they detach unselectively from bubbles due to bubble breakage and coalescence.

3) Considering the flow of particles under steady-state conditions, arriving at the pulp-froth interface depicted in Figure 2.2, particles which remain attached to bubbles will report to the concentrate launder following the bubble flow patterns. Some of the particles initially attached to bubbles will not survive the flow conditions within the froth and will return to the pulp. As such the fraction of particles attached to bubbles will be reduced. In this regard,

a potentially very useful empirical relationship between froth recovery of floatable minerals and froth retention time, defined as the ratio of the froth volume to the concentrate volumetric flow rate, has been observed in several flotation systems (Harris, 1998; Gorain *et al*, 1998). This was shown in Fig. 1.15, where it can be seen that the relationship between froth recovery and froth retention time was essentially independent of cell size (0.25 m^3 and 2.8 m^3), cell mechanism (Dorr-Oliver, Batequip and Outokumpu) or cell operating conditions (different froth depths, gas rates and impeller speeds).

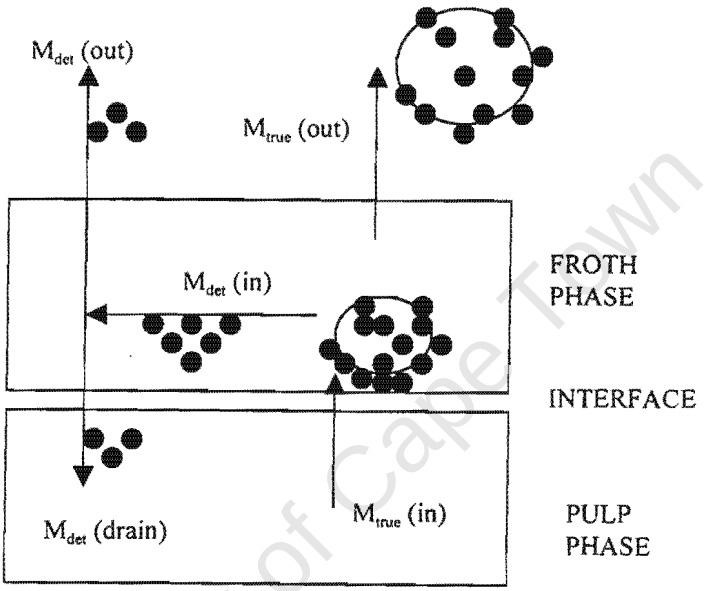

Figure 2.2 Various paths followed by true floating particles within the froth phase

On the basis of the relationship observed in Fig. 1.15, it is postulated that the recovery of particles to the concentrate launder that remain attached to bubbles, R_{fa}, can be described by a simple exponential function of FRT (i.e. froth decay follow first-order kinetics):

$$R_{fa} = exp(-\beta * FRT) \qquad (2.4)$$

where FRT is the froth retention time defined as the ratio of the effective liquid froth volume to the concentrate volumetric slurry flow rate (equation 2.1), and β is a derived parameter which could be related to the rate at which the bubbles are coalescing and breaking-up.

Equation (2.4) must obviously conform to the following boundary conditions:

- as $\beta \rightarrow 0$, $R_{fa} \rightarrow 1$

- as $\beta \rightarrow \infty$, $R_{fa} \rightarrow 0$

The β parameter as used in equation (2.4), however, is a function of a number of flotation variables which might include air flow rate, frother concentration, particle size, percent solids, etc. However, to simplify and reduce the number of parameters required during modelling, this parameter is initially assumed to be a function of frother concentration only.

4) The fraction of detached particles, viz. $(1-R_{fa})$, have a chance of being either recovered into the concentrate launder via an entrainment mechanism or settling back to the pulp phase due to gravitational force. It is assumed that there is no reattachment of these particles. If it is assumed that the settling rate of detached particles of component i (classified by either size or mineral type) returning to the pulp phase is proportional to the mass of these particles within the froth (Moys, 1989), then the fraction of component i remaining in the froth after time t, $m_{f,i}(t)$ (i.e. the ratio of the mass of component i at any time t to the initial mass of component i at time zero), is given by the following expression:

$$m_{f,i}(t) = exp(-\omega_i t) \tag{2.5}$$

where ω_i can be regarded as the settling rate constant of component i.

Therefore, the output mass flow rate of component i, $M_{det(i)}$ (out), is related to the input mass flow rate of component i, $M_{det(i)}$ (in), by the convolution integral (Fogler, 1992):

$$M_{\det(i)}(out) = \int_0^\infty M_{\det(i)}(in)\exp(-\omega_i t)E_C(t)dt \tag{2.6}$$

where E_c (t) is the residence time distribution of detached particles at any time t.

If it is assumed that the fraction of detached particles is well distributed within the froth phase in a perfectly mixed flow manner, then $E_c(t)$ is given by:

$$E_C(t) = \frac{1}{\tau_f}\exp(-\frac{t}{\tau_f}) \tag{2.7}$$

where τ_f is the mean froth residence time, approximated by FRT in this study as explained above.

Substituting equation (2.7) into equation (2.6) and solving for the ratio of the output mass flow rate to the input mass flow rate of component i gives,

$$\frac{M_{\det(i)}^{(out)}}{M_{\det(i)}^{(in)}} = \frac{1}{1+\omega_i \tau_f} \tag{2.8}$$

It should be obvious in equation (2.8) that the ratio of the output mass flow rate to the input mass flow rate of component i represents the fraction of detached particles reporting to the concentrate launder via entrainment. Hence, the froth recovery of these particles, $R_{fe(i)}$, is given by:

$$R_{fe(i)} = \frac{1}{1+\omega_i \tau_f} \tag{2.9}$$

Equation (2.9) is similar to a classification function proposed by Bisshop and White (1976) to describe entrainment of hydrophilic particles in bench-scale flotation cells:

$$CF_i = \frac{1+\xi r}{1+\lambda_i r} \tag{2.10}$$

where ξ and λ_i are empirically derived parameters, and r is the froth residence time (defined the same as FRT).

The results obtained by these authors indicated that the numerator in the above equation was very close to unity (i.e. $\xi \rightarrow 0$). Under such a condition equation (2.10) has essentially the same form as equation (2.9) with $\omega_i \cong \lambda_i$.

5) It is possible that some particles will not be recovered from the froth owing to froth transport inefficiencies. These particles will be recycled within the froth phase and also be subjected to the possibility of being recovered via entrainment. However, to simplify the analysis here, all particles arriving at the froth surface are assumed to be recovered into the concentrate launder (a condition most likely to be met in bench-scale flotation cells).

Based on the five postulates listed above, the ultimate recovery of floatable particles of component i within the froth phase is then given by:

$$R_{f(i)} = R_{fa} + [1-R_{fa}]*R_{fe(i)} \tag{2.11}$$

Substituting for R_{fa} and $R_{fe(i)}$ from equations (2.4) and (2.9) above gives the relationship:

$$R_{f(i)} = \exp(-\beta * FRT) + [1 - \exp(-\beta * FRT)] * [\frac{1}{1+\omega_i FRT}] \quad (2.12)$$

2.5.2 Froth Recovery of Entrained Non-Floating Material, R_{fn}

Particles can undergo non-selective transfer into the base of the froth by being suspended in the water between the bubbles (Moys, 1978) or by being trapped in the bubble wakes (Yianatos *et al*, 1986) or they can be mechanically pushed up by ascending swarms of bubbles (Smith and Warren, 1989). Depending on the hydrodynamic conditions within the froth phase, some of these particles have a chance of being washed back to the pulp phase or recovered into the concentrate launder. At the moment, there is no reliable model for describing the recovery of entrained particles within the pulp phase and within the froth phase separately. To simplify the analysis in this work, it is assumed that the entrained and detached particles will behave the same within the froth phase. As such, equation (2.9), which describes the entrainment mechanism of detached particles, can also be used for describing the behaviour of particles which entered the froth zone in the first instance via an entrainment mechanism. This implies that the particle settling rate parameter within the froth phase, ω, will be determined by the size and density of the mineral species. The manner in which these particles are transferred into the froth phase does not influence their drainage characteristics. Since the amount of entrained solids can be considered to be proportional to the amount of water recovered (Engelbrecht and Woodburn, 1975), the recovery of entrained particles can therefore be related to the water recovery. A methodology for extracting the model parameters for use in the proposed equations is now discussed.

2.6 PROPOSED METHODOLOGY FOR EXTRACTING FROTH MODEL PARAMETERS FROM BATCH DATA

2.6.1 Introduction

So far, the previous sections have been dealing with the identification and derivation or development of froth models which could be used to adequately describe froth behaviour. The proposed froth recovery models have parameters that are not physically measurable at this stage. These parameters can be estimated by fitting the performance equations to data from continuous systems. However, this approach requires an extremely large number of data points in order for the derived parameters to have statistical significance. As such, it is most convenient to derive these parameters using batch tests. However, the nature of batch floats requires a method for describing flotation performance that takes into account the non-steady

state behaviour of froths found in batch systems. The aim of this section, therefore, is to present a proposed methodology for extracting the required parameters from batch data. To achieve this the froth phase influence is decoupled from the pulp phase performance.

2.6.2 Decoupled Flotation Process

In general, flotation performance is mainly described in terms of recovery and grade of the concentrate. In this study, however, only recovery is considered. This is because the overall flotation recovery is easily measured in any flotation system. The problem with using the overall (pulp + froth) flotation recovery, however, is that it encompasses processes occurring both within the froth and pulp phases. As such, it is very difficult to distinguish between the effect of froth and pulp processes on the mineral flotation response. In the methodology proposed here, the pulp phase mineral recovery, for both floatable and entrained minerals, is decoupled from the froth phase mineral recovery. To achieve this, a mass balance approach of treating the dropback of material from the froth to the pulp phase as a recycle (Contini *et al*, 1988; Falutsu and Dobby, 1989; Finch and Dobby, 1990; Savassi, 1998; Harris, 1999) is adopted, with some modifications. This approach is now discussed.

2.6.3 Recovery Equations

A mass balance equation proposed recently by Savassi (1998) to describe flotation performance is as follows:

$$R_{o,i} = \frac{R_c R_f (1-R_w) + Ent_i R_w (1-R_c)}{(1-R_w)(1-R_c+R_c R_f) + Ent_i R_w (1-R_c)} \qquad (1.15)$$

where R_o is the overall or global flotation recovery of a particular mineral, R_c is the pulp phase mineral recovery, R_w is the global water recovery based on the feed water flow rate, R_f is the froth recovery of particles that remain attached to bubbles, Ent_i is the global entrainment factor defined as the ratio of the recovery of suspended or entrained solids within the froth to the recovery of water based on the tails water flow rate, and i is the particle size class.

This equation was chosen for use in this study because it provides a means of simultaneously accounting for flotation of minerals by both true flotation and entrainment mechanisms. In addition, its form allows for the evaluation of various models describing froth recovery and entrainent. Explicit mathematical descriptions of each factor in equation (1.15), and the manner in which they are used in describing overall flotation recovery in a batch cell, are discussed in section 2.6.4 below.

Despite its preference for use in this study, several drawbacks are worth mentioning with regard to equation (1.15). This equation considers entrainment as a global process (i.e. does not separate entrainment within the pulp phase from that in the froth phase). In addition, the recycling of the entrained material that drops back from the froth into the pulp phase is not considered. Furthermore, equation (1.15) does not consider the processes occurring at the pulp-froth interface explicitly. It is believed that most of the processes associated with selectivity occur at the pulp-froth interface. It was considered necessary to develop an alternative recovery equation which addresses some of the issues raised above. The derivation of the alternative global flotation recovery equation is considered next.

2.6.3.1 Proposed global flotation recovery equation

A sequence of events that occurs during flotation, under steady-state conditions, which lead to particles, initially in the feed, reporting to either the concentrate or tails can be represented by the probability network in Figure 2.3. In this figure, the recovery of particles by entrainment and the recovery of particles by true flotation within the pulp phase is decoupled from the recovery of particles attached to bubbles and the recovery of entrained particles within the froth phase. In addition, it is assumed that the mechanism whereby particles are transferred from the froth phase to the concentrate launder by entrainment will be similar to that of particles which have detached from bubbles within the froth. The fraction of these particles which would eventually report to the concentrate launder is determined by only particle size, density and froth residence time. The symbol X represents a fraction of particles recycled back to the pulp phase for reattachment.

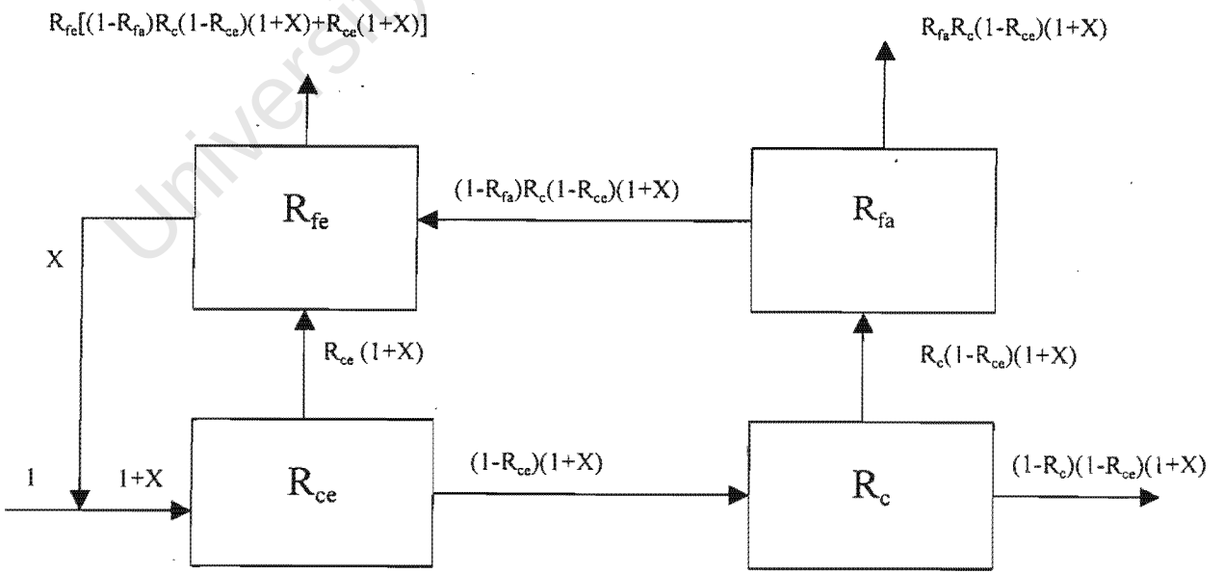

Figure 2.3 Proposed mass balance scheme

Solving for the overall flotation recovery in the network presented in Figure 2.3 gives the following equation:

$$R_w = \frac{1}{1-\left[(1-R_{fa})R_c(1-R_{ce})+R_{ce}-R_{fe}(1-R_{fa})R_c(1-R_{ce})-R_{fe}R_{ce}\right]} * \left\{R_{fe}\left[(1-R_{fa})R_c(1-R_{ce})+R_{ce}\right]+R_{fa}R_c(1-R_{ce})\right. \quad (2.13)$$

where R_{ce} is the recovery of non-floating particles within the pulp phase by entrainment, R_c is the recovery of particles within the pulp phase by true flotation, R_{fe} is the recovery of particles within the froth phase by entrainment, R_{fa} is the recovery of particles that remain attached to bubbles within the froth phase.

From section 2.5.1, the recovery of floatable particles of component i within the froth phase by entrainment is given by:

$$R_{fe(i)} = \left[\frac{1}{1+\omega_i * FRT}\right] \quad (2.9)$$

The recovery of particles that remain attached to bubbles within the froth is given by:

$$R_{fa} = \exp(-\beta FRT) \quad (2.4)$$

Engelbrecht and Woodburn (1975) showed that there is a linear relation between the recovery of entrained material and the recovery of water. This relation could be described by the following equation:

$$R_{e,i} = e_i R_w \quad (2.14)$$

where e_i is the entrainment factor of particles with size diameter i, and R_w is the overall cell water recovery.

It is worth mentioning here that the entrainment factor e_i used in equation (2.14) is very similar to the entrainment factor, Ent_i, proposed for describing entrainment in equation (1.15) (Savassi, 1998). The difference between these two factors (viz, e_i and Ent_i) is that the entrainment factor used in equation (1.15), Ent_i, is considered to represent the recovery of entrained particles occurring only within the froth phase. On the other hand, e_i represents the classification of particles, with size diameter i, within both the pulp and the froth phases.

When applied to the entrainment of particles within the pulp phase, equation (2.14) becomes:

$$R_{ce,i} = e_{c,i} R_{wc} \tag{2.15}$$

where $e_{c,i}$ is the entrainment factor of particles, with size diameter i, within the collection or pulp phase, and R_{wc} is the recovery of water within the pulp phase (i.e. at shallow froth).

It is proposed to use the following empirical partition curve, developed by Johnson (1972), to describe the entrainment factor of component i within the collection zone:

$$e_{c,i} = \frac{2}{\exp(1.317(\frac{dp_i}{\varsigma}))+\exp(-1.317(\frac{dp_i}{\varsigma}))} \tag{2.16}$$

where dp_i is the particle size diameter and ς is an empirical constant.

To describe the recovery of minerals within the pulp phase by true flotation, it is proposed to use a simple first-order kinetic equation (Gorain, 1998):

$$R_{c,i} = \frac{P_i S_b \tau_c}{1+P_i S_b \tau_c} \tag{2.17a}$$

where P_i is the floatability parameter of particles found in particle size class i, S_b is the bubble surface area flux and τ_c is the pulp residence time. In this equation, both τ_c and S_b are measurable.

In the case of plug-flow or batch behaviour, the recovery of floatable minerals within the pulp phase is:

$$R_{c,i} = 1 - exp\,(-P_i S_b \tau_c) \tag{2.17b}$$

The practical use of the above equations in the analysis of batch and continuous froth performance is presented next.

2.6.4 Synthesis and Analysis of Batch Data

All the models presented above are applicable to data obtained from continuously operated flotation cells. As such, they are not directly applicable to batch data. To apply them to non-

steady state systems, batch data need to be treated in a special way. Cumulative flotation recovery data obtained from non-steady state systems, either from bench-scale flotation cells or down the bank in commercial industries, represent a number of continuous cells in series (Figure 2.4). Therefore, it is proposed that batch data be treated as a series of continuously operated flotation cells. However, the nature of batch tests is such that the froth characteristics change with flotation time. As such, the froth parameters in the proposed froth recovery models are expected to vary with flotation time, introducing many unknown parameters during modelling. This situation requires a lot of measured data points at similar flotation conditions to derive the necessary parameters. The use of data obtained from industrial flotation cells to test these models is therefore limited. As such, modelling of the froth phase is preferably performed using data obtained mainly from bench-scale flotation cells. To achieve this, the description of the flotation recovery in batch cells must accommodate the changing froth characteristics with flotation time. Two approaches are proposed in this regard: (i) modifying a batch cumulative recovery equation to accommodate the influence of the froth, and (ii) dividing each batch test into n number of discrete continuous flotation cells or stages based on the flotation time interval, and describing overall recovery in each stage. These two approaches are now discussed.

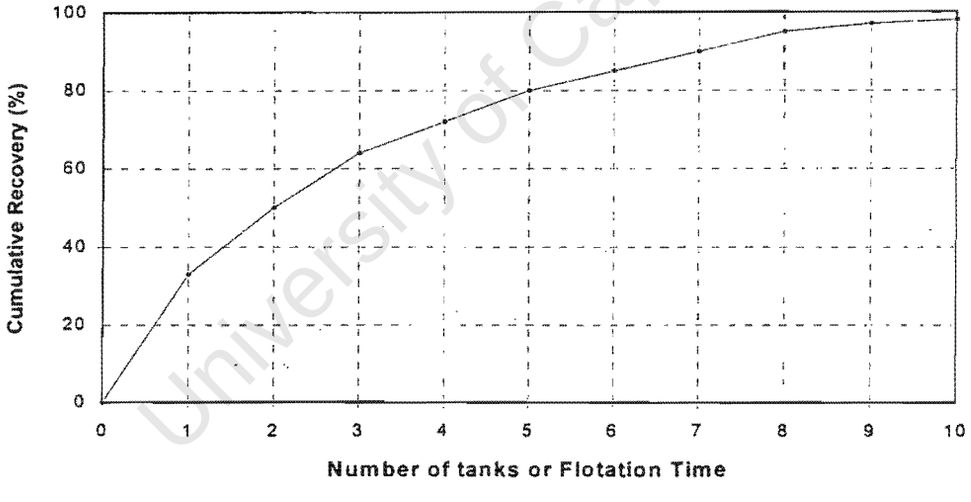

Figure 2.4 **Typical cumulative recovery as a function of number of cells in series or flotation time**

(i) Transformed batch recovery equation

The first-order rate expression for describing cumulative mineral recovery in a batch flotation cell is given by the equation:

$$R = 1 - exp(-k\,t) \qquad (2.18)$$

where k is the overall flotation rate constant and t is the cumulative flotation time.

If a batch test is regarded as comprising of a sequence of tests carried out in continuous plug-flow flotation cells, the cumulative recovery of particles by true flotation can be approximated by the sum of particle recoveries obtained from each flotation interval as follows:

$$R_{True(batch)} = 1 - \exp\left\{ \sum_{j=1}^{n} \left[(-k_j (t_j - t_{j-1})) \right] \right\} \tag{2.19}$$

where n is the number of time intervals and j is the "cell number".

It has been shown by Gorain *et al* (1998) that the overall flotation rate constant can be decoupled as follows:

$$k = P S_b R_f \tag{2.20}$$

where P is the floatability parameter and S_b is the bubble surface area flux, which is measurable.

Substituting equation (2.20) into equation (2.19) leads to the following expression:

$$R_{True(batch)} = 1 - \exp\left\{ \sum_{j=1}^{n} \left[(-P S_b R_{f(j)} (t_j - t_{j-1})) \right] \right\} \tag{2.21}$$

where R_f is given by equation (2.12).

Treating batch data in this manner allows for the P parameter for a particular particle size class to be kept constant for the entire batch flotation time during modelling. Only the mass fraction of a particular particle size class would vary from one flotation time interval to another. The bubble surface area flux, S_b, is also assumed not to be a function of flotation time. Most importantly, this method of analysing batch data allows for the R_f factor to vary with flotation time, which in turn enables the extraction of froth parameters that can be used to predict the performance of the froth in continuous tests.

Including entrainment,

$$R_{Total} = R_{True} * (1-R_e) + R_e \tag{2.22}$$

where entrainment recovery, R_e, could be described by the following expression (Engelbrecht and Woodburn, 1975; Trahar, 1981; Warren, 1985):

$$R_{e,i} = e_i * R_w \tag{2.23}$$

where R_w is the overall cell water recovery.

If it is assumed that the recovery of water is described by first-order kinetics, $R_{e,i}$ is given by:

$$R_{e,i} = e_i * (1-exp(-k_w * t)) \tag{2.24}$$

where k_w is the "recovery rate constant" of water.

Therefore, substituting equations (2.21) and (2.24) into equation (2.22), R_{Total} is:

$$R_{Total(batch),i} = 1 - \exp\left\{ \sum_{j=1}^{n} \left[(-P_i S_b R_{f(j),i} (t_j - t_{j-1})) \right] \right\} * \left[1 - e_i + e_i * \exp(-k_w t) \right] + e_i * \left[1 - \exp(-k_w * t) \right] \tag{2.25}$$

Despite its apparent complexity, equation (2.25) represents a very conventional description of batch flotation data, in the form of cumulative recovery with flotation time. The global nature of some parameters used in this equation, however, offers very little potential for better understanding and insight into some of the key froth sub-processes. For instance, the above equation considers entrainment of non-floating material as a global process (i.e. does not separate entrainment of non-floating particles within the pulp phase from that in the froth phase). In addition, the recycling of some of the entrained non-floating material that dropback from the froth into the pulp phase is not considered. Development of detailed and more realistic models for describing these froth sub-processes is difficult using equation (2.25). This can only be achieved by using a more tractable method for describing the recovery in a batch test. This method should allow for the decoupling of mineral recovery by entrainment and true flotation as a function of time. In addition, it should allow for the variation of some of the froth sub-processes or factors with flotation time. The information derived from such a method could then be used to modify equation (2.25) to represent a more realistic description of the batch flotation performance. It is believed that this can only be achieved by analysing flotation performance per individual stage in a batch flotation test. This method is now discussed.

(ii) Discrete stages in a batch test

An alternative approach is to divide each batch test into a number of discrete continuous flotation stages, which can be treated as if they are independent flotation cells operated under plug-flow conditions, based on the flotation time intervals. The mass charged into the cell at the start of a batch test is treated as the feed to the first stage. The feed to the next stage is determined by subtracting the mass recovered in the concentrate from that initially inside the cell. The recovery is then calculated for each stage based on the ratio of solids mass (which could be by size and/or mineral and/or liberation) in the concentrate to the mass of solids in the "feed". This procedure is repeated until the last stage. A schematic representation of this procedure is shown in Figure 2.5.

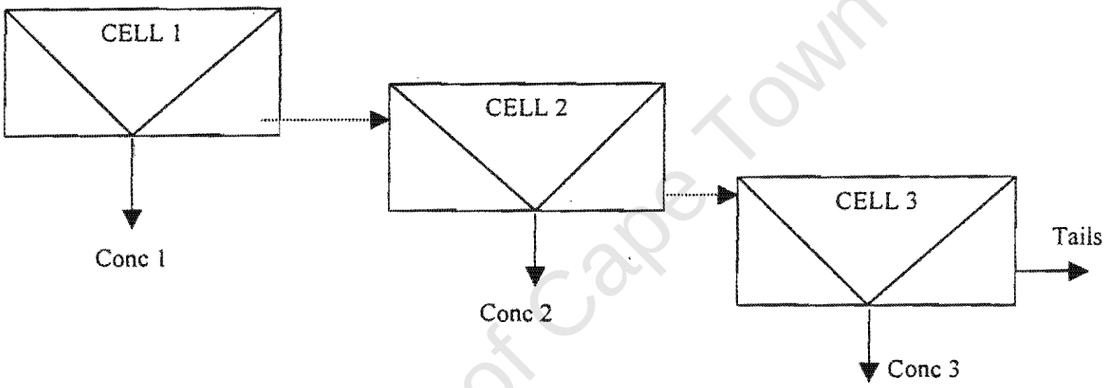

Figure 2.5 Synthesis of batch data

The main reason for adopting this approach is that it allows for the use of the recovery equations describing continuous flotation performance discussed in section 2.6.3. The manner in which these equations apply to this method is discussed in the next paragraph. The other reason for adopting this method is that the results, particularly the parameters derived from batch data, are readily transferable to continuous flotation tests. Depending on the operating conditions and the observed froth characteristics, this approach also makes it easier to vary some parameters, if necessary, by stage. Generally, froth characteristics, such as froth mobility, loading and stability, change with flotation time as frother and solids concentrations are depleted. The parameters describing or associated with froth characteristics can therefore be allowed to change by stage during modelling. In addition, this method allows for the assignment of different errors associated with recovery during each flotation stage. The mathematical expressions used to apply this method are now presented and discussed.

To illustrate the use of equations discussed in section 2.6.3 in this method, it is assumed that the recovery is only a function of particles found in particle size class i. For example, the

recovery of particles found in particle size class i in the first stage of a batch test is given by the following equation:

$$Ro_{1,i} = \frac{Rc_{1,i}\,Rf_{1,i}(1-Rw_1)+Ent_{1,i}\,Rw_1(1-Rc_{1,i})}{(1-Rw_1)(1-Rc_{1,i}+Rc_{1,i}\,Rf_{1,i})+Ent_{1,i}\,Rw_1(1-Rc_{1,i})} \qquad (2.26)$$

where $R_{c,1}$, i refers to the collection zone recovery, in stage 1, of particles found in particle size class i, $R_{f,1,i}$ refers to the froth recovery, in stage 1, of particles found in particle size class i, R_{w1} is the overall water recovery, in stage 1, and $Ent_{t,i}$ is the entrainment factor, in stage 1, of particles found in particle size class i.

The equations describing the individual factors used in equation (2.26) are as follows:

$$Rc_{1,i} = 1-\exp(-P_i\,S_b\,\tau_1) \qquad (2.27)$$

$$R_{f\,1,i} = \exp(-\beta\,FRT_1)+\left(1-\exp(-\beta\,FRT_1)\right)*\frac{1}{1+\omega_i\,FRT_1} \qquad (2.28)$$

$$Ent_{1,i} = \left(\frac{1}{1+\omega_i\,FRT_1}\right)/\,Rw_1 \qquad (2.29)$$

where P_i is the floatability parameter of particles found in size class i, which was assumed not to vary with cell number or flotation time interval; S_b is the bubble surface area flux, which was also assumed not to vary with cell number, only vary with air flow rate; ω is the drainage parameter, assumed to vary with particle size class i. τ_1 and FRT_1 are pulp and froth retention times in stage 1, respectively, which are measurable.

A more detailed explanation on how the above equations are applied to other particle size classes and batch flotation stages, is provided in Appendix D.

2.6.5 An Algorithm for Estimating Model Parameters

In the present work, the recovery equations are used to predict concentrate masses. The predicted concentrate masses are then compared with experimentally measured concentrate masses. Thereafter, the differences between predicted and measured concentrate masses are minimised using a linear regression tool (Solver) in Microsoft Excel software. An abbreviated algorithm of this procedure is shown in Figure 2.6. A more detailed example illustrating the application of the methodology is provided in Appendix D.

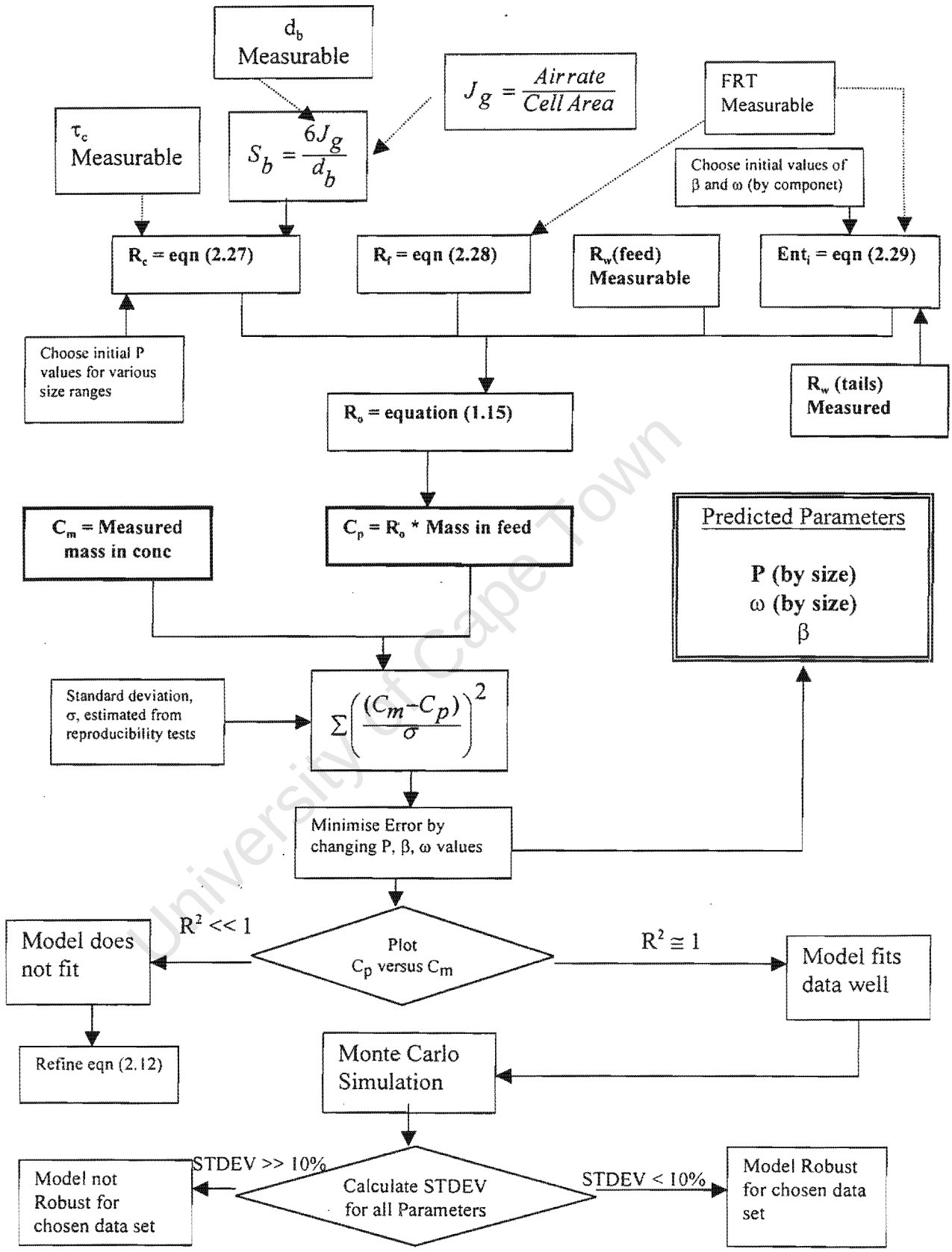

Figure 2.6 Modelling algorithm

2.7 SUMMARY

A descriptive froth recovery model of floatable particles has been presented in this chapter, namely:

$$R_{f(i)} = \exp(-\beta * FRT) + [1 - \exp(-\beta * FRT)] * [\frac{1}{1+\omega_i FRT}] \quad (2.12)$$

It was also shown how this model could be used in the analysis of batch data. Two methods were proposed in this regard. The first method is based on using a transformed equation describing the batch cumulative recovery which accommodates explicit descriptions of the froth and pulp processes. The use of this method, however, is believed to be very limited. This is mainly because it uses global parameters for describing some of the flotation mechanisms, such as the recovery of non-floating material and the recovery of water. Subsequently, an alternative method was proposed. This method is based on dividing each batch test into a number of discrete continuous flotation cells or stages, which could be plug-flow or perfectly mixed cells, based on the flotation time intervals. As such, each stage is treated, separately, as a continuous cell. The main reason for adopting this approach is that it allows for the use of the recovery equations describing continuous flotation performance. The other reason for adopting this method is that the results, particularly the parameters derived from batch data, are readily transferable to continuous flotation tests. Lastly, this method allows for the assignment of different errors associated with recovery during each flotation stage.

In summary, the mathematical expressions used in this method are as follows:

The overall recovery of particles found in particle size class i, per stage j, is described by:

$$Ro_{j,i} = \frac{Rc_{j,i} Rf_{j,i}(1-Rw_j) + Ent_{j,i} Rw_j (1-Rc_{j,i})}{(1-Rw_j)(1-Rc_{j,i}+Rc_{j,i} Rf_{j,i}) + Ent_{j,i} Rw_j (1-Rc_{j,i})} \quad (2.26)$$

where,

$$Rc_{j,i} = 1 - \exp(-P_i Sb \tau_j) \quad (2.27)$$

$$R_{f_{j,i}} = \exp(-\beta FRT_j) + \left(1 - \exp(-\beta FRT_j)\right) * \frac{1}{1+\omega_i FRT_j} \quad (2.28)$$

$$Ent_{j,i} = \left(\frac{1}{1+\omega_i FRT_1}\right) / Rw_j \quad (2.29)$$

A methodology for estimating or extracting parameters used in these equations from batch data was also presented in this chapter. The manner in which the derived parameters could then be used to describe froth behaviour in continuous systems was also outlined. The next chapter deals with experimental work conducted to test the practical use of the proposed methodology of modelling batch data and evaluate model parameters used in the proposed recovery equations.

CHAPTER 3

Evaluation of Model Parameters using Laboratory Procedures

CHAPTER 3: EVALUATION OF MODEL PARAMETERS USING LABORATORY PROCEDURES

3.1 EXPERIMENTAL TESTWORK

3.1.1 Introduction

The overall objective of this experimental testwork was to conduct flotation tests in batch and continuous modes, with the aim of correlating froth parameters derived from both systems. Parameters of interest included froth retention time, pulp residence time, bubble surface area flux, flotation rate constants, and parameters proposed in Chapter 2 to describe froth recovery. To simplify experimental tests and analysis it was necessary to conduct these tests with a bench-scale flotation cell using a very simple system.

3.1.2 Equipment Used

3.1.2.1 Flotation Cell

A 3.5 ℓ bottom driven Leeds type flotation cell was chosen for this investigation, and was used for conducting both batch and continuous flotation tests. This cell was chosen for various reasons, including the possibility of extending the top section of the cell to allow for flotation tests to be conducted with deep froths. In addition, the scraping of the froth layer, when necessary, was not restricted. The cell is equipped with a variable agitator speed control panel. Air is fed through a small stainless steel pipe (approximately 2 mm ID) to the bottom of the cell, and dispersed by the impeller. The impeller has a diameter of 7 cm. The cell is also equipped with a pulp level controller, which uses a constant head to adjust the volume of liquid inside the cell. In some instances, it was necessary to add water manually during flotation to compensate for the slow response of the constant head device in filling up the water to the set level. The cross-sectional area at the top of the cell was measured to be 207 cm^2. A schematic diagram of this flotation cell is shown in Figure 3.1.

3.1.2.2 Continuous Flotation Set-Up

In addition to the 3.5 ℓ Leeds cell, equipment used for these tests included a 250 ℓ stainless steel holding tank, fitted with a blade type impeller for mixing. A circulation pump was used to further mix the slurry inside the tank. The feed to the flotation cell was bled off from the circulation line. Feed was fed into a small feed box, made out of plastic, to reduce turbulence and ensure a smooth flow of the slurry into the back side of the flotation cell. A plastic launder was placed at the front side of the cell to collect the concentrate. The launder was

replaced with a plastic bucket whenever flow rate measurements were taken. Figure 3.2 shows a schematic diagram of the continuous flotation set-up.

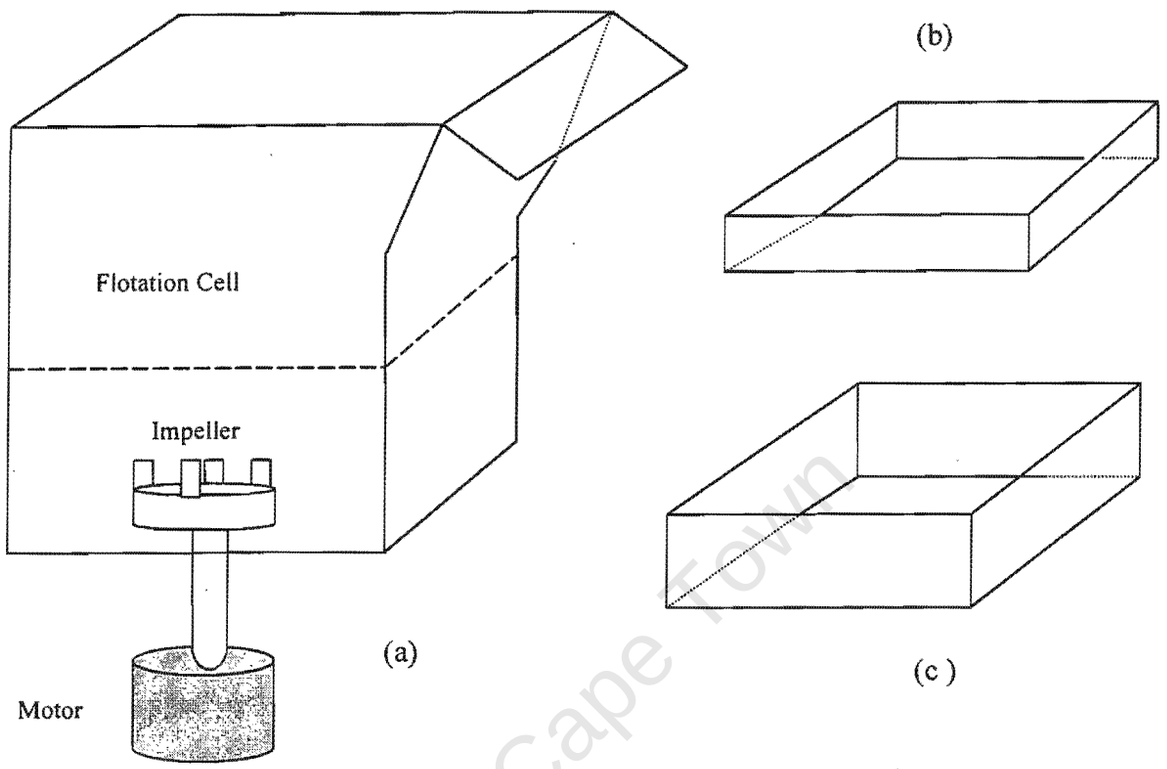

Figure 3.1 (a) Modified Leeds cell, (b) 2 cm extension piece, (c) 4 cm extension piece

3.1.2.3 Set-Up for Batch Tests With Wash Water

The flotation cell described in section 3.1.2.1 was used for this work. Due to an increase in froth volume, it was necessary to extend the upper part of the cell using the 4 cm extension piece described above. Wash water, mixed with a frother to achieve the same concentration as that inside the cell, was added using a coiled PVC pipe of approximately 0.5 cm inside diameter. Small holes of approximately 0.01 mm were drilled into the bottom part of the coiled pipe. A 25 litre bucket was used to hold wash water. Water was then fed into the spray water pipe using a pump. A schematic diagram of this set-up is shown in Figure 3.3.

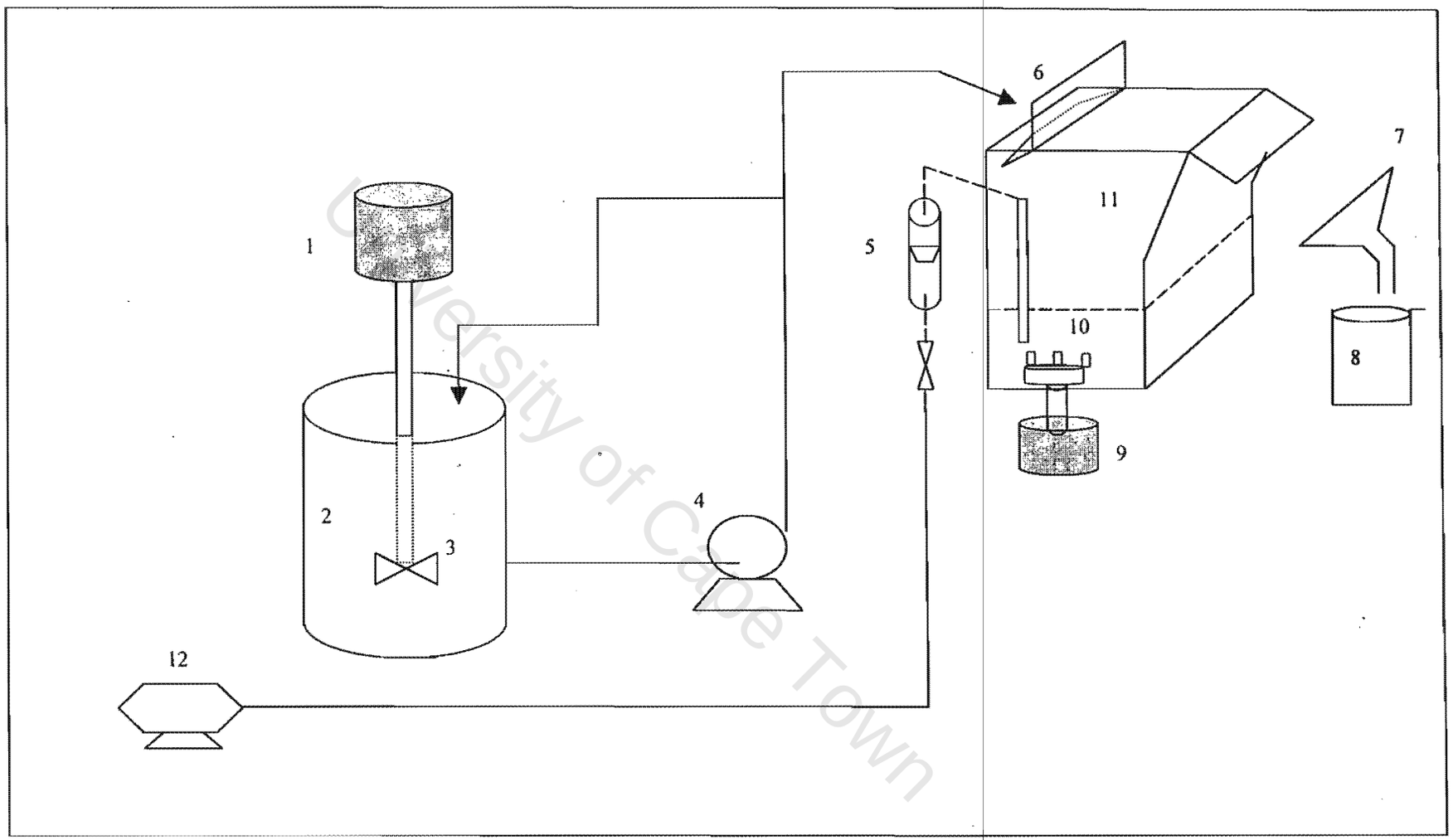

Figure 3.2 Continuous flotation set-up

1. Motor, 2. Holding tank, 3. Impeller 4. Circulation pump, 5. Rotameter, 6. Feed box, 7. Plastic-made launder, 8. Bucket, 9. Motor, 10. Impeller, 11. Flotation cell, 12. Compressor

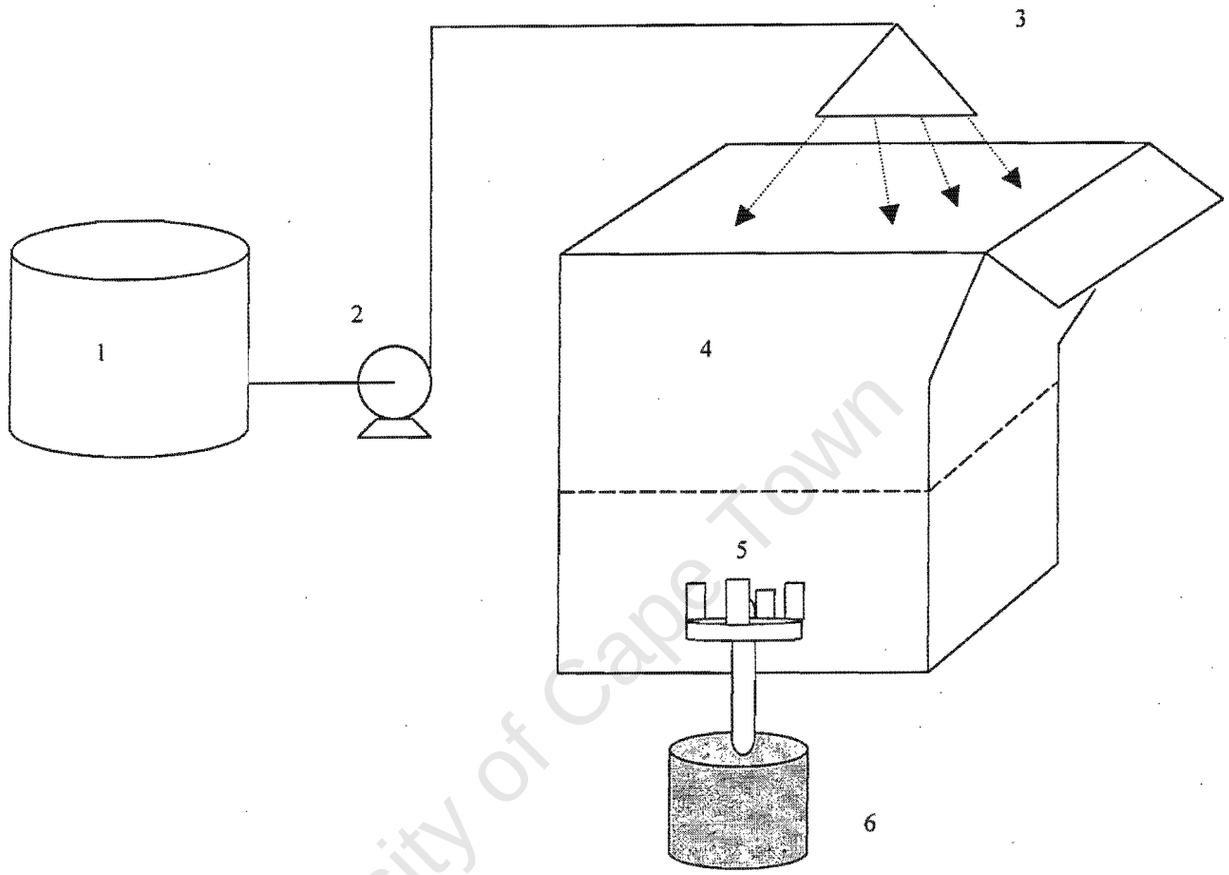

Figure 3.3 Batch tests with wash water set-up
1. Wash water tank, 2. Pump, 3. Water spray, 4. Flotation cell, 5. Impeller, 6. Motor

3.1.3 Choice of Ore

High purity quartz was chosen as the probe ore to be used in this study. This mineral has been used by several researchers to study the influence of the froth phase in flotation (Mular and Musara, 1991; Falutsu and Dobby, 1989; Contini *et al*, 1988). This is because of its low cost, availability, and the fact that it is obtainable at high purity. As such, any problems associated with mineral liberation and locking are eliminated. Quartz is an anionic (i.e. negatively charged over most of the pH range) non-metallic mineral and is naturally hydrophilic. Therefore, the mineral can be conditioned with reagents to achieve any desired level of hydrophobicity. In this way, the amount or rate of transfer of material from the pulp phase to the froth phase can be controlled. These advantages of quartz simplify the analysis of the concentrate, which enables researchers to focus on the problem at hand.

3.1.4 Preparation of the Ore

3.1.4.1 Milling and Screening

Bags of No. 2 Foundry sand, with a quartz purity of more than 99.6%, were obtained from Consol Industrial Minerals in Cape Town. The sand was then milled to obtain different size distributions. It was considered necessary to use a feed material with a size distribution representative of the particle size distribution in most flotation systems, with +/-75% of the floating material usually below 106 μm in particle diameter. Accordingly, one of the size fractions chosen for the experimental testwork was to be milled to approximately 75% passing 106 μm after calcining it. A coarser particle size fraction (+150 to 300 μm) was also selected. This was used in a number of tests to facilitate the study of the effect of dropback of particles within the froth phase.

A 300mm Polaris Mill, charged with 20 stainless steel rods of approximately 13 cm in length and 1 cm diameter, was used to mill the sand in 2 Kg batches, at 56 rpm. The sand was milled to 60% passing 106 μm, using a milling time of 55 minutes. This material was bulk screened to produce a nominally 60% passing 106 μm sample, and a nominally 150 to 300 μm sample.

3.1.4.2 Calcining of the Quartz

The bulk screened fractions of sand (nominally 60% passing 106 μm, and +150 to 300 μm) were calcined at 500 degrees for 2 hours to burn off any impurities and organic materials coated on the surface of the particles. These calcining conditions were established by Breytenbach (1995) who calcined the same quartz mineral for use in studying the mineral collection efficiency in different flotation systems. The particle size distribution of the calcined quartz sample, originally nominally 60% passing 106 μm, is shown in Table 3.1 below. From this table, it can be seen that approximately 75% of the particles were below 106 μm. One can conclude that calcining the quartz either caused a reduction in the diameter of the particles, or, more likely, improved the screening characteristics of the sand by removal of organic material coating these particles. The removal of impurities from the surface of the quartz particles was also evident from the change of color on the surface of the particles from grey to light pink. On this basis, the 150 to 300 μm fraction was also rescreened after calcining to remove any oversize and undersize material.

Table 3.1 Particle size distribution of the originally nominally 60% passing 106 μm calcined quartz

Particle Size Range (μm)	% Mass
Sub 10	5.48
10 to 25	10.91
25 to 45	15.77
45 to 75	20.02
75 to 106	24.92
106 to 225	22.89

3.1.5 Choice of Reagents

For this study, hexadecyl pyridiniumchloride (HPYC), $C_{21}H_{38}NCL$, was chosen as a collector. This collector has been shown to work well with the quartz used in this study (Breytenbach, 1995; Brack and Harris, 1996). It is supplied by Sigma Chemical Company, St Louis, USA.

A previous study conducted using quartz (Breytenbach, 1995) also showed that a Senmin 6010 frother works very well with the selected collector. Therefore, Senmin 6010 was chosen to be the only frother used in this study. Senmin 6010 is a blend of 90% dimethyl phthalate and 10% polyglycol ether. Only small amounts of frother were needed because of the frothing properties of the collector. The specific amounts of the frother and collector dosages used are discussed in section 3.1.7.1 below.

3.1.6 Choice of Operating Parameters

The operating conditions selected for the tests conducted in this study are summarised in Table 3.2 below. A pulp density of 3% was selected for the flotation of the 150 to 300 μm size fraction feed material. The main aim was to create a dilute and well dispersed system, which would favour first-order kinetics. However, it was found that this pulp density was not appropriate for the nominally 75% passing 106 μm feed material. This was due to the very fast and uncontrollable rate at which the particles in this size range were recovered into the concentrate launder. As a result, a pulp density of 10% was selected for this material.

A pH of 7 was chosen for this study. This pH has been found in previous studies to represent a suitable value for flotation of quartz (Breytenbach, 1995). Collector dosage was kept

constant at 150 g/ton of ore. This was based on previous batch tests conducted at UCT using quartz to study the effect of hydrophobicity in a laboratory flotation cell (Breytenbach, 1995; Brack and Harris, 1996). The frother concentration was also kept constant, at 6.5 micro-litres per litre of pulp volume. This corresponds to about 70 g/ton of ore. According to Crozier (1992) most industrial plants float quartz with 50 to 200 g/ton of the collector and with 50 to 100 g/ton of the frother. Thus, the chosen dosages of reagents fall within these ranges.

Table 3.2 Choice of operating parameters

Fixed Conditions		Variable Conditions
Pulp density:	3% (150 to 300 μm feed material)	Froth height: varied between 5 and 50 mm
	10% (nominally 75% passing 106 μm feed)	Air flow rate: varied between 2 and 8 ℓ/min
pH:	7	
Impeller speed:	1000 rpm	
Collector concentration:	150 g/ton of ore	
Frother concentration:	6.5 μℓ per litre of pulp volume ≅ 70 g/ton of ore	

Impeller speed was kept constant at 1000 rpm. This level had been shown to be appropriate in a variety of previous studies on the chosen flotation cell (Goodall, 1992; Breytenbach, 1995; Harris and Brack, 1996). Froth height and air flow rates were selected to span the effective operating range for the type of cell used in this study. Generally, air flow rate was varied between 2 and 8 ℓ/min. This parameter was varied to achieve a wide range of bubble size distribution. Physical characteristics of the cell and froth characteristics determined the limits of the froth height that could be used. Where possible, the froth height was varied between 0.5 and 5 cm. It was also part of the experimental plan to vary froth height and air flow rates to achieve a wide range of froth retention times and water recovery.

3.1.7 Operating Procedures

3.1.7.1 Pulp Conditioning

Firstly, the required amount of quartz, for the desired pulp density was charged into the cell which contained some water to keep the mineral particles in suspension. Whilst agitating, additional water was added to raise the pulp level inside the cell to the predetermined mark. The speed of the impeller would then be adjusted to 1000 rpm. Thereafter the pH of the slurry was adjusted (by using small quantities of HCl or NaOH) to a pH of 7. After this, the required

amount of collector (150 g/ton) was added and conditioned for 5 minutes. Frother (6.5 $\mu\ell$ per ℓ of cell volume) was then added and the slurry was then conditioned for a further 5 minutes.

3.1.7.2 Batch Tests

Once the pulp had been conditioned, the air was turned on. A short time was allowed for the froth to build up before scraping was begun. Froth was scraped 6 times per minute at intervals of 10 seconds. This was continued whilst collecting concentrates at desired intervals until no further froth build-up was observed to occur. Wash bottles filled with a known amount of water were used to wash floated particles off the concentrate launder into pre-weighed dishes. The dishes with concentrates were then weighed to determine the amounts of wet slurry and water recovered.

3.1.7.3 Continuous Tests

Slurry feed for continuous flotation tests was held in a large conditioning tank fitted with recirculation flow and a mixer. After conditioning the pulp with a collector and a frother as in the batch tests, the slurry was fed into the cell feed box by bleeding off some slurry from the recirculation line. While the material inside the cell was being agitated, the air and head level control water was turned on. The system was allowed 10 to 15 minutes to reach steady-state before sampling took place. This procedure was followed each time the flotation conditions inside the cell were varied. Mass and volumetric flow rate of concentrate and feed samples were measured using a bucket and a stopwatch.

3.1.7.4 Batch tests with wash water

Conditioning of the pulp was performed as previously described in section 3.1.7.1. Wash water was mixed with frother to achieve the same concentration of frother as that inside the cell. This was done to maintain the froth stability during flotation. The use of water resulted in an increase in mass flow of water to concentrate and more deep froths at the very start of a batch float. The increase in mass flow of water to concentrate facilitated the free overflowing of the froth into the concentrate dish. For this reason, no scraping was necessary. Concentrate samples were collected every 10 seconds over a period of 3 to 4 minutes.

3.1.8 Tests Conducted

3.1.8.1 Batch Tests (+ 150 to 300 μm)

The initial batch tests were carried out by floating samples of the coarse fraction (-300 to + 150 μm) of calcined quartz. These tests were conducted at different flotation conditions, varying froth height, 0.5 to 5 cm, and air flow rate between 2 and 6 ℓ/min. Concentrate samples were collected at cumulative flotation times from 1 minute up to 5 minutes. To ensure continuous removal of froth, it was necessary to scrape 6 times every minute. It was found that the coarse nature of this particle size range limited the range of flotation conditions that could be used for this preliminary testwork. This was mainly due to the fast flotation rate of the material in this particle size range. Most material floated within the first minute. The operating parameters and fixed conditions used in some of these tests are summarized in Tables 3.3 and 3.4, respectively. The analysis of these results is reported in section 3.2 below. Appendix A shows all the results obtained from this work.

Table 3.3 Operating conditions used during flotation of the 150 to 300 μm feed material

Test Number (see Appendix A)	Froth Height (mm)	Air Flow Rate (ℓ/min)
27	10	4
30	25	2
31	25	3
32	25	4
33	25	5
35	25	6
17	40	4
15	50	4

Table 3.4 Fixed conditions used during flotation of the 150 to 300 μm feed material

Parameter	Setting
Collector Type	HPYC
Collector Dosage(g/ton)	150
Frother Type	Senmin 6010
Frother Dosage (g/ton)	71
Pulp Density	3%
Impeller Speed	1000 rpm
pH	7

3.1.8.2 Batch Tests (nominally 75% passing 106 μm)

Calcined quartz (10% solids) was charged into the cell and conditioned following the procedure described in section 3.1.7.1. The particle size distribution of the feed material, measured using a Malvern Sizer, to each test is shown in Table 3.5. The conditions used in these tests are summarised in Tables 3.6 and 3.7. The same chemical dosages used to treat the coarse feed material were also used for these tests. Froth removal was achieved by hand scraping at a constant rate of 6 scrapes/min. Concentrate samples were collected at cumulative flotation times of 30 seconds or 1 minute, depending on the mass pull, up to 5 minutes. These samples were then weighed, wet and dry, and analysed for particle size distribution using a Malvern Sizer. All raw data from these tests are shown in Appendix B-1.

Table 3.5 Particle size distribution of the nominally 75% passing 106 μm feed material used for batch tests

Test Number (see Appendix B-1)	Feed Size Distribution (%)					
	Sub 10 (μm)	10 to 25 (μm)	25 to 45 (μm)	45 to 75 (μm)	75 to 106 (μm)	106 to 225 (μm)
1	5.76	12.60	17.35	20.13	23.53	20.64
2	6.64	13.66	17.69	20.37	23.60	18.05
3	6.99	14.35	18.44	19.92	21.92	18.36
4	6.25	12.76	17.45	20.01	22.95	20.56
5	5.28	10.01	15.30	20.35	25.83	23.25
6	4.99	9.66	14.71	20.25	26.40	24.00
7	4.84	9.07	14.16	19.94	26.55	25.45
8	5.23	10.63	15.66	20.09	25.13	23.24
9	4.81	9.08	14.20	19.75	26.24	25.91
10	4.74	9.17	14.15	19.53	26.02	26.39
11	5.26	10.10	15.11	19.88	25.39	24.25
12	5.07	9.79	15.07	19.98	25.53	24.57

Table 3.6 Operating conditions used during batch flotation of the nominally 75% passing 106 μm feed material

Test Number (see Appendix B-1)	Froth Height (mm)	Air Flow Rate (ℓ/min)
9	5	3
10	5	4
11	5	5
12	5	6
5	25	3
6	25	4
7	25	5
8	25	6
1	45	3
2	45	4
3	45	5
4	45	6

Table 3.7 Fixed conditions used during batch flotation of the nominally 75% passing 106 μm feed material

Parameters	Setting
Collector Type	HPYC
Collector Dosage (g/ton)	150
Frother Type	Senmin 6010
Frother Dosage (g/ton)	71
Pulp Density	10%
Impeller Speed	1000 rpm
pH	7

3.1.8.3 Continuous Tests (nominally 75% passing 106 μm feed)

26 continuous flotation tests were conducted at various froth heights and air flow rates (see Table 3.8). Air flow rate was varied between 4 and 8 ℓ/min. Fixed conditions are shown in Table 3.9. The particle size distribution of the feed material to each test is shown in Table 3.10. A comparison among some tests, especially Test 11, 13 and 27, indicates that there are large variations in the masses of the 106 to 225 μm. For Test 11 and 13, the variation could be associated with the change in the feed density. For Test 13 and 27, the variation in percentage size distribution of the masses of the 106 to 225 μm could be due to the change in froth height. In the final analysis, these variations would have very little impact since masses within each particle size range are treated separately. The free overflowing nature of the froths obtained in continuous tests did not necessitate scraping for the tests conducted at shallow froths (below 2 cm). However, this limited the range of froth height that could be used, as it was not possible to conduct flotation tests with deep froths without scraping. The data from these tests are shown in Appendix B-2.

Table 3.8 Operating conditions used during continuous flotation of the nominally 75% passing 106 μm feed material

Test Number (see Appendix B-2)	Froth Height (cm)	Air Flow Rate (ℓ/min)	Feed %Solids
23	0.5	4	6.02
8	0.8	4	2.56
42	1	4	6.76
24	1.5	4	3.26
43	2	4	6.75
4	0.5	5	6.53
22	0.5	5	3.83
35	0.5	5	7.11
9	0.8	5	7.31
25	1	5	2.33
41	1	5	6.60
40	1	5	2.42
15	2	5	6.60
3	0.5	6	7.42
26	1	6	5.70
11	2	6	3.24
16	2	6	7.43
36	2.5	6	2.34
27	1	7	3.30
30	1	7	3.83
13	2	7	1.83
2	0.5	8	7.20
19	0.5	8	6.34
32	0.5	8	3.24
31	1.5	8	3.30
18	2	8	6.41

Table 3.9 Fixed conditions used during continuous flotation of the nominally 75% passing 106 μm feed material

Parameters	Setting
Collector Type	HPYC
Collector Dosage (g/ton)	150
Frother Type	Senmin 6010
Frother Dosage (g/ton)	71
Impeller Speed	1000 rpm
pH	7

Table 3.10 Feed size distribution used during continuous flotation of the nominally 75% passing 106 μm feed material

Test Number (see Appendix B-2)	Feed Size Distribution (%)					
	Sub 10 (μm)	10 to 25 (μm)	25 to 45 (μm)	45 to 75 (μm)	75 to 106 (μm)	106 to 225 (μm)
23	11.01	11.44	12.84	13.93	18.76	31.98
8	8.53	9.67	13.24	16.41	22.75	29.40
42	7.15	7.89	11.97	16.10	21.72	35.19
24	11.25	12.48	14.23	14.39	18.01	29.62
43	7.55	9.67	12.59	15.81	21.71	32.64
4	8.19	10.17	14.67	17.58	22.43	26.97
22	11.04	12.15	13.66	14.25	18.39	30.48
35	8.10	8.97	12.25	15.13	21.38	34.18
9	7.80	9.92	14.84	18.03	23.05	26.36
25	11.36	11.97	13.40	14.32	18.93	30.00
41	6.63	6.97	11.76	16.73	22.46	35.46
40	7.65	8.23	12.55	16.38	21.77	33.42
15	11.95	13.16	14.73	14.42	17.74	27.96
3	7.65	8.88	13.43	17.70	24.23	28.07
26	13.58	14.11	15.84	16.42	19.52	20.47
11	13.64	17.53	23.08	20.79	16.03	8.94
16	10.61	11.25	13.13	14.48	18.98	31.55
36	10.67	12.25	18.29	19.55	20.55	18.65
27	18.45	19.47	20.84	17.44	14.30	9.47
30	6.78	7.62	11.74	15.58	22.03	36.25
13	18.12	23.22	26.59	18.21	9.84	4.04
2	8.43	10.28	13.59	15.70	21.74	30.25
19	11.48	12.64	14.28	14.99	19.24	27.39
32	7.05	8.75	12.54	15.17	20.99	35.52
31	7.42	8.21	11.34	14.55	20.92	37.53
18	11.67	12.66	14.57	14.99	18.63	27.46

3.1.8.4 Batch Tests with Wash Water (nominally 75% passing 106 μm)

To minimise entrainment as far as possible, some batch tests were conducted whilst spraying water on top of the froth. Wash water was added at approximately 1200 mℓ/min. The average particle size distribution of the feed material is shown in Table 3.11. The conditions used in these tests are summarised in Tables 3.12 and 3.13. All concentrate samples were weighed, wet and dry, and analysed for particle size distribution. The data obtained is given in Appendix B-3.

The addition of wash water, however, made it very difficult to control froth level. This is because of the slow response of the level controller in the chosen cell. As such, the froth height varied between 5 and 30 mm.

Table 3.11 Particle size distribution of the feed material used for batch tests with wash water

Particle Size Range (μm)	% Mass
Sub 10	9.40
10 to 25	9.90
25 to 45	12.91
45 to 75	15.73
75 to 106	20.95
106 to 225	31.13

Table 3.12 Operating conditions used during batch flotation of the nominally 75% passing 106 μm feed material (with wash water)

Test Number (see Appendix B-3)	Froth Height (mm)	Air Flow Rate (ℓ/min)
30	5 to 30	4
31	5 to 30	5
32	5 to 30	6
33	5 to 30	7
34	5 to 30	8
35	5 to 30	3

Table 3.13 Fixed conditions used during batch flotation, with wash water, of the nominally 75% passing 106 μm feed material

Parameters	Setting
Collector Type	HPYC
Collector Dosage (g/ton)	150
Frother Type	Senmin 6010
Frother Dosage (g/ton)	71
Impeller Speed	1000 rpm
PH	7
%Solids	10%

3.1.9 Bubble Size Measurements

Bubble size measurements were performed using the UCT bubble sizer. These measurements were conducted in the presence of water and frother only. It has been shown that the effect of solids on bubble size is relatively minimal at the pulp density used in this study (Goodall, 1992). The operation of the bubble sizer has been discussed very extensively in several

publications (Tucker *et al*, 1994; Gorain, 1998; Deglon, 1998), and will therefore be described only briefly here.

In the UCT Bubble Size Analyser, bubbles from the flotation cell are sucked through a bell-shaped glass capillary into a burette via a detector head. Within the detector head, two pairs of light-emitting diodes (LED) measure for each bubble the difference in intensity of the light as the bubble passes the detectors, due to the difference in refractive index of water and air. These two pairs of detectors measure the length and velocity of the bubble as it passes. Approximately 4000 bubbles are sampled per measurement. The total bubble volume captured in the burette together with the length and velocity readings are used by the computer software to generate results such as the Sauter mean bubble diameter, mean bubble volume and mean total bubble surface area of the bubbles sampled. The Sauter mean bubble diameter is the variable used in the calculation of the bubble surface area flux, S_b. Details of the method for calculating the Sauter mean bubble diameter from experimental data using the total bubble surface area S and volume V has been given in Tucker *et al* (1994), also shown in Appendix C. A schematic diagram of the UCT bubble sizer is shown in Figure 3.4. Table 3.14 shows the bubble sizes and bubble surface area flux obtained at different air flow rates.

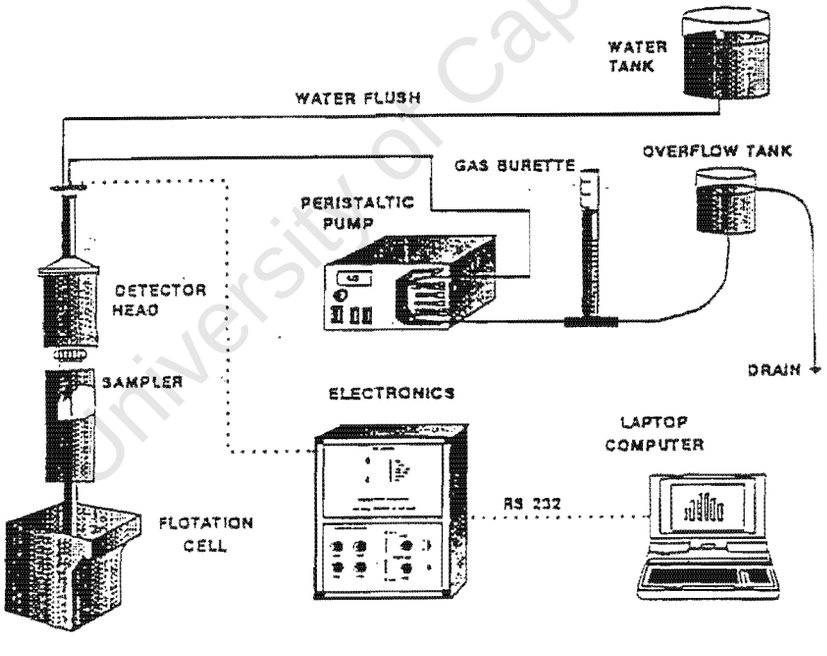

Figure 3.4 **UCT bubble sizer equipment (from Tucker *et al*, 1994)**

Table 3.14 Bubble size results

Airflow (ℓ/min)	Bubble Size, d_b Sauter Mean Diameter(mm)	Bubble Flux, Sb (1/min)
3	1.37	634
4	1.38	840
5	1.39	1042
6	1.49	1167
7	1.56	1300
8	1.60	1449

3.2. RESULTS AND DISCUSSION

3.2.1 Data Analysis

A mass balance program (Gay *et al*, 1999) was used to extract statistically reliable data from the tests that were conducted whilst operating the flotation cell continuously. Raw data of the feed, concentrate and tails flows (solids and water flow rates) were entered into the spreadsheet of the mass balance program. A standard deviation of 10% was assigned to each data point. The data was then reconciled based on the fact that mass is conserved (i.e. input mass into a flotation cell must equal mass coming out). With respect to batch tests, the data was used without any mass balancing.

For continuous data, the recovery was determined by the ratio of the dry solids mass flow rate in the concentrate to the dry solids mass flow rate in the feed. Likewise, water recovery was determined by the ratio of water mass flow rate in the concentrate to the mass flow rate of water in the feed. The batch tests mass recoveries were determined by the ratio of the cumulative mass of solids or water in the concentrate to the mass of dry solids or water initially inside the flotation cell. The flotation rate constants were calculated by fitting the first-order rate equation to experimental recovery data using the solver routine in Microsoft Excel. For batch data, the recovery was described using the following equation:

$$R = 1 - \exp(-k\,t) \qquad (1.3)$$

where k is the overall (froth and pulp) flotation rate constant, and t is the flotation time.

For continuous data, the recovery of particles was described using the following equation:

$$R = \frac{k\,\tau}{1 + k\,\tau} \qquad (1.7)$$

where τ is the flotation cell mean retention time based on tails flow rate.

The recovery data from batch and continuous tests were subsequently used to analyse the effect of operating parameters, such as particle size, froth height, air flow rate and froth retention time, on flotation performance. The data was also used to test how well the proposed equations in Chapter 2 can be used to model or describe flotation recovery. Firstly, a discussion on the experimental results obtained from using the conventional approach to analyzing laboratory data (i.e. deriving flotation rates by fitting equations 1.3 or 1.6 and 1.7) is provided. Thereafter, a discussion on the modeling results obtained from using the methodology proposed in chapter 2 is presented.

3.2.1 Experimental Results

3.2.1.1 Reproducibility

Tests conducted in a batch mode were repeated, randomly, in order to test the reproducibility of the results. Although achieving good reproducibility in flotation tests is often difficult, Figure 3.5 indicates that good reproducibility was achieved in this study. The standard deviation for data points was less than 3 percent. With respect to continuous flotation tests, Table 3.15 shows the results of the tests that were repeated at comparable conditions. In general, the standard deviation varied by not more than 4 percent.

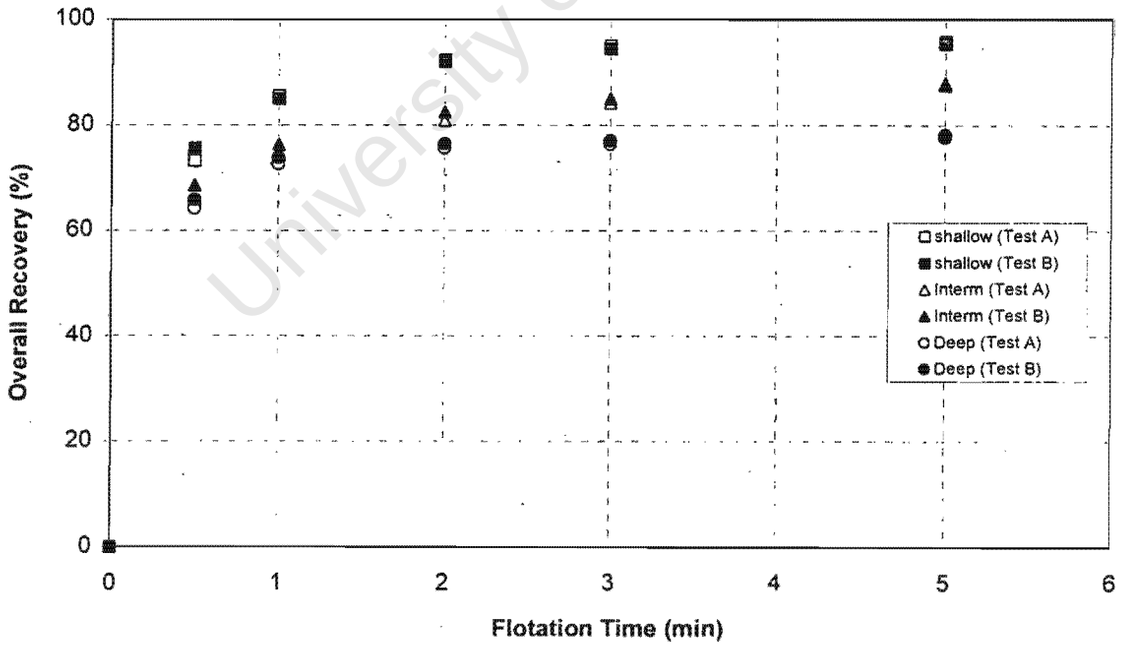

Figure 3.5 Batch reproducibility for different froth heights at an air flow rate of 5 litres/min

Table 3.15 Continuous tests reproducibility

Air flow (ℓ/min)	Froth Height (cm)	Pulp Density (%)	Recovery (%)		STDEV (%)
			Test A	Test B	
4.00	0.50	7.00	80.00	75.00	3.54
5.00	1.00	5.00	80.46	83.40	2.08
6.00	0.50	7.40	95.00	91.20	2.69

3.2.1.2 Effect of froth height on recovery

Figure 3.6 shows the effect of froth height on the overall flotation recovery of solids in the cell operated in a batch mode treating the 150 to 300 μm feed material. It can be seen that an increase in froth depth lead to a reduction in overall flotation recovery of solids. This can be explained by increased possibility of drainage of material (solids and water) as froth depth increases. Deep froths result in high froth residence time. In turn high froth residence time may allow significant coalescence of bubbles, which will, in turn, lead to high drainage rate of solid particles, both floating and entrained, and water. Likewise, increase in froth depth leads to a reduction in the overall water recovery (Figure 3.7). The same influence of froth height on overall recovery of solids and water was observed for the nominally 75% passing 106 μm fraction quartz mineral, both in batch and continuous flotation tests (Figures 3.8, 3.9, 3.10 and 3.11).

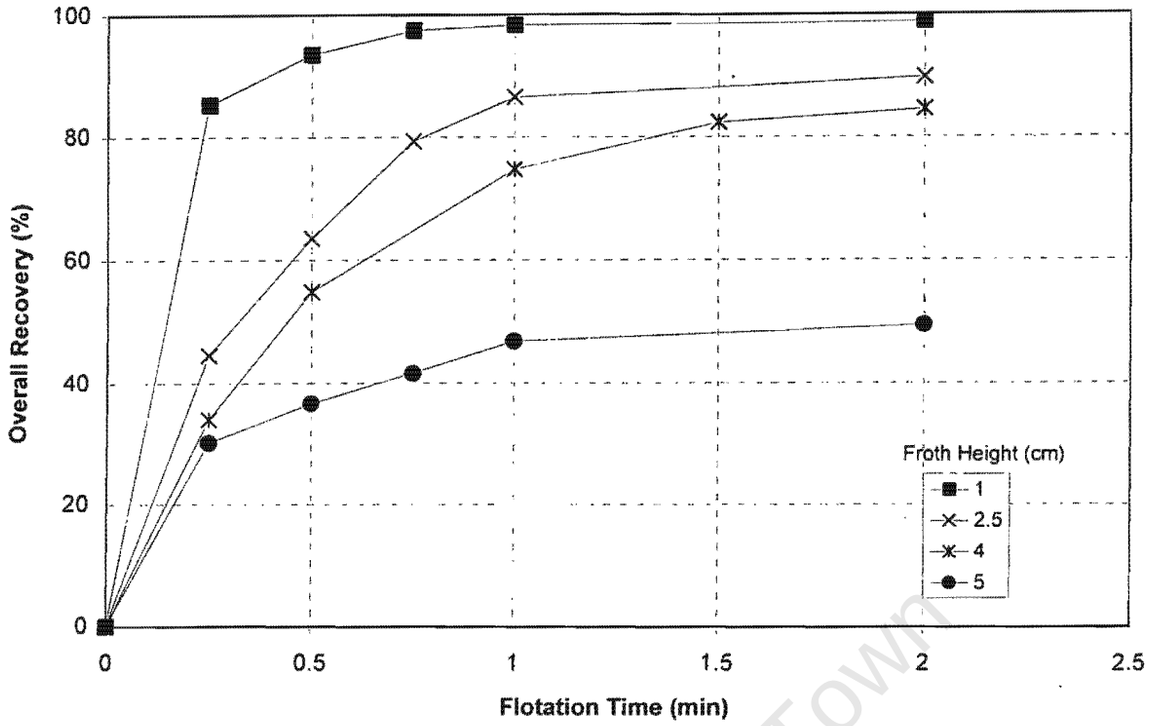

Figure 3.6 Effect of froth height on the overall flotation recovery for the 150 to 300 μm size fraction floated in a batch mode at 4 ℓ/min

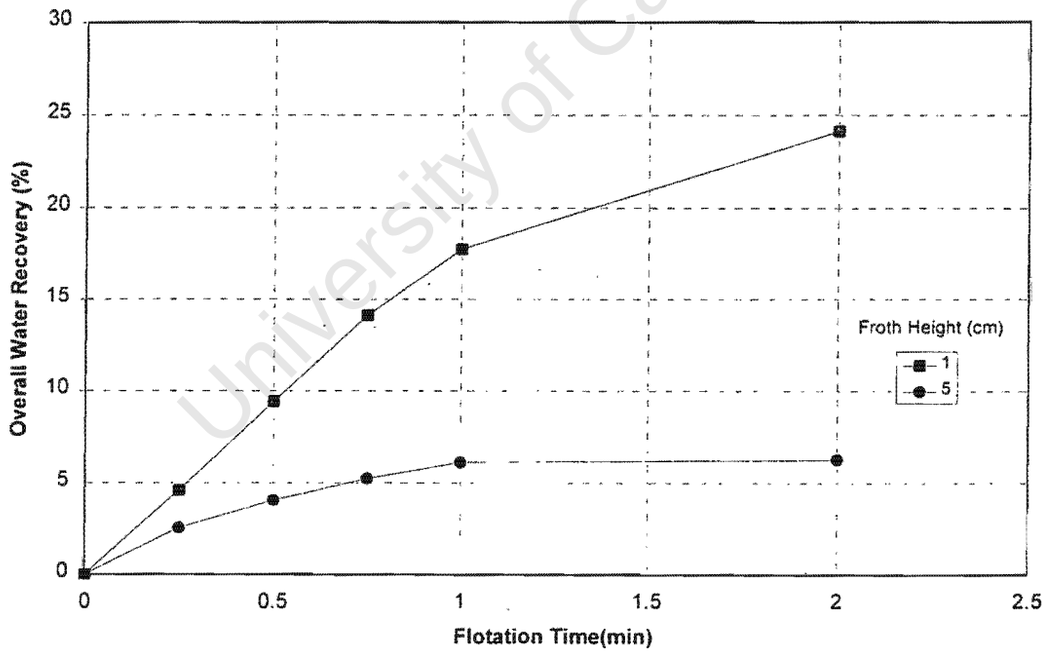

Figure 3.7 Effect of froth height on water recovery during batch flotation of the 150 to 300 μm feed material at 4 ℓ/min

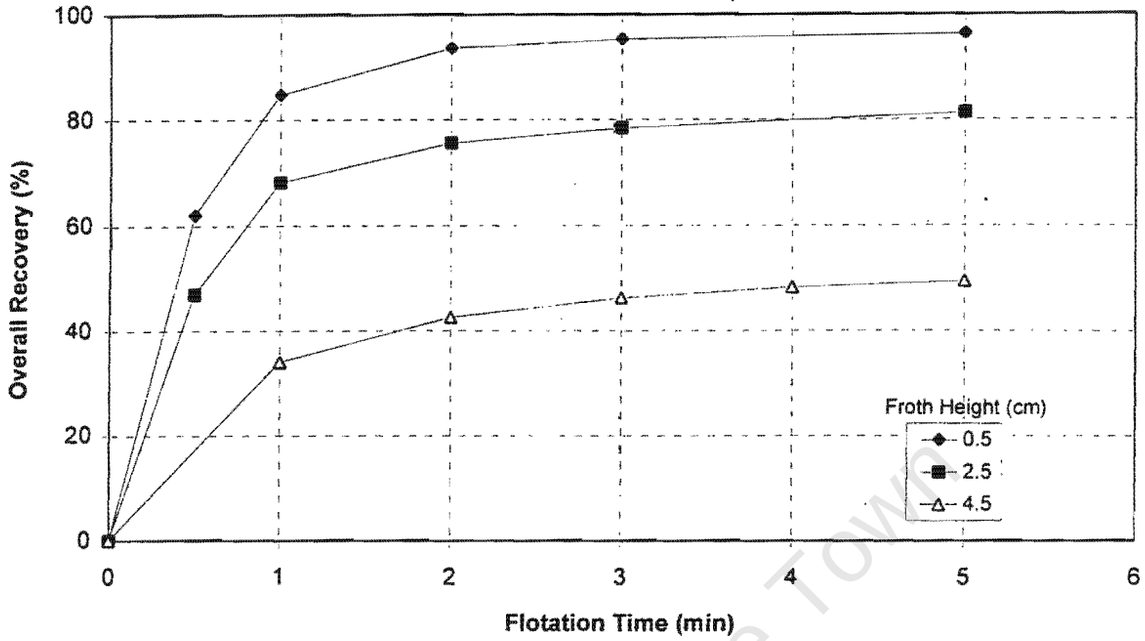

Figure 3.8 Effect of froth height on the overall flotation recovery for the nominally 75% passing 106 μm size fraction floated in a batch mode at an air flow rate of 6 ℓ/min

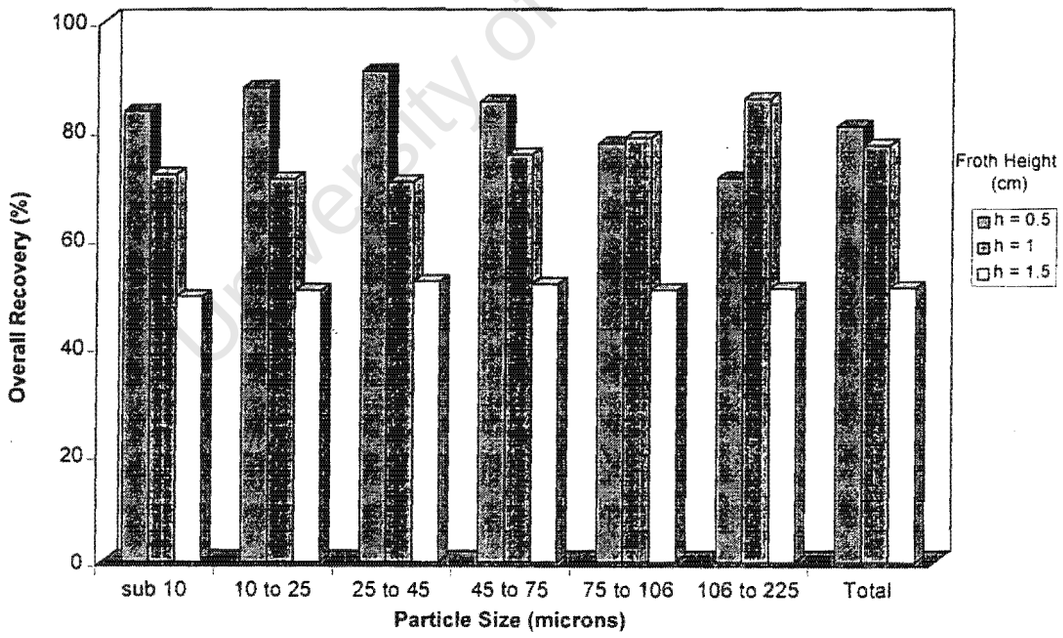

Figure 3.9 Effect of froth height on the overall flotation recovery for the nominally 75% passing 106 μm size fraction floated in a continuous mode at an air flow rate of 4 litres/min

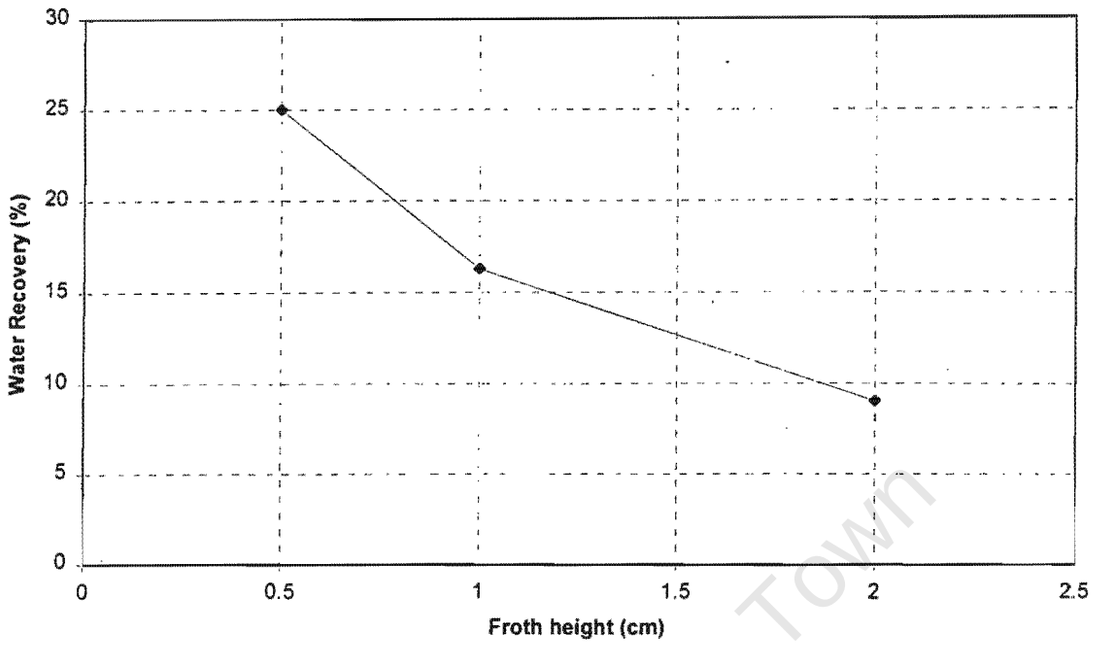

Figure 3.10 Effect of froth height on the overall water recovery for the nominally 75% passing 106 μm size fraction floated in a continuous mode at 4 ℓ/min

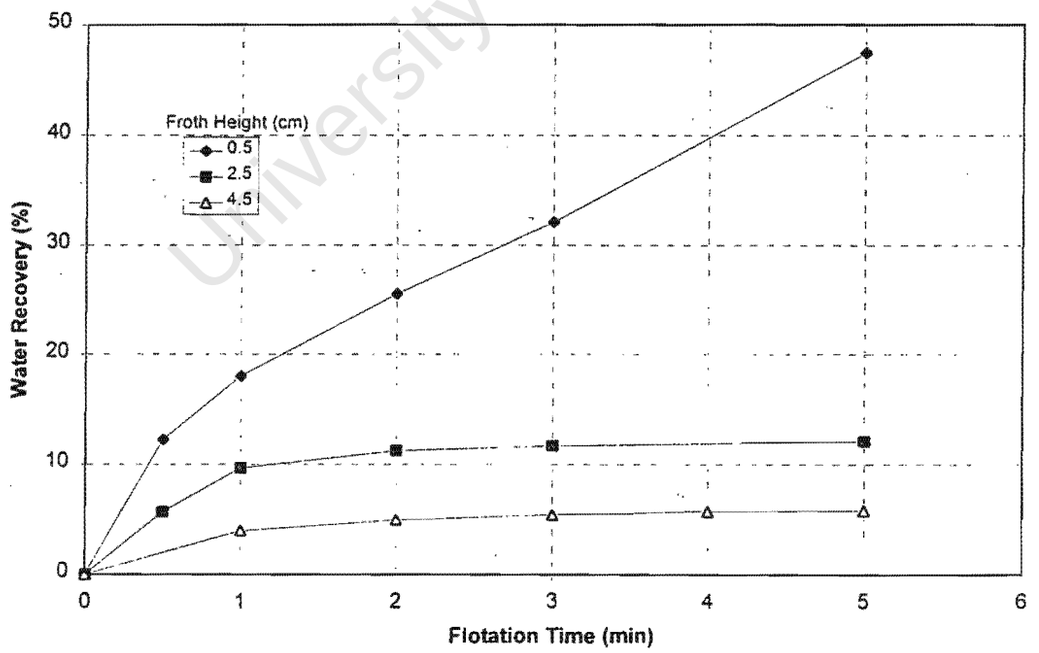

Figure 3.11 Effect of froth height on the overall water recovery for the nominally 75% passing 106 μm size fraction floated in a batch mode at 4 ℓ/min

The above results clearly show that the froth height is a very important parameter in flotation, and can be manipulated to achieve desired relative recovery between minerals. However, the use of this parameter in scale-up or comparison of flotation performance from different cells, is limited. This is because froth height is system specific. In addition, the results obtained when froth height is used as a variable, such as the results presented above, provide very little insight into some of the key froth sub-processes within the froth phase. Nevertheless, these results suggest that froth height should be considered as one of the key variables when developing a froth recovery model.

3.2.1.3 Variation of recovery with particle size

Figure 3.12 shows the variation of recovery with particle size for tests carried out in a batch mode at an air flow rate of 4 ℓ/min and a froth height of 2.5 cm. Under these conditions, the highest recovery was obtained in the 106 to 225 μm size fraction, with recovery decreasing with particle size. Typically, there is a "peak" in the recovery versus particle size curve. For sulphide minerals, this "peak" is in the range of 10 to 100 μm (Fig. 3.13). For the quartz mineral, however, which is relatively light when compared to some of the sulphide minerals, this "peak" is expected to be found at a higher particle size range. Analysis of previous study on quartz flotation in a batch cell (Breytenbach, 1995), at comparable conditions, indicate a possible "peak" at around 150 μm (Fig. 3.14).

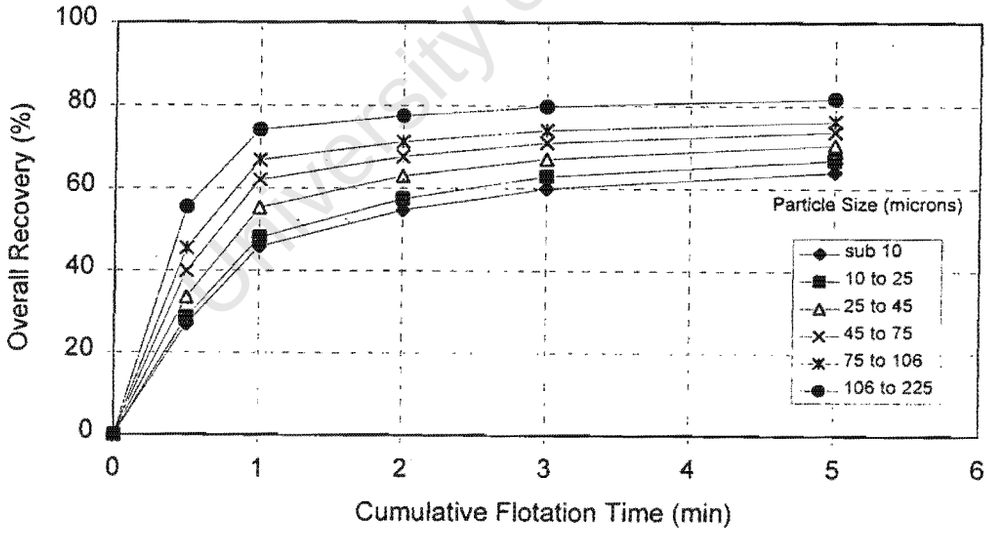

Figure 3.12 **Effect of particle size on the overall flotation recovery for tests carried out in a batch mode using the nominally 75% passing 106 μm size fraction. Recoveries obtained at an air flowrate of 4 ℓ/min and intermediate froth level (froth height of 2.5 cm)**

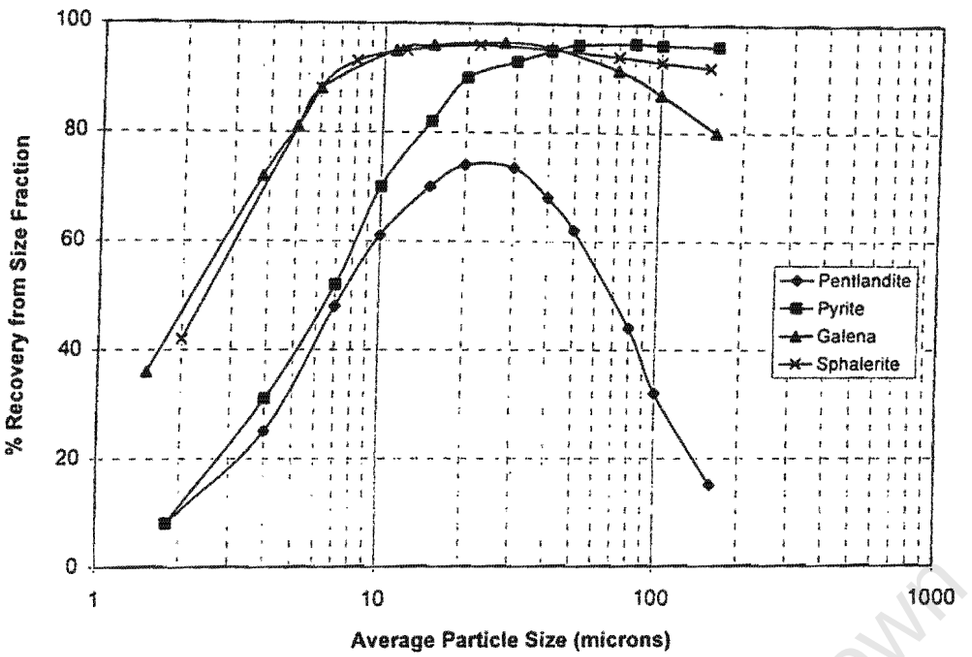

Figure 3.13 Size-by-size recovery of some sulphide minerals in batch flotation tests (Goodall, 1992)

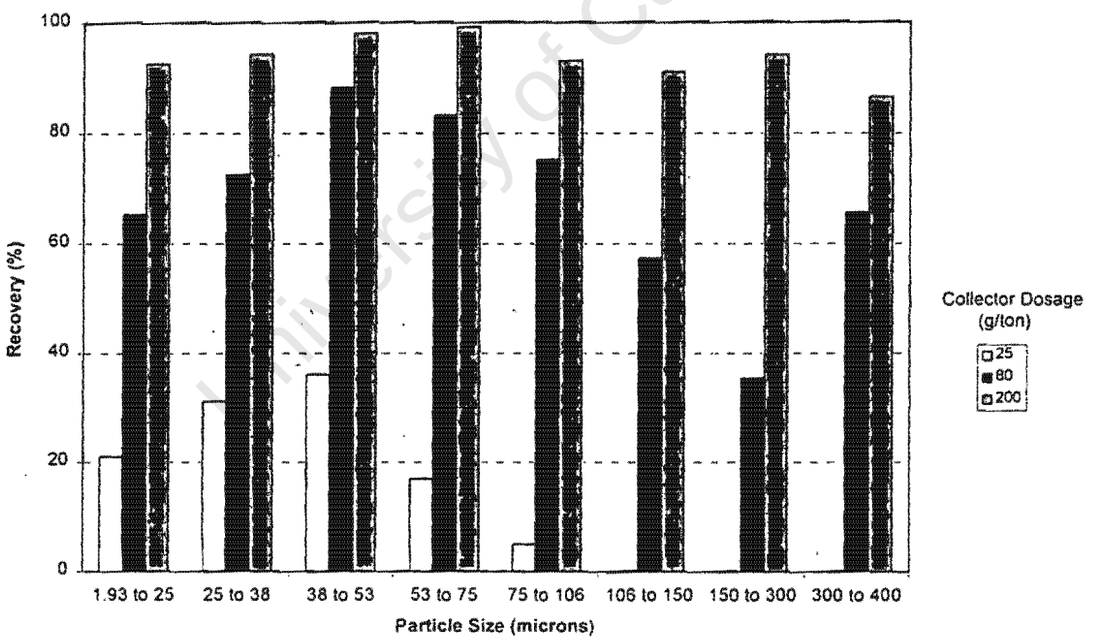

Figure 3.14 Variation of flotation recovery with particle size in a laboratory batch cell at different collector dosages. Pulp density kept constant at 10%, froth height equal to 2 cm, air flow rate equal to 3 ℓ/min, and impeller speed equal to 1470 rpm (Breytenbach, 1995)

At shallow froths, high recoveries were observed for all particle size classes (Figure 3.15). It can be seen also that the various particle size classes are recovered at different rates at the

start of a batch test. However, the recovery rate for all particle sizes was almost the same toward the end of the batch tests. This can probably be attributed to poor separation of the particles within the froth phase due to instability of the froth toward the end of a batch float. Again, the highest recovery was obtained in the 106 to 225 μm particle size range. As the froth depth was increased, the results indicated a significant drop in flotation recovery for all particle size ranges (Figure 3.16). More interesting was the observed significant decrease in the recovery of the fine (sub 10 μm) and the coarse (106 to 225 μm) size classes. This can be ascribed to the influence of froth residence time on the overall flotation performance. As mentioned earlier, deep froths result in high froth residence time, which, in turn, lead to significant dropback of particles and water. Particles found in the coarse size range (106 to 225 μm) probably dropback because of their weight. The particles in the fine size range (sub 10 μm), on the other hand, probably dropback because they tend to follow water flows. In Figures 3.10 and 3.11, it was shown that an increase in froth depth lead to a reduction in the recovery of water, which obviously influenced the recovery of the particles found in the fine size class. These results suggest that water recovery has a major influence on the overall recovery of solids, both true floating and entrained. Therefore, a successful overall flotation recovery model would probably depend on being able to accurately predict water recovery.

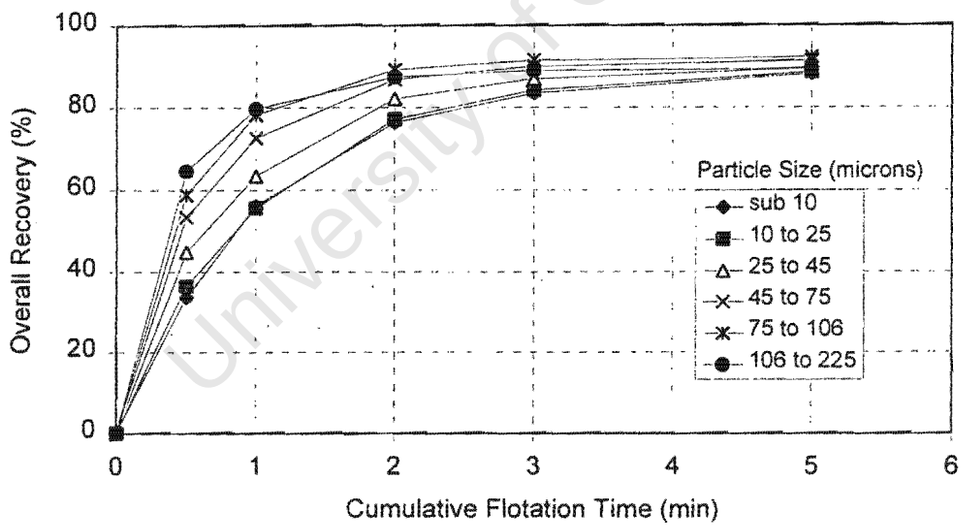

Figure 3.15 **Effect of particle size on the overall flotation recovery for tests carried out in a batch mode using the nominally 75% passing 106 μm size fraction. Recoveries obtained at an air flow rate of 4 ℓ/min and shallow froth level (froth height of 0.5 cm)**

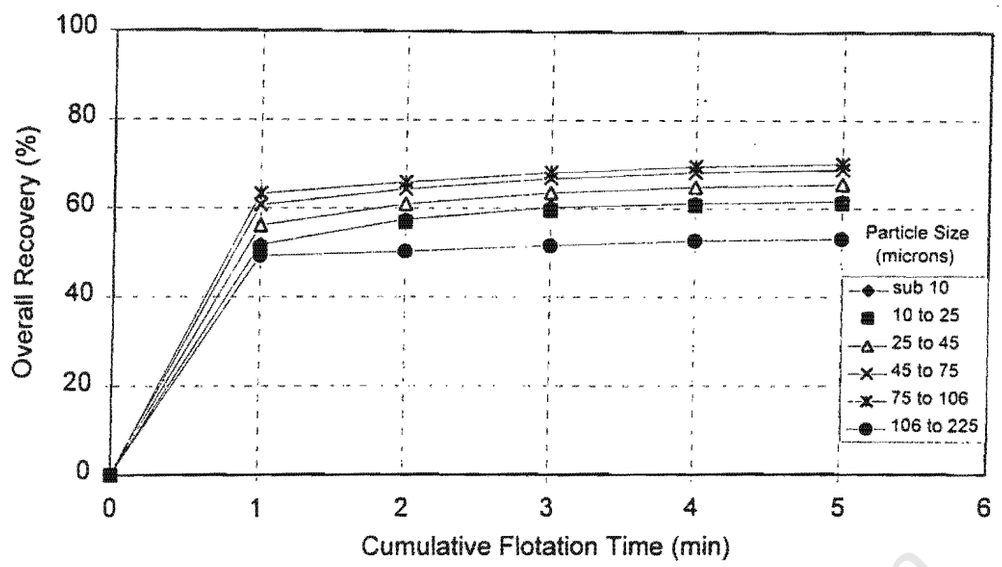

Figure 3.16 **Effect of particle size on the overall flotation recovery for tests carried out in a batch mode using thenominally 75% passing 106 μm size fraction. Recoveries obtained at an air flowrate of 4 ℓ/min and deep froth level (froth height of 4.5 cm)**

3.2.1.4 Effect of air flow rate on recovery

Figures 3.17 and 3.18 show the effect of air flow rate for the tests carried out in the batch cell operated in a batch mode using the nominally 75% passing 106 μm and the 150 to 300 μm feed material, respectively. They indicate that an increase in air flow rate increased the overall recovery, as expected. Also, the fast floating nature of coarse particles is evident in the short flotation times used to recover most of the 150 to 300 μm feed material.

However, when deep froths were used, an increase in air flow rate had a negative effect on the overall flotation recovery (see Figure 3.19). This is probably the result of destabilisation of the froth phase at high air flow rates. This is supported by Ross (1991b) who floated three size fractions (-150 to 75 μm, 75 to 38 μm, and sub 38 μm) of a pyritic sulphide ore and phosphate ore using an equilibrium flotation cell. His results indicated an increase in drainage rate of the (-150 to 75 μm) fraction of the ore with an increase in air flow rate. However, the water drainage decreased with an increase in air flow rate. The implications of the observed effect of air flow rate on froth performance is discussed in the next section.

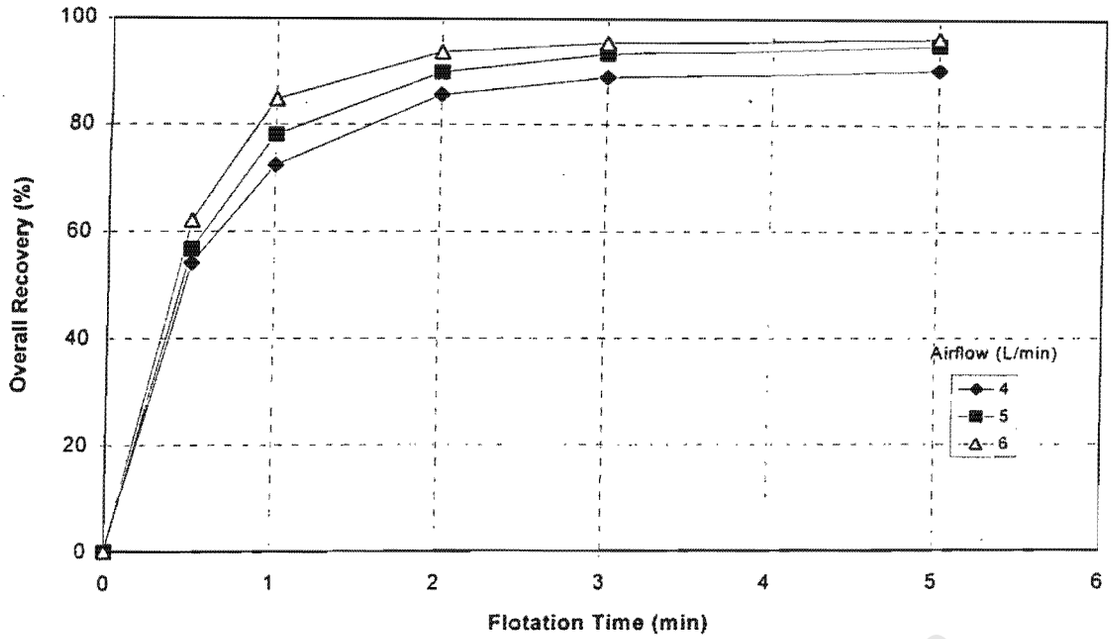

Figure 3.17 Effect of air flow rate on the overall flotation recovery for the tests carried out in a batch cell using the nominally 75% passing 106 μm size class. Recoveries obtained at shallow froth height

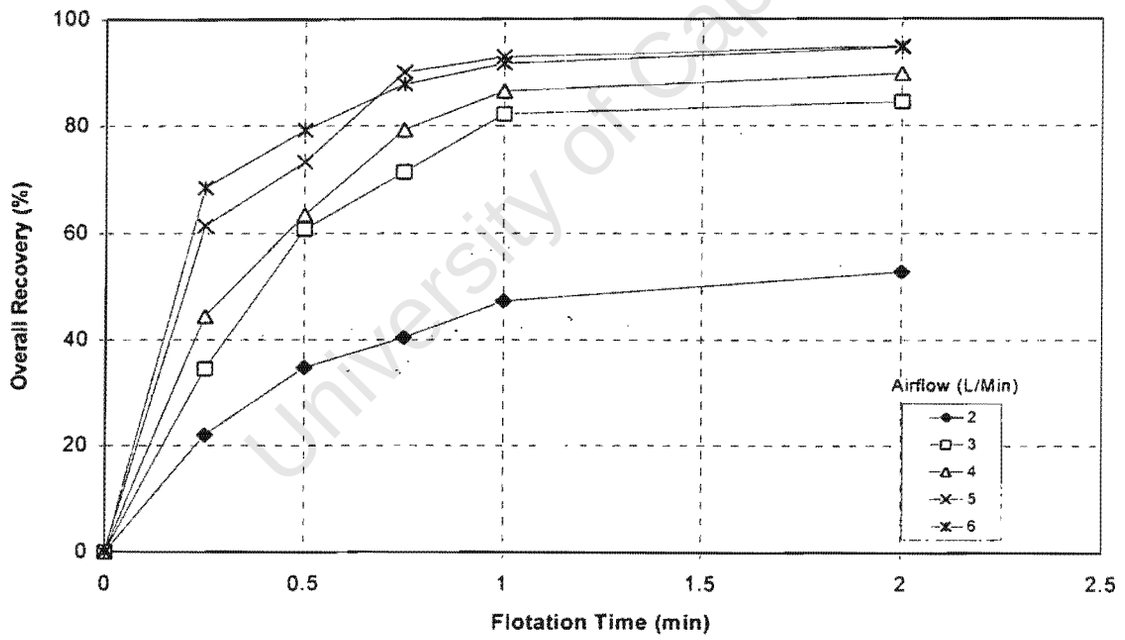

Figure 3.18 Effect of air flow rate on the overall flotation recovery for the tests carried out in a batch cell using the 150 to 300 μm size class at a froth height of 2.5 cm

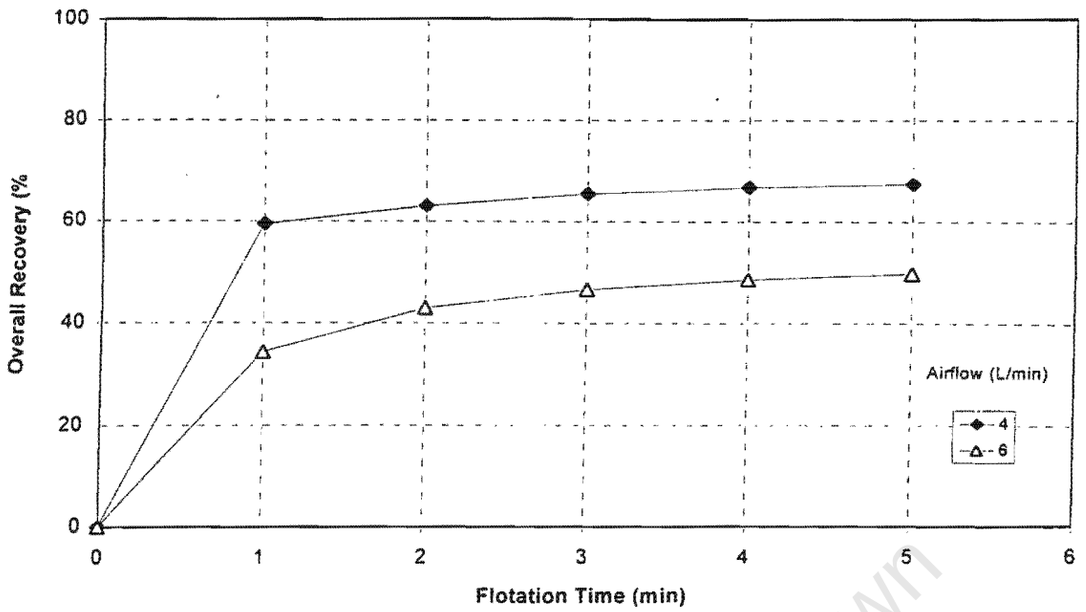

Figure 3.19 **Effect of air flow rate on the overall flotation recovery for the tests carried out in a batch cell using the nominally 75% passing 106 μm size class. Recoveries obtained at a froth height of 4.5 cm**

To show the effect of air flow rate on flotation by size, three size fractions were chosen, viz. sub 10 μm, 45 to 75 μm and 106 to 225 μm. Plots of recovery of the chosen particle size classes versus flotation time, at different air flow rates, are shown in Figures 3.20, 3.21 and 3.22. Figure 3.20 shows the effect of air flow rate, at various froth depths, on the recovery of particles found in the coarse particle size range (106 to 225 μm). At shallow froths, increase in air flow rate leads to an increase in recovery of these particles. This is consistent with what was observed for the recovery of the bulk mass into the concentrate (see Figure 3.17). At intermediate froth levels, an increase in air flow rate lead to a decrease in recovery. For the tests conducted at low and high air flow rates, in this case 4 and 6 ℓ/min, respectively, under deep froths conditions, the results showed a drop in the overall recovery of the particles found in this particle size range. However, for the tests conducted at an air flow rate of 5 ℓ/min, with deep froths, the recovery of these particles was high. This suggests that, under these conditions, the optimum air flow rate was at 5 ℓ/min. By analyzing data in this manner, however, it is not possible to know whether the observed optimum flotation performance at an air flow rate of 5 ℓ/min is due to the influence of the improved performance within the froth phase or due to improved performance within the pulp phase. This can only be achieved if the influence of the froth phase is decoupled from that of the pulp phase on flotation.

Figure 3.21 shows the effect of air flow rate on the recovery of the particles found in the fine particle size range (sub 10 μm). At shallow froths, no significant differences were observed

between the recovery versus flotation time curves obtained at various air flow rates, suggesting high degree of entrainment at all gas rates. At intermediate froth levels, the recovery of the fines was high at an air flow rate of 6 ℓ/min, suggesting that entrainment was probably reduced, to some extent, at lower air rates. For deep froths, however, an increase in air flow rate resulted in low recovery of the particles found in this size class.

To indicate the effect of air flow rate on the behaviour of the "truly" floating particles, a recovery-time curve of the 45 to 75 μm fraction at three different air flow rates was chosen. This is shown in Figure 3.22. It can be seen in this figure that an increase in recovery with an increase in air flow rate was observed at shallow and intermediate froth levels. For deep froths, however, low recovery of the particles found in this particle size range was observed at an air flow rate of 6 ℓ/min when compared to the recovery of these particles at an air flow rate of 4 and 5 ℓ/min. This suggests that particles originally attached to bubbles are probably detached. It is strongly believed that the possible detachment of these truly floating particles is probably due to bubble coalescence. Bubble coalescence is usually a consequence of high drainage rate of water between bubbles, especially when deep froths are employed. The following section discusses the results obtained when wash water was added into the froth.

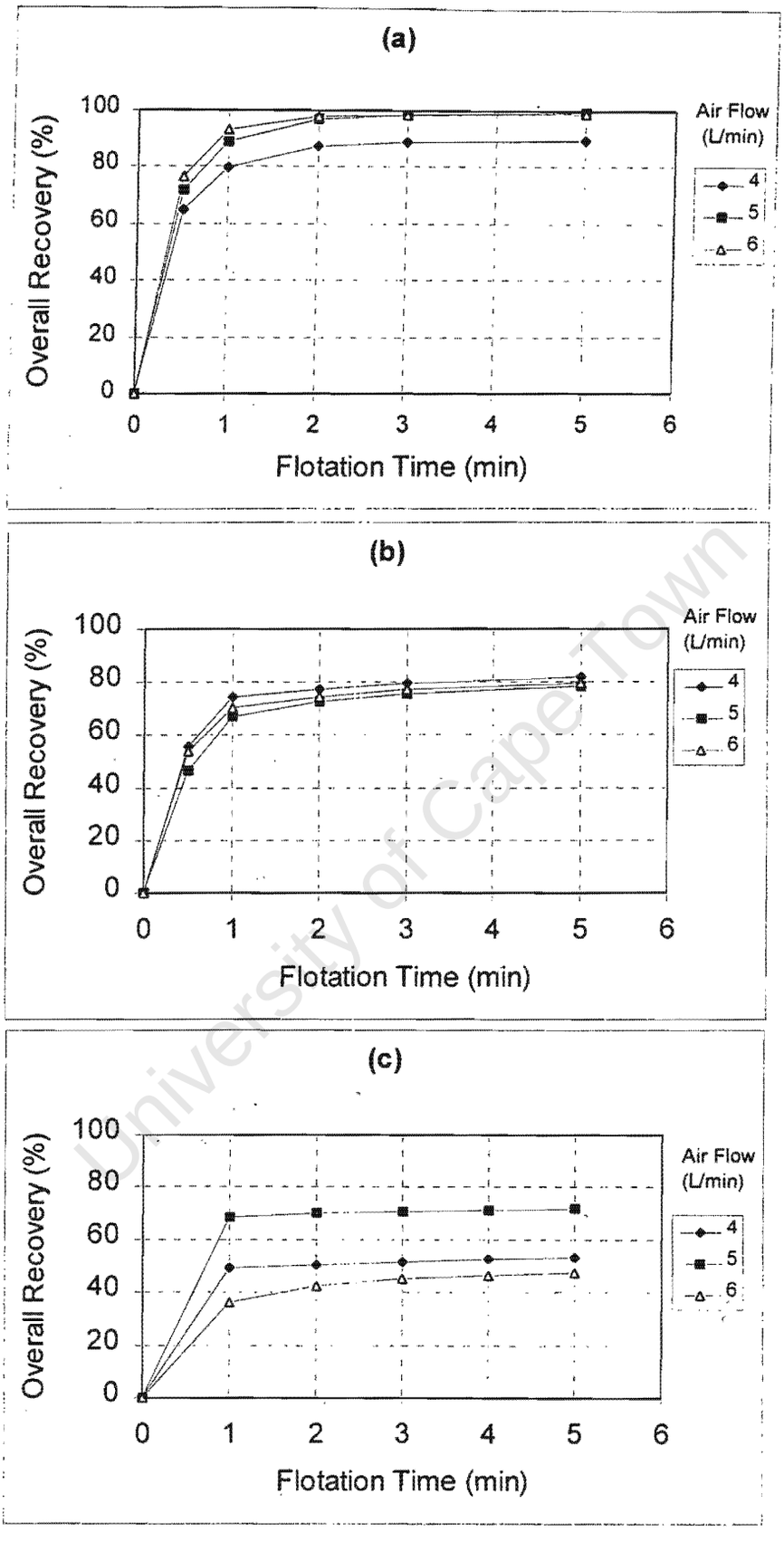

Figure 3.20 **Effect of air flow rate on the recovery of the coarse particle size range (106 to 225 μm) at various froth depths. (a) shallow froth level (0.5 cm); (b) intermediate froth level; (c) deep froth level (4.5 cm)**

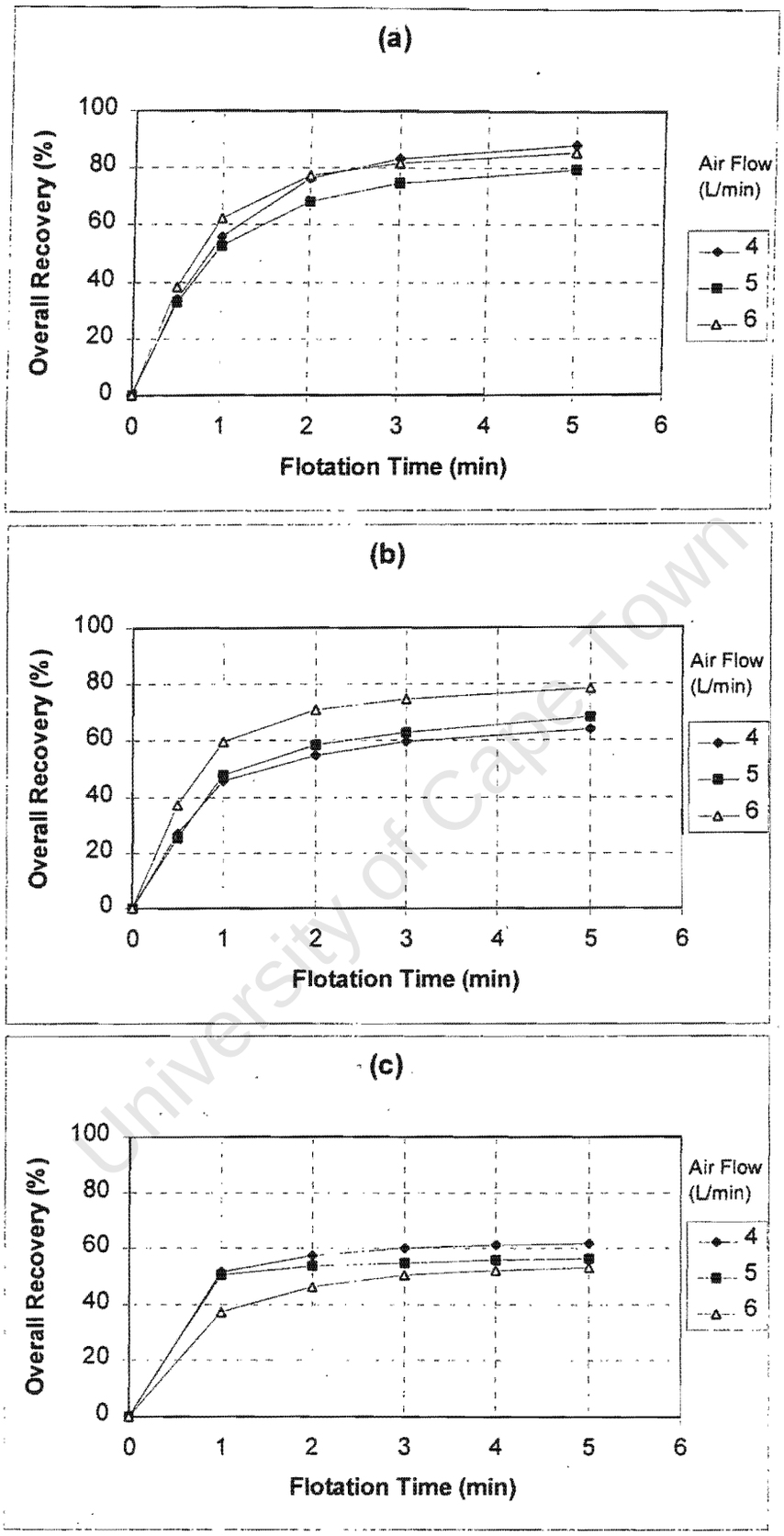

Figure 3.21 Effect of air flow rate on the recovery of the fines (sub 10 μm). (a) shallow froth level (0.5 cm); (b) intermediate froth level; (c) deep froth level (4.5 cm)

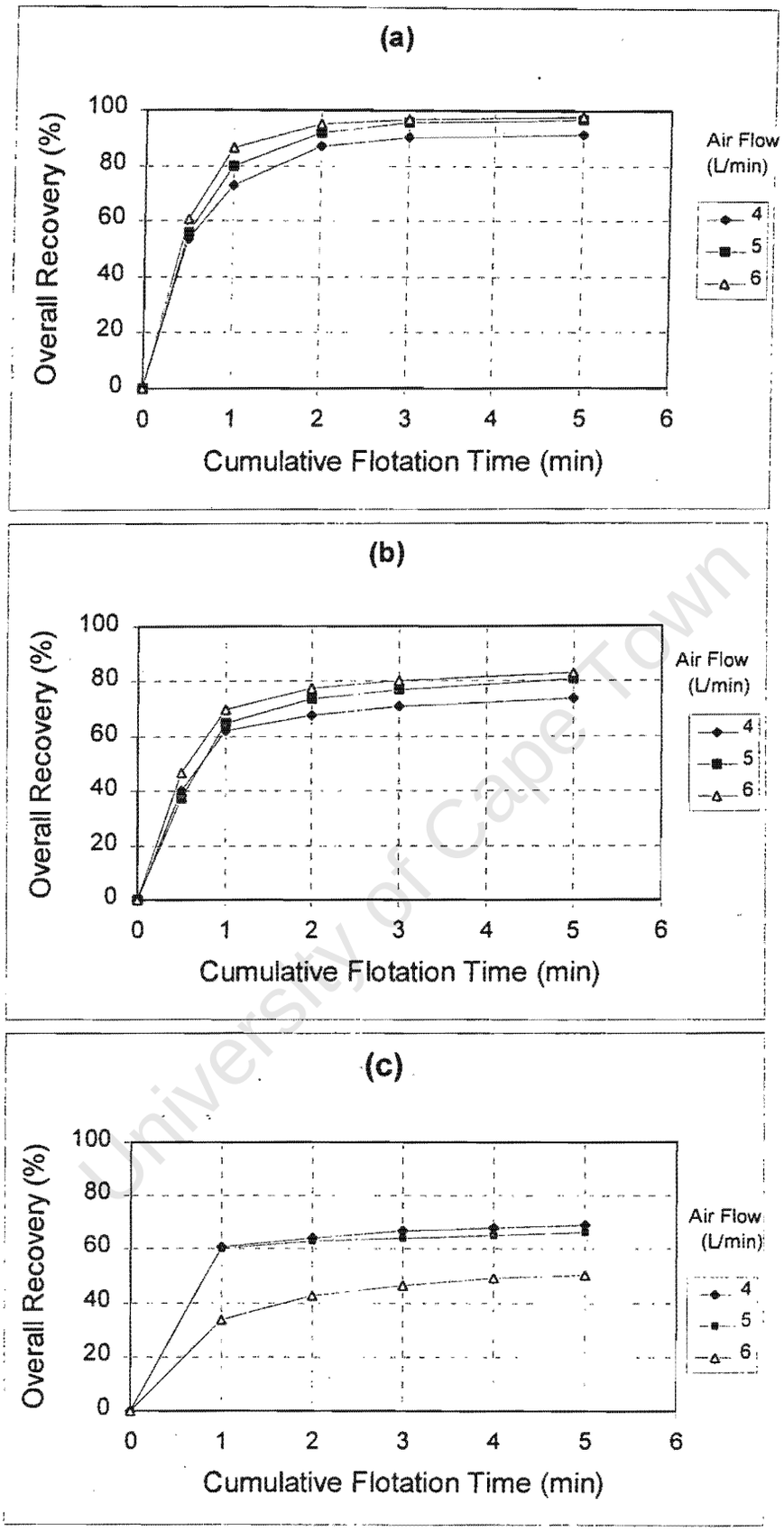

Figure 3.22 **Recovery-time curve of the 45 to 75 μm fraction at three different air flow rates. (a) shallow froth level (0.5 cm); (b) intermediate froth level; (c) deep froth level (4.5 cm)**

3.2.1.5 Effect of wash water

In the previous sections, it was shown that there is a significant drop in the recovery of particles for the flotation tests conducted with deep froths. It was also shown that this drop in the recovery of particles in these tests, increases with an increase in air flow rate. In addition, it was observed that an increase in air flow rate, in flotation tests conducted with deep froths, lead to a reduction in water recovery. Flotation tests conducted whilst adding wash water, where it is expected that the drainage rate of water would be high, are reported and discussed below.

Figure 3.23 shows the recovery-time curves obtained from the batch tests conducted whilst adding wash water. It shows that an increase in air flow rate resulted in an increase in the initial recovery of the bulk mass into the concentrate. For the high air flow rate (8 ℓ/min), however, the recovery decreased toward the end of the flotation test. Again, this can probably be ascribed to a decrease in froth stability toward the end of the flotation test when this air flow rate was used.

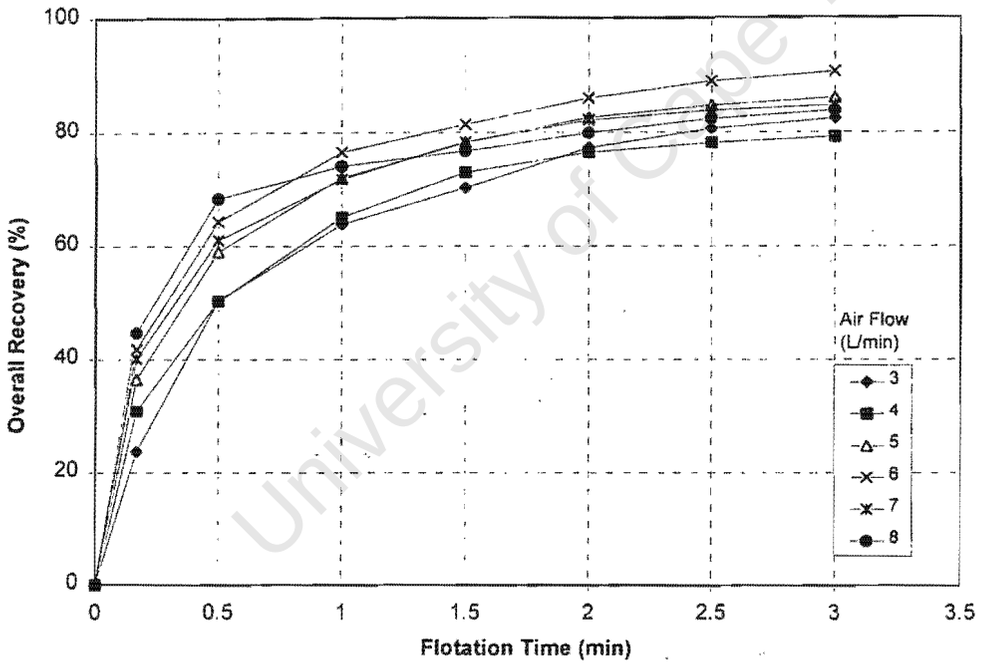

Figure 3.23 Recovery-time curves obtained from the batch tests conducted whilst adding wash water

To show the effect of air flow rate on flotation by size, three particle size fractions were again chosen, viz. sub 10 μm, 45 to 75 μm and 106 to 225 μm. At an air flow rate of 4 ℓ/min, the initial recovery of the particles found in the 106 to 225 μm size fraction was high when compared to the recovery of the particles found in the sub 10 μm and in the 45 to 75 μm size

fraction, with the sub 10 μm being the lowest (Fig. 3.24). Increase in air flow rate from 4 to 5 ℓ/min resulted in a decrease in recovery of the particles in the 106 to 225 μm size fraction to below the recovery of the particles in the sub 10 μm and the 45 to 75 μm size fractions. The same trend as above was observed for the results obtained at an air flow rate of 6 ℓ/min, except that the gap between the recovery of the coarse size fraction (106 to 225 μm) and the recovery of the other particles in the sub 10 μm and the 45 to 75 μm size fractions increased. These results suggest that a high drainage of the coarse particles existed when wash water was used.

Due to significant variation in froth depth during batch processing of the material used in these tests, it is very difficult to directly compare the results with batch data collected without the addition of wash water. However, the trends observed with regard to the effect of particle size and air flow rate on overall flotation recovery were somewhat very similar to the trends obtained from the analysis of the tests conducted without the addition of wash water.

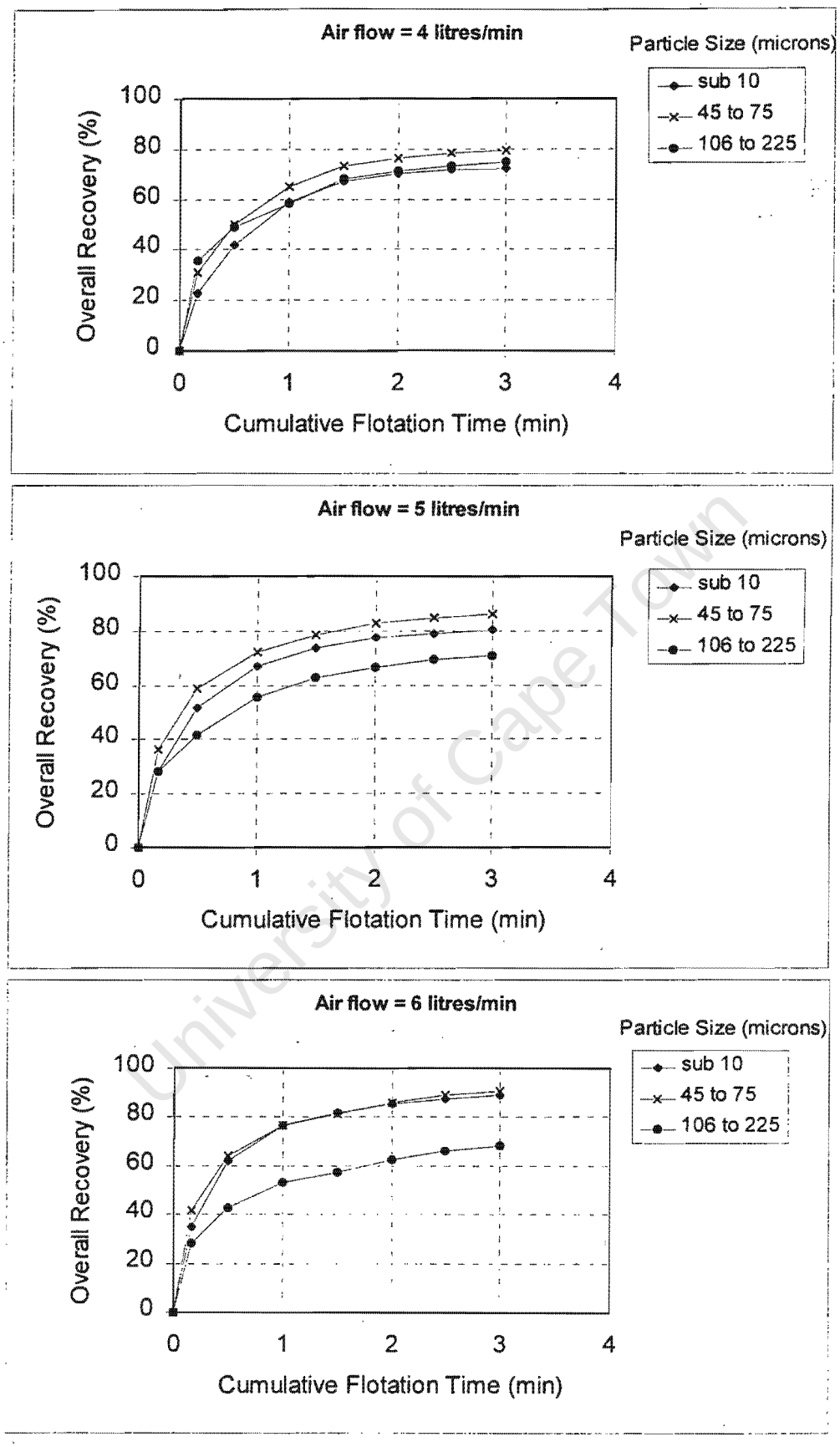

Figure 3.24 Recovery of the particles found in the 106 to 225 μm, sub 10 μm and 45 to 75 μm during batch flotation of quartz with wash water

3.2.1.6 Comparison of froth recovery in batch and continuous tests

In the previous sections it was shown that very little understanding of the process, especially the influence of the froth phase on flotation, is gained by comparing batch and continuous flotation performance on the basis of overall recovery obtained at various froth heights and air flow rates. This is because the influence of the individual flotation phases, viz. froth and pulp phases, on the overall flotation performance is not clear. This can only be achieved if the influence of the froth phase on flotation is decoupled from that of the pulp phase. To achieve this, the use of a froth recovery factor has been proposed in the literature. This section discusses results obtained when this factor was used to compare batch and continuous froth performances.

Figure 3.25 shows the relationship between the froth recovery and froth height for flotation tests carried out in a batch mode at different air flow rates. In this case, equation (1.21), shown below, was used to calculate the froth recovery factor. The froth recovery factor was defined as follows (Finch and Dobby, 1990):

$$R_f = \frac{k}{k_c} \tag{1.21}$$

where k is the overall (froth and pulp) flotation rate constant and k_c is the collection/pulp zone flotation rate constant.

The flotation rate constants, k and k_c, were calculated by fitting the first-order kinetic equations to mass recovery data. For batch data, the recovery equation used is as follows:

$$R = 1 - \exp(-k\,t) \tag{1.3}$$

The froth recovery values were calculated using the first two concentrates (1 minute interval). This was done because the froth recovery is expected to change with flotation time as the solids and frother concentrations within the froth phase decrease. In addition, the conditions at the very start of a batch test were thought to be more comparable to the conditions expected in a continuous flotation system.

For continuous data, the recovery was described by the following equation:

$$R = \frac{k\,\tau}{1+k\,\tau} \tag{1.7}$$

It appears, from Fig. 3.25, that the froth recovery decreases almost linearly with an increase in froth height. A similar behaviour of the froth recovery as a function of froth height was

observed when quartz data collected from a cell operated in batch mode (Mular and Musara, 1991) was used. Mular and Musara (1991) reported results showing a linear relationship between the flotation rate constant and froth height. Using equation (1.21), shown above, it follows that froth recovery factor decreased linearly with an increase in froth height.

In the case of the continuous tests, Figure 3.26 shows a curve that appears to be an exponential decrease in froth recovery with an increase in froth height.

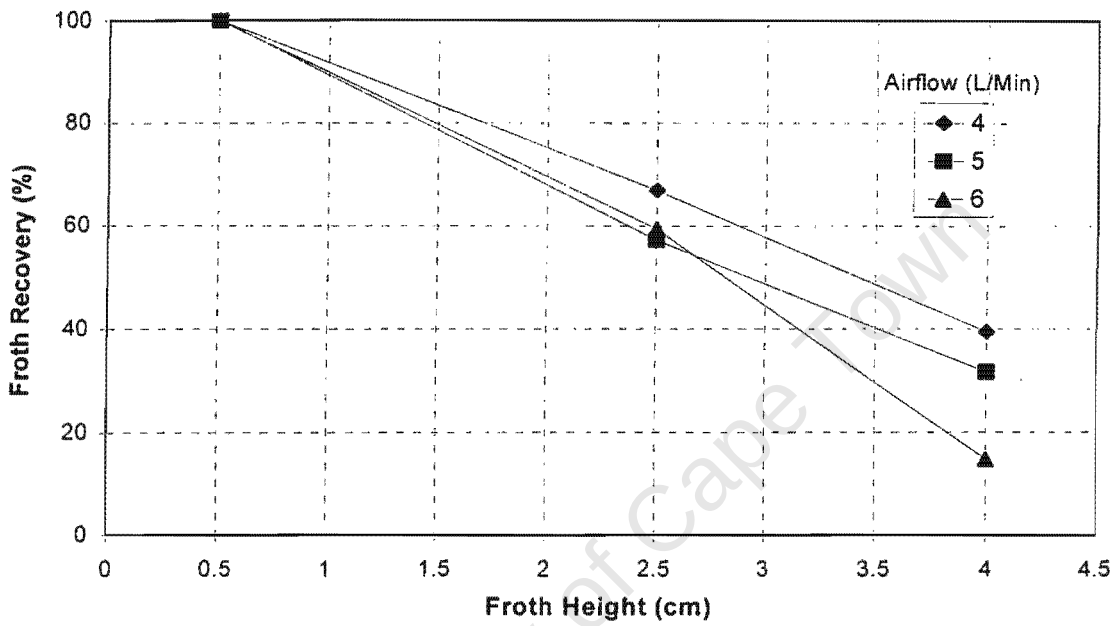

Figure 3.25 **Effect of froth height on froth recovery in batch tests floating the nominally 75% passing 106 microns fraction quartz mineral**

The froth recovery values obtained from continuous tests can also be presented as a function of froth retention time. This is shown in Figure 3.27 (assuming a gas hold-up in the froth of 95%), where an exponential decay of froth recovery with an increase in froth retention time was observed, as expected. Interestingly, an exponential decay curve was also observed in the batch case when froth recoveries were plotted against froth retention time (Fig. 3.28).

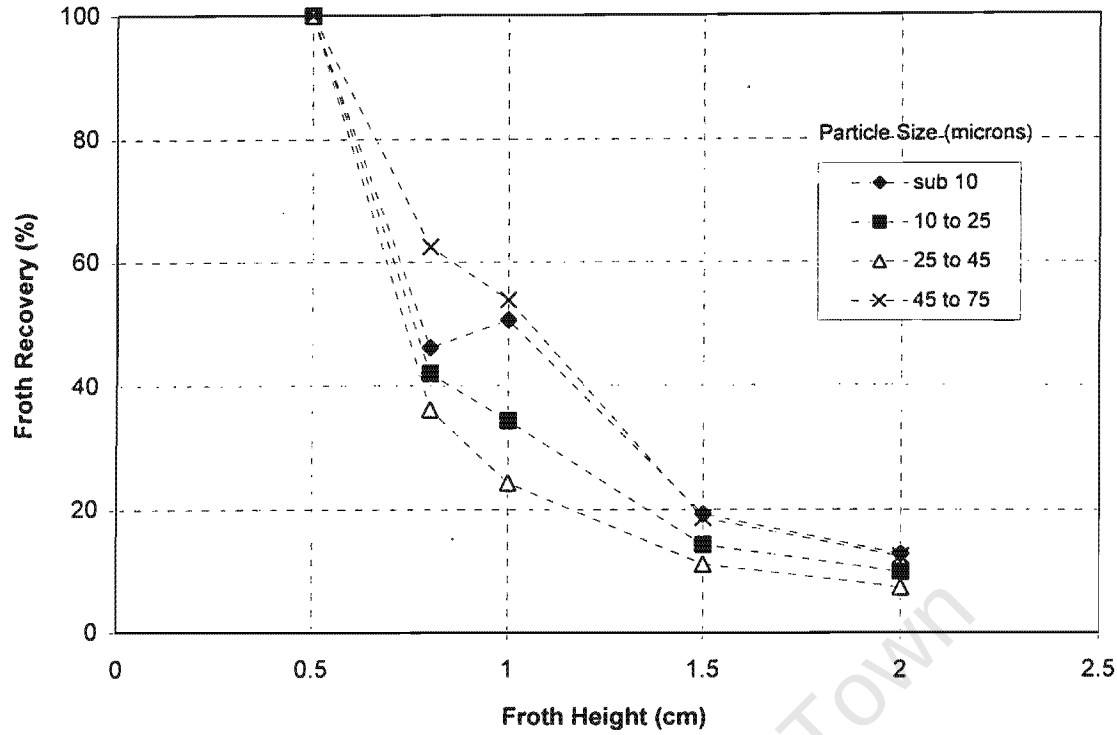

Figure 3.26 Effect of froth height on froth recovery in continuous tests floating the nominally 75% passing 106 microns fraction quartz mineral at an air flow rate of 4 ℓ/min

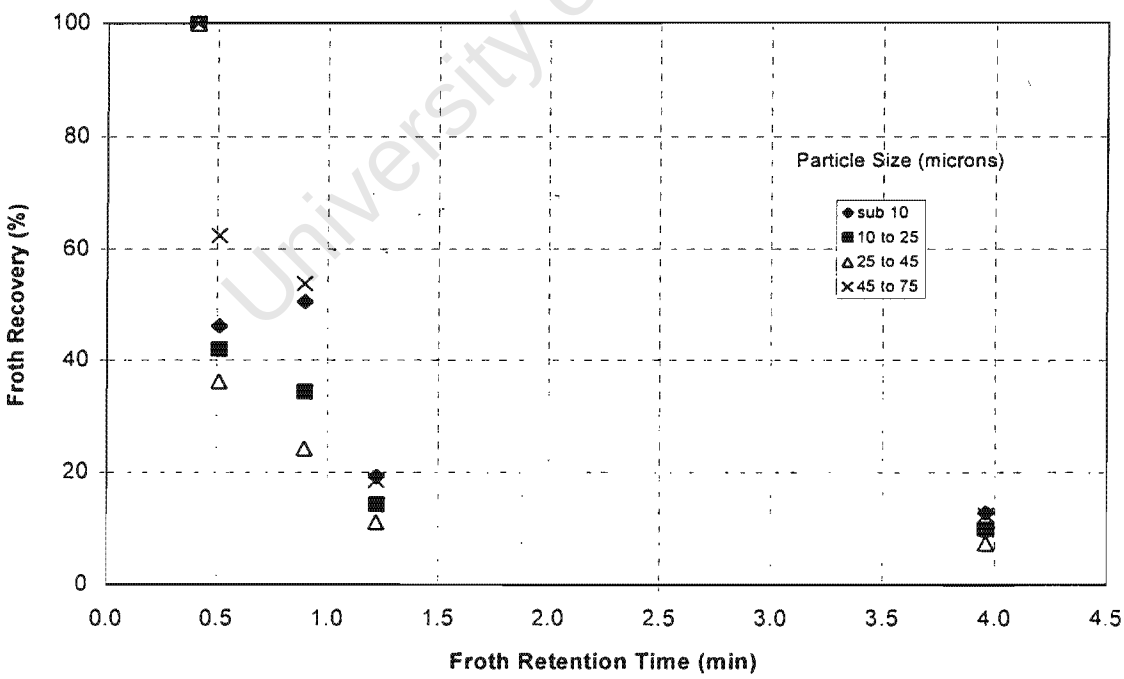

Figure 3.27 Effect of froth retention time on froth recovery in continuous tests during flotation of the nominally 75% passing 106 μm feed material at an air flow rate of 4 ℓ/min

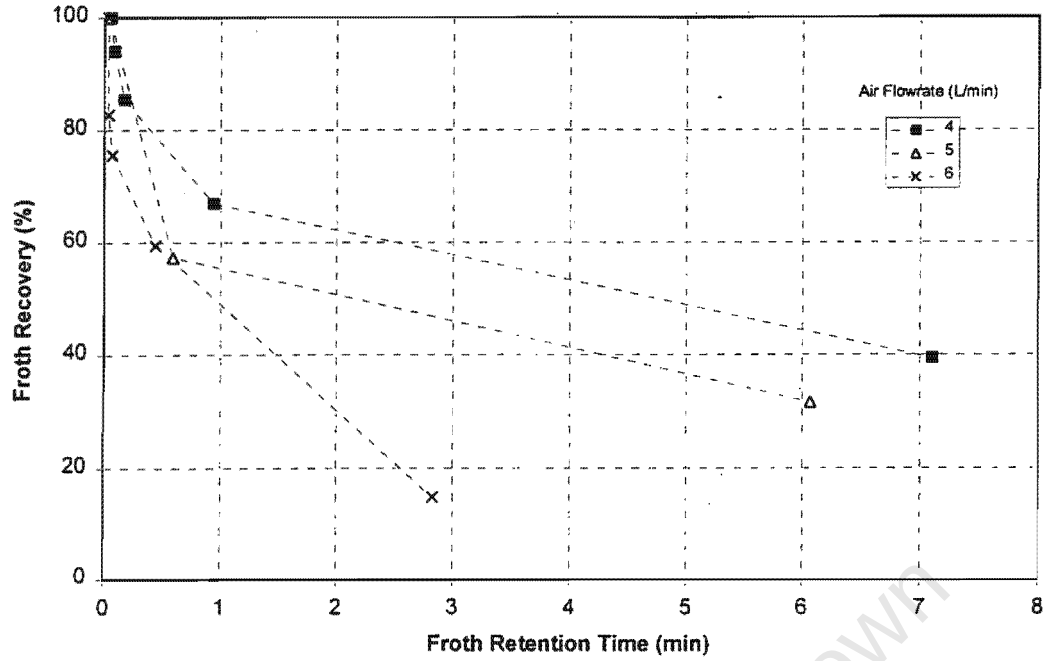

Figure 3.28 **Effect of froth retention time on froth recovery in a batch cell floating the nominally 75% passing 106 microns fraction quartz mineral**

While froth height is a very important design and control parameter in flotation, these results indicate that the use of the froth height to relate flotation performance from batch to continuous flotation cells is not useful and could lead to inaccurate scale-up procedures. This is due to the effect of substantial differences in operating variables used in cells of different sizes. The froth retention time, on the other hand, is a parameter which reflects a combination of all the major froth factors, and is moreover easily measured. The above results seem to indicate that the froth retention time is a good basis for comparing batch and continuous froth performances. However, consideration of the transfer rate constants, k_c and k, in the determination of the froth recovery factor is inadequate and can be misleading. For instance, in Figures 3.25, 3.26 and 3.27 the froth recovery values obtained at shallow froths are all 100 percent. This is because this approach of determining froth recovery uses the ratio of the flotation rate constant at any froth depth to the flotation rate constant obtained at shallow froths, which obviously limits the froth recovery to 100 percent at shallow froths. In froth systems with very unstable froths, the froth recovery is not expected to be 100 percent at shallow froths.

The approach discussed above obviously produces quantitative information about the effect of the operating variables on the froth phase. However, its use in comparing and scaling-up froth performance from batch to continuous flotation cells is limited. For very deep froths, the overall flotation rate constant is highly influenced by processes occurring within the froth phase. In addition, this parameter is influenced by froth removal technique in batch cells. Moreover, the poor understanding of the behaviour of the froth phase makes it difficult to

interpret the overall flotation rate constant in terms of the froth sub-processes. A more promising and practical approach is to describe froth recovery in terms of parameters that are not system specific. Nevertheless, the results obtained when using equation (1.21) in determining froth recovery are worth discussing further.

Figure 3.29 shows the influence of particle size on the froth recovery versus froth retention time relationship for quartz mineral floated in a batch cell. At shallow froths (i.e. low froth retention time), it appears as if the froth recovery is independent of particle size for the system studied here. However, as expected, when the froth retention time increases, fine particles have a relatively high probability of not returning to the pulp phase and consequently have higher froth recoveries. This can be associated with the low gravitational force exerted on fine particles and also because these particles can be easily retained in the bubble interstices. Conversely, coarse particles had low froth recoveries at high froth retention time. The above observations are supported by studies carried out in laboratory column cells (Falutsu and Dobby, 1989; Contini *et al*, 1988), which indicated a decrease in froth recovery with an increase in particle size. In the case of a continuous flotation system, the results were somewhat less conclusive, as shown in Fig. 3.27. The froth recovery values in the cell operated in a batch mode were generally greater than those obtained when the cell was operated continuously. This is probably due to rapid removal of the froth layer in the batch tests by scraping, which reduced the probability of particle drop back to the pulp phase.

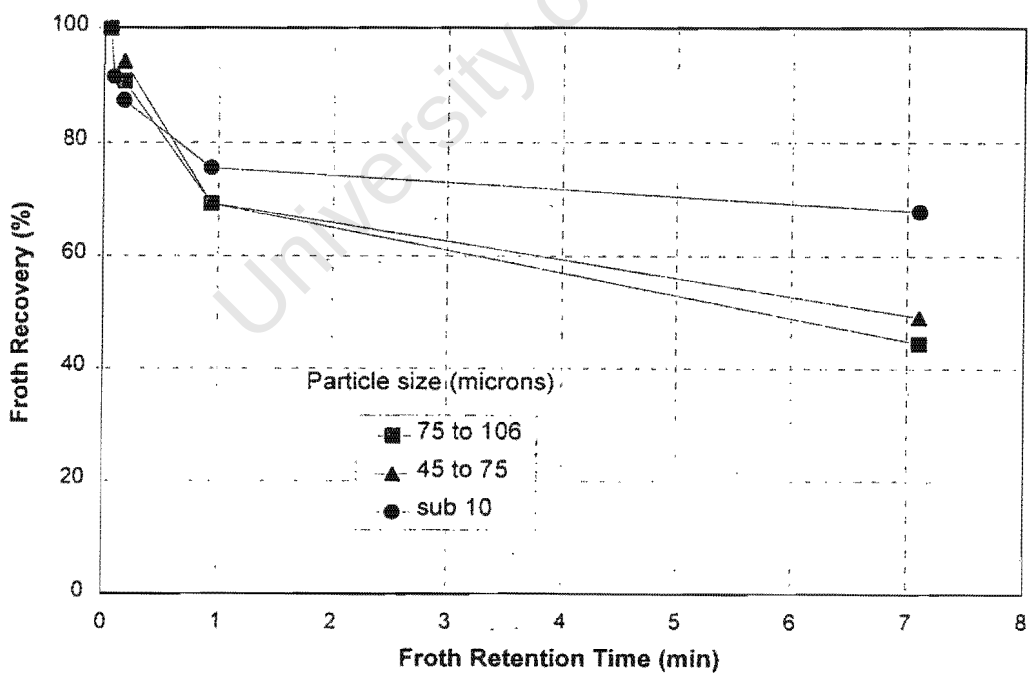

Figure 3.29 **Influence of particle size on the froth recovery versus froth retention time relationship for quartz mineral floated in a batch cell**

Figure 3.28 shows the relationship between froth recovery and froth retention time at three air flow rates. It indicates high froth recovery values at an air flow rate of 4 ℓ/min. Increasing air flow rate to 6 ℓ/min resulted in lower froth recovery values. One can conclude that increasing the air flow rate beyond an optimum level disturbs the froth phase. This is supported by Ross (1991b) who floated three size fractions (-150 to 75 μm, 75 to 38 μm, and sub 38 μm) of a pyritic sulphide ore and phosphate ore using an equilibrium flotation cell. His results indicated an increase in drainage rate of the (-150 to 75 μm) fraction of the ore with an increase in air flow rate. However, the water drainage decreased with an increase in air flow rate.

The above observations are in contrast to the results obtained by Cutting *et al* (1981) who also used an equilibrium flotation cell to float a sulphide ore. In this system, an increase in air flow rate resulted in an increase of froth recovery of arsenopyrite, sphalerite and pyrite minerals. The three minerals also behaved differently with pyrite having a high froth recovery and arsenopyrite the lowest. This may be associated with the strength of the hydrophobic forces bonding particles and bubbles.

In summary, the above results show that it is possible to relate batch froth performance to continuous froth if the factors influencing the froth phase in both systems are taken into account. The froth recovery values based on determining the overall and collection zone flotation rate constants in a batch cell, however, are not suitable for predicting froth recovery values in a continuous flotation cell. This is because froth recovery in batch systems changes with time. In addition, the overall and collection zone flotation rate constants are system specific (i.e. they depend on the cell geometry and the distance traveled by froth before reporting to the concentrate launder). It is proposed that a froth recovery model that takes into account the froth retention time, could well be the way in which to relate batch and continuous froth behaviour. The froth recovery model, equation (2.12), proposed in Chapter 2 can be used to describe froth performance in both batch and continuous flotation cells. The results obtained when the methodology for extracting froth recovery model parameters, also proposed in Chapter 2, was applied to quartz data are discussed next.

3.2.2 Modelling

3.2.2.1 Comparison of model predictions with experimental data

The approach of treating a batch test as comprising of a series of discrete continuous cells was used in deriving the required model parameters. To describe the overall flotation performance, equation (1.15), shown below, was used.

$$R_{o,i} = \frac{R_{c,i} R_{f,i}(1-R_w)+Ent_i R_w(1-R_{c,i})}{(1-R_w)(1-R_{c,i}+R_{c,i} R_{f,i})+Ent_i R_w(1-R_{c,i})} \quad (1.15)$$

where R_w is the recovery of water, Ent_i is the entrainment factor of particles in particle size class i, $R_{c,i}$ is the recovery of floatable particles found in particle size class i within the collection zone, and $R_{f,i}$ is the froth recovery factor of particles found in particle size class i.

In this equation the recovery of non-floating material by entrainment mechanism was described using equation (2.29), the collection zone recovery was described using equation (2.17b), and the proposed froth recovery model, equation (2.12), was used to describe the recovery of particles that arrive at the pulp-froth interface attached to bubbles. These equations are shown below:

$$Ent_i = \frac{1}{1+\omega_i FRT} / R_w \quad (2.29)$$

$$R_{c,i} = 1 - \exp(-P_i S_b \tau_c) \quad (2.17b)$$

$$R_{f(i)} = \exp(-\beta * FRT) + [1 - \exp(-\beta * FRT)] * [\frac{1}{1+\omega_i FRT}] \quad (2.12)$$

A detailed example showing how the parameters used in these equations were obtained is outlined in Appendix D. Figures 3.30a and 3.30b show how well these equations fit the data obtained from the batch tests (nominally 75% passing 106 μm) conducted in a 3.5 *l* flotation cell. It compares the experimental and predicted concentrate masses for the tests used in the modelling. The experimental data agree reasonably well with predicted concentrate masses. The plotted points had a correlation coefficient of 0.95. Parameters derived for this system are shown in Table 3.16. No significant differences were observed when equation (2.13) instead of equation (1.15) was used in describing the overall recovery performance. As such, all the results reported here are based on using equation (1.15). The derived parameters are now discussed.

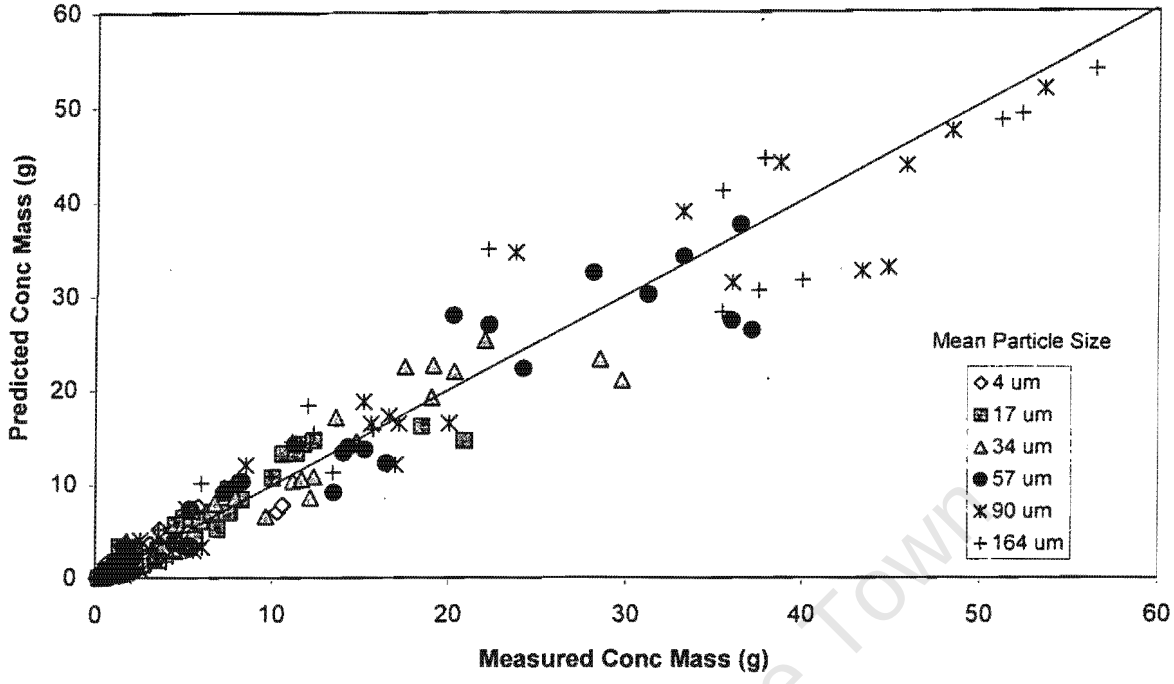

Figure 3.30a Batch tests experimental data plotted against predicted concentrate masses. Results of batch data obtained from floating the nominally 75% passing 106 μm fraction of the quartz mineral

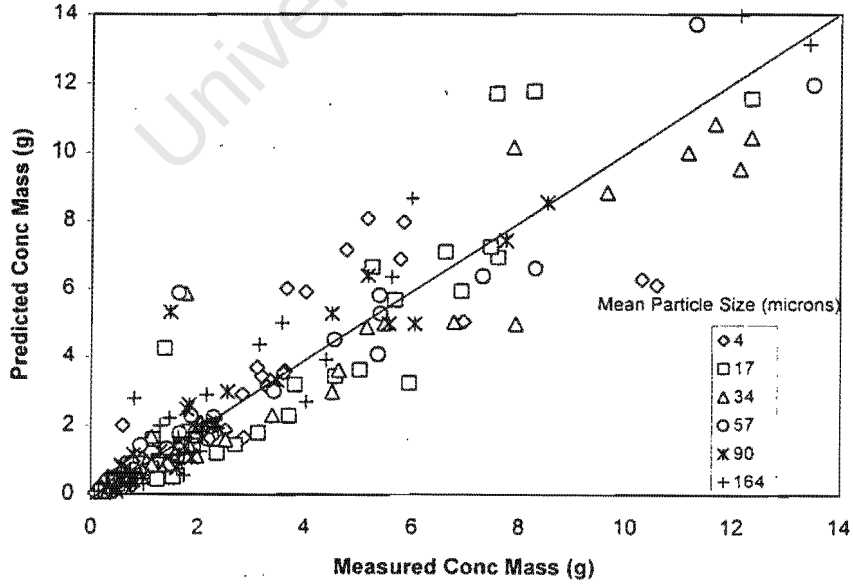

Figure 3.30b Batch tests experimental data plotted against predicted concentrate masses. Results of batch data obtained from floating the nominally 75% passing 106 μm fraction of the quartz mineral

Table 3.16 Froth and pulp phase parameters obtained from curve fitting

Size Range (μm)	Parameters		
	ω (1/min)	P	β
106 - 225	24.00	0.00181	2.80
75 - 106	11.25	0.00140	
45 - 75	7.68	0.00107	
25 - 45	5.05	0.00068	
10 - 25	3.89	0.00026	
sub 10	5.07	0.00024	

3.2.2.2 Derived parameters from curve fitting

(i) *Floatability, P*

Table 3.16 above shows the particle size dependency of the floatability parameter. Floatability was found to increase with an increase in particle size. This agrees well with the experimental results which showed that the flotation recovery increases with an increase in particle size. At very coarse particle sizes, however, the floatability parameter would be expected to be low. This is because of the effect of gravity on coarse particles.

(ii) *Froth stability parameter, β*

Equation (2.12) uses a parameter, β, which is believed to be related to froth stability. Any parameter associated with froth stability is expected to be influenced by the chemical environment, gas hold-up, percent solids and type of minerals within the froth phase. The conditions used for the flotation of quartz, however, tend to give rise to very stable froth. As such, the froth stability parameter was not allowed to vary (i.e. constrained) with any of the above variables. Allowing this parameter to vary with air flow rate during modelling did not provide any improvement in the fit to the experimental data in this study.

(iii) *Drainage parameter, ω*

The drainage parameter, ω, increased with an increase in particle size, except for very fine particle size class (Fig. 3.31). This can probably be attributed to the fact that the ultra-fine particles were recovered predominantly by entrainment. On this basis, a relatively higher

drainage of this class relative to the 10 to 25 μm class could well be considered a logical possibility.

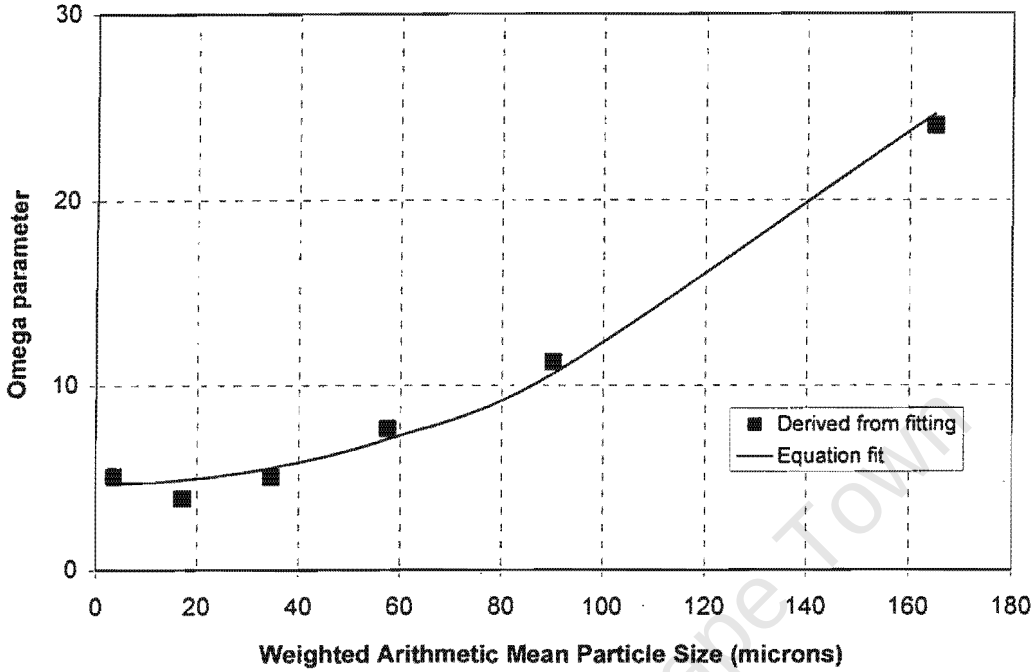

Figure 3.31 Effect of particle size on omega, ω

The relationship between ω and the mean particle size, d_p,was found to be well described by the following equation:

$$\omega_i = a + b * dp_i^2 \qquad (3.1)$$

In equation (3.1), the parameter, a, can be considered to represent the water drainage rate under the froth conditions (frother type and concentration, solids characteristics) arising in this study, while the parameter b represents a proportionality constant, expected to vary with mineral type, for particle drainage rate as a function of size under these froth conditions. If it is assumed that particles are settling predominantly via bubble Plateau borders, i.e., the intersections of the three bubble films, in which water is draining over a distance h at a uniform rate, a, and the particles settle freely over this distance, the b parameter could well be considered to be described by the Stokes' equation (Coulson and Richardson, 1988; Wills, 1997):

$$b = g\,(\rho_s - \rho_f)/18\,\eta\,h \qquad (3.2)$$

where g is the gravitational acceleration, ρ_s is the density of the solid, ρ_f is the density of the fluid and η is the fluid viscosity. In this context, η in equation (3.2) would represent an "apparent" viscosity of the fluid in the plateau borders, which would be expected to be related to factors such as solids concentration and solids characteristics in the froth, and the frother type and concentration.

According to Taggart (1945), free settling predominates when percent of solids is less than 15%(m/m) in well-dispersed systems. For the system studied here, the pulp density was less than 10%. Hence, Stokes' equation was chosen for use in describing the settling behaviour of particles. On consideration of equation (3.1), it was considered very likely that the water drainage rate parameter, a, would be directly related to the β parameter, as the rate at which water drains within the froth phase is a direct consequence of the rate at which bubbles coalesce. To test this hypothesis, equations (3.1) and (3.2) were incorporated into the proposed froth recovery model, and the new equation was refitted to the batch data set. The refined model was fitted to the data in two forms. In the first case, the fit was performed with a and β as independent parameters, while in the second case, a was assumed to be equal to β. These results are presented in Table 3.17. It can be seen that setting a equal to β did not significantly affect the model fit that was obtained. However, when the froth recovery equation is used in this form, the number of model fit parameters is reduced. On this basis, it was decided to adopt this form for the recovery equation in subsequent data analysis.

The modified R_f equation is therefore given by the following expression:

$$R_{f(i)} = \exp(-\beta * FRT) + [1 - \exp(-\beta * FRT)] * \left[\frac{1}{1+(\beta + \frac{g(\rho_s - \rho_f)}{18\,\eta\,h} dp_{(i)}^{\,2})* FRT}\right] \quad (3.3)$$

Table 3.17 Results from fitting froth recovery models

Froth Recovery Equation	No of parameters	Mean Error per data point
Original equation (2.12)	7	0.879
Refined equation, a and b independent	3	0.880
Refined equation, a = b	2	0.883

3.2.2.3 Modelling results using a modified R_f equation

The model fit with respect to the batch data using equation (3.3) is shown in Fig. 3.32, on a sized basis. It can be seen that the model was able to describe the performance of the batch cell reasonably well over a wide range of operating conditions and particle sizes. The derived β and η parameters were found to be 2.90 (1/min) and 3.02×10^{-3} (N.s/m^2), respectively. It is interesting to note that the derived apparent viscosity of the concentrate slurry is higher than that of water (8.5×10^{-4} N.s/m^2), but of the same order of magnitude, as would be expected. This is obviously encouraging with respect to the assumptions adopted in the development of equation (3.3). However, the reader should bear in mind that the derived apparent viscosity represents an average value, as conditions in a batch test froth vary with flotation time.

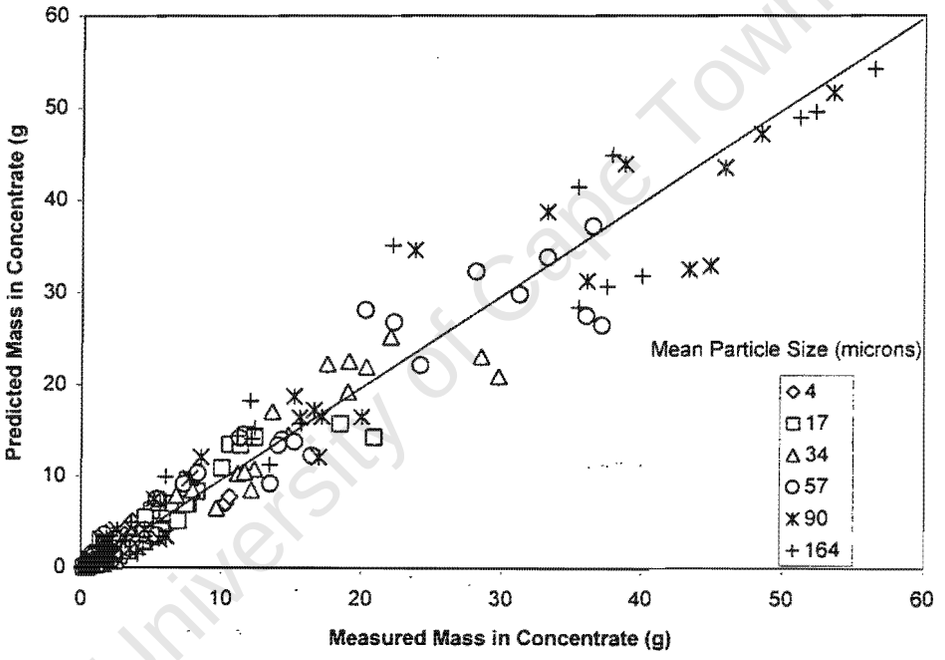

Figure 3.32 Model fit with respect to the batch data using modified R_f equation

3.2.2.4 Error analysis

Due to the empirical approach used in this work and the errors associated with experimental data points, an estimate of the confidence limits on the derived parameters was performed using a Monte Carlo error estimation technique. The purpose of performing this exercise was to test the robustness of the modelling methodology and froth recovery model. Five types of Monte Carlo methods are most commonly encountered. Firstly, the classical Monte Carlo method involves drawing samples from a probability distribution to obtain thermodynamic properties, molecular structures and rate coefficients. Secondly, the quantum Monte Carlo

method, often referred to as random walks method, which is typically used to compute quantum-mechanical energies and wave functions. Next is the path-integral quantum Monte Carlo method which is typically used to estimate starting points. There is also simulation Monte Carlo method which is typically used to generate initial conditions for trajectory simulations. Lastly, there is the volumetric Monte Carlo method which randomly generate numbers. The latter Monte Carlo method is the one used in this study. This was achieved by running a Monte Carlo program (Appendix E) in Visual basic within an Excel spreadsheet. A Monte Carlo simulation was performed by allowing the experimental data to vary by 10% deviation. This was run simultaneously with Solver in Excel to minimise the sum of error-squared, generating a set of P, for the chosen size classes, β and η parameters. One thousand sets of these parameters were generated and used to calculate the standard deviation, s, and confidence limits of n number of predicted parameters. Confidence limits were calculated using a method described by Napier-Munn (1995). In this method the true value of the mean value of a derived parameter, say x, is said to lie between $((x - zs/\sqrt{n})$ and $((x + zs/\sqrt{n})$, with a degree of confidence, z, given by the probability level (Spiegel, 1992). The results are shown in Table 3.18.

It can be seen in Table 3.18 that the confidence limits for all parameters are significantly lower (95% confident) than the average values. This indicates a high level of certainty in the derived parameters for the system studied here. It also shows robustness (no major variation in derived parameters based on slight variation in starting values) in parameters. Figures 3.33 and 3.34 show the frequency distributions of the predicted froth parameters. Although these figures show that there are parameters that were off the mean range, the distribution of most parameters appeared to be normally distributed. This suggests that the approach used in deriving the parameters for this system is reasonably accurate.

Table 3.18 Monte Carlo results

Parameters			
Floatability (P)		Froth stability (1/min) (β)	Viscosity (N.s/m^2) (η)
Particle Size (microns)	P		
Sub 10	4.86 E-7 +/- 3.90 E-7	2.94 +/- 0.0129	0.00284 +/- 4.25 E-5
10 to 25	1.44E--4 +/- 6.25 E-6		
25 to 45	6.26 E-4 +/- 3.88 E-6		
45 to 75	10.33 E-4 +/- 3.32 E-6		
75 to 106	13.95 E-4 +/- 3.66 E-6		
106 to 225	18.66 E-4 +/- 5.05 E-6		

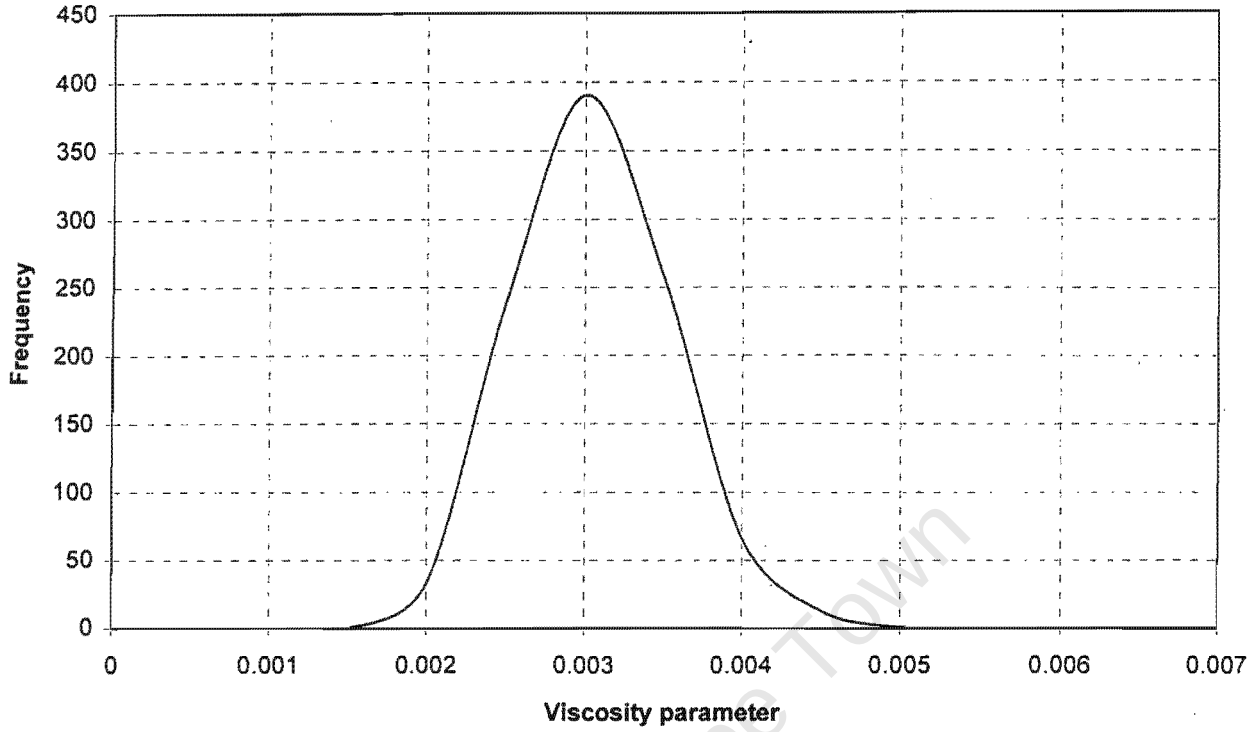

Figure 3.33 Frequency distribution of derived parameter, η, using Monte Carlo

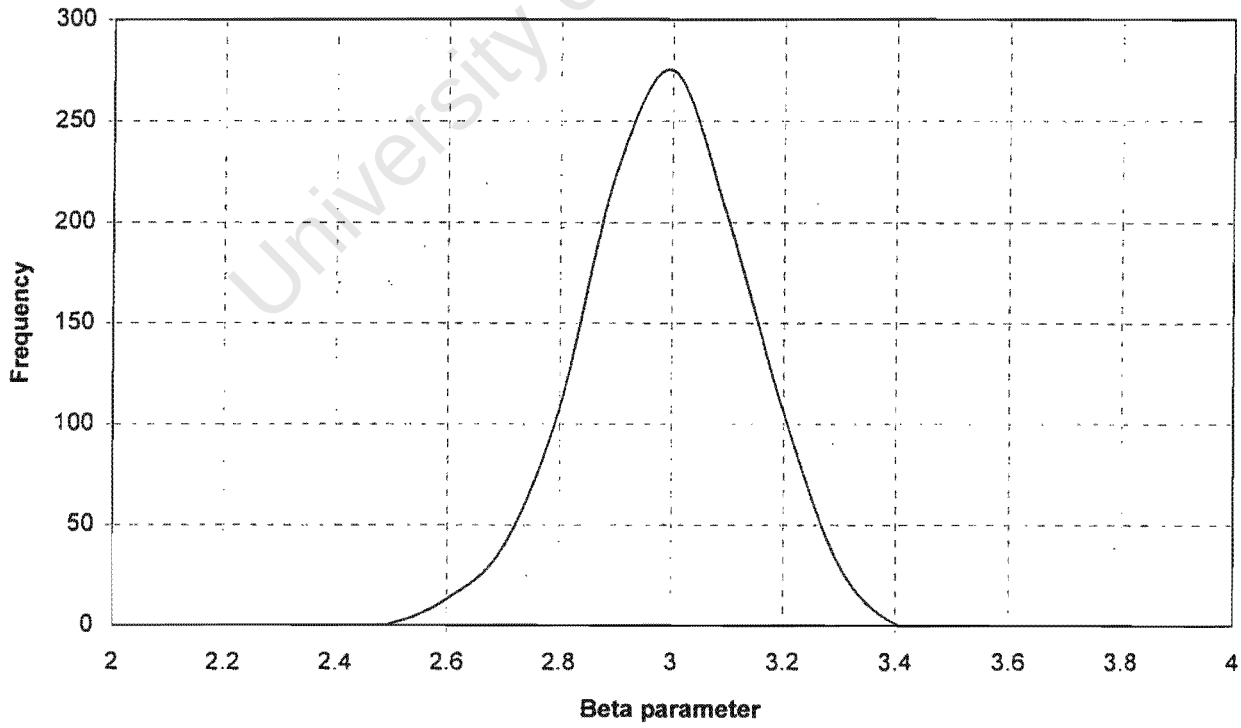

Figure 3.34 Frequency distribution of derived parameter, β, using Monte Carlo

3.2.2.5 Prediction of batch flotation performance using Monte Carlo results

The model parameters derived from the Monte Carlo simulation were used to predict batch flotation performance. The results are presented in the form of recovery versus time curves. Fig. 3.35 shows the results obtained for the batch tests conducted using an air flow rate of 4 ℓ/min at various froth depths. It can be seen in this figure that the predicted bulk recovery of quartz mineral at shallow and intermediate froth levels correlates reasonably well to the measured recovery. Similar trends were observed for the tests carried out using 5 and 6 ℓ/min air flow rates at shallow and intermediate froth levels (see Figure 3.36 and 3.37). For the test carried out with deep froth level at an air flow rate of 4 ℓ/min, the predicted recoveries were below those recoveries obtained experimentally, suggesting a possible under-prediction of the models. A good correlation was observed between the predicted and measured recoveries obtained for the test conducted with deep froths at an air flow rate of 5 ℓ/min. For the batch tests carried out with deep froth level, at an air flow rate of 6 ℓ/min, the predicted recoveries were higher than those recoveries obtained experimentally, suggesting a possible over-prediction of flotation performance at high gas rates. This can be ascribed mainly to the possible inaccurate prediction of the froth parameters. The parameters used in the froth recovery model represent average values for the system studied here. For instance, the froth stability parameter, β, is assumed not to vary by stage or air flow rate in a batch flotation cell.

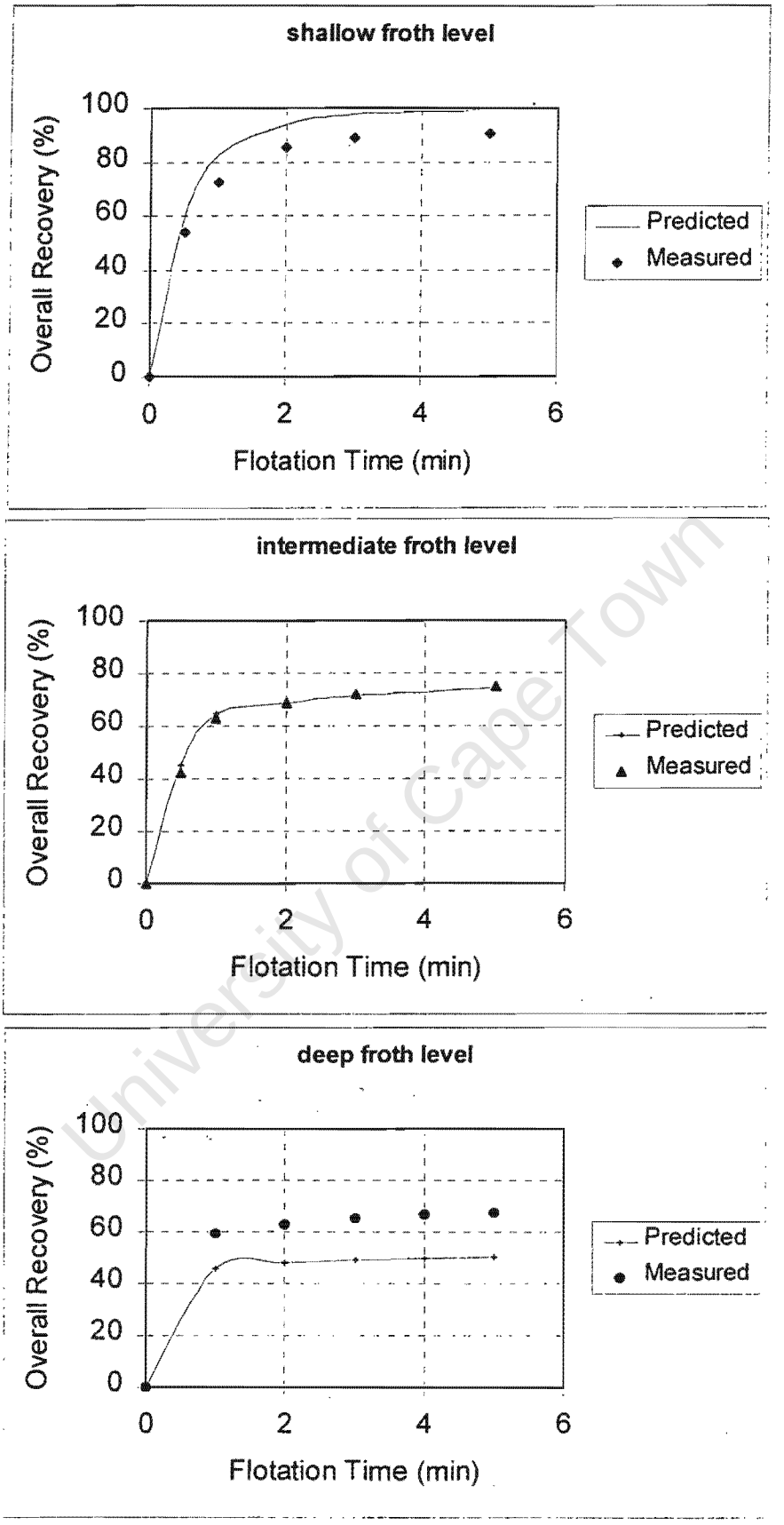

Figure 3.35 **Comparison between predicted and measured batch flotation recovery versus flotation time for tests conducted using an air flow rate of 4 ℓ/min**

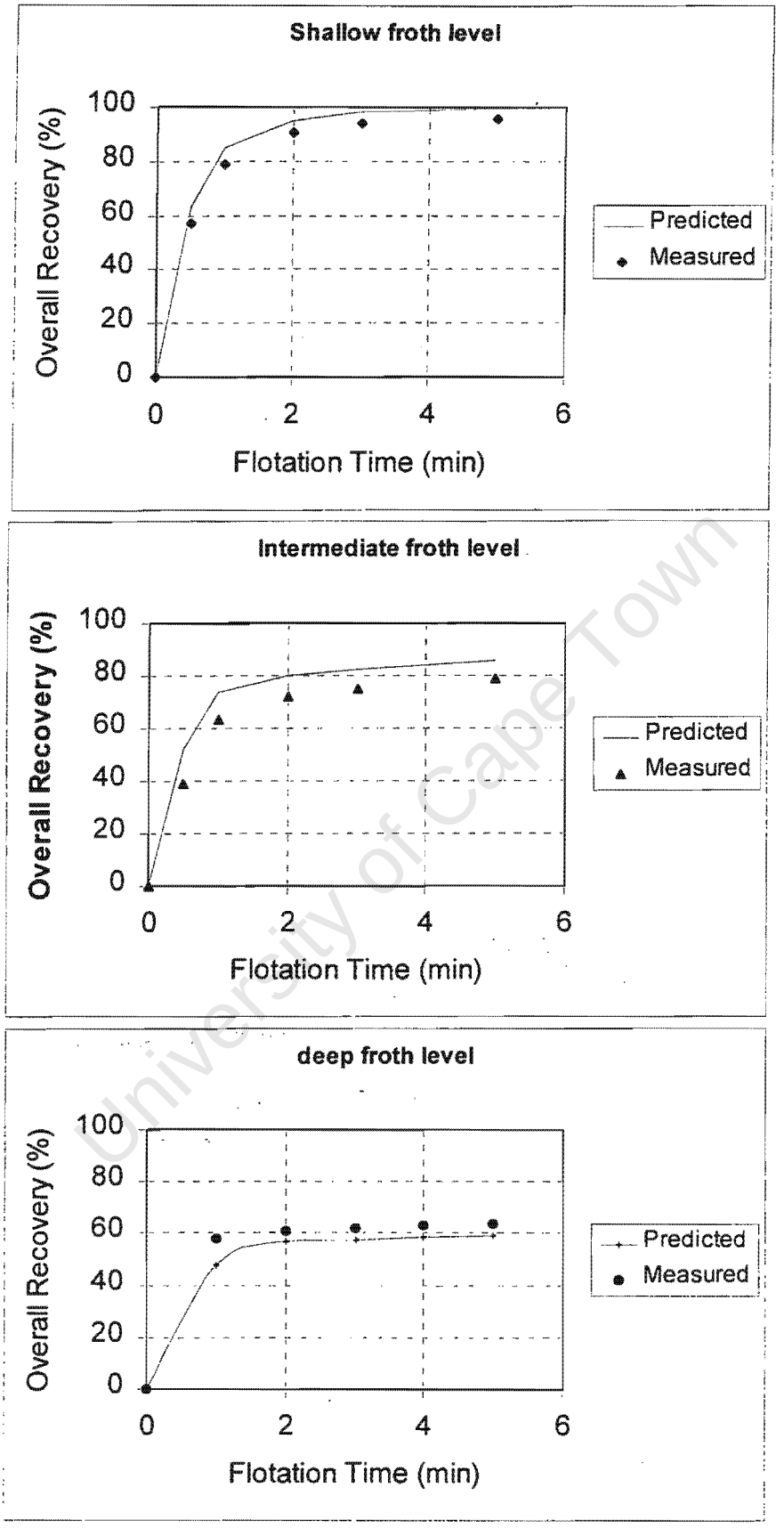

Figure 3.36 Comparison between predicted and measured batch flotation recovery versus flotation time for tests conducted using an air flow rate of 5 ℓ/min

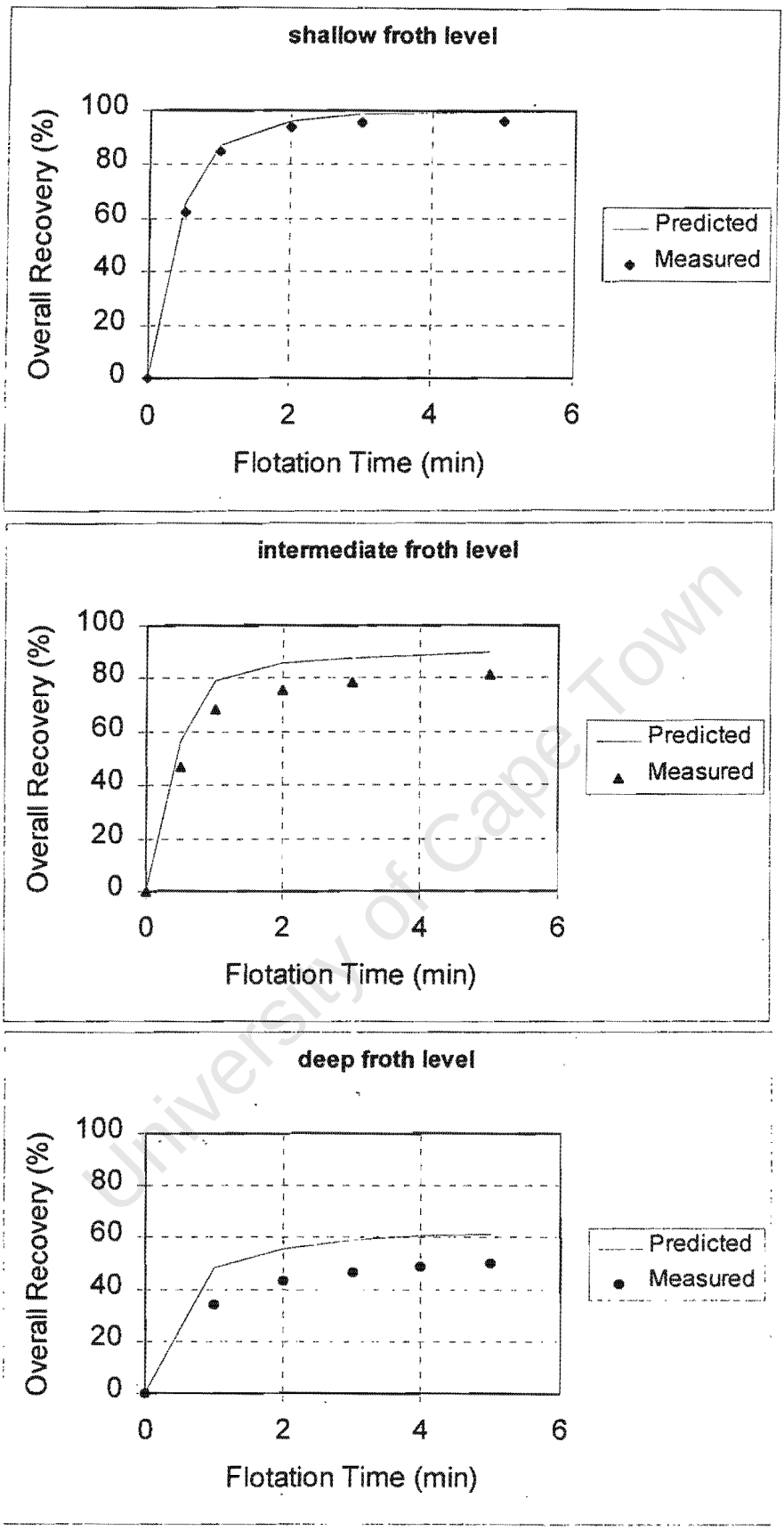

Figure 3.37 **Comparison between predicted and measured batch flotation recovery versus flotation time for tests conducted using an air flow rate of 6 ℓ/min**

To show how well can the proposed models be used in predicting the influence of the operating parameters, such as particle size and air flow rate, on flotation, results obtained whilst floating quartz mineral under intermediate froths conditions were chosen. Figure 3.38a shows the predicted influence of particle size on recovery for a batch test conducted using an air flow rate of 4 ℓ/min. The predicted results obtained compare very well with measured recoveries (see Figures 3.38a and 3.38b). Figure 3.39a shows the predicted influence of the air flow rate on recovery of solids in a batch test. It shows that an increase in air flow rate lead to an increase in recovery, as observed from the experimental data (Fig 3.39b). This suggests that the proposed flotation modeling equations can be used to describe batch data. In addition, the above results suggest that the proposed methodology for extracting model parameters from batch data is reasonable accurate. For deep froths, however, more detailed equations are required.

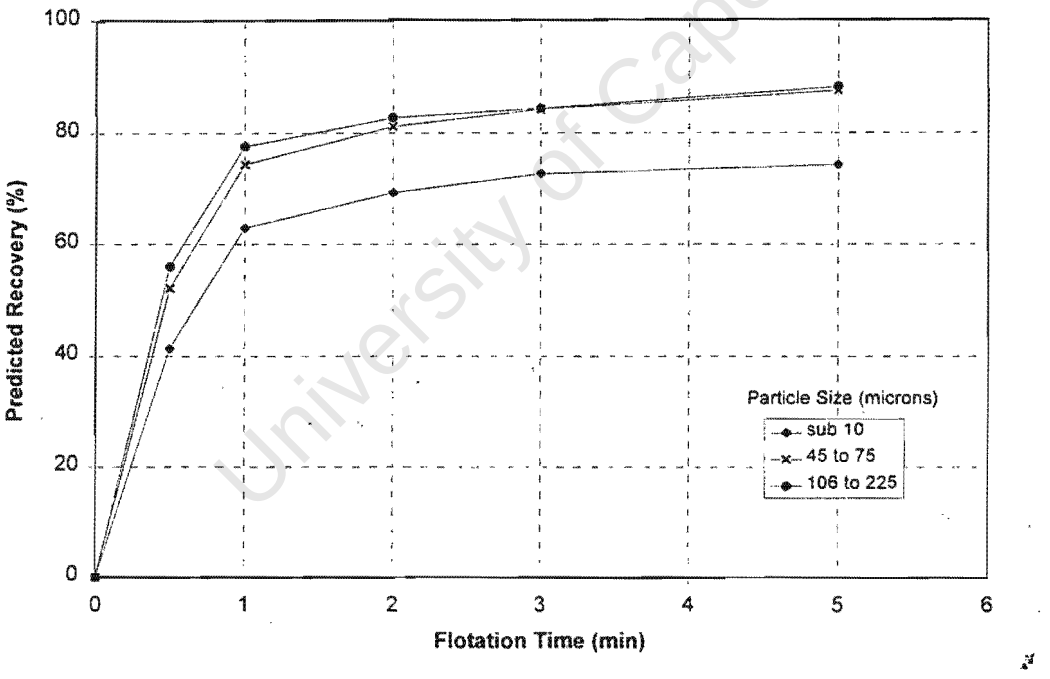

Figure 3.38a Predicted batch flotation recovery, by size, versus flotation time for a test conducted at an air flow rate of 4 ℓ/min

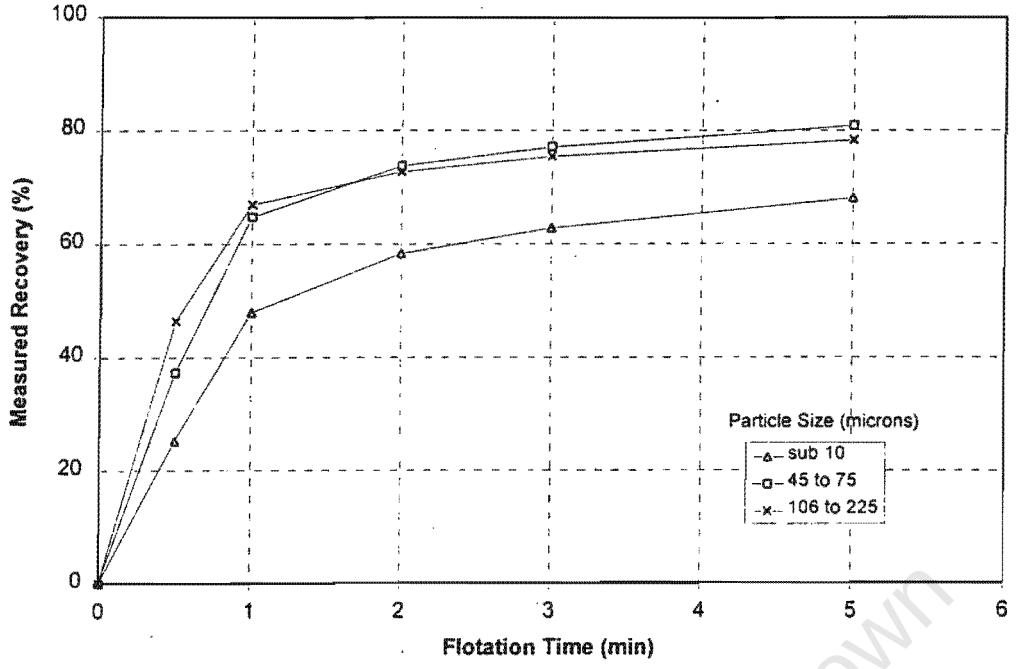

Figure 3.38b Measured batch flotation recovery, by size, versus flotation time for a test conducted at an air flow rate of 4 ℓ/min

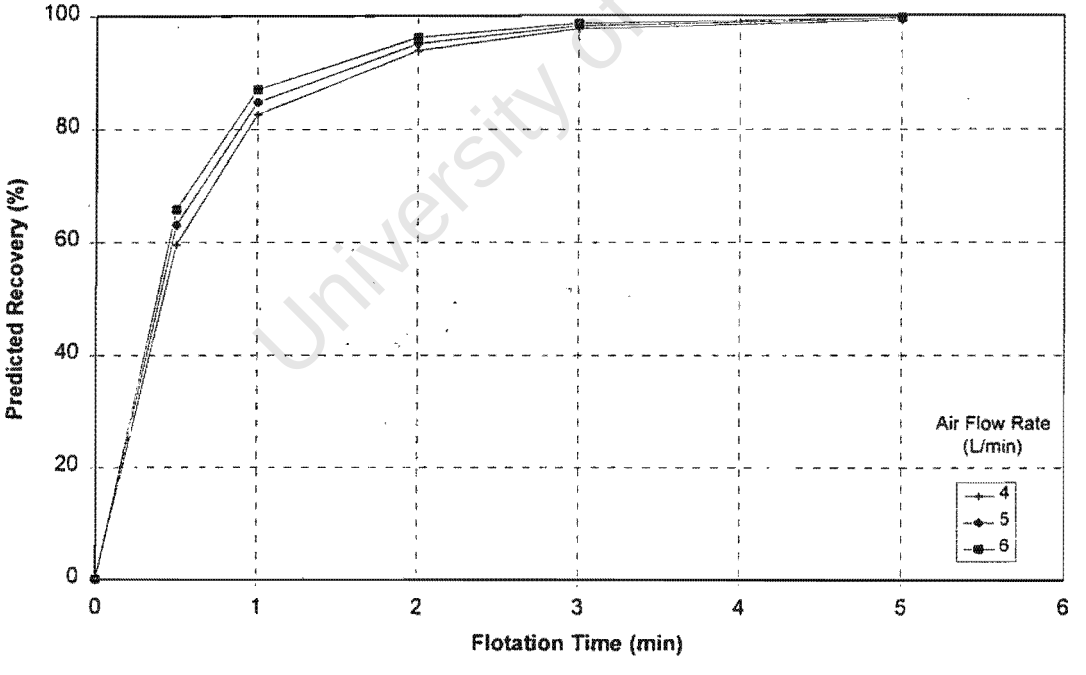

Figure 3.39a Predicted batch flotation recovery versus flotation time at various air flow rates

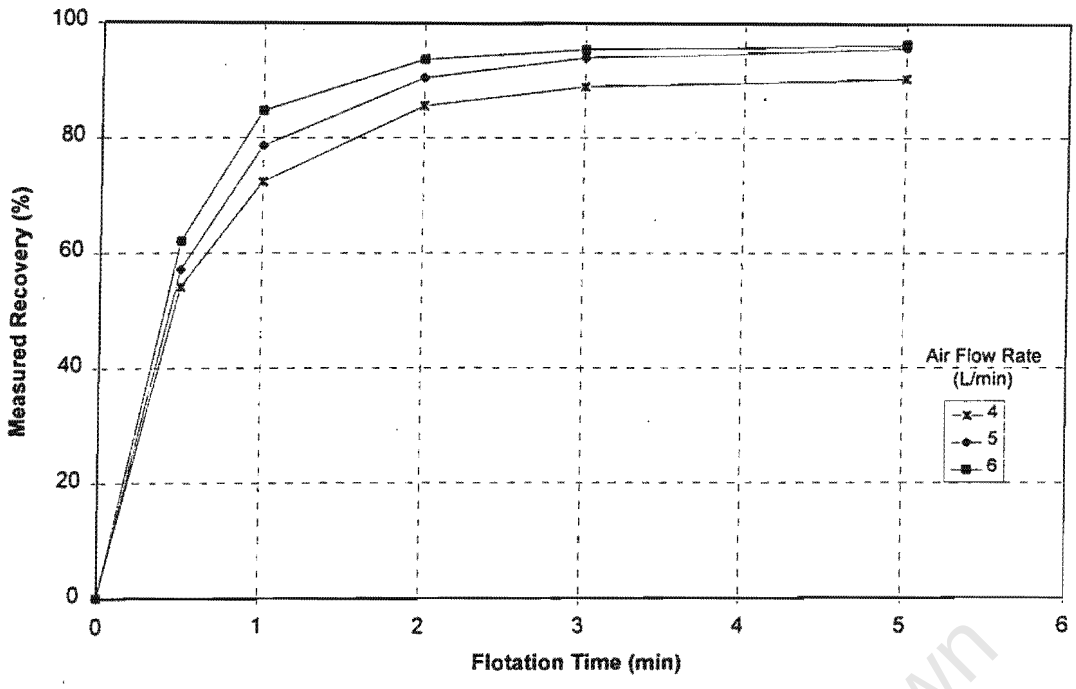

Figure 3.39b Measured batch flotation recovery versus flotation time at various air flow rates

3.2.2.6 Prediction of continuous flotation performance using parameters derived from batch data

One of the objectives of this modeling exercise was to use model parameters derived from the batch data to predict flotation performance in the same cell, using the same ore, under continuous, steady state operating conditions for a range of different froth heights and gas rates. Two strategies were developed to achieve this objective. Firstly, parameters were derived using only batch data. These parameters were then used to predict flotation performance observed from a continuously operated system. A schematic representation of this procedure is outlined in Figure 3.40. Table 3.19 shows the parameters obtained when using this method. Figure 3.41 compares the experimental and predicted concentrate masses, on a sized basis, for these tests. The correlation coefficient for the data depicted in Fig. 3.41 was found to be 0.9. It can be seen that the prediction of the continuous cell performance using model parameters derived from batch test data is very good. This is despite the fact that the froth stability parameter, β, derived from the batch tests represents an "averaged" characteristic froth drainage behaviour over the duration of the batch test, given the fact that the stability of the froth decreases with time, owing to the depletion of both frother and solids contents. By the same token, the viscosity parameter is expected to vary with flotation time. Despite these apparent drawbacks, the good agreement between predicted and measured concentrate masses by size demonstrates the potential use of this approach for relating the performance of batch flotation data to flotation cells operated under continuous conditions.

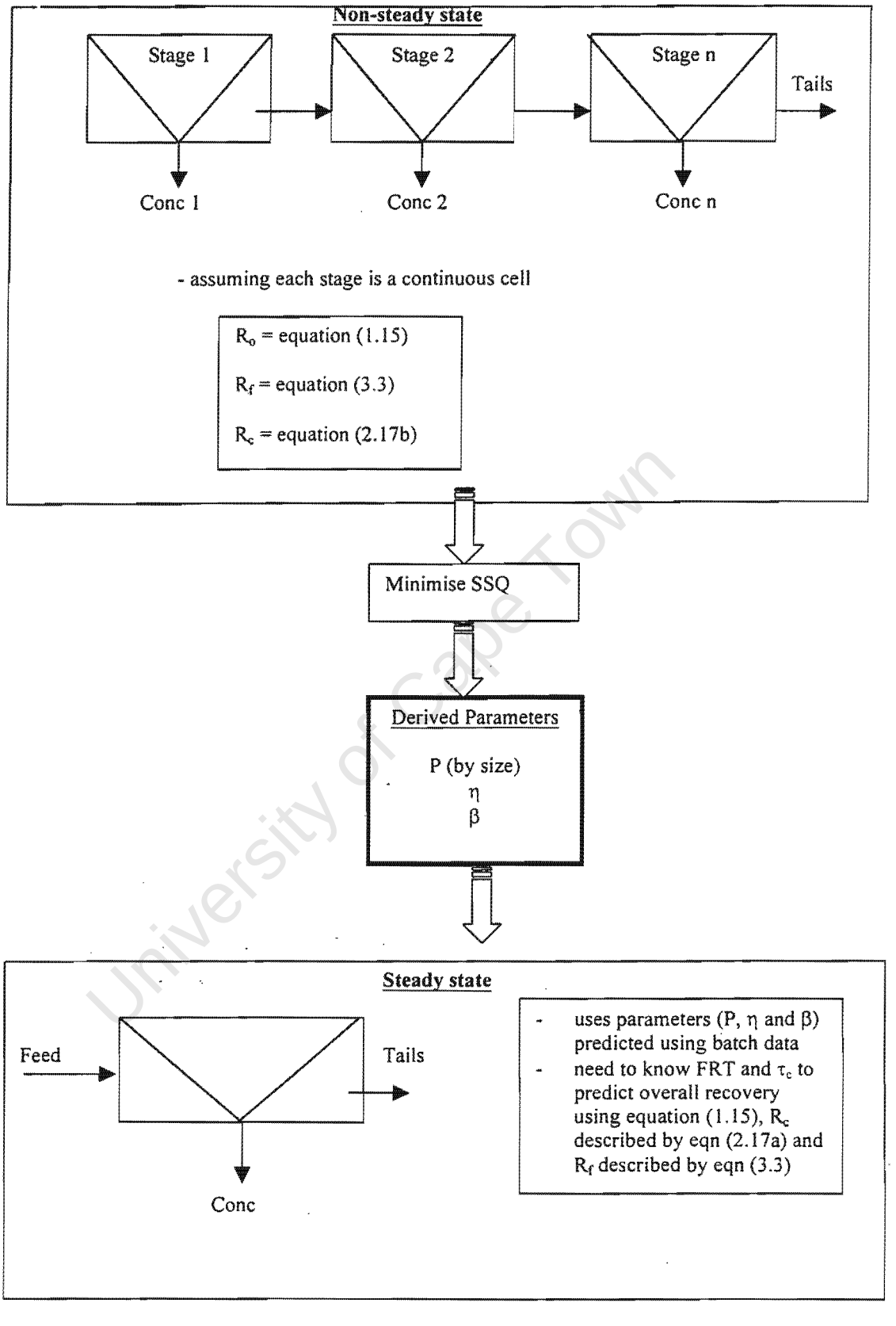

Figure 3.40 Froth modeling methodology (method 1)

Table 3.19 Derived parameters using method 1

Mean error per data point = 0.883			
Floatability (P)		Froth stability (1/min) (β)	Viscosity (N.s/m^2) (η)
Particle Size (microns)	P		
Sub 10	1.0 E-7	2.94	0.00284
10 to 25	1.50 E-4		
25 to 45	6.16 E-4		
45 to 75	10.20 E-4		
75 to 106	13.78 E-4		
106 to 225	18.42 E-4		

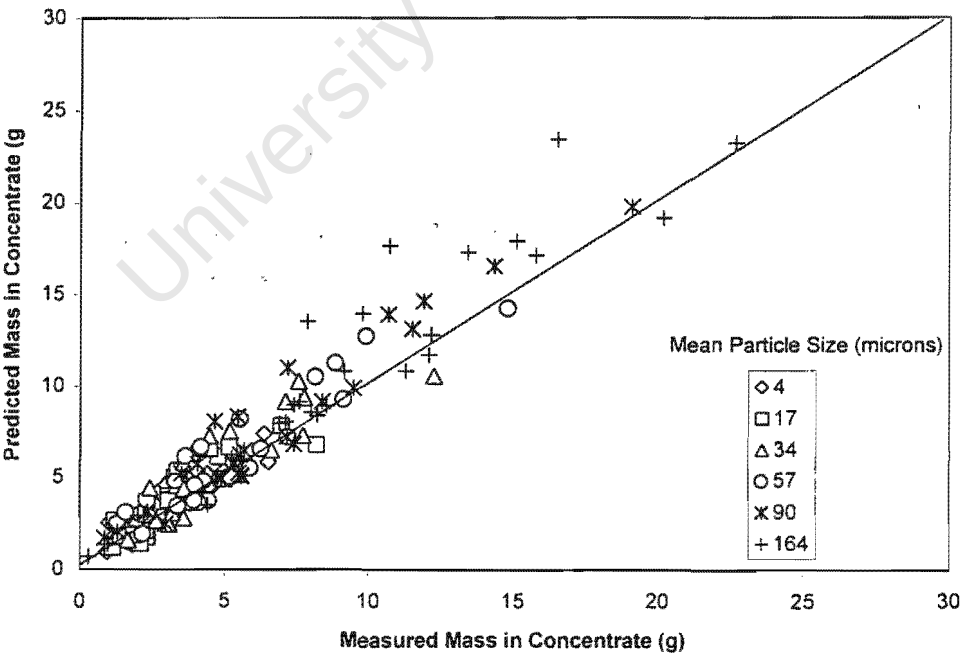

Figure 3.41 Comparison between experimental and predicted concentrate masses on a sized basis in a continuous cell

Secondly, combined data sets from batch and continuous tests were used to derive parameters by sum-of-error squares minimisation (see Fig. 3.42). This strategy has the advantage of using a large database to derive model parameters. Figure 3.43 compares the experimental and predicted concentrate masses, on a sized basis, for this method. The correlation co-efficient for the data depicted in Fig. 3.43 was found to be 0.93. The derived parameters are shown in Table 3.20. It can be seen from this table that there are no significant differences between the derived parameters and the parameters reported in Table 3.19. When comparing the mean-error per data point, however, it is clear that using combined batch and continuous data to derive parameters produced a better fit. Since the main focus of this study is on the use of batch data to derive parameters that are transferable to continuous systems, the following discussion will be based on parameters derived using only batch data (method 1).

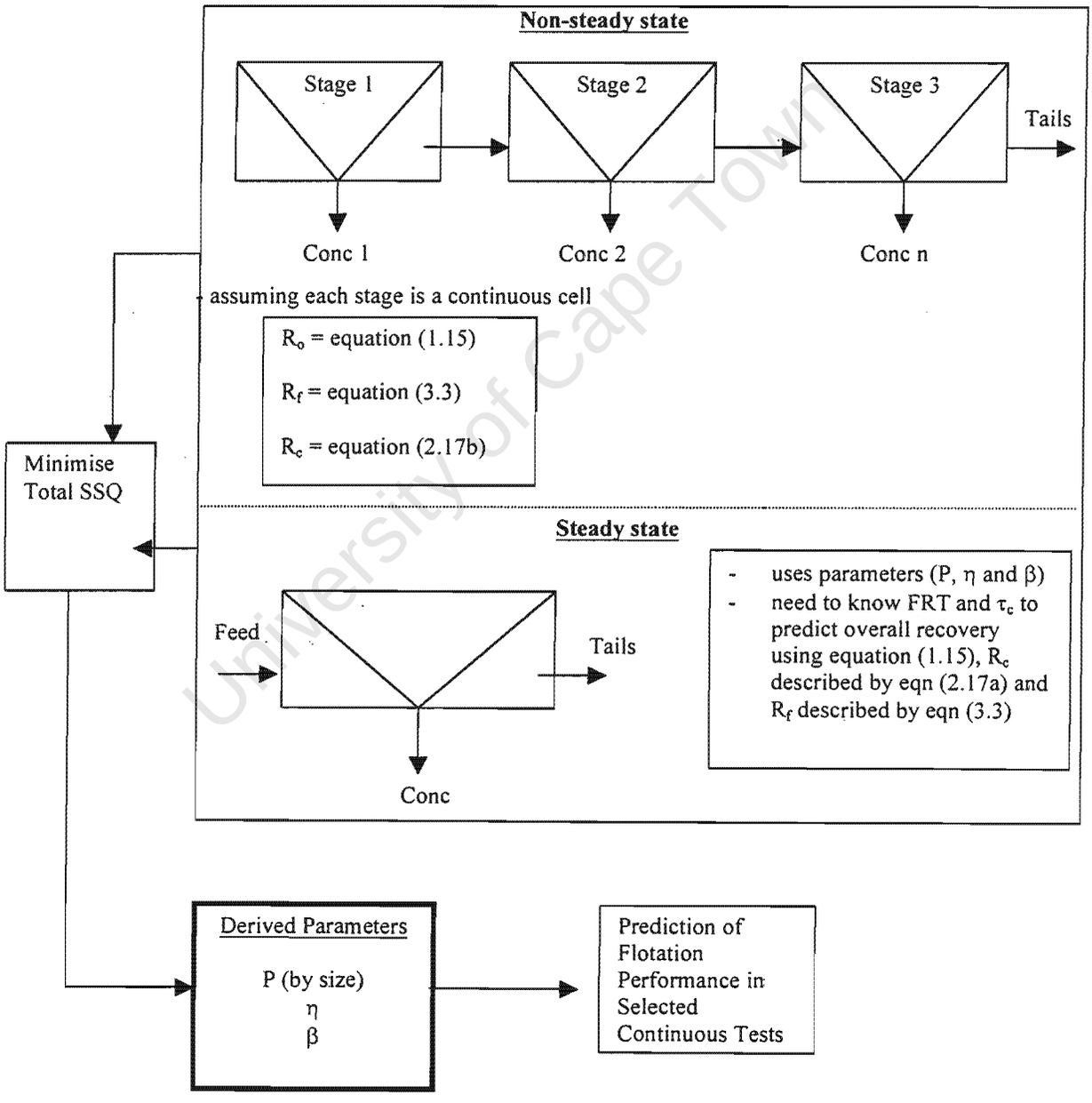

Figure 3.42 Froth Modelling Methodology (method 2)

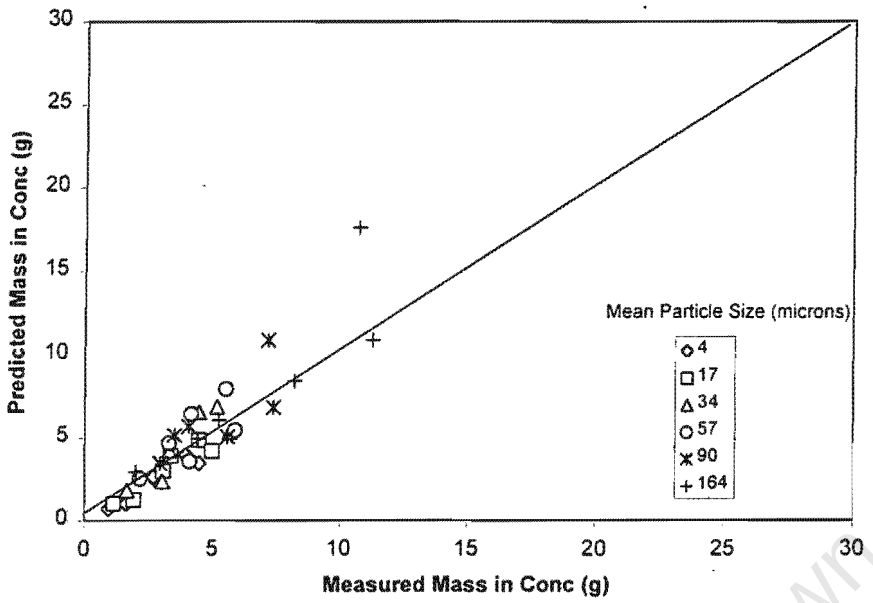

Figure 3.43 **Comparison between experimental and predicted concentrate masses, on a sized basis, using parameters derived from combined batch and continuous data to predict continuous performance**

Table 3.20 **Derived parameters using method 2**

Mean error per data point = 0.68			
Floatability (P)		Froth stability (1/min) (β)	Viscosity (N.s/m^2) (η)
Particle Size (microns)	P		
Sub 10	6.65 E-5	2.97	0.00294
10 to 25	1.70 E-4		
25 to 45	5.78 E-4		
45 to 75	10.07 E-4		
75 to 106	13.77 E-4		
106 to 225	18.46 E-4		

3.2.2.7 Predicted Froth Recovery Behaviour

Figure 3.44 shows the plot of froth recovery against froth retention time profiles for different particle size ranges. The symbol marks are included in this figure to facilitate comparison between the curves. Figure 3.44 indicates that froth recovery decreases with an increase in particle size. As mentioned earlier, this could be due to the effect of gravity. The other

interesting observation is that when the predicted froth recovery values from batch and continuous tests were plotted against froth retention time on the same graph, they lay on the same curve (Fig. 3.45). In the case of batch system only, Figure 3.46 indicates that froth recovery changes with flotation time. This has serious implications on most work that uses parameters derived from batch tests.

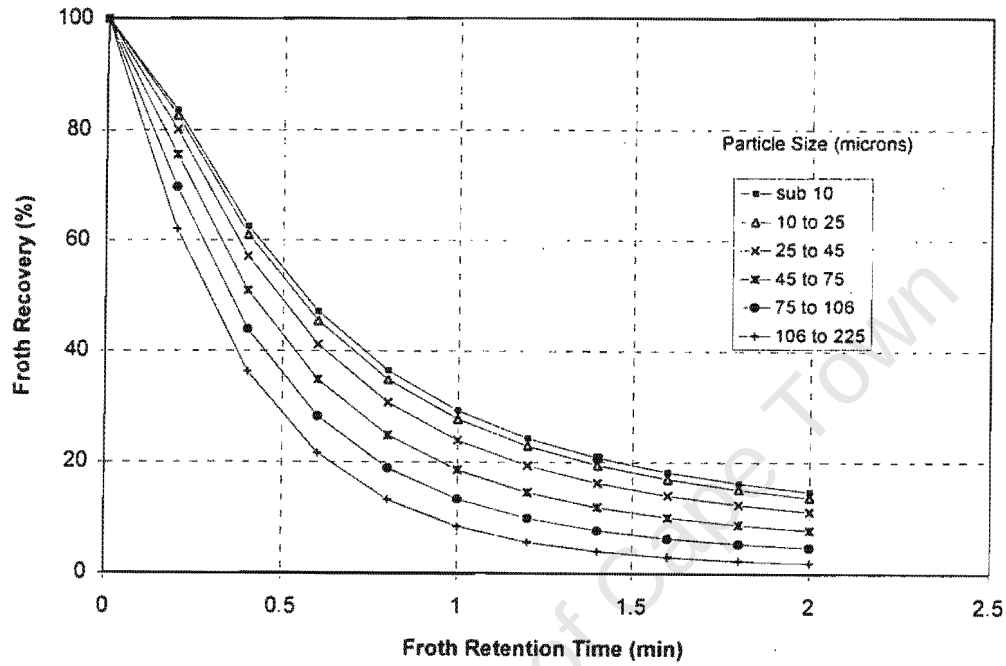

Figure 3.44 **Effect of froth retention time for different particle size ranges on froth recovery in a continuous cell**

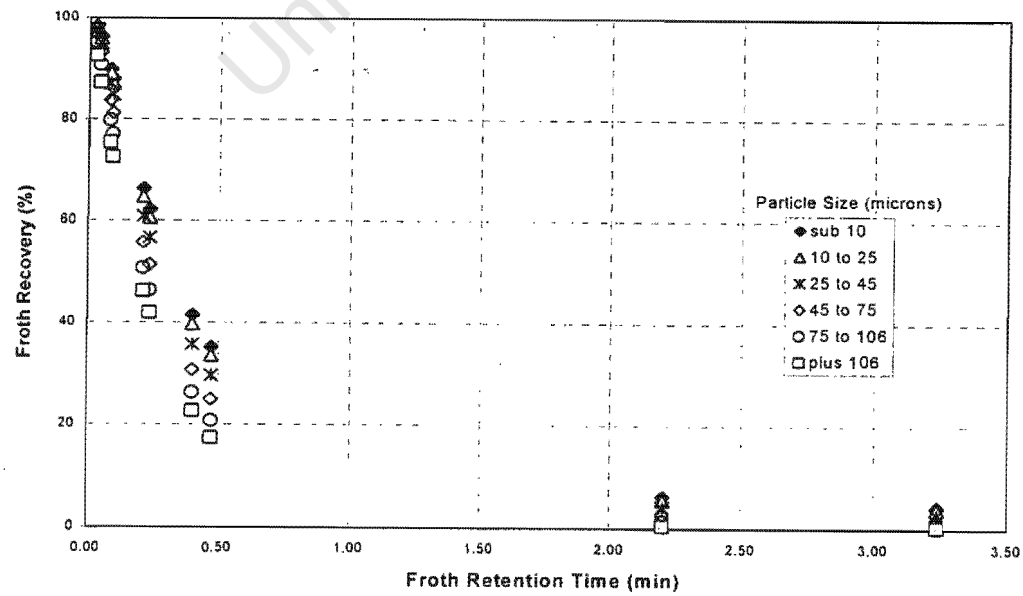

Figure 3.45 **Effect of froth retention time on froth recovery for both batch and continuous tests**

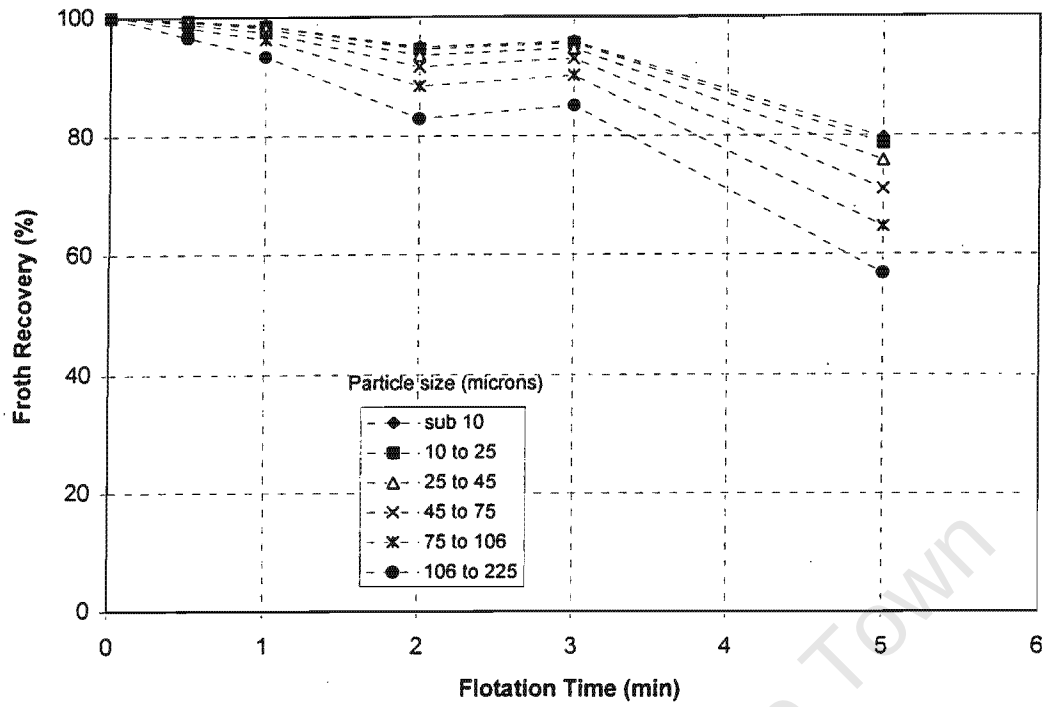

Figure 3.46 Change in froth recovery with batch flotation time

3.2.2.8 Prediction of batch flotation performance (with wash water) using parameters derived from batch data collected without the addition of wash water

Parameters derived from the batch tests carried out without the addition of wash water were used to predict batch flotation performance for the tests conducted whilst adding wash water. Addition of wash water, however, is expected to increase the drainage rate of water within the froth phase. As such, the drainage parameter, β, was allowed to vary in order to obtain a realistic prediction of the batch flotation tests conducted whilst adding wash water. The other parameters for P, at various size classes, used in this exercise were exactly the same as those reported in Table 3.19.

Figure 3.47 shows the prediction obtained for these tests. It compares the measured masses, by size, to the predicted masses in the concentrate. Although there is some scatter in the reported data, generally it can be seen that the prediction was satisfactory. The correlation co-efficient for the data depicted in Fig. 3.47 was found to be 0.82. The drainage parameter, β, was found to be 28.46 (1/min). Clearly, this value supports the claim that the addition of wash water increases water drainage within the froth phase. This is because the derived value is a lot higher than that one obtained from the batch tests conducted without the addition of wash water (see Table 3.19).

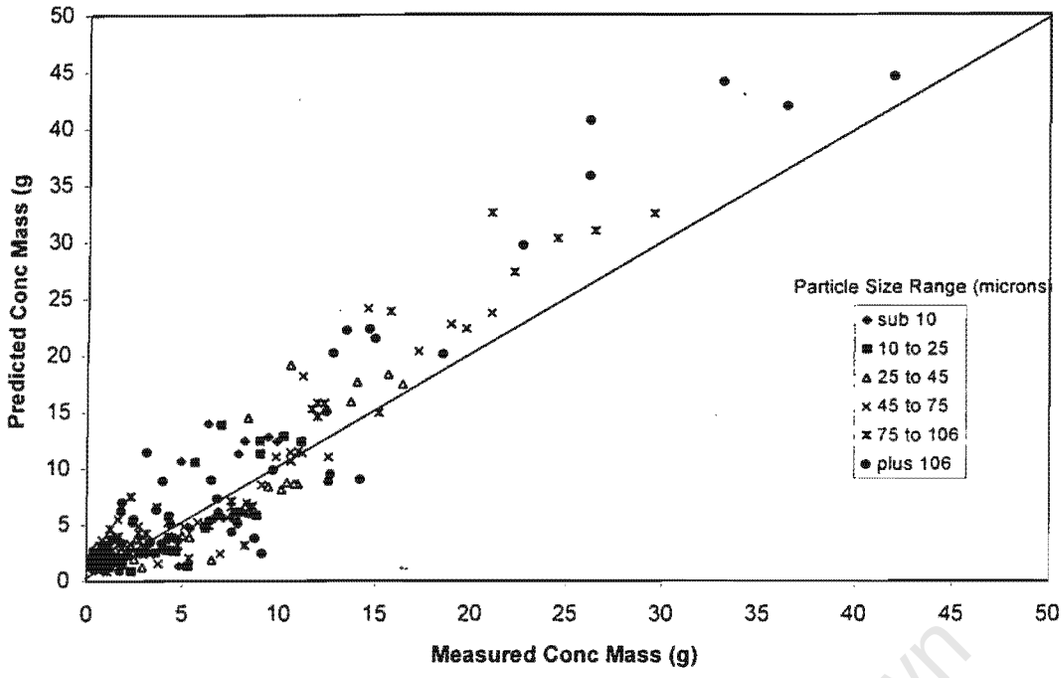

Figure 3.47 **Prediction of concentrate masses on a sized basis, using parameters derived from batch tests conducted without wash water, with respect to batch tests conducted whilst adding wash water**

3.3 A CASE STUDY: EXTRACTION OF MODEL PARAMETERS IN A BINARY SYSTEM

3.3.1 Source of the experimental data set

To test the general applicability of the froth modelling methodology and froth recovery model proposed in this thesis, viz. equation 3.3, it was decided to use data from the literature, generated by Feteris (1983). Some raw data from this work is also found in Feteris *et al* (1987). This set of data was chosen mainly because it was generated in a laboratory flotation cell very similar in size and design to the one used for studying the quartz system. They studied the influence of the froth height in flotation using an artificial galena/silica system, generating data at different froth depths using a 4 *l* modified Leeds flotation cell. The concentrate masses were reported in terms of mineral type and particle size. For simplicity, and to eliminate problems associated with describing the recovery of gangue material, silica in this case, the analysis provided here pertains to the recovery of the floatable mineral, galena, only. Masses of galena in each size range are shown in Table 3.21 below.

Table 3.21 Mass of galena in each size range (Feteris *et al*, 1987)

Time (min)	Size range (μm)	Froth depth (mm)					
		42	38	34	28	22	15
0-0.5	>17.3	16.786	18.748	20.760	20.490	21.078	22.857
	8.2-17.3	2.627	2.191	3.285	2.777	3.587	3.730
	3.3-8.2	0.359	0.305	0.503	0.556	0.654	0.984
	<3.3	0.180	0.173	0.114	0.260	0.275	0.384
0.5-1	>17.3	2.793	3.491	2.807	3.618	2.783	3.849
	8.2-17.3	1.471	1.361	1.542	1.894	1.982	2.322
	3.3-8.2	0.212	0.165	0.274	0.400	0.415	0.759
	<3.3	0.081	0.078	0.192	0.152	0.142	0.249
1-2	>17.3	1.984	2.941	1.785	1.724	1.406	1.107
	8.2-17.3	1.403	1.517	1.396	1.650	1.514	1.540
	3.3-8.2	0.288	0.268	0.468	0.535	0.578	0.949
	<3.3	0.081	0.098	0.127	0.191	0.210	0.285
2-4	>17.3	1.320	1.149	0.595	0.538	0.735	0.337
	8.2-17.3	0.848	0.920	0.686	0.810	0.649	0.487
	3.3-8.2	0.426	0.333	0.417	0.547	0.618	0.714
	<3.3	0.098	0.113	0.108	0.183	0.230	0.274
4-8	>17.3	-	-	0.451	0.229	0.128	0.064
	8.2-17.3	-	-	0.244	0.312	0.201	0.130
	3.3-8.2	-	-	0.246	0.411	0.418	0.389
	<3.3	-	-	0.085	0.180	0.213	0.227

3.3.2 Operating conditions

Six tests were conducted by Feteris (1983) at various froth depths (Table 3.22). Collector and frother, Potassium ethyl xanthate (0.1%) and Dowfroth 250 (0.25%), respectively, were added to the pulp at the rate of 0.4 mℓ of each per 100 mℓ of pulp. Pulp density was kept constant at approximately 13%. All tests were conducted at an air flowrate of 7 litres/min and an impeller speed of 900 r.p.m. A "sweaty plate" through which water flowed at 20 mℓ/min was put at the top of the cell to aid the removal of the froth.

Table 3.22 Operating conditions

Test number	Actual pulp volume (ml)	Pulp density (%)	Froth depth (mm)	Air flowrate (litres/min)	Froth volume (ml)
1	2864	13.71	42	7	1046
2	2972	13.71	38	7	938
3	3072	13.74	34	7	838
4	3226	13.66	28	7	684
5	3348	13.74	22	7	562
6	3484	13.81	15	7	426

3.3.3 Curve fitting of model parameters

The same procedure outlined in Chapter 2 and at the beginning of section 3.2.2.1 was used to extract model parameters for this system, except that the froth recovery was described using equation 3.3. It was, however, necessary to estimate the bubble surface area flux, S_b, as it was not measured in the original data provided by this study. This was estimated by measuring the bubble flux in a similar flotation cell using the same chemical conditions and air flow rate used by the authors of the original data. The S_b value measured was 16 (cm^2 air /cm^2 cell . s).

Results from this work indicate a good correlation of the total masses of galena recovered to the concentrate with the fitted values (Fig. 3.48). For this comparison, the plotted points had a correlation coefficient of 0.91. Figure 3.49 shows the relationship between froth recovery and froth retention time for the three particle size ranges used in the modelling. The coarse particle size range of galena (plus 17.3 μm) was not used in this modelling exercise. This is because the average particle size could not be calculated in this size range since the maximum size was not given in the original data. Figure 3.49 indicates that froth recovery in this system was not strongly depended on particle size. The model parameters are provided in Table 3.23.

From Table 3.23, the value of β, "the rate at which water is draining, which is related to the rate at which bubbles are coalescing", from this system was very small. This indicates that most particles reported to the concentrate launder attached to bubbles. In addition, it can be seen that the β parameter is significantly smaller than the drainage rate parameter obtained from the quartz system. This can be attributed to the big difference in wash water flow rates used in the two systems. In the quartz system water addition rate was approximately 1200 mℓ/min, whereas in the galena/silica system it was 20 mℓ/min. As expected, the floatability (P) parameter was particle size dependent, increasing with an increase in particle size.

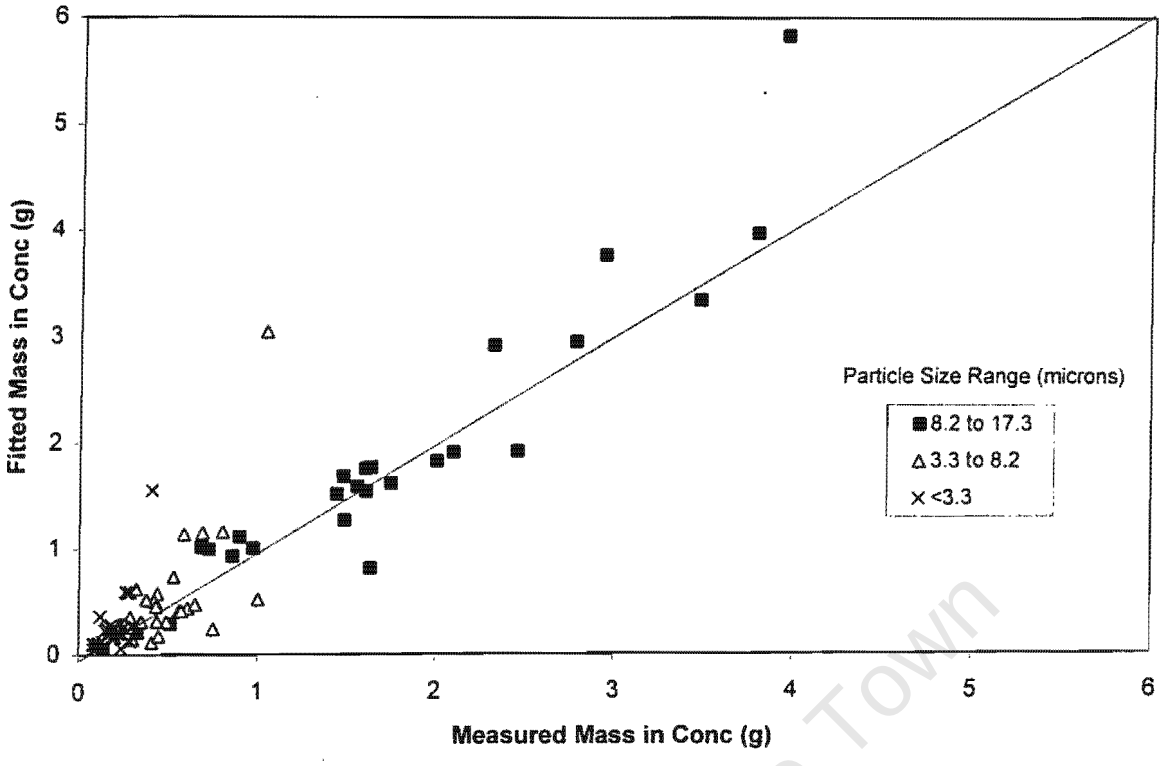

Figure 3.48 Comparison between measured and fitted masses of galena mineral in the concentrate launder

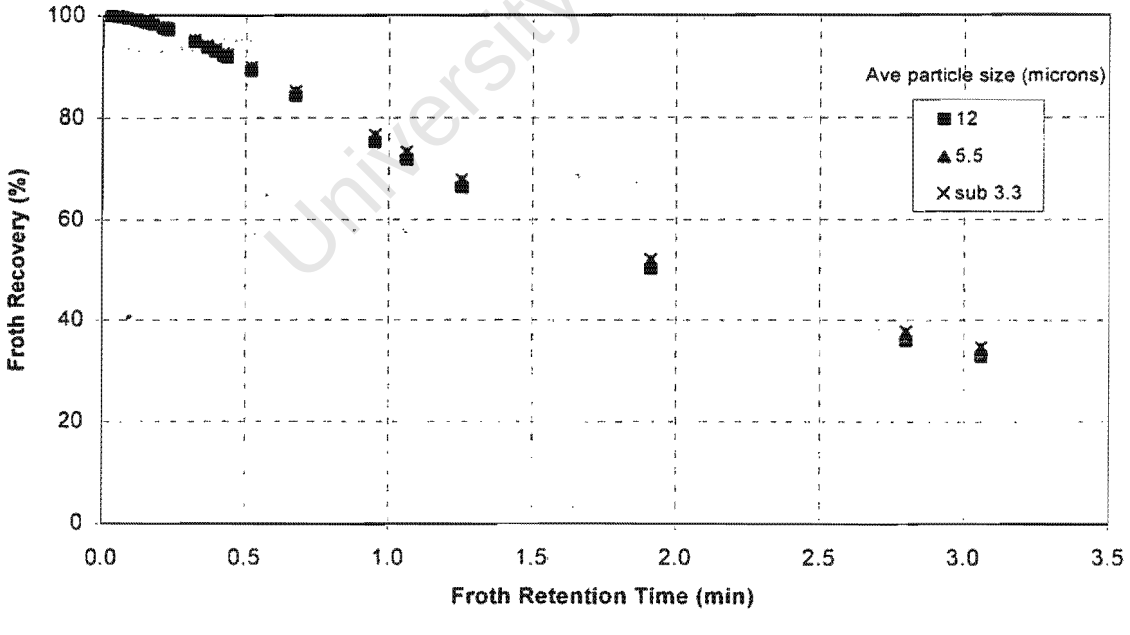

Figure 3.49 Effect of froth retention time on froth recovery

Table 3.23 Froth and pulp phase parameters obtained from curve fitting galena data

Parameters			
Floatability (P)		Froth stability (1/min) (β)	Viscosity (N.s/m^2) (η)
Particle Size (microns)	P		
Sub 3.3	0.000080	0.8090	0.0215
3.3 to 8.2	0.000885		
8.2 to 17.3	0.002957		

3.4 SUMMARY

This chapter has described the equipment and raw material used to conduct experimental testwork. The procedures followed for conducting batch and continuous tests were outlined. Sources of raw data were also indicated. It also dealt with the interpretation of data contained in cited sources. Results obtained from the use of the raw data in extracting kinetic parameters describing the batch and continuous systems were reported and discussed.

It was demonstrated that the froth modelling approach proposed in Chapter 2 can be used successfully to derive kinetic parameters (for describing both pulp and froth performances) from batch data. Subsequently, these parameters were shown to be transferable to a continuous flotation system. It was also shown that some of these parameters, such as the drainage rate parameter, ω, can be correlated with operating variables such as particle size. The observed correlation between the drainage rate parameter and particle size was used to refine the froth recovery model.

Furthermore, data obtained from the literature was used to test the final form of the froth recovery equation. The data set used was collected by Feteris (1983) who floated an artificial mixture of galena/silica using a 4 litre flotation cell. Modelling results obtained from this exercise showed that the refined froth recovery model can be used successfully to describe the froth phase influence on the overall flotation performance in a binary mineral system.

In the next chapter, the refined froth recovery model, equation 3.3, is tested, using plant data, to determine its applicability in describing the performance of the froths found in real ore flotation systems.

CHAPTER 4

Evaluation of Model Parameters using Plant Data: A Case Study of Flotation Testwork at Impala Platinum Ltd

CHAPTER 4: EVALUATION OF MODEL PARAMETERS USING PLANT DATA: A CASE STUDY OF FLOTATION TESTWORK AT IMPALA PLATINUM LTD

4.1 INTRODUCTION

In the previous chapter, a froth recovery model (equation 2.12) and a methodology for extracting pulp and froth kinetic parameters from batch data, proposed in Chapter 2, were evaluated using laboratory data. Subsequently, a semi-empirical froth recovery model (equation 3.3) was derived. In the case of a single mineral, quartz, floated in batch and continuous modes without the addition of wash water, parameters derived from batch tests were used successfully to describe flotation performance in continuous tests. The proposed froth recovery model (equation 3.3) was further evaluated using a binary system (viz. galena and silica) based on data reported in the literature (Feteris, 1983). The analysis of both these systems, however, was limited to particle size classification of a single floating mineral species. It was therefore considered necessary to extend and test the proposed froth recovery model and the methodology for extracting kinetic parameters from batch data using a more realistic, and complex, ore flotation system.

As far as could be ascertained, there is no study to date which has been able to usefully quantify the influence of the operating variables on the behaviour of different minerals within the froth phase in complex flotation systems. An application of the proposed froth modelling methodology to a real ore system was therefore seen as a possible way of establishing appropriate conditions for attaining high froth recoveries of desired minerals, along with a satisfactory degree of gangue mineral rejection. However, it was considered that the extension of the proposed methodology to a real ore system could not be satisfactory achieved using a 3.5 ℓ flotation cell. As a result, a 60 ℓ flotation cell, operated in parallel with an operating flotation plant, was chosen. It was thought that this cell would be suitable for generating more representative data for use in describing froth processes. This chapter presents an application of the proposed froth modelling methodology to testwork which was carried out at Impala Platinum's Merensky plant in the North West province, South Africa. The focus is mainly on the evaluation of model parameters obtained from the use of plant data, and testing the validity and limitations of the proposed methodology of using kinetic parameters derived from batch data to predict froth performance in a continuous system.

4.2 FLOWSHEET STRUCTURE AND OPERATIONAL PRACTICES AT IMPALA PLATINUM (MERENKSY PLANT)

Impala Platinum operates Platinum-Group-Minerals (PGMs) concentrators. Of the total annual production, a significant amount of PGMs is produced by the Merensky plant, which is the largest of the three Platinum concentrators. The other two being the MF2 (Mill-Float-Mill-Float) and UG2 (Upper Group 2) concentrators. At the time that this testwork was undertaken, March 1998, the Merensky plant consisted of 15 sections. Each section had three stages, viz, storage of ore in silos, milling and recovery of PGMs through flotation. Figure 4.1 shows a typical flowsheet of a section (only up to the rougher stage) in the Merensky plant.

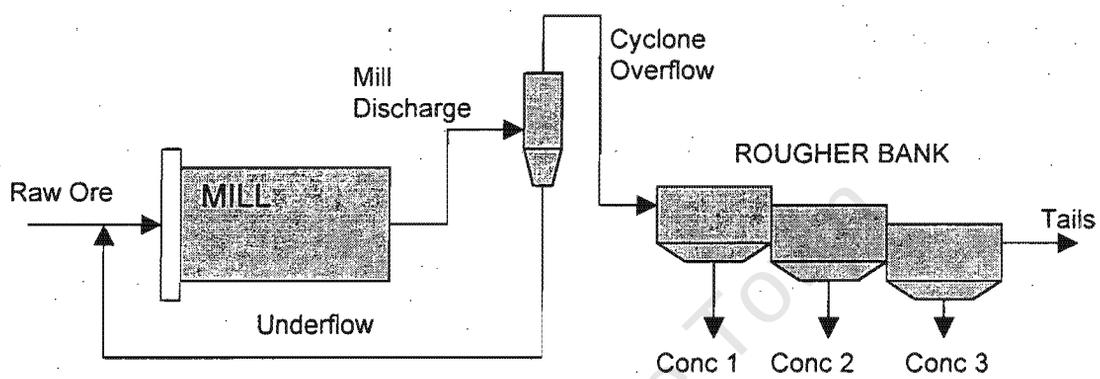

Figure 4.1 A typical section of the Merensky plant

No further details of the flowsheet structure of the Merensky plant will be provided since such information is regarded as confidential, and not relevant to this study, as the testwork carried out on the 60 ℓ flotation cell pertained only to the rougher stage of this flotation plant. The location of the 60 ℓ flotation cell on section 10 of the Merensky plant is shown in Figure 4.2.

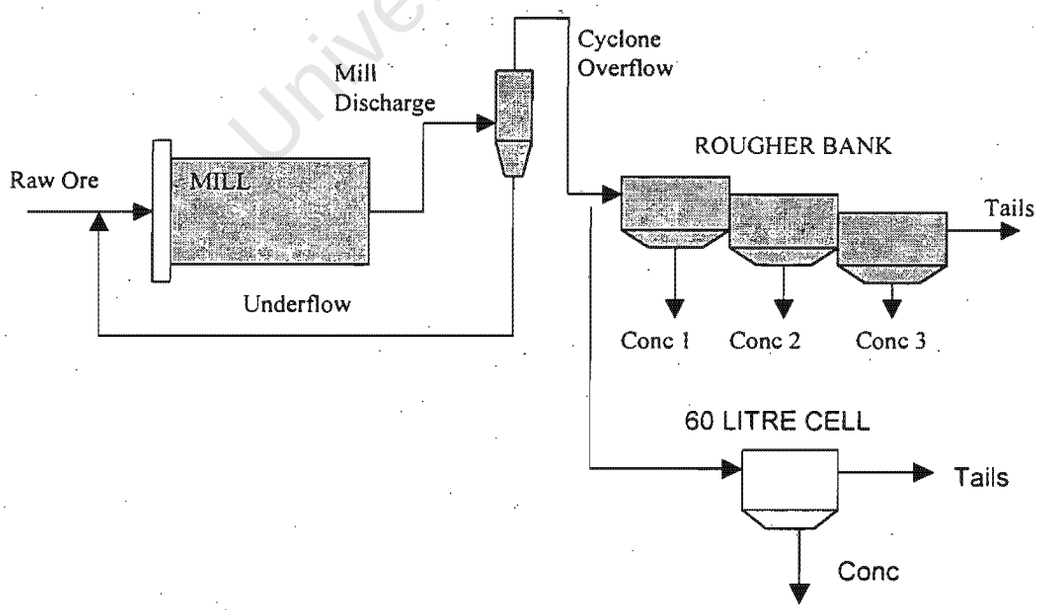

Figure 4.2 Location of the 60 ℓ flotation cell

4.3 DESCRIPTION OF THE 60 ℓ FLOTATION CELL

The flotation cell used in the pilot circuit was constructed of stainless steel, with a Bateman-type impeller (see Figure 4.3). The rotational speed of the impeller and the volumetric flow rate of air could be altered by the operator. In addition, an overflow weir system allowed one to change the pulp level in the cell. Instruments measured and displayed the impeller speed (in revolutions per minute) and the air flow rate (in cubic meters per minute). The cell had a top cross sectional area of approximately 1716 cm^2, and a height of 38 cm. A schematic diagram of this cell is shown in Figure 4.4.

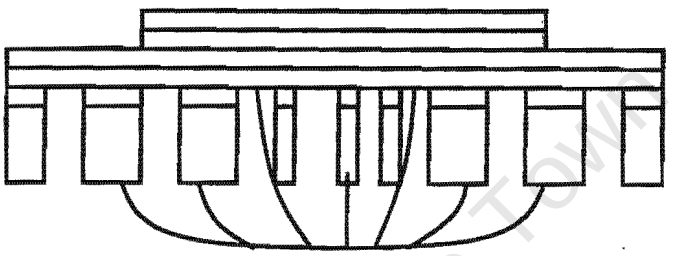

Figure 4.3 Batequip impeller and stator (after Gorain, 1998)

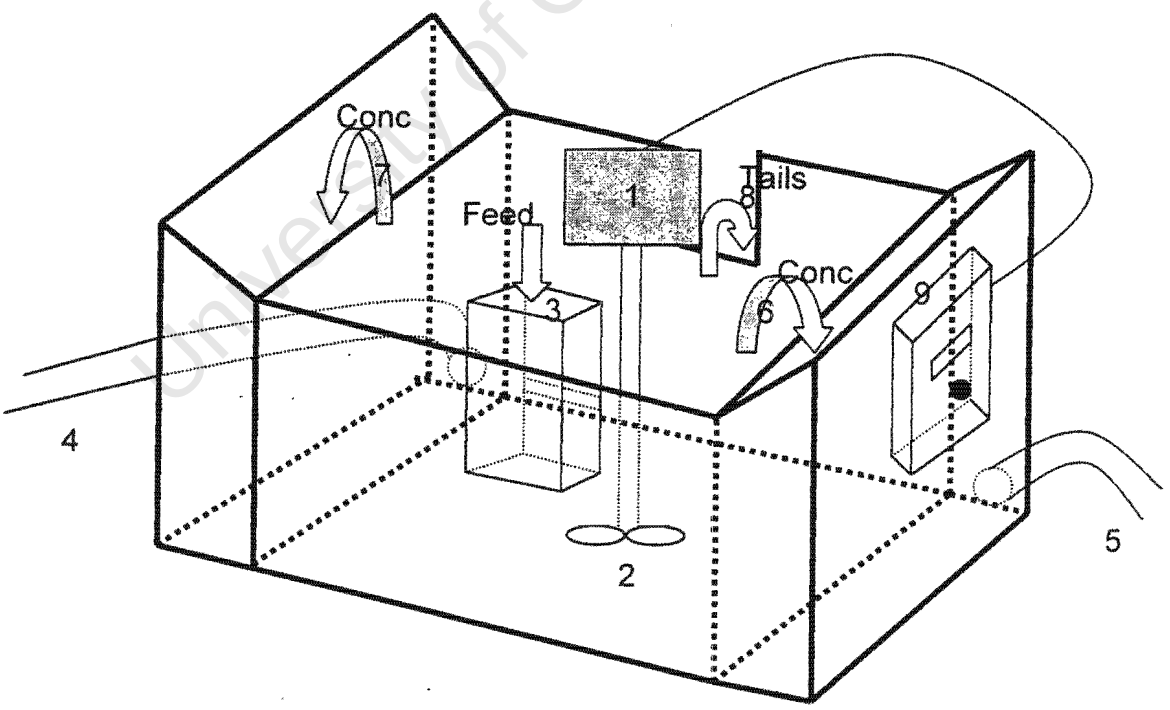

Figure 4.4 Sketch of the 60 ℓ flotation cell
1. Motor; 2. Impeller; 3. Feed box; 4. Concentrate-2 pipeline; 5. Concentrate-1 pipeline; 6. Concentrate 1; 7. Concentrate 2; 8. Tails; 9. Impeller speed control box

4.4 DESCRIPTION OF THE ORE

The ore used in the pilot circuit comes from the bushveld complex, a gigantic layered intrusive, which underlies an area of about 40 000 km^2, situated in North West and Northen provinces, and some parts of Gauteng province, of South Africa (Hochreiter *et al*, 1985). Two types of ores are mined from the Bushveld complex, viz. UG2 and Merensky. The ore used in this study is the Merensky ore. Typical mineral abundances in the Merensky ore, cyclone overflow, are shown in Table 4.1. It can be seen in this table that sulphide minerals account for approximately 1.22 percent of the total ore. By far, the dominant sulphide mineral is pyrrhotite. Other sulphide minerals include sphalerite and galena. From Table 4.1, it can be seen also that silicates are present in significant proportion, more than 96%, when compared to the sulphide minerals, oxides and carbonates in the head sample. The major gangue minerals are orthopyroxene, feldspar, clinopyroxene and chromite. Chromite is a major undesirable mineral in the down stream processing stages. The limit of the chromite content in the flotation concentrate is +/- 3%, as greater chromite content can form components that may be stable up to temperatures as high as 2000 °C during smelting (Theron, 1998). These solid phases in the furnace reduce the efficiency of the smelting process. Consequently, the flotation cells must be operated under conditions that minimise the amount of problematic components such as chromite.

Table 4.1 Summary of mineral abundances (wt.%) in the Merensky ore (Latti, 1997)

MINERAL	CYCLONE OVERFLOW
Sulphides	
Pyrrhotite	0.46
Pyrite	0.09
Pentlandite	0.36
Chalcopyrite	0.20
Other_Sulphides*	0.09
Silicates	
Feldspar	40.32
Orthopyroxene	42.90
Talc	0.35
Clinopyroxene	8.43
Other_Silicates**	4.39
Oxides	
Chromite	1.90
Other***	0.51
TOTAL	100

* sphalerite and galena
** olivine, serpentine, chlorite, mica and quartz
*** Fe-oxides and carbonates

4.5 EXPERIMENTAL PROGRAM

4.5.1 Flotation cell set-up

The main aspects of the experimental program were finalised on site in consultation with Mrs Jenni Sweet (Sweet, 1999), who was using the cell to study chemical scale-up. A schematic representation of the equipment used is shown in Figure 4.5. The conditioners used were designed to simulate plant conditions as far as possible. This aspect is discussed in the next section.

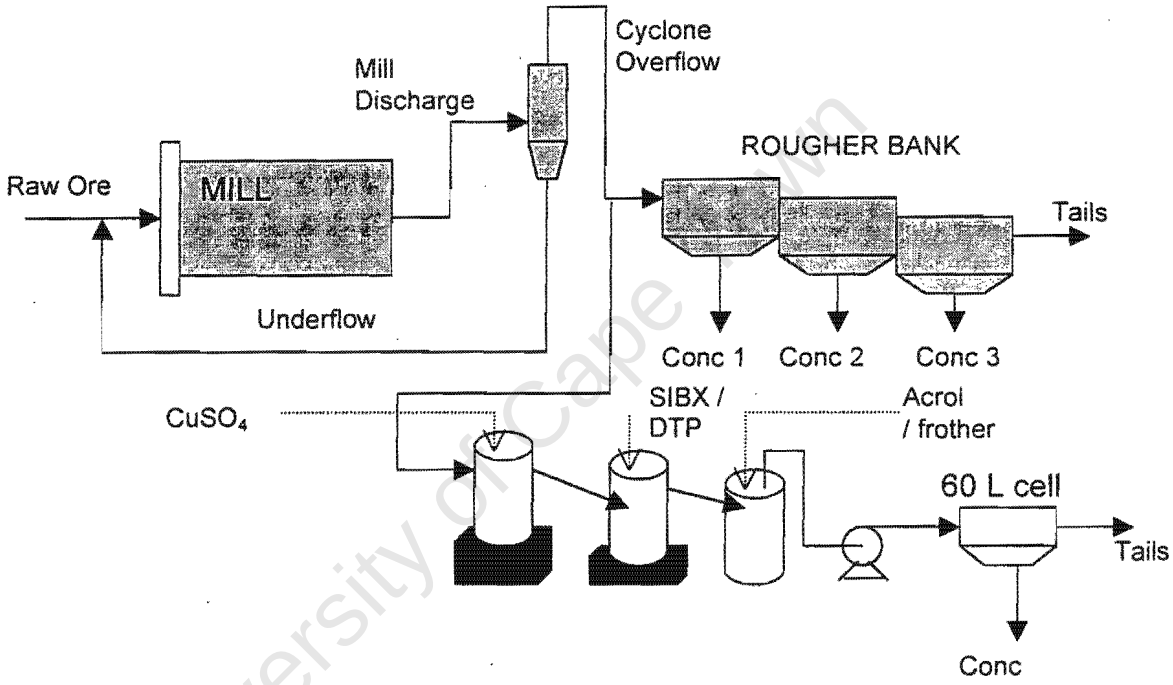

Figure 4.5 Schematic representation of the flotation set-up at Impala

4.5.2 Chemical Conditioning

Three conditioning tanks were employed. The feed flow rate (approximately 10 ℓ/min) allowed for approximately 14 minutes residence time in the first two tanks, and 10 minutes in the last tank. Plant cyclone overflow was pumped into the first tank, where copper sulphate ($CuSO_4$) was added as an activator. Activated slurry from the first tank was allowed to overflow into the second tank where the collector, a mixture of sodium isobutyl xanthate (SIBX) and dithiophosphate (DTP), was added. In the last tank, a depressant, carboxy-methyl-cellulose or guar gum (Acrol, IMP4), and a frother, cresylic acid, were added prior to transferring the slurry to the flotation cell. The actual dosages used are discussed in the next sections.

4.5.3 Tests conducted

4.5.3.1 Exploratory tests

The first phase of the experimental testwork was geared toward establishing appropriate operating conditions and testing for reproducibility. Test R1 and R2 were conducted, using conditions, shown in Tables 4.2a and 4.3, aimed at simulating the plant performance (Sweet, 1999). For this set of tests, activator ($CuSO_4$) and collector (SIBX/DTP) were added into the first and second conditioning tanks respectively, as previously described. The poor froth mobility observed, visually, in these tests, necessitated adjustments of the operating conditions to boost froth performance. In the second set of tests (tests 1S to 5S), $CuSO_4$ dosage was decreased from 60 to 50 g/ton, and the frother dosage was increased from 80 to 100 g/ton. The purpose of changing these chemical dosages was to ensure a continuous overflow of the concentrate into the launder. The reagent dosages used for these flotation tests are summarised in Table 4.2a. These flotation tests were conducted using a range of air flow rates and froth heights (see Table 4.3). For continuous tests, the system was operated for approximately two hours to ensure steady state operation before sampling. Flow rates of tails, feed and concentrate were measured using a bucket and a stopwatch. Samples were weighed and dried before sending them to the laboratory for assaying. Detailed experimental data for these tests is presented in Appendix F.

Furthermore, a number of tests (Test 1N in Tables 4.2b and 4.3) were performed in which the 60 ℓ cell was operated in a batch mode to test the feasibility of performing batch tests using this type of a cell. These tests were performed by cutting out the air supply and allowing unconditioned pulp to pass through the cell. After some time, the feed was stopped and the pulp inside the cell was conditioned manually like in a typical batch float. During flotation, pulp level was kept constant by adding small amounts of water with frother, same concentration as the feed pulp. A sample of conditioned feed was taken before turning on air supply. Concentrate samples were collected over a period of about 25 minutes at various time intervals depending on the froth characteristics. Froth concentrates were allowed to overflow freely without scraping. To achieve this it was necessary to increase the frother dosage from 80 to 100 g/ton. The results obtained from this exercise are reported and discussed in section 4.6.1.

4.5.3.2 Modelling flotation tests

The second phase of the experimental testwork involved using the procedures established in the first phase to conduct relevant batch and continuous flotation tests suitable for modelling purposes. This set of tests (Tests 7S to 12S, and 2N to 4N) was performed with feed (cyclone overflow) already activated and conditioned with collector, as these reagents were added to the plant mill feed. The operating conditions and reagent dosages for these tests are shown in

Tables 4.2a, 4.2b and 4.3. Continuous tests carried out at shallow froth were not successful due to vigorous mixing conditions employed. For completeness, these tests (13S, 14S & 15S) are included in the detailed experimental data presented in Appendix F.

Table 4.2a Continuous flotation reagent dosages

Test No.	Dosages (g/ton)			
	$CuSO_4$	SIBX/DTP	Acrol	Cresylic Acid
R1	60	60	70	80
R2	60	60	70	80
1 S	50	60	70	100
2 S	50	60	70	100
3 S	50	60	70	100
4 S	50	60	70	100
5 S	50	60	70	100
7 S	90	60	70	100
8 S	90	60	70	100
9 S	90	60	70	100
10 S	90	60	70	100
11 S	90	60	70	100
12 S	90	60	70	100

Table 4.2b Batch flotation reagent dosages

Test no.	Dosages (g/ton)			
	$CuSO_4$	SIBX/DTP	Acrol	Cresylic Acid
1N	50	60	70	100
2N	90	60	70	100
3N	90	60	70	100
4N	90	60	70	100

Table 4.3 Operating conditions for batch and continuous tests

BATCH			CONTINUOUS		
Test no.	Froth height (cm)	Air rate (ℓ/min)	Test no.	Froth height (cm)	Air rate (ℓ/min)
1N (x3)	7	140	R1	7	140
2N (x6)	7	160	R2	7	140
3N (x4)	7	160	1 S	7	140
4N (x1)	2.5	160	2 S	7	160
			3 S	7	180
			4 S	7	140
			5 S	7	180
			7 S	7	160
			8 S	7	180
			9 S	7	140
			10 S	7	160
			11 S	7	180
			12 S	7	140

4.5.4 Bubble size measurements

The froth modelling methodology proposed in Chapter 2 uses a bubble surface area flux parameter, S_b, which is a function of bubble size. As such, it was necessary to perform bubble size measurements on the 60 ℓ cell. The UCT bubble sizer, described in Chapter 3, was used to measure bubble size distribution in the collection zone. This was carried out at different operating conditions in the presence of all the chemical reagents used during flotation. A detailed description of how bubble sizes are measured in industrial flotation cells is given in Deglon (1998) and Gorain (1998). The results obtained from the 60 ℓ cell are presented in Table 4.4.

Table 4.4 Bubble surface area flux results

Test	Airflow (L/min)	Mean d_b (mm)	Bubble size deviation from the mean (mm)	S_b (1/min)
1*	120	1.4230	0.7684	2969.40
2*	140	1.6420	0.7498	3001.80
3*	160	1.7067	0.7576	3300.60
4*	180	1.8568	0.7532	3413.40
5**	120	1.3925	0.6465	3034.20
6**	140	1.5593	0.7214	3160.80
7**	160	1.7756	0.8166	3172.80
8**	180	1.9213	0.7948	3298.80

* Frother dosage = 80 g/ton

** Frother dosage = 100 g/ton

4.5.5 Residence Time Distribution measurements

The residence time distribution (RTD) of a flotation cell is a characteristic of the mixing that occurs in the flotation cell. The residence time distribution of particles within the pulp and froth phases significantly affects flotation performance. In this study, RTD tests were conducted on the 60 ℓ cell in order to: (i) verify that the mixing in the 60 ℓ flotation cell can be well approximated as an ideal continuously mixed reactor, and (ii) compare the calculated pulp residence time, based on tails flow rate, with measured mean cell residence time.

The RTD measurements were performed by introducing a tracer (Sodium Chloride) to the flotation cell feed stream. A conductivity meter was used to measure the history of tails stream conductivity before and after the introduction of the tracer at different time intervals. The conductivity readings were then converted to concentration values, which were used to calculate the mean residence time. The method described in Fogler (1992) was followed for determining the residence times. Figure 4.6 shows the results obtained. The mean residence time obtained over the range of conditions tested was found to be very close to the expected value of 6 minutes, based on the total volume of the cell (60 ℓ) and the average feed flow rate of 10 ℓ/min. From Figure 4.6 it can be seen that the measured RTD function resembles that one of a perfect mixer. The mean residence times obtained at various air flow rates are shown in Table 4.5.

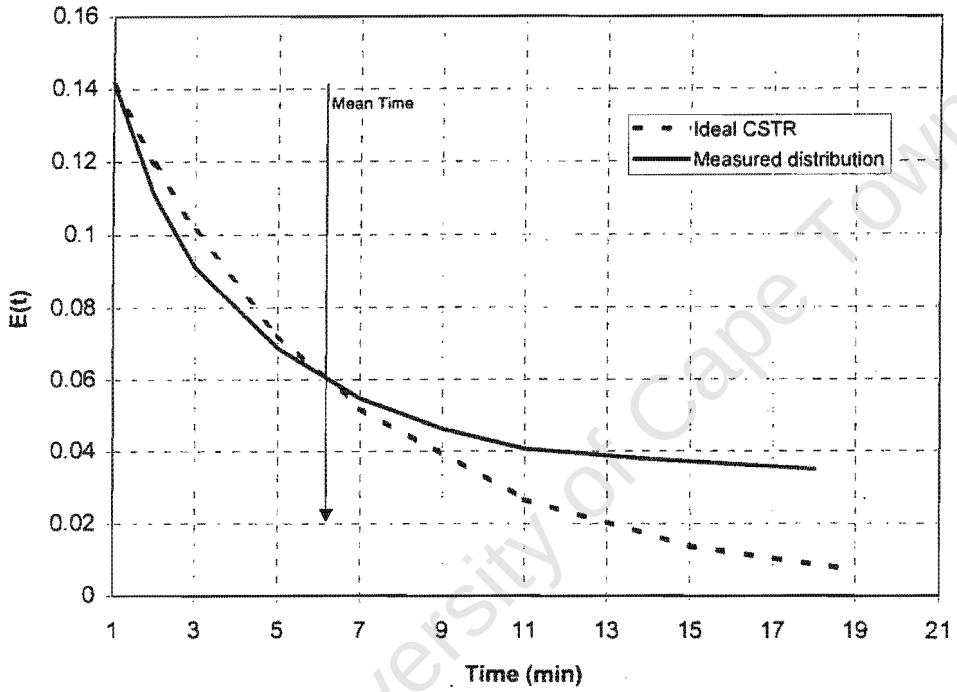

Figure 4.6 Residence time distribution in a 60 ℓ flotation cell

Table 4.5 Measured mean residence times at different air flow rates

Airflow (ℓ/min)	Mean Residence Time (min)
140	5.90
160	5.83
180	6.66
Average	6.13

4.6 EXPERIMENTAL RESULTS AND DISCUSSION

4.6.1 Exploratory Tests

4.6.1.1 Reproducibility

Table 4.6 shows the reproducibility for the continuous and batch flotation tests in a 60 ℓ cell. Although reproducibility is often very poor when floating plant ore, the results obtained were regarded as satisfactory. Reproducibility for batch tests was better than that one of the continuous tests. This observation can be associated with difficulties experienced in trying to operate the system at steady states.

Table 4.6 Reproducibility tests

	Continuous			Batch (after 7 minutes)		
Assay Type	Recovery (%)		STDEV (%)	Cum Recovery (%)		STDEV (%)
	Test R1	Test R2		Test 1	Test 2	
Nickel	52.71	43.12	6.78	39.50	39.00	0.35
Copper	50.15	49.69	0.33	40.00	38.00	1.41
Sulfur	43.17	39.24	2.77	45.00	49.00	2.83

4.6.1.2 Assays

All samples submitted to Impala Platinum Laboratory were analysed for total Ni, Cu, Cr_2O_3 and, where sufficient mass was available, pgms. Total sulphur analysis was obtained for each sample at UCT using a LECO sulphur analyser. Selected samples were also analysed for total iron content at UCT. Assays give a good indication of the flotation response of different minerals. For instance, Ni is associated with pentlandite, copper is associated with chalcopyrite, and Cr_2O_3 is associated with chromite. Chromite is a gangue mineral which is known to be recovered almost exclusively by entrainment, and therefore Cr_2O_3 is a good indicator of the contribution of entrainment. The flotation response of suphur serves as a good indicator of the flotation response of all base metal sulphides (BMS) minerals. Fe is present both as sulphide, mainly pyrrhotite, but also in a variety of the gangue minerals. This makes it difficult to use the total Fe content which would generally be measured using laboratory methods. A portion of these results is shown in Table 4.7. Detailed results are presented in Appendix G. In general, the head samples had a fairly similar elemental composition, with an average Ni composition of about 0.13%, 0.07% Cu, 1.25% Cr_2O_3 and 0.35% S. For all the measured elemental compositions, the standard deviation was less than 10% (see Table 4.7).

The concentrate and tail assays, however, varied, depending on the operating conditions. Generally, increase in air flow rate, at constant chemistry, increased the mass pull of different elements at the expense of grade (see Table 4.8). Decrease in froth height is expected to have a similar effect of decreasing grade whilst increasing the elemental mass pull. In the case of batch tests, the elemental grades of the concentrate decreased with flotation time (Table 4.9), indicating more recovery of gangue with an increase in flotation time.

Table 4.7 Elemental compositions in the head samples

	Test Number							Deviation (%)
Assays	R1	R2	1S	2S	3S	4S	5S	
Cu	0.083	0.099	0.071	0.074	0.054	0.081	0.085	0.015
Ni	0.120	0.135	0.139	0.142	0.113	0.162	0.184	0.024
S	0.410	0.410	0.368	0.376	0.220	0.261	0.380	0.075
Cr_2O_3	1.25	1.25	0.99	0.91	2.41	2.46	1.38	0.645

Table 4..8 Effect of increasing air flow rate on the concentrate grade

Test Number	Operating conditions			Head			Conc			Tails		
	Froth Height (cm)	Air Rate (ℓ/min)	Feed %solid	Cu	Ni	Cr_2O_3	Cu	Ni	Cr_2O_3	Cu	Ni	Cr_2O_3
R1	7	140	32.59	0.083	0.120	1.25	5.37	8.16	0.52	0.062	0.093	2.37
1S	7	140	38.35	0.071	0.139	0.99	6.38	8.28	0.23	0.038	0.118	0.94
2S	7	160	41.23	0.074	0.142	0.91	2.84	5.07	0.42	0.055	0.103	2.25
3S	7	180	41.46	0.054	0.113	2.41	1.47	2.75	1.43	0.020	0.059	2.54
4S	7	140	41.92	0.081	0.162	2.46	4.63	7.30	0.52	0.023	0.060	2.37
5S	7	180	38.62	0.085	0.184	1.38	13.55	15	0.30	0.023	0.130	1.30

Table 4.9 Variation of elemental composition with flotation time in a batch test

Test	Sample	Cu	Ni	Cr_2O_3
1N	Head	0.09	0.13	1.25
	C1	2.55	4.70	0.38
	C2	1.00	1.85	0.40
	C3	0.80	1.19	0.42
	C4	0.76	1.00	0.40

4.6.1.3 Flotation response

Table 4.10 indicates that Cu, Ni, Cr_2O_3 and S recoveries and grades for the continuous tests conducted at air flow rates of 140, 160 and 180 ℓ/min, whilst the froth height was kept constant at 7 cm. At an air flow rate of 140 ℓ/min, Cu and Ni were recovered in significant proportions when compared to Cr_2O_3. As the air flow rate increased from 140 to 160 ℓ/min, the recovery of all elements increased. At the same time, the grade of Cu, Ni, and S decreased.

More interesting in Table 4.10 is the observation that the grade of Cr_2O_3 increased with an increase in air flow rate. To some extent, this indicates that chromite is recovered predominantly via entrainment mechanism.

Table 4.10 Effect of increasing air flow rate in continuous tests

Test	Air Rate	Recovery (%)				Conc Grade (%)			
	(ℓ/min)	Cu	Ni	Cr_2O_3	S	Cu	Ni	Cr_2O_3	S
1 S	140	44.82	29.71	0.12	32.19	6.38	8.28	0.23	23.75
2 S	160	45.53	42.36	0.55	51.27	2.84	5.07	0.42	16.25
3 S	180	52.01	46.50	1.13	70.52	1.47	2.75	1.43	8.12

In the case of batch tests, Figure 4.7 shows the flotation response of different elements. It can be seen that nickel floats faster than copper and iron, iron being the least floatable element. To the contrary, the results obtained from the continuous tests showed that copper floats faster than nickel. Given the fact that this data was collected on-site, a number of factors, such as feed particle size distribution, percentage solids in the feed, froth retention time, etc, could have contributed to this discrepancy. For instance, a comparison between percentage solids found in batch concentrates and percentage solids found in continuous tests showed that the percentage solids in batch concentrates was lower than the one found in concentrates from continuous tests. Since the data depicted in Figure 4.7 represents the global response of the floatable elements, it is not clear how the froth phase behaviour impacts on these results. More insight with this regard can be obtained if the froth phase behaviour is decoupled from that of the pulp phase. To achieve this, the proposed froth modelling methodology and froth recovery equation developed in Chapter 3 are used in the following sections to gain more insight into the influence of the froth phase in flotation. Firstly, the flotation results obtained from the tests used in the modelling are discussed in the next section. This is followed by a discussion on the modelling results in section 4.7.

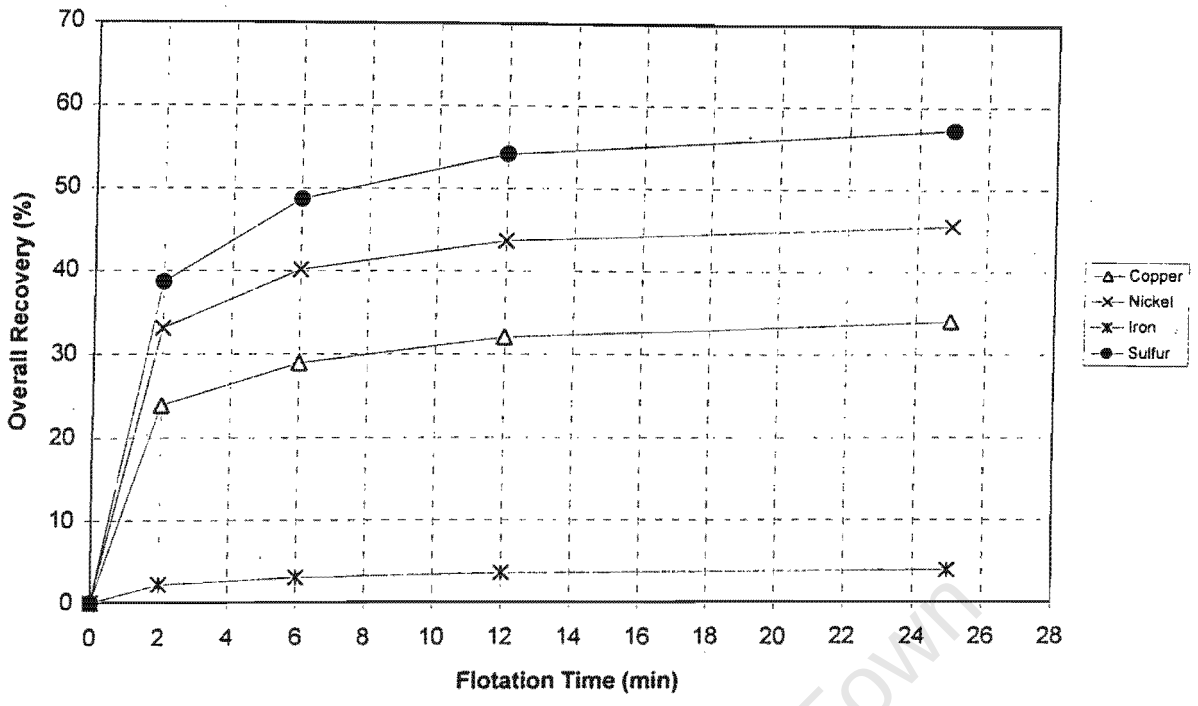

Figure 4.7 Flotation response of different elements

4.6.2 Modelling flotation tests

4.6.2.1 Mineralogical results

Table 4.11 shows a summary of the mineral abundance data. In the head samples, a significant proportion of the samples consisted of silicates (approximately 95%). In the concentrate samples, however, silicates composition was less (approximately 75%). In the BMS group, the Fe-Sulphides existed in significant proportions when compared to Pentlandite, Chalcopyrite and other sulphides. This observation applies to both head and concentrate samples. Detailed mineral abundance data for all samples analysed by Billiton Laboratories are shown in Appendix H.

Particle size distribution (shown in Table 4.12) indicates that concentrate samples had a significant amount of mass in the fine size class (sub 10 microns). In turn, the fine size class had a significant amount of Fe-S when compared with the other sulphide minerals (see Table 4.13). This, to some extent, indicated that Fe-S grains recovered into the concentrate launder were mostly liberated. Approximately 70 % by volume of the Fe-Sulphides, Pentlandite, and Chalcopyrite were at least 90 % liberated in the concentrate samples. This differed significantly when the 100% liberated (monominerallic) fraction was considered. Pentlandite was the least liberated, followed by chalcopyrite (Table 4.14). The fully liberated fractions of some sulphide minerals increased slightly in the concentrate samples. The procedure used to

calculate these fully liberated fractions is outlined in Appendix I. The fractions of the fully liberated (monominerallic) particles, by size, are shown in Appendix J.

Table 4.11 Summary of sulphide minerals abundance

Mineral	Head		Conc	
	10 S	12 S	11 S	12 S
Chalco	0.19	0.19	4.72	10.85
Pent	0.30	0.33	8.04	18.27
Fe-S	0.42	0.45	9.63	18.69
Other sulphides	0.02	0.02	0.15	0.31
Silicates	95.26	94.63	75.69	48.73

Table 4.12 Particle size distribution

Size (microns)	10 S Head	12 S Head	11 S Conc	12 S Conc
Plus 425	0.4	0.0	0.0	0.0
212 to 425	5.1	6.1	4.7	3.5
106 to 212	24.7	26.1	4.1	4.9
53 to 106	29.2	29.1	6.9	11.2
25 to 53	17.5	16.1	12.0	16.1
10 to 25	6.8	7.8	13.7	16.9
2 to 10	16.3	14.8	58.5	47.5

Table 4.13 Fully liberated fractions of sulphide minerals

Monominerallic Mineral	Conc							
	11 S				12 S			
	+106	+53	+25	+10	+106	+53	+25	+10
Fe-Sulphides	6.8	15.9	35.2	58.3	3.3	18.6	33	54.2
Pentlandite	0	1.3	2.8	6.5	0	2.5	2	4.6
Chalcopyrite	3.3	5.7	1.3	26.3	0.3	4	9.6	15.3

Table 4.14 Calculated fractions of fully liberated sulphide minerals

Continuous Tests

Mineral	Head	Conc
Fe-S	0.43	0.51
Pent	0.08	0.07
Chalco	0.11	0.15

Batch Tests

Sample	Chalco	Pent	Fe-S
Head	0.12	0.08	0.46
Conc 1	0.14	0.06	0.51
Conc 2	0.15	0.04	0.56
Conc 3	0.09	0.03	0.48

The calculated average particle sizes of the fully liberated fraction were found to be 8.5 μm for Fe-S, 10 μm for Pentlandite and 12 μm for Chalcopyrite. Since it was established during the exploratory tests, Fig. 4.7, that Fe-Sulphides float at a slower rate, it is to be expected that a significant proportion of Fe-S grains would be transferred from pulp to froth via an entrainment mechanism. If chalcopyrite and pentlandite grains remain attached to bubbles within the froth, one would expect the draining floatable material to consist mainly of Fe-S grains, which in turn can lead to low overall recoveries of Fe-S. These issues, however, will never be completely resolved if the flotation process is continued to be studied using global flotation parameters, such as the overall flotation rate constant. To achieve better understanding of the behaviour of the minerals within the froth phase, their behaviour in the froth phase must be decoupled from that in the pulp phase.

4.6.2.2 Correlation between calculated and measured mineral compositions

As there were few samples analysed by Billiton for mineral compositions, it was considered necessary to convert elemental assays to mineral composition for use in the analysis of the effect of operating parameters and froth modelling. Stoichiometric coefficients of Ni, Cu, Fe and S were used to convert assay data to mineral compositions. All copper was assumed to be associated with chalcopyrite, which then allowed for the estimation of the sulphur associated with chalcopyrite. Nickel associated with pentlandite was determined by assuming that approximately 30% of nickel in the feed is associated with gangue. Residual sulphur, calculated by subtracting sulphur associated with pentlandite and chalcopyrite from total sulphur, was assumed to be associated with iron-sulphides. Detailed assumptions involved in this procedure are outlined in Appendix K. A comparison of the calculated and measured mineral compositions is shown in Table 4.15 below. It can be seen from this table that the correlation of the calculated and measured compositions was satisfactory. For the sake of comparison, the data in Table 4.15 is graphically represented in Figure 4.8, where it can be seen that the correlation of chalcopyrite and Fe-Sulphides mineral compositions was better than that one of pentlandite. The correlation co-efficients for chalcopyrite, pentlandite and iron-sulphides data were found to be 0.98, 0.94 and 0.97, respectively. The calculated compositions were then used to calculate recoveries of the sulphide minerals, viz. chalcopyrite, pentlandite and Fe-sulphides. The effect of froth height and particle size on the recovery of sulphide minerals is discussed next.

Table 4.15 Correlation of the calculated and measured mineral compositions

Continuous

Test		Chalco		Pent		Fe-S	
		QEM*SEM	CALC	QEM*SEM	CALC	QEM*SEM	CALC
10S	HEAD	0.19	0.18	0.3	0.21	0.42	0.48
	CONC	4.81	7.08	8.09	13.82	9.49	8.94
11S	HEAD		0.20		0.26		0.43
	CONC	4.72	4.25	8.04	7.98	9.63	7.04
12S	HEAD	0.19	0.19	0.33	0.25	0.45	0.44
	CONC	10.85	10.77	18.27	22.01	18.69	17.67

Batch

Test		Chalco		Pent		Fe-S	
		QEM*SEM	CALC	QEM*SEM	CALC	QEM*SEM	CALC
2N	Head	0.16	0.21	0.3	0.27	0.47	0.51
	Conc1	9.2	10.05	17.77	20.55	23.33	22.25
	Conc2	5.1	5.34	8.48	9.89	16.32	14.61
	Conc3	2.48	2.54	3.49	4.60	8.78	7.06

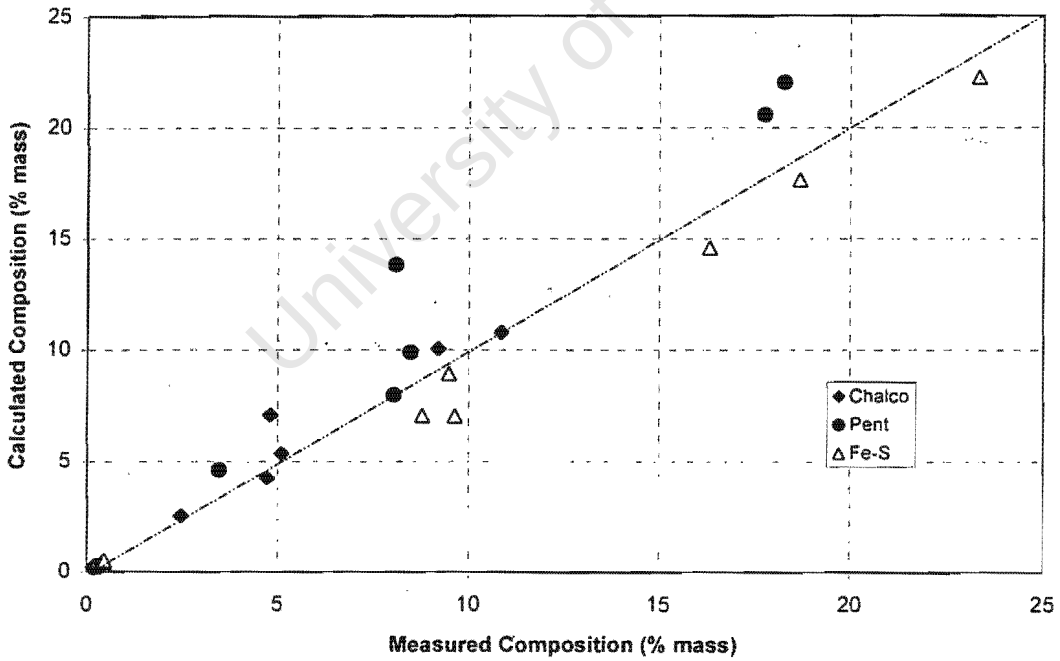

Figure 4.8 Correlation between calculated and measured compositions

4.6.2.3 Flotation response

At shallow froth, the initial flotation response of the three sulphides minerals was the same, whilst pentlandite was recovered in significant proportion with increase in flotation time (Figure 4.9). For deep froth, however, chalcopyrite and Fe-sulphides floated slower than pentlandite (Figure 4.10).

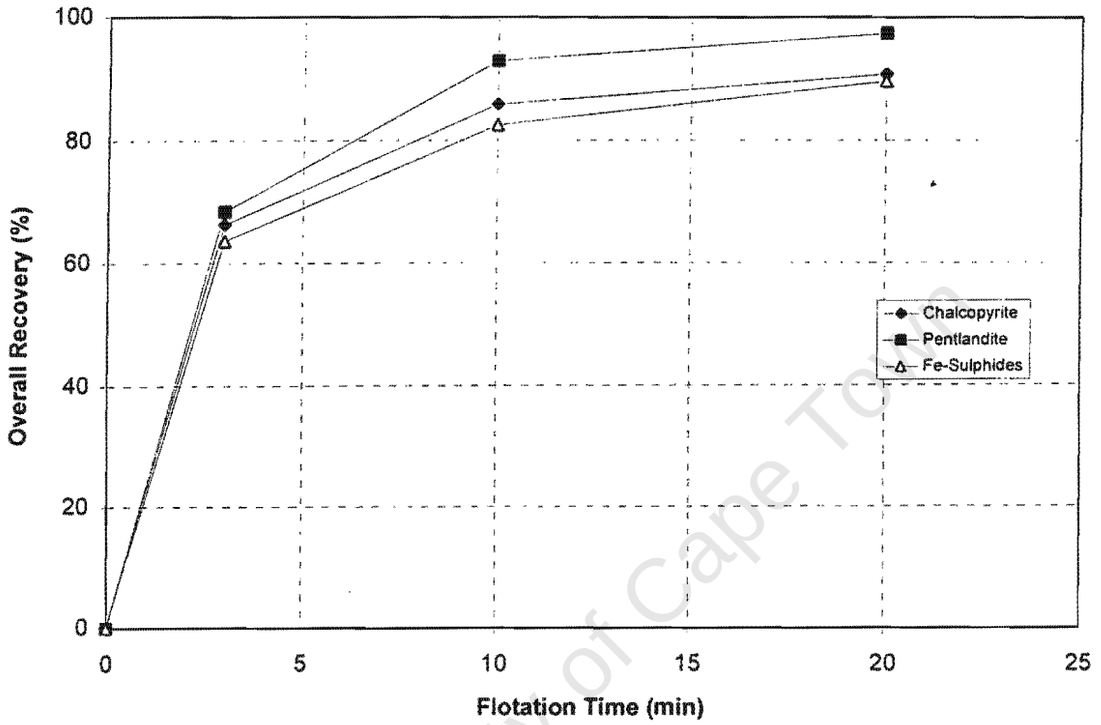

Figure 4.9 Flotation response of sulphide minerals at shallow froth

Figure 4.11 shows the effect of particle size on the sulphide mineral overall flotation rate constant, calculated using equation (1.3), for various sizes. From Figure 4.11, there seems to be an optimum size range where most of the minerals float fast. However, the optimum size range for chalcopyrite seems to be slightly higher than those of pentlandite, iron-sulphides and other sulphide minerals. This could lead to either more chalcopyrite dropping back from the froth phase into the pulp phase if it is loosely attached to bubbles within the froth or more recovery of chalcopyrite within the froth if no detachment of particles takes place. Quantitative evaluation of the behaviour of these minerals within the froth phase, using the froth recovery model proposed in Chapter 3, is considered in section 4.7. In the next section, the traditional approach of using the overall flotation rate constants derived from batch data to predict continuous performance is discussed.

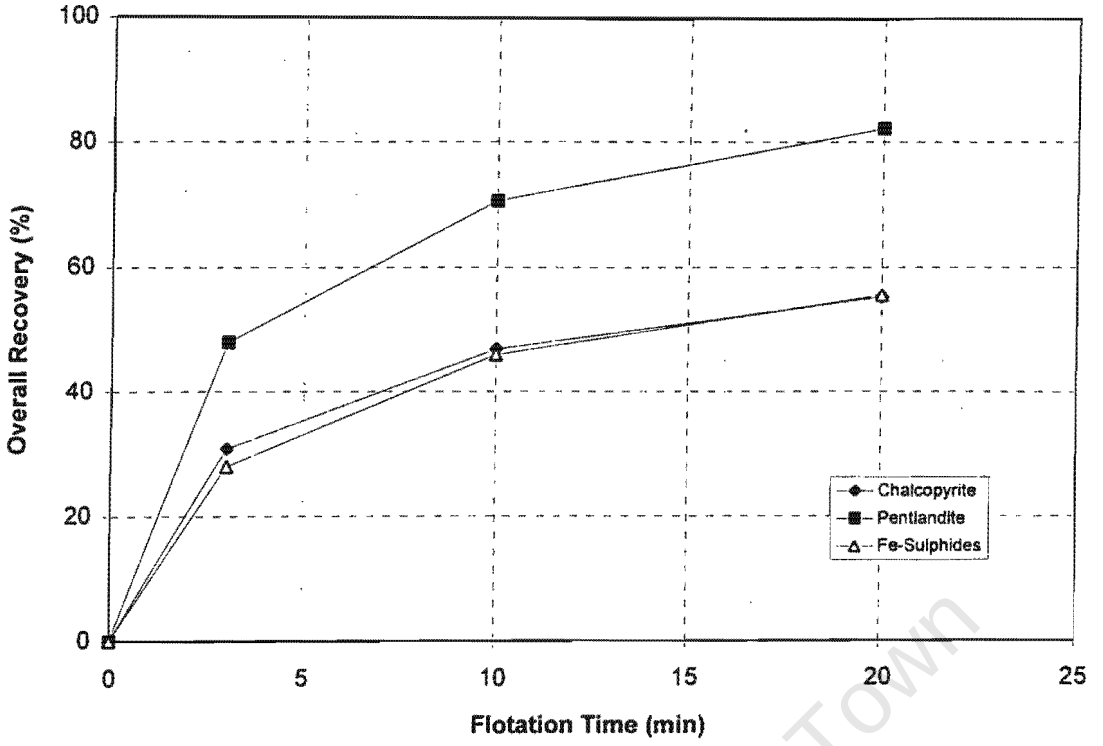

Figure 4.10 Flotation response of sulphide minerals for deep froths

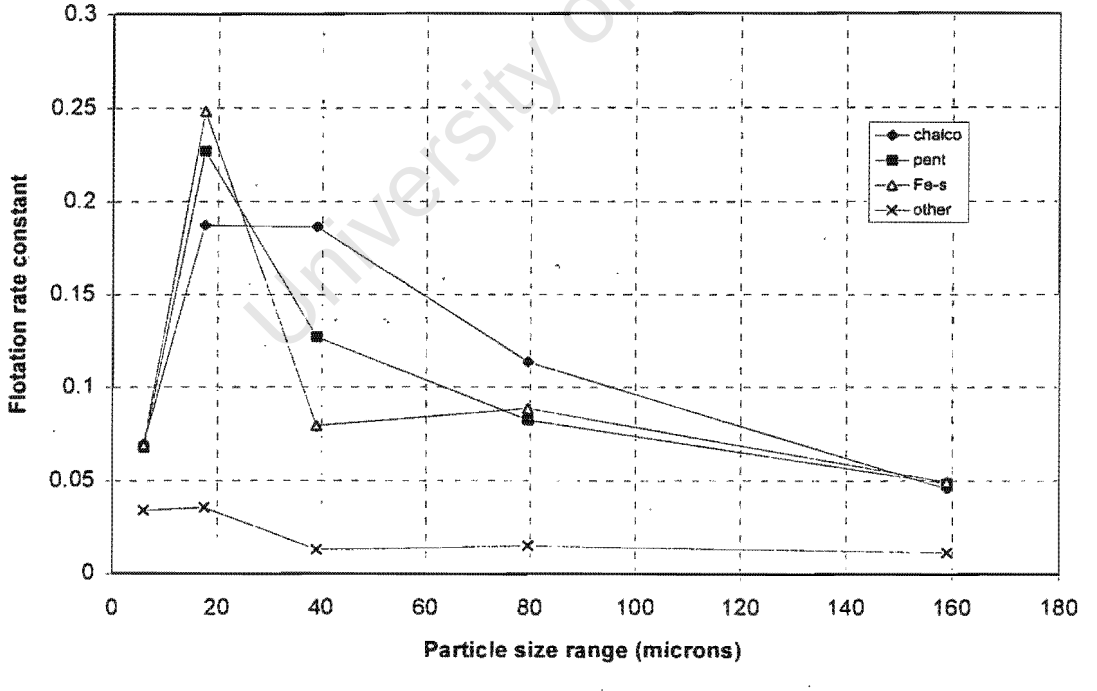

Figure 4.11 Effect of particle size on the sulphide mineral flotation rate constant for various sizes

4.6.2.4 Prediction of continuous flotation performance using overall flotation rate constant derived from batch data

In this section the conventional method of correlating batch and continuous flotation performance using flotation rate constants derived using batch data is used to illustrate its shortcomings. Overall flotation rate constants derived for three particle size ranges (viz. 2 to 10, 10 to 25, and 25 to 53 microns) using batch data (Test 2N) were used to predict overall recovery of different sulphide minerals in these particle size ranges for a continuous test (test 12 S). The measured versus predicted recoveries for test 12 S are shown in Figure 4.12. The scattered data indicates the poor correlation observed from this exercise. It is hypothesised that the poor predictions obtained are associated with the use of the overall flotation rate constant derived from batch data. The overall flotation constant encompasses the influence of the pulp and froth phases. As mentioned in the introduction, the influence of the froth phase in batch flotation cells is significantly different to that one found in continuously operated flotation cells. As such, a successful method for use in correlating batch and continuous flotation performance should decouple the influence of the froth phase on flotation from that of the pulp phase. This is illustrated in the next section.

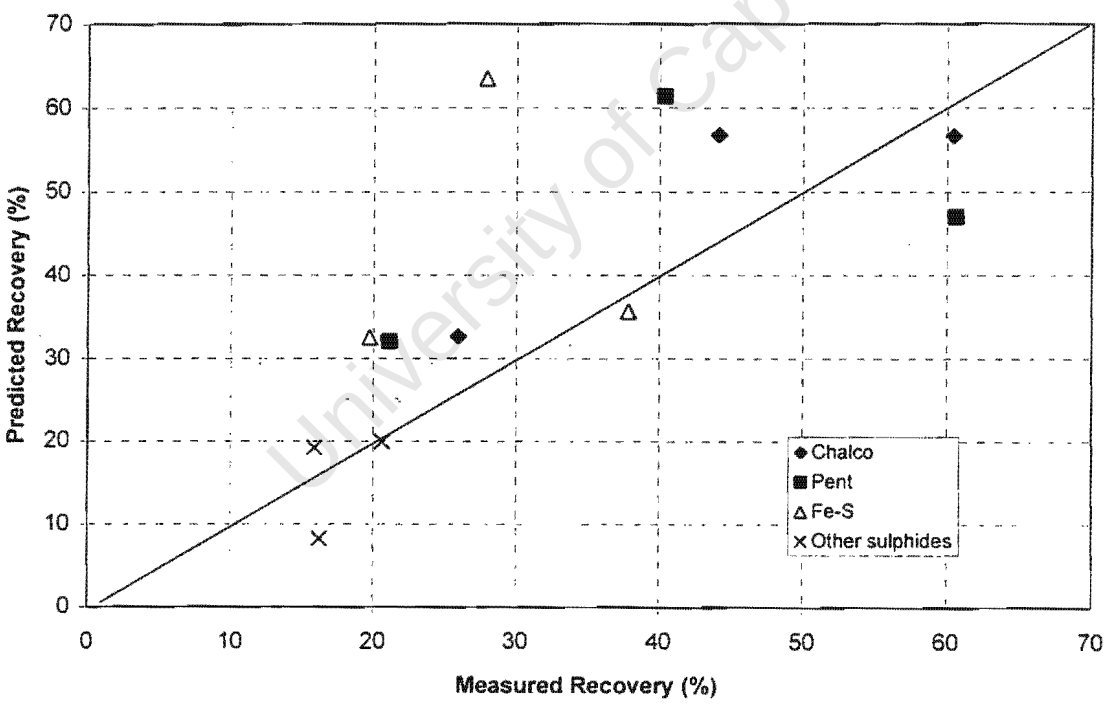

Figure 4.12 **Correlation between measured and predicted overall recovery of sulphide minerals for test 12 S**

4.7 MODELLING RESULTS AND DISCUSSION

4.7.1 Approach

A similar approach used to analyse the influence of the froth phase in the quartz system was adopted here. Insufficient particle size distribution data for some key samples forced the analysis to be limited to lumped particle sizes for pentlandite, chalcopyrite and Fe-S. This was done for the purpose of generating sufficient data points for modelling, which could not be achieved by using QEM-SEM data only. It was decided to limit the modelling to 100% liberated (monominerallic) fractions of pentlandite, chalcopyrite and Fe-Sulphides. The reasoning behind this was that the monominerallic fractions report to the concentrate mainly by true flotation. In addition, it was only possible to calculate the average particle sizes of the fully liberated sulphide minerals in the feed and concentrate samples. This information was required for use in the froth recovery model, which is explicitly expressed in terms of particle size, to estimate froth recoveries of the three sulphide minerals. Limiting the analysis to fully liberated sulphide minerals also allowed for the use of the recovery equations discussed in Chapter 2 to describe the flotation response of these minerals within the pulp and froth phases. It must be pointed out, however, that the proposed equations and froth modelling methodology in Chapter 3 can be applied to other floating classes if sufficient mineralogical data is available. For instance, analysis can be performed using a fully liberated sulphide mineral class, a class of sulphide minerals in binary with gangue, a class of sulphide minerals in composite with gangue, etc. The challenge will be in trying to estimate the specific gravity and average particle sizes of these classes. For the work reported in this chapter, which considers only liberated masses, a procedure showing how the liberated masses of the sulphide minerals were calculated is provided in Appendix I.

Two sets of data from batch and continuous tests carried out at exactly the same chemical conditions, tests 7S to 12S and tests 2N to 4N in Tables 4.1, 4.2 and 4.3, were chosen to test the proposed froth recovery model and a methodology for extracting model parameters. This was done because the froth stability parameter, β, in the proposed froth recovery model is expected to vary with chemistry. As such, suitable data for use in correlating batch and continuous parameters must be at constant chemistry.

As was the case for the quartz system, the required parameters to describe flotation performance in a continuous system were derived from batch data. A spreadsheet was prepared for performing most of the calculations. An outline of the procedure followed during the analysis of batch and continuous data is shown in Figure 4.13.

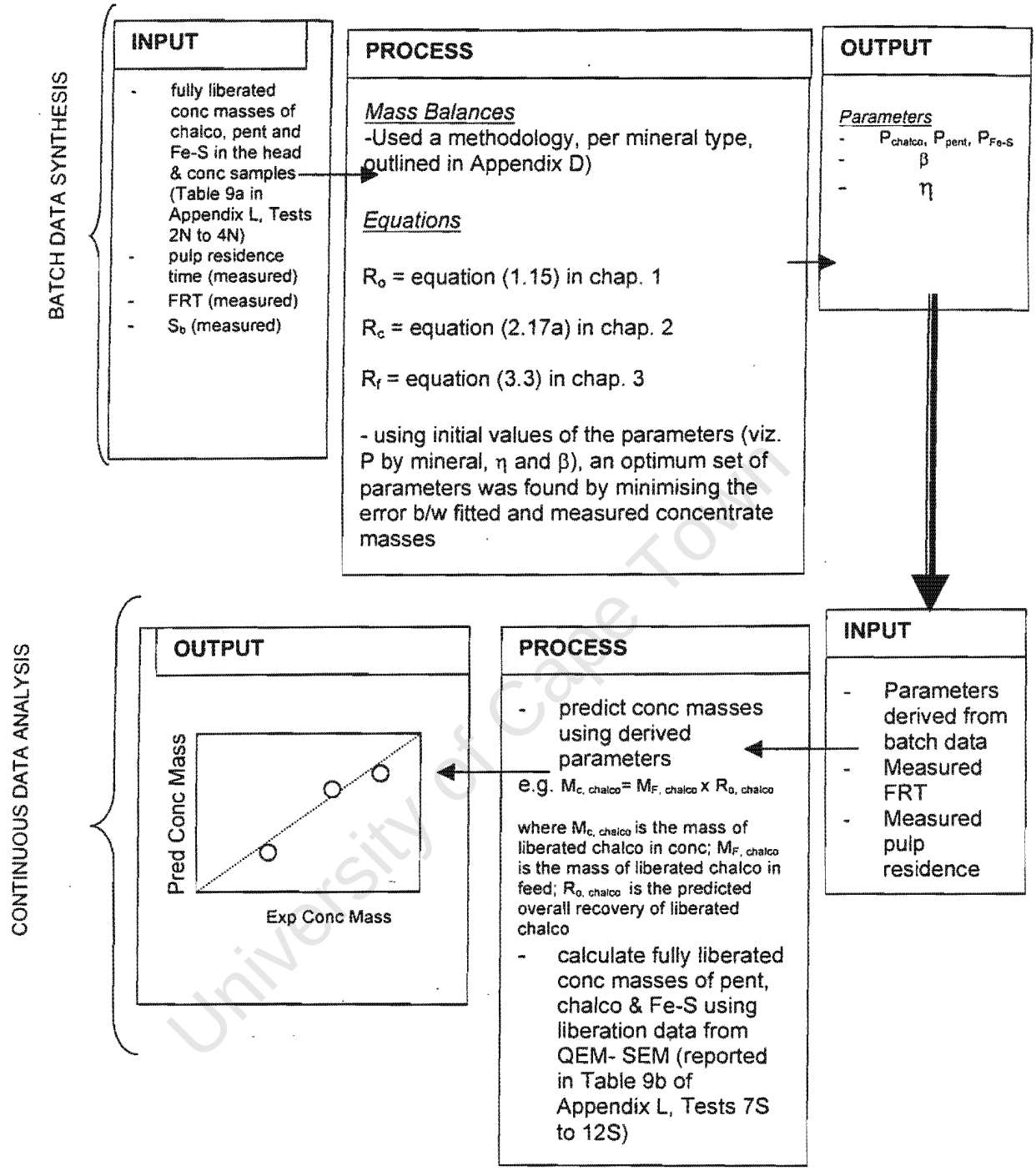

Figure 4.13 **Outline of the procedure followed to correlate batch and continuous performance**

4.7.2 Modelling Results

Figure 4.14 shows the plot of the calculated batch concentrate mineral masses, using parameters derived from batch data, against measured batch concentrate masses. The plotted data points indicate a linear dependence of the predicted values on measured values, with an

average correlation coefficient of 0.9. The parameters derived from this exercise are shown in Table 4.16 below. These parameters were in turn used to predict the flotation performance for the tests carried out continuously. The results of this exercise are reported and discussed in section 4.7.3.2.

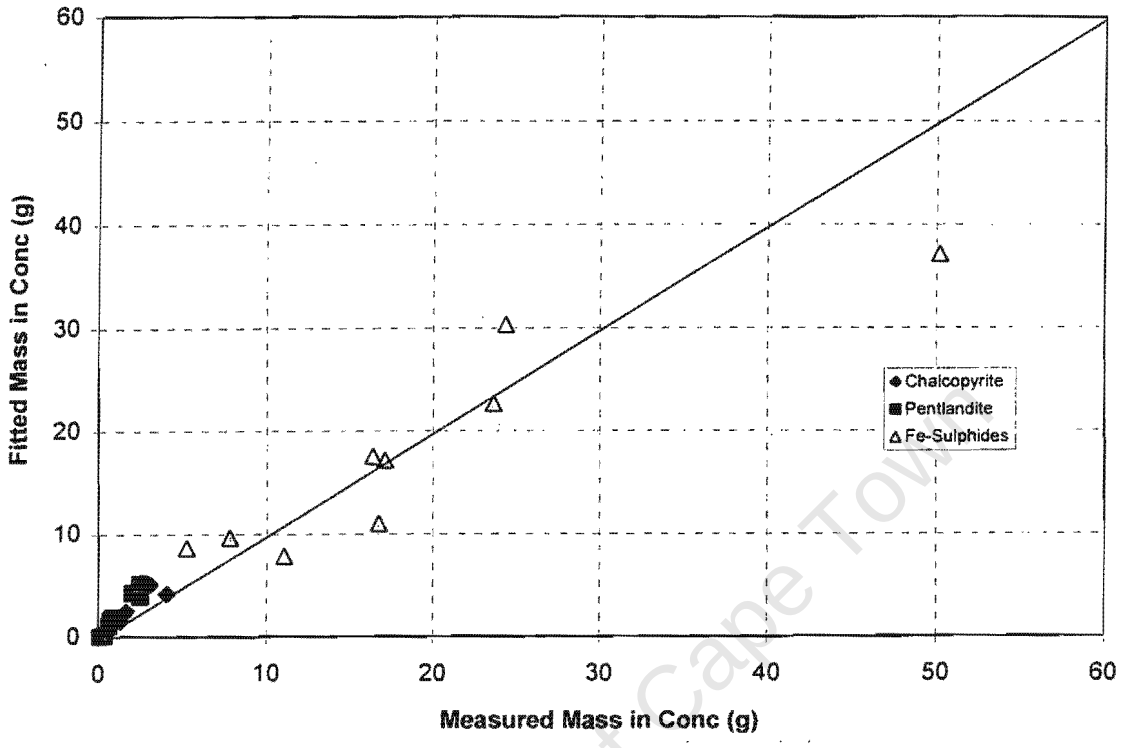

Figure 4.14 **Comparison between fitted and measured mass in concentrate for batch flotation of the Merensky ore in a 60 litre cell**

Table 4.16 **Fitted parameters derived from the Merensky ore system**

Parameters	Derived parameters		
β	0.25		
η	0.12		
	Chalco	Pent	Fe-S
P	6.6 x E-5	9.4 x E-5	2.3 x E-6

4.7.3 Discussion

4.7.3.1 Fitted parameters

The fitted floatability parameter, P, obtained for the three mineral sulphides varied with mineral type. The floatability values for Chalcopyrite and Pentlandite were higher than that of Fe-Sulphides, indicating the fast floating nature of chalcopyrite and pentlandite within the pulp phase. This observation confirms the slow floating behaviour of iron-sulphides.

Froth stability parameter, β, was kept constant throughout the modelling. This parameter, however, represents an average value from batch data. This is because froth stability in a batch cell changes with flotation time. As such, the derived value of 0.25 (1/min) could be an underestimation of the true rate at which bubbles were coalescing. It is therefore very difficult to make any definite conclusions with regard to the significance of this number. Generally, this value indicates that there was very little drainage in the froths found in this work. This could be the result of the high frother dosages used to enhance continuous overflow of the concentrate into the launder.

By the same token, the above argument of changing froth characteristics with flotation time in a batch cell applies equally to the apparent viscosity parameter, which was found to be 0.125 ($N.s/m^2$). It is worth noting, however, that this value is higher than that of water viscosity. This, to some extent, indicates that this parameter has a potential meaning.

4.7.3.2 Prediction of continuous performance from batch derived parameters

The parameters derived from batch data were used to predict the flotation performance of the tests carried out when the cell was operated continuously. Figure 4.15 indicates a slight scattering of data ($r^2 = 0.9$) in the correlation between predicted and measured concentrate masses of the fully liberated sulphide minerals. Firstly, this can be associated with the average values of the froth stability and the apparent viscosity parameters derived from batch data. Secondly, the experimental errors associated with collecting data on plant site can be very significant in this type of work. In addition, the estimation of the fully liberated masses, based on average values obtained from samples analysed for mineral liberation, might not have been very accurate for some samples. Clearly, this represents the major source of errors in this type of work, and perhaps the biggest challenge toward validating proposed froth recovery models in the literature. When dealing with complex ores, liberation data seem to be one of the key information required to perform the analysis proposed in this work, which obviously requires more refinement of the current approach. Insufficient data prevented the analysis of the current work by liberation, size and mineral type. Nevertheless, some useful information was obtained from the limited data set used for modelling, and the findings are discussed next.

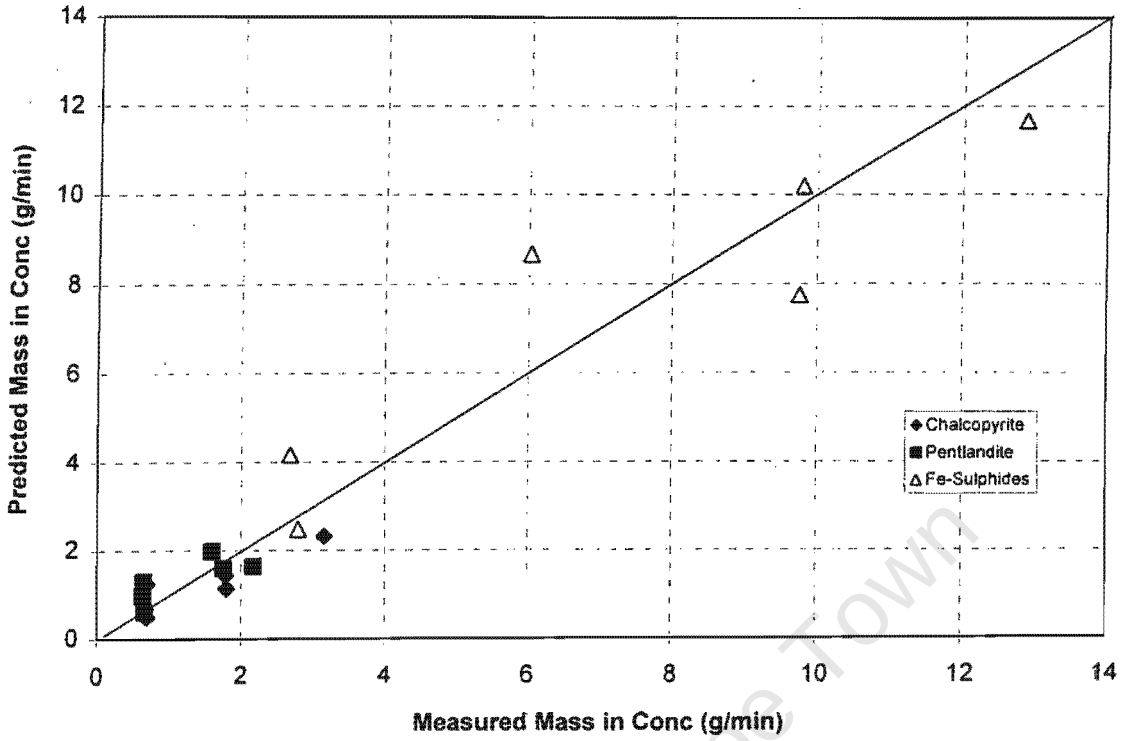

Figure 4.15 Prediction of continuous performance from batch derived parameters in a 60 litre flotation cell

4.7.3.3 Prediction of froth recovery behaviour

Fig 4.16 shows the plot of froth recovery against froth retention time for the three minerals studied in this system. The symbol marks on this figure do not represent data points. They are included to merely facilitate comparison between the curves. As expected, Fig. 4.16 indicates no significant differences in the froth recovery values of the fully liberated chalcopyrite, pentlandite and Fe-Sulphides masses. This data was statistically tested and indeed proved that there is no difference among the chalcopyrite, pentlandite and Fe-sulphides froth recovery curves. This observation was not suprising since the mineral density of these sulphide minerals are very close to each other.

Figure 4.17 shows the plot of predicted froth recovery of sulphide minerals, represented by chalcopyrite, versus froth retention time per size of the fully liberated mineral grains. From Fig. 4.17, it is clear that an increase in particle size has a negative effect on froth recovery, particularly at high froth retention times (i.e. deep froths). A similar behaviour of the froth recovery as a function of froth retention time, per size, was observed for pentlandite and iron-sulphide minerals.

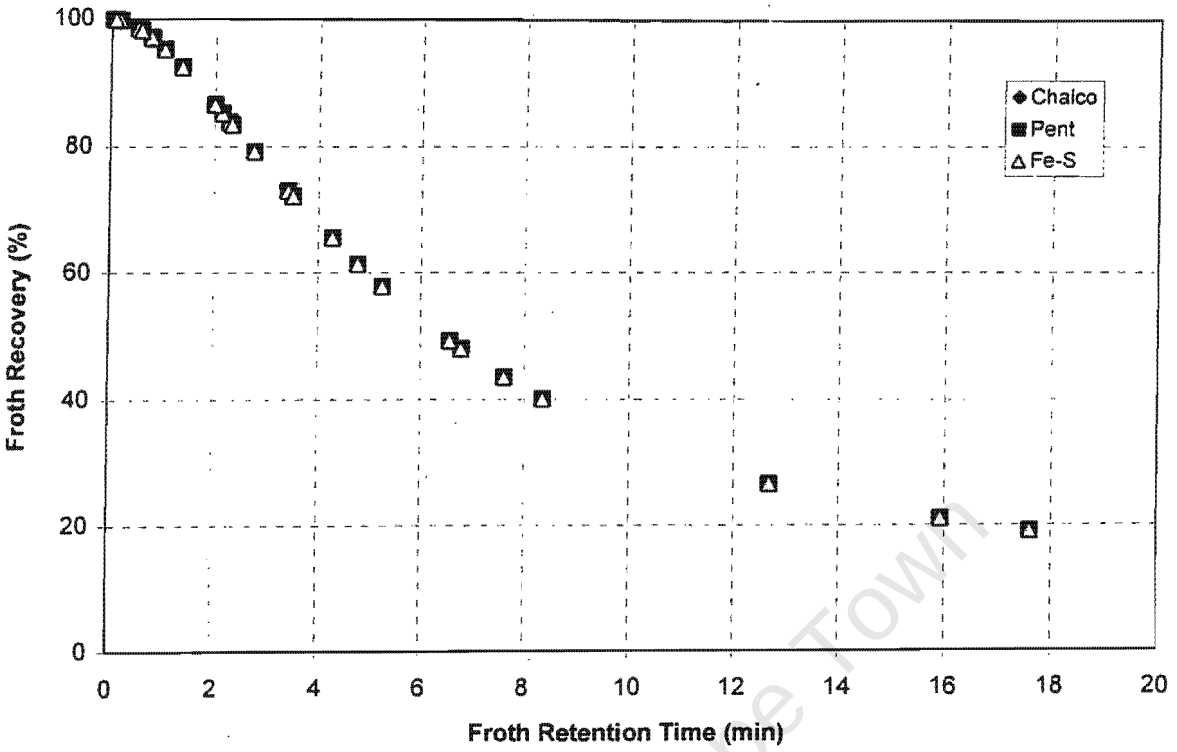

Figure 4.16 Combined froth recovery behaviour in both batch and continuous tests for the Merensky system

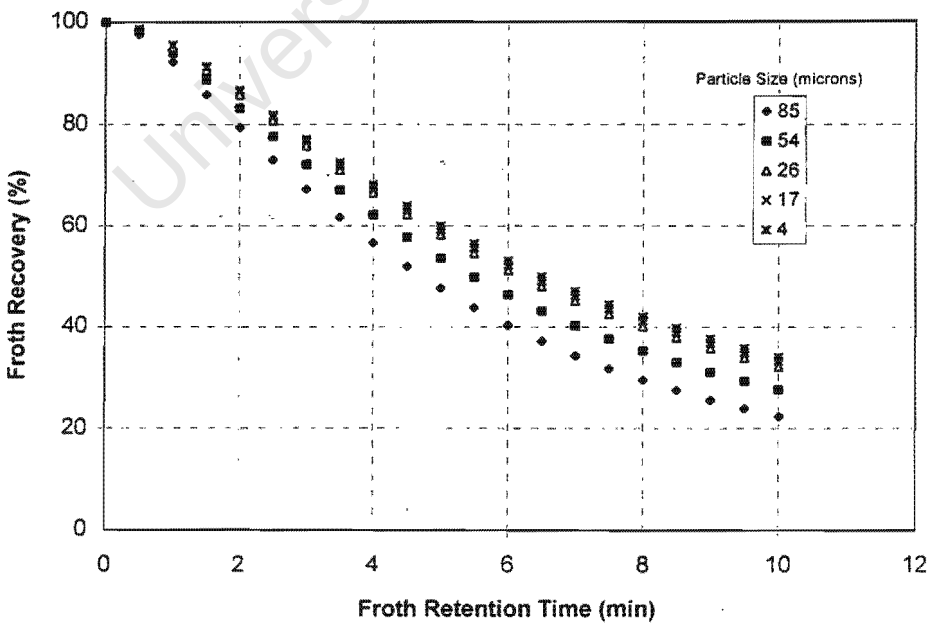

Figure 4.17 Predicted froth recovery of chalcopyrite, per size, as a function of froth retention time

Furthermore, the derived froth parameters were used to predict the froth recovery of the chromite mineral, assuming that most chromite grains are liberated. The observed froth recovery versus froth retention time curve of the chromite mineral is shown in Figure 4.18. Again this figure indicates that an increase in particle size has a negative effect on froth recovery, even for the minerals that are transferred from the pulp phase to the froth phase via entrainment. For the sake of comparison, the predicted froth recovery versus froth retention time relationship for the floating and entrained particles, within the same particle size range, are plotted on the same graph (see Figure 4.19). From Figure 4.19, it can be seen that chromite mineral, which is slightly denser than the sulphide minerals, has a relatively low froth recovery when compared to the sulphide minerals at the same froth retention time value. However, the difference between the froth recovery values of chromite and the sulphide minerals decreases with an increase in froth retention time, indicating a possibility of the froth recovery of the valuable and gangue minerals approaching the same value at deep froths.

To illustrate the influence of the observed froth behaviour on the overall mineral recovery, the predicted overall recovery (using equation 1.15) and the froth recovery of the sulphide minerals, represented by chalcopyrite, is plotted against cell number, for test 1N, in Figure 4.20. Predicted chromite froth recovery and the calcuated overall recovery of chromite are also included on the same plot for purposes of comparison. In Figure 4.20, it can be seen that the froth recovery of the sulphide minerals and chromite decreased with stage or flotation time interval. For the sulphide minerals, a decrease in froth recovery with stage resulted in a decrease in the overall recovery. For chromite mineral, however, it appears as if a decrease in froth recovery with stage has very little effect on the overall recovery of chromite per stage. This is because the recovery of chromite, which is a gangue mineral, is driven by water recovery. Therefore, it can be concluded that if one is interested in minimising the recovery of chromite, a reduction in water recovery might be the answer. This implies operating the flotation cells with deep froths. Since high froth retention times also lead to loss in recovery of desired minerals, operating the cell at moderate froth retention times appears to be the best option.

Industrial flotation cells are operated under conditions that give rise to a wide range of froth retention times, which often do not represent optimum conditions for the froth phase. Typically, froth retention times in platinum flotation cells range between 1 to 18 minutes (Theron, 1998). This is assuming a gas hold-up of approximately 90% within the froth phase. It is believed that the proposed froth modelling and analysis approach outlined in this study could be very useful with regard to establishing optimum conditions for the froth phase in industrial flotation cells.

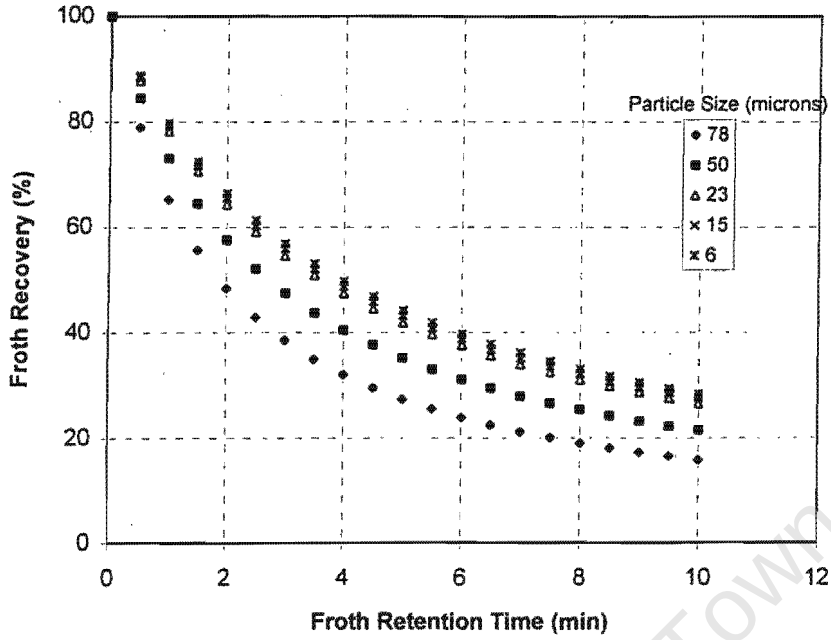

Figure 4.18 Predicted froth recovery of chromite, per size, as a function of froth retention time

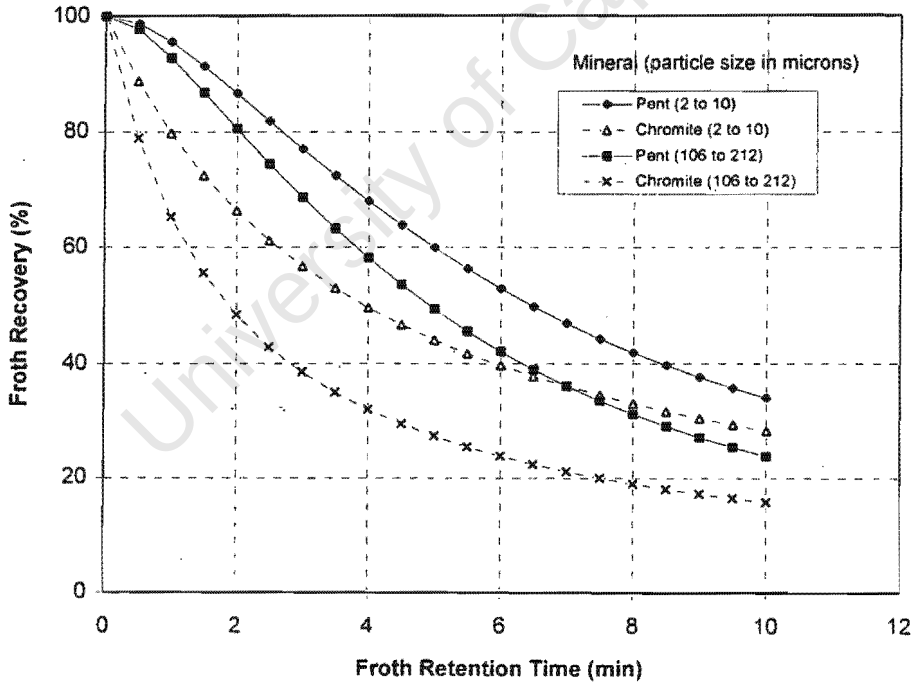

Figure 4.19 Predicted froth recovery for pentlandite and chromite minerals versus froth retention time

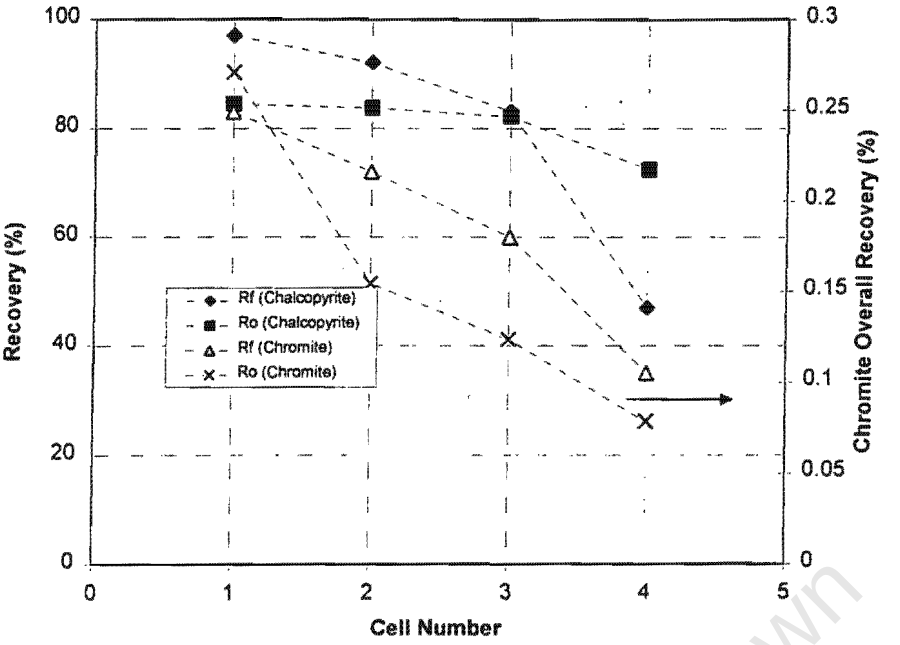

Figure 4.20 **Overall and froth recovery of chromite and chalcopyrite per batch flotation stage**

4.8 SUMMARY

In this chapter the froth recovery model developed in Chapter 3, and the methodology for extracting model parameters proposed in Chapter 2, were tested using a complex ore. Batch and continuous tests were conducted using a 60 ℓ flotation cell on plant site, floating a Merensky ore, with a view of correlating kinetic parameters derived from batch data with continuous flotation performance. The complexity of the mineralogy of the chosen ore necessitated that the analysis be limited to fully liberated sulphide minerals.

Results obtained from this system indicate that chalcopyrite, pentlandite and Fe-Sulphide minerals seem to have similar froth recoveries, at least for the fully liberated mass fractions. Most importantly, it was again shown that froth parameters derived from batch data can be used to predict froth performance in a continuous cell. Furthermore, the application of the proposed froth modelling methodology showed that it has a potential use in studying the influence of the froth phase in flotation.

Whilst the proposed froth modelling methodology and froth recovery model seem to be applicable to real ore analysis, the amount of information required to implement this approach is overwhelming. Firstly, dry samples need to be analysed for elemental compositions, per particle size class. Secondly, some information about locking associations of sulphide minerals needs to be obtained, using very expensive and time consuming technique (QEM-

SEM). The other complication is that the mineralogical compositions of the head samples vary with time. Furthermore, the mineralogical compositions of the concentrate samples is also expected to vary with operating conditions such as air flow rate, chemical dosages, etc, all of which require QEM-SEM analysis of each and every sample to achieve accurate predictions.

Despite the above obvious drawbacks when dealing with a real ore, this work is seen as a very valuable exercise which can potentially form a basis for any future work on correlating batch derived parameters to continuous flotation systems. However, a refinement of the proposed froth recovery model and the methodology for extracting model parameters is required. Recommendations on how this could be achieved are discussed in the next chapter.

CHAPTER 5

Concluding Remarks and Recommendations

CHAPTER 5: CONCLUDING REMARKS AND RECOMMENDATIONS

5.1 SIGNIFICANCE OF THIS INVESTIGATION

The current work investigated the flotation process (froth zone in particular) both in global terms and at the level of sub-processes. Most importantly, it investigated the practical significance of proposed froth models, and how they can be used in correlating batch and continuous froth performance. Firstly, a comprehensive analysis of the froth investigations and froth models was compiled and presented in this thesis. This analysis is believed to be a unique and unparalleled research work that has never been conducted before. The manner in which the information on froth modelling is presented in this work greatly simplifies the complexity of froth modelling studies reported in the literature. This information will assist mineral processing researchers in formulating relevant research questions to be addressed by future froth studies. It will also help flotation cell manufacturers, to incorporate qualitatively and quantitatively the influence of the froth phase, during design of new cells and analysis of existing flotation cells and circuits. However, none of the proposed froth models found in the literature could be used to quantify or describe, adequately, the influence of the froth phase on flotation recovery. Hence a froth recovery model was developed in this thesis.

The proposed froth recovery model, which accounts for the possibility of the recovery of detached particles within the froth phase via entrainment mechanism, is the first of its kind in which the froth recovery is described in terms of primary flotation variables, such as particle size and particle density - with the exception of the description of bubble coalescence.

Furthermore, this is the first work that attempts to derive meaningful froth kinetic parameters from batch flotation tests and correlate them with froth kinetic parameters obtained from continuously operated flotation systems.

Lastly, the successful use of the proposed methodology of dealing with batch data when extracting froth kinetic parameters demonstrates the soundness of the assumptions involved in the development of this approach. More importantly, this method of analysing batch data adds more value to the current use of batch tests. As mentioned in the introduction, Chapter 1, batch tests are mainly used for two purposes: (i) to extract pulp kinetic parameters such as flotation rate constants, floatability parameters, P values, and the mass fractions of different floating classes, m values; and (ii) to generate grade-recovery curves to study the influence of changing the physical and chemical parameters. In addition to the above, batch data can now be used to (i) study the influence of operating parameters on froth recovery; and (ii) extract intrinsic froth parameters that can be used to describe continuous flotation systems (even if the parameters are used as initial estimates for feasibility studies or proposed pilot-plant or

industrial flotation circuit schemes). Moreover, the proposed methodology can be used to derive initial values of the froth kinetic parameters in the current flotation simulation packages. This will help the search engines used by these softwares to at least start searching from realistic ranges, which obviously will increase the confidence in the simulated flotation schemes.

5.2 FINDINGS

5.2.1 Flotation Review in General

To achieve optimum design and efficient operation of industrial flotation cells, intrinsic parameters that describe both physical and chemical processes, and possibly their interaction with each other, within the froth and pulp phases are required. The description of processes occurring within the pulp phase is relatively well established. However, accurate description of froth processes is not yet established. This situation makes it difficult to determine, accurately, the most profitable design and circuit layout before constructing a large-scale plant or to optimise existing flotation cells or circuits. In addition, the use of bench-scale flotation equipment in the derivation of meaningful parameters is not possible.

5.2.2 Critical Review on Froth Modelling

A considerable amount of fundamental knowledge about the behaviour of froths has been established by froth investigations presented in the literature. However, describing froth behaviour, mathematically, continues to be a daunting task. This is due to a large number of interactive factors, both physical and chemical related, which influence the ultimate recovery of particles within the froth phase (also known as R_f). Proposed R_f models are largely descriptive. In addition, the parameters used in these models cannot be measured or independently determined. This problem emanates from the lack of reliable froth sampling techniques, particularly in conventional flotation cells. Furthermore, the parameters used in these models are global in nature (i.e. lump all major factors influencing froth performance into one parameter). As such, it is very difficult to know what are the intrinsic froth parameters that need to be extracted from bench-scale testwork, particularly from batch flotation cells. This goes to the heart of the most frequently asked question: what's the relevance of batch data in predicting continuous performance? From this observation it was concluded that unless a realistic froth model is developed the use of batch data in deriving kinetic parameters will continue to be a problem. Hence, a froth recovery model, which is believed to be realistic and practical, was proposed in this thesis.

5.2.3 Evaluation of the Proposed Froth Recovery Model and Methodology for Linking Batch and Continuous Froth Performance

In the work presented in this thesis, empirical and semi-empirical froth models were proposed and tested. The empirical model seems to describe the froth behaviour very well. However, the parameters used need to be determined from large dynamic data sets, which could prove costly. The semi-empirical approach, on the other hand, uses relatively few, more meaningful parameters, but these cannot be directly determined on continuous cells at this stage. However, these parameters can be extracted from bench-scale flotation tests.

5.2.3.1 Evaluation of model parameters using laboratory procedures

In the case of batch tests, an empirical methodology of extracting froth parameters is proposed in this thesis (chapter 2). It has been shown that this can be used for the prediction of continuous performance from dynamic batch data in simple systems. In this method, the effects of pulp processes are separated from the influence of the froth phase. Parameters that describe pulp and froth performances are then derived from the observed data. A correlation between the drainage parameter, ω, and particle size, d_p, was observed, which was shown to be well described by the following expression:

$$\omega_i = a + b\, d_{p(i)}^2$$

In the above equation, the parameter, a, is considered to represent the water drainage rate under the froth conditions arising in the flotation cell (frother type and concentration, solids characteristics, etc), while the parameter b represents a proportionality constant for particle drainage rate as a function of size. The b parameter was further described as follows:

$$b = g\,(\rho_s - \rho_f)/18\,\eta\,h$$

where g is the gravitational acceleration, ρ_s is the density of the solid, ρ_f is the density of the fluid, η is the fluid viscosity and h is the froth height through which particles have to settle.

The model for describing the overall froth recovery of floatable particles proposed in this thesis is therefore as follows:

$$R_{f(i)} = \exp(-\beta * FRT) + [1 - \exp(-\beta * FRT)] * \left[\frac{1}{1 + (\beta + \frac{g(\rho_s - \rho_f)}{18\,\eta\,h} dp_{(i)}^2) * FRT}\right]$$

A good correlation between predicted and measured concentrate mass flow rates was observed when froth and pulp parameters derived using batch data were used to describe continuous performance. Furthermore, the results from this work indicate that, in principle, if the intrinsic parameters of the flotation process are known, any type of a flotation cell may be designed by introducing the physical dimensions and hydrodynamic factors associated with the type of equipment used.

It must be pointed out, however, that the nature of batch froths (i.e. non-steady-state behaviour) might introduce some limitations where the froth characteristics are changing rapidly with flotation time. Scale-up of bench-scale data will have a much better chance to succeed if the laboratory and commercial operations are carried out in the same type of system (i.e. continuous mode). The foregoing comments do not imply that the proposed methodology of linking batch data to continuous performance has no value. Such method can provide an important initial evaluation of projected pilot or industrial plant flotation performance and costs. This methodology can also be used to study the influence of the froth phase in batch cells, which obviously enhances the current use of batch data.

From a modelling point of view, the proposed froth recovery model can be very useful in describing existing flotation data. It uses the FRT parameter which has been shown to have great potential for purposes of scaling-up bench-scale froth performance to industrial flotation cells (Gorain *et al*, 1998; Harris, 1998). It was further demonstrated in this work that the proposed froth recovery equation can be used to describe froth performance in complex systems. Several issues, however, with regard to the use of the proposed froth recovery equation in complex flotation systems still need further attention.

5.2.3.2 Evaluation of model parameters using plant data

Application of the proposed methodology to real ore systems has not yet been refined. At the moment, it is only possible to quantify the influence of the froth phase on flotation in batch and continuous systems for the minerals that are fully liberated and report to the concentrate launder predominantly via true flotation mechanism. Results from the Merensky ore system, Chapter 4, seem to suggest that the froth recovery of the fully liberated fractions of the sulphide minerals is the same. Several recommendations on how the findings presented above could be advanced further are discussed in section 5.4 below.

5.3 IMPLICATIONS OF THIS WORK TO SCALE-UP

This investigation focused on correlating parameters derived from the data obtained using the same flotation cell, in terms of size and design, operated in batch and continuous modes. Although the

results obtained indicated a good correlation between predicted and measured flotation performance in all flotation systems studied here, scaling up from laboratory batch cells to full-scale cells is expected to be difficult. With regard to the pulp phase, the floatability parameters, P's, obtained from laboratory scale flotation cells is expected not to vary much when compared to the floatability values expected in full-scale flotation cells. This is most likely to be true provided the power input, pulp density, chemical adsorption on the surface of the particles, particle size distribution, solids suspension and the bubble surface area flux, S_b, are the same in both laboratory and commercial scale flotation cells. As such, the pulp parameters extracted or derived from a laboratory batch cell data could be used to predict flotation performance within the pulp phase in a full-scale flotation cell.

The froth phase parameters derived from batch cell data, however, are expected to vary significantly when compared to the froth parameters expected in full-scale flotation cells. This is because froth parameters derived from batch data represent an average value over the entire batch flotation period. As such, there might be some discrepancies between predicted and measured froth performance in full-scale cells. In addition, there is an issue of froth mobility. The transportation of froths into the launder in laboratory cells is very rapid, leading to less bubble coalescence and break-up on the surface. On the other hand, high froth retention time found in full-scale cells might lead to significant bubble coalescence within the froth phase, and bubble break-up on the surface. It is clear, therefore, that a more detailed froth model which accounts for some of the issues discussed above is necessary. This is discussed further in the recommendations section next.

5.4 RECOMMENDATIONS

On the basis of this study and the above conclusions, the following recommendations are suggested:

Further batch and continuous testwork using a real ore system is required to validate and confirm findings from the present study. This should include a comprehensive description of the response of the non-floating material.

Descriptive correlations of the floatability parameter, P, with factors such as particle size, chemical adsoprtion, etc, need to be considered. Such correlations will reduce the number of measurements that need to be taken for modelling purposes.

Incorporation of the variation of froth stability with flotation time in batch tests can improve the correlation of predicted and measured performance. This can also increase the reliability of parameters derived from batch data.

As a long-term objective, extensive refinement or further development of robust froth and pulp phase performance equations, preferably using fundamental approaches, should now be seriously considered. This should include detailed description of the froth sub-processes, especially the rate at which bubbles coalesce, and their interaction with each other. Bubble coalescence is influenced by a number of factors, both physical and chemical. In dynamic froths, where the froth transportation plays a crucial role, this phenomenon is even more complicated. Again, the approach that is envisaged to address this issue is to decouple physical and chemical factors. This approach, however, will eliminate the significance of the interaction of these factors. This could lead to development of unrealistic froth models. Above all, the challenge will be in quantifying, in a measurable manner, the influence of changing chemistry (i.e. frother concentration and type). It would be advisable to start by quantifying this in relatively simple systems. Currently, this is being attempted by several workers in the field of mineral processing. Better co-ordination and collaboration among these researchers, rather than working individually, could well see the problem solved sooner. It is also believed that there are now sufficient data bases, knowledge and computer resources to at least begin testing comprehensive flotation process models.

By the same token, more effort should be directed toward developing and improving froth sampling techniques. It is important to note that froth is not just like any other fluid such as liquid or uniformly mixed gas. Froth is a very complex fluid consisting of solids (of different types and compositions), liquid, and air. Under these circumstances, the sampling techniques create another dilemma in froth flotation. It is therefore imperative that considerable effort be put into developing better ways of sampling froths and measuring dynamic froth stability or froth decay. This could include the use of image processing techniques to extract meaningful surface froth information, including identification of minerals covering bubbles. This will form a very important part in model validation and testing in the near future.

Another obstacle, aluded to in this work, is in quantifying froth removal efficiency. It is believed that this factor will play a crucial role in the scale-up of froth models derived using bench-scale cells to industrial cells. Generally, as the flotation cell volume increases, the froth removal becomes more important. As such, froth models should incorporate the froth removal efficiency. Therefore, more work should be conducted on existing plant flotation circuits to develop correlations of froth discharge or froth removal efficiency as a function of operating variables such as particle size, airflow rate, froth height, etc. To develop reliable correlations, the use of image analysis should be considered. Image analysis has the advantage of making it possible to develop correlations from large data bases.

Once all the above mentioned aspects of froth modelling are accomplished, it will be much easier to formulate a predictive froth model. It is strongly believed, however, that a successful froth model will be a combination of empirical correlations from dynamic data and mechanistic description of the froth processes. Deriving a fundamental froth model for describing froth influence in the current flotation cell design types is almost impossible. The design nature of flotation cells, which is essentially a mixture of a contact reactor and a froth separator, makes it very difficult to mathematically describe the two units together using only a fundamental engineering approach.

References

REFERENCES AND BIBLIOGRAPHY

REFERENCES

Agar, G.E., Chia, J. and Requis-c, L., 1998. Flotation rate measurements to optimise an operating circuit. *Minerals Engineering*, 11(4), 347-360.

Arbiter, N. and Harris, C.C., 1962. Flotation Kinetics. In: D.W. Fuerstenau(Ed.) Froth Flotation., *50th Anniversary Volume, AIME.*, New York.

Barigou, M, Greaves, M., 1992. Bubble size in the impeller region of a Rushton turbine, *Trans. I ChemE*, Part A (70): 153-160.

Bascur, O.A. and Herbst, J.A., 1982. Dynamic modelling of a flotation cell with a view toward automatic control. *CIM XIV International Mineral Processing Congress*, October 17-23, Toronto, Canada, pp. III-11.1 - III-11.22.

Bikerman, J.J., 1938. The unit of foaminess. *Trans. Faraday Soc.*, 34: 634-638.

Bisshop, J.P. and White, M.E., 1976. Study of particle entrainment in flotation froths, *Trans. Inst. Min. Met.*, 85: C191-C194.

Bourassa, M., Barbery, G., Broussaud, A. and Conil, P., 1988. Flotation Kinetic Scale-up: Comparison laboratory batch test to pilot plant processing. *XVI International Mineral Processing Congress*, edited by E. Forssberg, pp. 579-587.

Brack, B. and Harris, T.A., 1996. Scale-up of flotation rate / bubble surface area flux dependence. Internal Report, Department of Chemical Engineering, University of Cape Town.

Breytenbach, J.N., 1995. An investigation of particle collection efficiency in different particle-bubble contacting environments in flotation. *MSc Thesis*. University of Cape Town.

Buswell, M., 1998. The use of electrochemical measurements in characterization of flotation pulp chemistry on laboratory and plant scale. UCT report, Department of Chemical Engineering.

Contini, N.J., Wilson, S.W., and Dobby, G.S., 1988. Measurement of the rate data in flotation columns. *Column Flotation '88 Proceedings*, Sastry, K.V.S. (ed), SME Annual Meeting, Phoenix, US, pp. 81-89.

Coulson, J.M. and Richardson, J.F., 1988. Chemical Engineering, Vol 2. Pergamon Press, Oxford.

Crozier, R.D., 1992, Flotation, Theory, reagents and ore testing. Pergamon Press, Oxford.

Cutting, G.W., 1989. Effect of Froth Structure and Mobility on Plant Performance. *Mineral Processing and Extractive Metallurgy Review*, 5: 169-201.

Cutting, G.W., Watson, D., Whitehead, A. and Barber, S.P., 1981. Froth Structure in Continuous flotation Cells: Relation to the Prediction of Plant Performance from Laboratory Data using Process Models. *Int. J. Miner. Process*, 7: 347-369.

Cutting, G.W., Barber, S.P. and Watson, D., 1982. Prediction of Flotation Plant Performance from Batch Tests Using Process models: Effect of Froth Structure. *CIM. XIV Int. Min. Proc. Congr.*, Oct 17-23, Toronto, Canada, pp IV-14.1 - IV-14.20.

Cutting, G.W., Barber, S.P. and Newton, S., 1986. Effects of Froth Structure and Mobility on Performance and Simulation of Continuously Operated Flotation Cells. *Int. J. Miner. Process.*, 16: 43-61.

Deglon, D.A., 1998. A hydrodynamic investigation of fine particle flotation. *PhD Thesis*. University of Cape Town, South Africa.

Deglon, D.A., Sawyerr, F. and O'Connor, C.T., 1999. A model to relate the flotation rate constant and the bubble surface area flux in mechanical flotation cells. *Minerals Engineering*, 12(6): 599-608.

Dippenaar, A., 1978. The effect of particles on the stability of flotation froths. National Institute for Metallurgy, Report No. 1988.

Dobby, G.S., Yianatos, J.B. and Finch, J.A., 1988. Estimation of bubble diameter in flotation columns from drift flux analysis. *Canadian Metallurgical Quarterly*, 27(2): 85-90.

Engelbrecht, J.A. and Woodburn, E.T., 1975. The Effects of froth height, aeration rate, and gas precipitation on flotation. *J. of SA Inst. of Min. and Metallurgy*. October Special issue, 76: 125-132.

Falutsu, M. and Dobby, G.S., 1989. Direct Measurement of Froth Drop Back and Collection Zone Recovery in a Laboratory Flotation Column. *Minerals Engineering*, 2: 377-386.

Falutsu, M. and Dobby, G.S., 1992. Froth Performance in Commercial Sized Flotation Columns. *Minerals Engineering*, 5: 1207-1223.

Feteris, S.M., 1983. Flotation-The froth phase, *MSc thesis,* University of Melbourne.

Feteris, S.M., Frew, J.A. and Jowett, A., 1987. Modelling the Effect of Froth Depth in Flotation. *Int. J. Miner. Process.*, 20: 121-135.

Fichera, M.A. and Chudacek, M.W.,1992. Batch cell flotation models - A Review. *Minerals Engineering*, 5(1): 41-55.

Finch, J.A. and Dobby, G.S., 1990. Column Flotation. Pergamon Press, Oxford, Chap. 3.

Fogler, H.S., 1992. Elements of Chemical Reaction Engineering, 2nd Edition, Prentice-Hall International, Inc.

Gay, S., Stoll, J. and Andrusiewicz, M., 1999. The JKMRC two dimensional mass balance system VBMBAL2D. Internal Report, Julius Kruttschnitt Mineral Research Centre, University of Queensland, Australia.

Goodall, C.M., 1992. The effects of flotation variables on the bubble size, mixing characteristics and froth behaviour in column flotation cells. *PhD thesis*, University of Cape Town, South Africa.

Gorain, B.K., 1998. The effect of bubble surface area flux on the kinetics of flotation and its relevance to scale-up. *PhD Thesis*, JKMRC, Department of Mining, Minerals and Materials Engineering, University of Queensland.

Gorain, B.K, Franzidis, J-P. and Manlapig, E.V., 1996. Bubble surface area flux: A new criterion to evaluate flotation cell performance. *Proceedings of an International Conference: Minerals and Materials'96*, Somerset West, South Africa, **1**, pp. 326-334.

Gorain, B.K, Franzidis, J-P., Manlapig, E.V. and Harris, M.C., 1998. The effect of froth residence time on the kinetics of flotation. *Minerals Engineering*, 11(7): 627-638.

Gorain, B.K., Franzidis, J-P.and Manlapig, E.V. 1999. The empirical prediction of bubble surface area flux in mechanical flotation cells from cell design and operating data. *Minerals Engineering*, 12(3): 309-322.

Harris, M.C., 1998. The use of flotation plant data to simulate flotation circuits. *Conf. Proc. of the South African Inst. of Min and Metallurgy*, Technikon SA, South Africa, 3-4 Sept, pp. 1-27.

Harris, M.C., 1999. An Evaluation of the Savassi Equation for Overall Flotation Recovery Determination. Technical Note, Mineral Processing Research Unit, University of Cape Town.

Hochreiter, R.C., Kennedy, D.C., Muir, W. and Woods, A.I., 1985. Platinum in South Africa. *Journal of South African Mining and Metallurgy*, 85(6): 165-185.

Hosten, C. and Tezcan, A. 1990. The influence of frother type on the flotation kinetics of a massive copper sulphide ore. *Minerals Engineering*. 3(6): 637-640.

Jameson, G.J., Nam, S. and Moo Young, M., 1977. Physical factors affecting recovery rates in flotation. *Minerals Science and Engineering*, 9(3): 103-118.

Johansson, G. and Pugh, R.J. 1992. The influence of particle size and hydrophobicity on the stability of mineral froths. *International Journal of Mineral Processing*, 34: 1-21.

Johnson, N.W. 1972. The flotation Behaviour of some Chalcopyrite Ores. *PhD Thesis*, University of Queensland.

King, R.P., 1975. Simulation of flotation plants. *Trans. Soc. Min. Eng.*, AIME, 258: 286-293.

King, R.P., 1978. A pilot-plant investigation of a kinetic model for flotation. *Journal of the South African Institute of Mining and Metallurgy*, July: 325-338.

King, R.P., 1982. Principles of Flotation. *South African Institute of Mining and Metallurgy*, Johannesburg.

Kirjavainen, V.M., 1996. Review and analysis of factors controlling the mechanical flotation of gangue minerals. *Int. J. Mineral Process.*, 46: 21-34.

Klassen, V.I. and Mokrousov, V.A., 1963. An introduction to the theory of flotation. Butterworths, London.

Klimpel, R.R., 1980. Selection of chemical reagents for flotation, Mineral Processing Plant Design, 2nd edition, AIME, Denver, A. Mular and Bhappu, eds, chapter 45, pp. 907-934.

Laplante, A.R., Kaya, M. and Smith, H.W., 1989. The Effect of Froth on Flotation Kinetics - A Mass Transfer Approach. In *Frothing in Flotation* (Laskowski, J.S., ed.), Gordon and Breach Science Publishers, pp. 77-99.

Laplante, A.R., Toguri, J.M. and Smith, H.W., 1983a. The effect of air flow rate on the kinetics of flotation, Part 2: The transfer of material from the froth over the cell lip. *Int. J. Mineral Process.*, 11: 221-234.

Laplante, A.R., Toguri, J.M. and Smith, H.W., 1983b. The effect of air flow rate on the kinetics of flotation. Part 1: The transfer of material from slurry to the froth. *Int. J. Mineral Process.*, 11: 203-219.

Laskowski, J.S. and Ralston, J. (editors). 1992. Developments in Mineral Processing, vol. 12: Colloid Chemistry in Mineral Processing, Elsevier.

Latti, A.D. 1997. Qem*Sem investigation of section 10 merensky reef samples. Impala Platinum internal report.

Livshits, A.K. and Dudenkov, S.V., 1965. Some factors in flotation froth stability. In: N. Arbiter (Editor), *Proc. VIIth Int. Min. Proc. Congress. Gordon and Breach*, New York, N.Y., pp. 367-371.

Loveday, B.K. and Raghubir, S., 1995. Design and Optimisation of flotation circuits using simulation. In *Proceedings of the SAIMM Colloquium on interactions between Comminution and Downstream processing,* Mintek, South Africa, 5-6 June 1995, pp. 1-10.

Lynch, A.J., Johnson, N.W., Manlapig, E.V. and Thorne, C.G., 1981. Mineral and Coal Flotation Circuits: Their Simulation and Control, Elsevier Scientific Publishing Company, Amsterdam.

Malysa, K., Lunkenheimer, K., Miller, R. and Hartenstein, C., 1981. Colloids and Surfaces. Vol. 3, pp. 329.

Malysa, E., Malysa, K. and Czarnecki, J., 1987. A method of comparison of the frothing and collecting properties of frothers. *Colloids and Surfaces*, 23: 29-39.

Mathe, Z.T., Harris, M.C., O'Connor, C.T. and Franzidis, J-P., 1998. Review of froth modelling in steady state flotation systems. *Minerals Engineering*, 11(5): 397-421.

Mathe, Z.T., Harris, M.C.and O'Connor, C.T., 2000. A review of methods to model the froth phase in non-steady state flotation systems. *Minerals Engineering*, 13(2): 127-140.

Moys, M.H., 1978. A Study of a Plug Flow Model for Flotation Froth behaviour. *Int. J. Mineral Process.*, 5: 221-238.

Moys, M.H., 1984. Residence Time Distributions and Mass Transport in the Froth Phase of the Flotation Process. *Int. J. Mineral Process.*, 13: 117-142.

Moys, M.H., 1989. Mass Transport in Flotation Froths. *Int. J. Mineral Process.*, 5: 203-228.

Mular, A.L. and Musara, W.T., 1991. Batch column flotation: Rate data measurements. *Proceedings of an International Conference on Column Flotation*, Sudbury, Ontario, Canada. Vol. 1, pp. 63-74.

Napier-Munn, T.J., 1995. An introduction to comparative statistics and experimental design, Course Notes, 2nd edition, University of Queensland.

Perry, R.H. and Green, D.W. (eds), 1984. Perry's Chemical Engineer's Handbook. 6th edition, McGraw-Hill Book Company, New York.

Ross, V.E.and van Deventer, J.S.J., 1987. A computer model to predict froth behaviour in the scale-up of flotation cells. APCOM '87. *20th International Symposium on the Application of Mathematics and Computers in the Minerals Industries*, October 19-23, Johannesburg, SAIMM, pp. 73-88.

Ross, V.E.and van Deventer, J.S.J., 1988. Mass transport in flotation column froths. In: K.V.S. Sastry (Ed.), Column Flotation '88. *International Symposium on Column Flotation, SME - AIME Annual Meeting*, Phenix, Arizona, January 25-28, pp. 129-139.

Ross, V.E., 1988. Mass Transport in Flotation Froths. *PhD thesis,* University of Stellenbosch, South Africa.

Ross, V.E., 1991a. An investigation of sub-processes in equilibrium froths(I): the mechanisms of detachment and drainage. *Int. J. Mineral Process.*, 31: 37-50.

Ross, V.E., 1991b. An investigation of sub-processes in equilibrium froths (II): the effect of operating conditions. *Int. J. Mineral Process.*, 31: 51-71.

Rubinstein, J. B., 1995. Column Flotation: Processes, Designs and Practices. Gordon and Breach Science Publishers, USA.

Runge, K.C., Harris, M.C., Frew, J.A. and Manlapig, E.V., 1997. Floatability of streams around the Cominco Red Dog Lead cleaning circuit. In *Proceedings of the Sixth Mill Operators' conference*, Madang, Papua New Guinea, 6-8 October 1997, pp. 157-163.

Savassi, O.N., 1998. Direct estimation of the degree of entrainment and the froth recovery of attached particles in industrial flotation cells. *PhD Thesis*, JKMRC, University of Queensland, Australia.

Smith, P.G. and Warren, L.J., 1989. Entrainment of particles into flotation froths. *Mineral Processing and Extractive Metallurgy Review*, 5: 123-145.

Spiegel, M.R., 1992. Theory and problems of probability and statistics, Schaum's outline series, McGraw-Hill, Inc. New York.

Subrahmanyam, T.V. and Forssberg, E., 1988. Froth Stability, Particle Entrainment and Drainage in Flotation - A Review. *Int. J. Mineral Process.*, 23: 33-53.

Sun, S.C., 1952. Frothing characteristics of pine oils in flotation. *Trans AIME*, 193: 65-71.

Sweet, J., 1999. Investigation of a methodology to decouple physical and chemical effects for flotation circuit performance evaluation. *MSc Thesis*, Department of Chemical Engineering, University of Cape Town.

Sweet, C, Van Hoogstraten, J, Harris, M. and Laskowski, J.S., 1997. The effect of frothers on bubble size and frothability of aqueous solutions, *2nd University of British Columbia – McGill University Int. Symposium on "Fundamentals of Mineral Processing"*, Sudbury.

Taggart, A.F., 1945. Handbook of Mineral Dressing, Wiley, New York.

Theron, E., 1998. The characterization and modeling of the primary cleaning circuit at Impala Platinum's UG-2 concentrator. *MSc Thesis*, Department of Chemical Engineering, University of Cape Town.

Trahar, W.J., 1981. A rational interpretation of the role of particle size in flotation. *Int. J. Mineral Process.*, 8: 289-327.

Tucker, J.P., Deglon, D.A., Franzidis, J-P., Harris, M.C. and O'Connor, C.T., 1994. An evaluation of a direct method of bubble size distribution measurement in a laboratory batch flotation cell. *Minerals Engineering*, 7(5,6): 667-680.

Tuteja, R.K., Spottiswood, D.J. and Misra, V.N., 1994. Mathematical models of the column flotation process: A review. *Minerals Engineering*, 7(12): 1459-1472.

Vera, M.A., Franzidis, J-P. and Manlapig, E.V., 1999. Simultaneous determination of collection zone rate constant and froth zone recovery in a mechanical flotation environment. Minerals Engineering, 12(10): 1163-1176.

Vera, M.A., 1995. The determination of collection zone rate constant and froth zone recovery by column flotation. *MSc Thesis*, Julius Kruttschnitt Research Centre, The University of Queensland, Australia.

Vianna, 1999. JKMRC, University of Queensland, Personal Communication.

Warren, L.J., 1985. Determination of the contributions of true flotation and entrainment in batch flotation tests. *Int. J. Mineral Process.*, 14: 33-44.

Watson, D. and Grainger, T.J.N., 1974. Study of froth flotation by use of a steady-state technique. *Trans. Instn. Min. Metall. (Sect. C: Mineral Process. Extr. Metall.)*, 82: C103-C105.

Wills, B.A., 1997. Mineral Processing Technology. 6th Edition, Butterworth-Heinemann, Oxford.

Woodburn, E.T., Kropholler, H.W., Green, J.C.A. and Cramer, L.A., 1976. The Utility and Limitations of Mathematical Modelling in the Prediction of the properties of Flotation Networks. In *Flotation*, (M.C. Fuerstenau(Ed.)), A.M.Gaudin Memorial Volume, Vol II, AIME.,New York, pp. 638-674.

Woodburn, E.T., Austin, L.G. and Stockton, J.B., 1994. A Froth Based Flotation Kinetic Model. *Trans. Instn. Chemical Engineers*, 72(Part A): 211-226.

Woodburn, E.T. and Wallin, P.J., 1984. Decoupled kinetic model for simulation of flotation networks. *Trans. Instn. Min. Metall. (Sect. C: Mineral Process. Extr. Metall.)*, 93: C153-C161.

Yianatos, J.B., Finch, J.A. and Laplante, A.R., 1988. Selectivity in column flotation froths. *Int. J. Mineral Process.*, 23: 279-292.

Yoon, R.H. and Luttrell, G.H., 1989. The effect of bubble size on fine particle flotation. In *Frothing in Flotation*, (ed: J.S. Laskowski), pp. 101-122.

Yoon, R.H., Mankosa, M.J. and Luttrell, G.H., 1993. Design and scale-up criteria for column flotation. AusIMM - XVIII International Mineral Processing Congress, Sydney, Australia, pp. 785.

Yianatos, J.B., Finch, J.A. and Laplante, A.R., 1986. Apparent hindered settling in a gas-liquid-slurry counter-current column, *Int. J. Miner. Process*. 18: 155-165.

Yianatos, J.B., Bergh, L.G., Cortes, G.A., 1998. Froth zone modelling of an industrial flotation column, *Minerals Engineering*, 11(5): 423-435.

BIBLIOGRAPHY

Ahmed, N. and Jameson, G.J., 1989. Flotation Kinetics. In Frothing in Flotation (Laskowski, J.S., ed.), Gordon and Breach Science Publishers, pp. 77 - 99.

Castro, S.H. and Alvarez, J.(eds), **1988**. Froth Flotation, (Developments in Mineral Processing-Proceedings of the Latin-American Congress on Froth Flotation, Chile), Elsevier.

Crozier, R.D. and Klimpel, R.R., 1989. Frothers: Plant Practice. *Mineral Processing and Extractive Metallurgy Review*, 5: 257-279.

Dippenaar, A., 1982a. The destabilisation of froth by solids I: The mechanism of film rupture. *Int. J. Miner. Process*. 9: 1-14.

Dippenaar, A., 1982b. The destabilization of froth by solids II. The rate-determining step. *Int. J. Miner. Process.*, 9: 15-27.

Dobby, G.S. and Finch, J.A., 1986. Flotation column scale-up and modelling. *Canadian Inst. of Min. and Metall. Bulletin*, 79: 89-96.

Ek, C., 1992. Flotation Kinetics. In Innovations in Flotation Technology, Mavros, P. and Matis, K.A. (Eds), pp. 183-210.

Falutsu, M., 1991. Column flotation froth studies. *PhD thesis*, Toronto University.

Falutsu, M., 1994. Column flotation froth characteristics - stability of the bubble-particle system. *Int. J. Miner. Process.*, 40: 225 - 243.

Finch, J.A., Yianatos, J. And Dobby, G., 1989. Column Froths. *Mineral Processing and Extractive Metallurgy Review*, 5: 281-305.

Flint, L.R., 1973. Factors influencing the design of flotation equipment. *Minerals Science Engineering*, 5: 232-241.

Flynn, S.A. and Woodburn, E.T., 1987a. Development of a froth model for fine-particle beneficiation. *Trans Instn Min Metall.*, 96: C191-C1198.

Flynn, S.A. and Woodburn, E.T., 1987b. A Froth Ultra-Fine Model for the Selective Separation of Coal from Mineral in a Dispersed Air Flotation Cell. *Powder Technology*, 49: 127-142.

Fuerstenau, D.W., 1962. Froth Flotation, 50th Anniversary Volume, American Inst. of Mining, Metallurgical, and Petroleum Engineers, Inc., New York.

Fuerstenau, M.C. (ed.), 1976. Flotation, A.M. Gaudin Memorial Volume, American Institute of Mining, Metallurgical, and Petroleum Engineers, Inc., Vol. I, New York.

Fuerstenau, M.C. (ed.), 1976. Flotation, A.M. Gaudin Memorial Volume, American Institute of Mining, Metallurgical, and Petroleum Engineers, Inc., Vol. II, New York.

Goodall, C.M. and O'Connor, C.T., 1991. Pulp-Froth interactions in a laboratory column flotation cell. *Minerals Engineering*, 4: 951-958.

Gorain, B.K., Franzidis, J-P., Manlapig, E.V., 1995. Effect of bubble size, gas hold-up and superficial gas velocity on metallurgical performance in an industrial scale flotation cell, *Colloquium South Africa Inst Min Met*, Interactions between communication and down stream processing, pp. 5-6.

Greaves, M. and Allan, B.W., 1974. Steady-state and dynamic characteristics of flotation in a single cell. *Trans. Instn Chem. Engrs.*, 52: 136-148.

Harris, P.J., 1982. Frothing phenomena and frothers. In *Principles of Flotation* (King, R.P., ed.), South African Institute of Mining and Metallurgy, Johannesburg.

Harris, C.C. and Rimmer, H.W., 1966. Study of a two-phase model of the flotation process. *Trans. Instn. Min. Metall.* Sect C, 75: C153-C162.

Inoue, T., Nonaka, M. and Imaizumi, T., 1962. Flotation Kinetics-Its Macro and Micro Structure. In *Advances in Mineral Processing* (P. Somasundaran, ed.), Soc. Mining Engineers Inc., Colorado (1986), pp. 209-228.

Ives, K.J.(ed.), 1984. The Scientific Basis of Flotation. Martinus Nijhoff Publishers.

Kirjavainen, V.M., 1989. Application of a probability model for the entrainment of hydrophilic particles in froth flotation. *Int. J. Mineral Process.*, 27: 63-74.

Kirjavainen, V.M.. 1992. Mathematical model for the entrainment of hydrophilic particles in froth flotation. *Int. J. Mineral Process.*, 35: 1-11.

Klimpel, R.R., 1988. Considerations for improving the performance of froth flotation systems. *Mining Engineering*, pp. 1093-1100.

Klimpel, R.R. and Isherwood, S., 1991. Some industrial implications of changing frother chemical structure. *Int. J. Mineral Process.*, 33: 369-381.

Laskowski, J.S., 1989. Thermodynamic and Kinetic Flotation Criteria. *Mineral Processing and Extractive Metallurgy Review*, 5: 25-41.

Lekki , J. and Laskowski, J.S., 1975. A new concept of frothing in flotation systems and general classification of flotation frothers. *Proc. 11th International Mineral Processing Congress,* Cagliari, pp. 427.

Meyer, W.C. and Klimpel, R.R., 1982. Rate Limitations in Froth Flotation. *Trans. Soc. Min. Eng.* AIME, 274: 1852-1858.

Moolman, D.W., Aldrich, C., van Deventer, J.S.J. and Stange, W.W., 1995. The classification of froth structures in a copper flotation plant by means of a neural net. *Int. J. Mineral Process.*, 43: 193-208.

Moolman, D.W., Aldrich, C., Schmitz, G.P.J. and Van Deventer, J.S.J., 1996. The interrelationship between surface froth characteristics and industrial flotation performance. *Minerals Engineering*, 9 (8): 837-854.

Moolman, D.W., Eksteen, J.J., Aldrich, C. and van Deventer, J.S.J., 1996. The significance of flotation froth appearance for machine vision control. *Int. J. Mineral Process.*, 48: 135-158.

Moolman, D.W., Aldrich, C., Van Deventer, J.S.J., and Bradshaw, D.B., 1995. The interpretation of flotation froth surfaces by using digital image analysis and neural networks. *Chemical Engineering Science*, 50(22): 3501-3513.

Moon, K.S. and Sirois, L.L., 1988. Theory and Industrial Application of Column Flotation in Canada. *Column Flotation '88 Proceedings*. Sastry, K.V.S. (ed), SME Annual Meeting, Phoenix, US, pp. 81-89.

Murphy, D.G., Zimmerman, E.T. and Woodburn, E.T., 1996. Kinematic model of bubble motion in a flotation froth. *Powder Technology*, 87: 3-12.

Rajinder P. and Masliyah, J., 1990. Flow in Froth Zone of a Flotation Column. *Canadian Metallurgical Quarterly*, 29(2): 97-103.

Ross, V.E., 1991. The behaviour of particles in flotation froths. *Minerals Engineering*, 4: 959-974.

Ross, V.E., 1991. Comparison of methods for evaluation of true flotation and entrainment. *Trans. Min. Metall. (sect. C: Mineral Process. Extr. Metall.)*, 100: C121-170.

Ross, V.E., 1990. A study of the froth phase in large-scale pyrite flotation cells. *Int. J. Mineral Process.*, 30: 143-157.

Schuhmann, R., 1942. Flotation kinetics I: Methods for steady-state study of flotation problems. *J. Phys. Chem*, 46: 891-902.

Sutherland, K.L. and Wark, I.W., 1955. *Principles of Flotation*, Australasian Institute of Mining and Metallurgy (Inc.).

Tuteja, R.K., Spottiswood, D.J. and Misra, V.N., 1995. Column parameters: their effect on entrainment in froth. *Minerals Engineering*, 8(11): 1359-1368.

Van der Walt, T.J., Van Deventer, J.S.J. and Barnard, E., 1993. Neural nets for the simulation of mineral processing operation, Part I: Theoretical principles, *Minerals Engineering*, 6: 1127-1134.

Van der Walt, T.J., Van Deventer, J.S.J. and Barnard, E., 1993. Neural nets for the simulation of mineral processing operation, Part II: Applications. *Minerals Engineering*, 6: 1135-1153.

Woodburn, E.T., 1970. Mathematical Modelling of Flotation Processes. *Minerals Science Engineering*, 2: 3-17.

APPENDICES

APPENDIX A

150 TO 300 MICRONS BATCH DATA

APPENDIX A: 150 TO 300 MICRONS BATCH DATA

Run #21

Air Flow Rate			2 l/min			Water pH		8		
Measured Froth Depth			5 mm			Adjusted pH		7		
Sampl No	Pan Mass (g)	Froth + Pan Mass (g)	Quartz Dry Mass (g)	Bottle Mass Before (g)	Bottle Mass After (g)	Wash Water Mass (g)	Water Mass (g)	Cum Flot Time (min)	Cum Quartz Rec (%)	Cum Water (g)
1	382.70	620.02	64.34	459.82	454.57	5.25	167.73	0.25	71.49	167.73
2	363.47	572.67	24.09				185.11	0.5	98.26	352.84
3	374.77	588.02	0.69				212.56	0.75	99.02	565.40
4	354.87	534.02	0.06				179.09	1	99.09	744.49
Cumulative Quartz Recovery			**99.09**	%		Conditioning Time		5	min	
Cumulative Water (g)			**744.49**							

Run #22

Air Flow Rate			3 l/min			Water pH		8		
Measured Froth Depth			5 mm			Adjusted pH		7		
Sampl No	Pan Mass (g)	Froth + Pan Mass (g)	Quartz Dry Mass (g)	Bottle Mass Before (g)	Bottle Mass After (g)	Wash Water Mass (g)	Water Mass (g)	Cum Flot Time (min)	Cum Quartz Rec (%)	Cum Water (g)
1	367.93	690.90	73.56				249.41	0.25	81.73	249.41
2	362.02	579.36	15.33	454.57	449.83	4.74	197.27	0.5	98.77	446.68
3	345.70	550.75	0.23				204.82	0.75	99.02	651.50
4	354.80	557.08	0.00				202.28	1	99.02	853.78
Cumulative Quartz Recovery			**99.02**	%		Conditioning Time		5	min	
Cumulative Water (g)			**853.78**							

Run #23

Air Flow Rate			4 l/min			Water pH		8		
Measured Froth Depth			5 mm			Adjusted pH		7		
Sampl No	Pan Mass (g)	Froth + Pan Mass (g)	Quartz Dry Mass (g)	Bottle Mass Before (g)	Bottle Mass After (g)	Wash Water Mass (g)	Water Mass (g)	Cum Flot Time (min)	Cum Quartz Rec (%)	Cum Water (g)
1	383.84	678.60	77.28				217.48	0.25	85.87	217.48
2	346.20	535.92	11.13				178.59	0.5	98.23	396.07
3	356.93	535.81	0.45				178.43	0.75	98.73	574.50
4	358.93	534.46	0.01				175.52	1	98.74	750.02
Cumulative Quartz Recovery			**98.74**	%		Conditioning Time		5	min	
Cumulative Water (g)			**750.02**							

Run #24

Air Flow Rate			5 l/min			Water pH		8		
Measured Froth Depth			5 mm			Adjusted pH		7		
Sampl No	Pan Mass (g)	Froth + Pan Mass (g)	Quartz Dry Mass (g)	Bottle Mass Before (g)	Bottle Mass After (g)	Wash Water Mass (g)	Water Mass (g)	Cum Flot Time (min)	Cum Quartz Rec (%)	Cum Water (g)
1	363.90	745.34	80.58				300.86	0.25	89.53	300.86
2	374.06	640.48	8.21				258.21	0.5	98.66	559.07
3	367.77	637.12	0.29				269.06	0.75	98.98	828.13
4	369.90	630.94	0.00				261.04	1	98.98	1089.17
Cumulative Quartz Recovery			**98.98**	%		Conditioning Time		5	min	
Cumulative Water (g)			**1089.17**							

Run #34

Air Flow Rate			6 l/min			Water pH		8		
Measured Froth Depth			5 mm			Adjusted pH		7		
Sampl No	Pan Mass (g)	Froth + Pan Mass (g)	Quartz Dry Mass (g)	Bottle Mass Before (g)	Bottle Mass After (g)	Wash Water Mass (g)	Water Mass (g)	Cum Flot Time (min)	Cum Quartz Rec (%)	Cum Water (g)
1	367.93	904.46	86.80	398.01	376.22	21.79	427.94	0.25	96.44	427.94
2	354.87	639.46	2.09				282.50	0.5	98.77	710.44
3	346.20	720.70	0.08				374.42	0.75	98.86	1084.86
4	355.47	617.12	0.00				261.65	1	98.86	1346.51
	370.70	1123.10	0.00				752.40	1.5	98.86	2098.91
Cumulative Quartz Recovery			**98.86**	%		Conditioning Time		**5**	min	
Cumulative Water (g)			**2098.91**							

Run #36

Air Flow Rate			6 l/min			Water pH		8		
Measured Froth Depth			5 mm			Adjusted pH		7		
Sampl No	Pan Mass (g)	Froth + Pan Mass (g)	Quartz Dry Mass (g)	Bottle Mass Before (g)	Bottle Mass After (g)	Wash Water Mass (g)	Water Mass (g)	Cum Flot Time (min)	Cum Quartz Rec (%)	Cum Water (g)
1	345.70	882.90	84.34				452.86	0.25	93.71	452.86
2	361.86	670.34	4.26				304.22	0.5	98.44	757.08
3	369.90	746.70	0.33				376.47	0.75	98.81	1133.55
4	360.03	630.16	0.00				270.13	1	98.81	1403.68
	355.73	913.04	0.00				557.31	1.5	98.81	1960.99
Cumulative Quartz Recovery			**98.81**	%		Conditioning Time		**5**	min	
Cumulative Water (g)			**1960.99**							

Run #25

Air Flow Rate			2 l/min			Water pH		8		
Measured Froth Depth			10 mm			Adjusted pH		7		
Sampl No	Pan Mass (g)	Froth + Pan Mass (g)	Quartz Dry Mass (g)	Bottle Mass Before (g)	Bottle Mass After (g)	Wash Water Mass (g)	Water Mass (g)	Cum Flot Time (min)	Cum Quartz Rec (%)	Cum Water (g)
1	360.03	528.66	60.45	519.87	475.67	44.20	63.98	0.25	67.17	63.98
2	383.84	466.14	16.33	664.16	639.38	24.78	41.19	0.5	85.31	105.17
3	370.70	423.89	6.61	527.50	511.74	15.76	30.82	0.75	92.66	135.99
4	371.50	442.52	3.24	563.61	527.75	35.86	31.92	1	96.26	167.91
5	227.80	302.83	1.41	673.60	652.28	21.32	52.30	2	97.82	220.21
Cumulative Quartz Recovery			**97.82**	%		Conditioning Time		**5**	min	
Cumulative Water (g)			**220.21**							

Run #4

Air Flow Rate			3 l/min			Water pH		8		
Measured Froth Depth			10 mm			Adjusted pH		7		
Sampl No	Pan Mass (g)	Froth + Pan Mass (g)	Quartz Dry Mass (g)	Bottle Mass Before (g)	Bottle Mass After (g)	Wash Water Mass (g)	Water Mass (g)	Cum Flot Time (min)	Cum Quartz Rec (%)	Cum Water (g)
1	361.42	650.80	80.69	525.80	501.00	24.80	183.89	0.5	89.66	183.89
2	365.60	552.60	5.20	613.40	581.70	31.70	150.10	1	95.43	333.99
3	354.87	472.30	1.66	499.40	474.70	24.70	91.07	1.5	97.28	425.06
4	346.20	515.20	0.89	664.80	581.70	83.10	85.01	2.5	98.27	510.07
5	374.84	503.20	0.32	695.40	637.80	57.60	70.44	4	98.62	580.51
Cumulative Quartz Recovery			**98.62**	%		Conditioning Time		**5**	min	
Cumulative Water (g)			**580.51**							

Run #26

Air Flow Rate			3 l/min			Water pH		8		
Measured Froth Depth			10 mm			Adjusted pH		7		
Sampl No	Pan Mass (g)	Froth + Pan Mass (g)	Quartz Dry Mass (g)	Bottle Mass Before (g)	Bottle Mass After (g)	Wash Water Mass (g)	Water Mass (g)	Cum Flot Time (min)	Cum Quartz Rec (%)	Cum Water (g)
1	363.47	544.64	67.94	551.44	539.55	11.89	101.34	0.25	75.49	101.34
2	374.84	497.91	14.42	689.36	664.16	25.20	83.45	0.5	91.51	184.79
3	354.87	447.65	4.82	539.10	527.50	11.60	76.36	0.75	96.87	261.15
4	362.02	431.52	0.81	582.86	563.61	19.25	49.44	1	97.77	310.59
5	345.70	417.63	0.64	673.60	673.60	0.00	71.29	3	98.48	381.88
Cumulative Quartz Recovery			**98.48**	%		Conditioning Time		**5**	min	
Cumulative Water (g)			**381.88**							

Run #27

Air Flow Rate			4 l/min			Water pH		8		
Measured Froth Depth			10 mm			Adjusted pH		7		
Sampl No	Pan Mass (g)	Froth + Pan Mass (g)	Quartz Dry Mass (g)	Bottle Mass Before (g)	Bottle Mass After (g)	Wash Water Mass (g)	Water Mass (g)	Cum Flot Time (min)	Cum Quartz Rec (%)	Cum Water (g)
1	355.73	565.37	76.76	539.55	531.01	8.54	124.34	0.25	85.29	124.34
2	346.20	483.56	7.40	664.16	664.16	0.00	129.96	0.5	93.51	254.30
3	358.95	489.42	3.54				126.93	0.75	97.44	381.23
4	351.80	450.62	0.78				98.04	1	98.31	479.27
5	364.30	537.23	0.49				172.44	2	98.86	651.71
Cumulative Quartz Recovery			**98.86**	%		Conditioning Time		**5**	min	
Cumulative Water (g)			**651.71**							

Run #28

Air Flow Rate			5 l/min			Water pH		8		
Measured Froth Depth			10 mm			Adjusted pH		7		
Sampl No	Pan Mass (g)	Froth + Pan Mass (g)	Quartz Dry Mass (g)	Bottle Mass Before (g)	Bottle Mass After (g)	Wash Water Mass (g)	Water Mass (g)	Cum Flot Time (min)	Cum Quartz Rec (%)	Cum Water (g)
1	374.43	610.72	78.38	531.01	519.90	11.11	146.80	0.25	87.09	146.80
2	369.90	551.11	8.29				172.92	0.5	96.30	319.72
3	367.93	571.82	1.40				202.49	0.75	97.86	522.21
4	367.72	531.95	0.56				163.67	1	98.48	685.88
5	367.27	582.42	0.63				214.52	2	99.18	900.40
Cumulative Quartz Recovery			**99.18**	%		Conditioning Time		**5**	min	
Cumulative Water (g)			**900.40**							

Run #29

Air Flow Rate			6 l/min			Water pH		8		
Measured Froth Depth			10 mm			Adjusted pH		7		
Sampl No	Pan Mass (g)	Froth + Pan Mass (g)	Quartz Dry Mass (g)	Bottle Mass Before (g)	Bottle Mass After (g)	Wash Water Mass (g)	Water Mass (g)	Cum Flot Time (min)	Cum Quartz Rec (%)	Cum Water (g)
1	361.86	619.76	80.74				177.16	0.25	89.71	177.16
2	365.20	582.08	6.29				210.59	0.5	96.70	387.75
3	365.70	568.58	1.10				201.78	0.75	97.92	589.53
4	374.27	547.74	0.19				173.28	1	98.13	762.81
5	371.98	871.86	0.37				499.51	2	98.54	1262.32
Cumulative Quartz Recovery			**98.54**	%		Conditioning Time		5	min	
Cumulative Water (g)			**1262.32**							

Run #30

Air Flow Rate			2 l/min			Water pH		8		
Measured Froth Depth			25 mm			Adjusted pH		7		
Sampl No	Pan Mass (g)	Froth + Pan Mass (g)	Quartz Dry Mass (g)	Bottle Mass Before (g)	Bottle Mass After (g)	Wash Water Mass (g)	Water Mass (g)	Cum Flot Time (min)	Cum Quartz Rec (%)	Cum Water (g)
1	363.47	433.12	19.75	475.63	449.28	26.35	23.55	0.25	21.94	23.55
2	383.84	429.26	11.51	639.36	625.28	14.08	19.83	0.5	34.73	43.38
3	370.70	408.70	5.14	511.70	489.26	22.44	10.42	0.75	40.44	53.80
4	373.42	417.39	6.23	527.73	510.30	17.43	20.31	1	47.37	74.11
5	345.70	427.42	4.94	652.26	584.76	67.50	9.28	2	52.86	83.39
Cumulative Quartz Recovery			**52.86**	%		Conditioning Time		**5**	min	
Cumulative Water (g)			**83.39**							

Run #31

Air Flow Rate			3 l/min			Water pH		8		
Measured Froth Depth			25 mm			Adjusted pH		7		
Sampl No	Pan Mass (g)	Froth + Pan Mass (g)	Quartz Dry Mass (g)	Bottle Mass Before (g)	Bottle Mass After (g)	Wash Water Mass (g)	Water Mass (g)	Cum Flot Time (min)	Cum Quartz Rec (%)	Cum Water (g)
1	358.95	452.85	31.03	449.28	435.22	14.06	48.81	0.25	34.48	48.81
2	346.20	433.64	23.68	625.28	604.42	20.86	42.90	0.5	60.79	91.71
3	354.82	431.38	9.56	489.26	475.26	14.00	53.00	0.75	71.41	144.71
4	362.62	451.74	9.67	510.30	495.44	14.86	64.59	1	82.16	209.30
5	324.84	474.78	2.09	584.76	494.28	90.48	57.37	2	84.48	266.67
Cumulative Quartz Recovery			**84.48**	%		Conditioning Time		**5**	min	
Cumulative Water (g)			**266.67**							

Run #32

Air Flow Rate			4 l/min			Water pH		8		
Measured Froth Depth			25 mm			Adjusted pH		7		
Sampl No	Pan Mass (g)	Froth + Pan Mass (g)	Quartz Dry Mass (g)	Bottle Mass Before (g)	Bottle Mass After (g)	Wash Water Mass (g)	Water Mass (g)	Cum Flot Time (min)	Cum Quartz Rec (%)	Cum Water (g)
1	367.93	515.66	40.06	435.22	409.77	25.45	82.22	0.25	44.51	82.22
2	351.80	485.28	17.11	604.42	587.39	17.03	99.34	0.5	63.52	181.56
3	364.30	533.59	14.16				155.13	0.75	79.26	336.69
4	374.43	455.39	6.50				74.46	1	86.48	411.15
5	369.90	451.74	2.92	494.28	465.14	29.14	49.78	2	89.72	460.93
Cumulative Quartz Recovery			**89.72**	%		Conditioning Time		**5**	min	
Cumulative Water (g)			**460.93**							

Run #33

Air Flow Rate			5 l/min			Water pH		8		
Measured Froth Depth			25 mm			Adjusted pH		7		
Sampl No	Pan Mass (g)	Froth + Pan Mass (g)	Quartz Dry Mass (g)	Bottle Mass Before (g)	Bottle Mass After (g)	Wash Water Mass (g)	Water Mass (g)	Cum Flot Time (min)	Cum Quartz Rec (%)	Cum Water (g)
1	370.60	537.64	55.25	409.77	398.14	11.63	100.16	0.25	61.39	100.16
2	355.47	581.14	10.71				214.96	0.5	73.29	315.12
3	367.17	571.31	15.06				189.08	0.75	90.02	504.20
4	367.72	453.89	2.59				83.58	1	92.90	587.78
5	221.80	368.04	1.76	465.14	461.63	3.51	140.97	2	94.86	728.75
Cumulative Quartz Recovery			**94.86**	%		Conditioning Time		**5**	min	
Cumulative Water (g)			**728.75**							

Run #35

Air Flow Rate			6 l/min			Water pH		8		
Measured Froth Depth			25 mm			Adjusted pH		7		
Sampl No	Pan Mass (g)	Froth + Pan Mass (g)	Quartz Dry Mass (g)	Bottle Mass Before (g)	Bottle Mass After (g)	Wash Water Mass (g)	Water Mass (g)	Cum Flot Time (min)	Cum Quartz Rec (%)	Cum Water (g)
1	345.70	642.90	61.67	376.22	348.62	27.60	207.93	0.25	68.52	207.93
2	361.86	635.34	9.62				263.86	0.5	79.21	471.79
3	369.90	558.99	7.68				181.41	0.75	87.74	653.20
4	360.03	558.31	3.53				194.75	1	91.67	847.95
5	355.73	600.12	2.66				241.73	2	94.62	1089.68
Cumulative Quartz Recovery			**94.62**	%		Conditioning Time		**5**	min	
Cumulative Water (g)			**1089.68**							

Run #6

Air Flow Rate			3 l/min			Water pH		8		
Measured Froth Depth			40 mm			Adjusted pH		7		
Sampl No	Pan Mass (g)	Froth + Pan Mass (g)	Quartz Dry Mass (g)	Bottle Mass Before (g)	Bottle Mass After (g)	Wash Water Mass (g)	Water Mass (g)	Cum Flot Time (min)	Cum Quartz Rec (%)	Cum Water (g)
1	365.60	473.30	22.04	454.54	407.06	47.48	38.18	0.5	24.49	38.18
2	374.84	483.76	16.98	543.20	509.00	34.20	57.74	1	43.36	95.92
3	354.87	438.40	11.43	407.60	376.82	30.78	41.32	1.5	56.06	137.24
4	378.74	473.75	8.08	387.80	315.10	72.70	14.23	2.5	65.03	151.47
Cumulative Quartz Recovery			**65.03**	%		Conditioning Time		**5**	min	
Cumulative Water (g)			**151.47**							

Run #17

Air Flow Rate			4 l/min			Water pH		8		
Measured Froth Depth			40 mm			Adjusted pH		7		
Sampl No	Pan Mass (g)	Froth + Pan Mass (g)	Quartz Dry Mass (g)	Bottle Mass Before (g)	Bottle Mass After (g)	Wash Water Mass (g)	Water Mass (g)	Cum Flot Time (min)	Cum Quartz Rec (%)	Cum Water (g)
1	374.27	581.57	56.71			0.00	150.59	0.25	63.01	150.59
2	363.47	495.02	11.00			0.00	120.55	0.5	75.23	271.14
3	382.70	505.78	7.22			0.00	115.86	0.75	83.26	387.00
4	371.50	480.81	5.11			0.00	104.20	1	88.93	491.20
	370.51	546.64	8.04	484.28	477.91	6.37	161.72	2	97.87	652.92
Cumulative Quartz Recovery			**97.87**	%		Conditioning Time		**5**	min	
Cumulative Water (g)			**652.92**							

Run #14

Air Flow Rate			4 l/min			Water pH		8		
Measured Froth Depth			40 mm			Adjusted pH		7		
Sampl No	Pan Mass (g)	Froth + Pan Mass (g)	Quartz Dry Mass (g)	Bottle Mass Before (g)	Bottle Mass After (g)	Wash Water Mass (g)	Water Mass (g)	Cum Flot Time (min)	Cum Quartz Rec (%)	Cum Water (g)
1	361.42	545.20	49.33	509.00	476.30	32.70	101.75	0.5	54.81	101.75
2	362.02	498.60	17.90			0.00	118.68	1	74.70	220.43
3	345.70	474.80	6.84	653.20	607.00	46.20	76.06	1.5	82.30	296.49
4	346.20	387.00	1.95	583.80	553.20	30.60	8.25	2	84.47	304.74
Cumulative Quartz Recovery			**84.47**	%		Conditioning Time		**5**	min	
Cumulative Water (g)			**304.74**							

Run #8

Air Flow Rate			6 l/min			Water pH		8		
Measured Froth Depth			40 mm			Adjusted pH		7		
Sampl No	Pan Mass (g)	Froth + Pan Mass (g)	Quartz Dry Mass (g)	Bottle Mass Before (g)	Bottle Mass After (g)	Wash Water Mass (g)	Water Mass (g)	Cum Flot Time (min)	Cum Quartz Rec (%)	Cum Water (g)
1	346.20	714.80	73.56			0.00	295.04	0.5	81.73	295.04
2	345.70	651.70	7.73			0.00	298.27	1	90.32	593.31
3	358.95	511.30	3.74			0.00	148.61	1.5	94.48	741.92
4	370.30	509.20	0.94			0.00	137.96	3	95.52	879.88
Cumulative Quartz Recovery			**95.52**	%		Conditioning Time		**5**	min	
Cumulative Water (g)			**879.88**							

Run #15

Air Flow Rate			4 l/min			Water pH		8		
Measured Froth Depth			50 mm			Adjusted pH		7		
Sampl No	Pan Mass (g)	Froth + Pan Mass (g)	Quartz Dry Mass (g)	Bottle Mass Before (g)	Bottle Mass After (g)	Wash Water Mass (g)	Water Mass (g)	Cum Flot Time (min)	Cum Quartz Rec (%)	Cum Water (g)
1	365.70	461.22	27.18			0.00	68.34	0.25	30.20	68.34
2	371.50	418.40	5.78			0.00	41.12	0.5	36.62	109.46
3	382.70	418.74	4.47			0.00	31.57	0.75	41.59	141.03
4	370.51	399.20	4.66			0.00	24.03	1	46.77	165.06
5	374.27	409.55	2.39	512.88	484.30	28.58	4.31	2	49.42	169.37
Cumulative Quartz Recovery			**49.42**	%		Conditioning Time		5	min	
Cumulative Water (g)			**169.37**							

Run #16

Air Flow Rate			5 l/min			Water pH		8		
Measured Froth Depth			50 mm			Adjusted pH		7		
Sampl No	Pan Mass (g)	Froth + Pan Mass (g)	Quartz Dry Mass (g)	Bottle Mass Before (g)	Bottle Mass After (g)	Wash Water Mass (g)	Water Mass (g)	Cum Flot Time (min)	Cum Quartz Rec (%)	Cum Water (g)
1	365.60	540.63	38.78			0.00	136.25	0.25	43.09	136.25
2	367.93	467.43	13.06			0.00	86.44	0.5	57.60	222.69
3	367.72	470.69	14.62			0.00	88.35	0.75	73.84	311.04
4	354.87	419.66	8.29			0.00	56.50	1	83.06	367.54
	374.72	460.51	3.01	543.79	485.76	58.03	24.75	2	86.40	392.29
Cumulative Quartz Recovery			**86.40**	%		Conditioning Time		5	min	
Cumulative Water (g)			**392.29**							

Run #7

Air Flow Rate			6 l/min			Water pH		8		
Measured Froth Depth			50 mm			Adjusted pH		7		
Sampl No	Pan Mass (g)	Froth + Pan Mass (g)	Quartz Dry Mass (g)	Bottle Mass Before (g)	Bottle Mass After (g)	Wash Water Mass (g)	Water Mass (g)	Cum Flot Time (min)	Cum Quartz Rec (%)	Cum Water (g)
1	367.72	700.20	51.10			0.00	281.38	0.5	56.78	281.38
2	374.84	635.10	18.61			0.00	241.65	1	77.46	523.03
3	354.87	449.10	7.84			0.00	86.39	1.5	86.17	609.42
4	378.74	514.60	1.72			0.00	134.14	3	88.08	743.56
Cumulative Quartz Recovery			**88.08**	%		Conditioning Time		5	min	
Cumulative Water (g)			**743.56**							

Run #5

Air Flow Rate	3 l/min	Water pH	8
Measured Froth Depth	20 mm	Adjusted pH	7

Sampl No	Pan Mass (g)	Froth + Pan Mass (g)	Quartz Dry Mass (g)	Bottle Mass Before (g)	Bottle Mass After (g)	Wash Water Mass (g)	Water Mass (g)	Cum Flot Time (min)	Cum Quartz Rec (%)	Cum Water (g)
1	378.74	626.40	52.64			0.00	195.02	1	58.49	195.02
2	367.72	568.10	16.14			0.00	184.24	2	76.42	379.26
3	354.87	472.20	4.60			0.00	112.73	3	81.53	491.99
4	346.20	554.60	3.59			0.00	204.81	5	85.52	696.80

Cumulative Quartz Recovery	**85.52**	%	Conditioning Time	**5**	min
Cumulative Water (g)	**696.80**				

Run #18

Air Flow Rate	4 l/min	Water pH	8
Measured Froth Depth	20 mm	Adjusted pH	7

Sampl No	Pan Mass (g)	Froth + Pan Mass (g)	Quartz Dry Mass (g)	Bottle Mass Before (g)	Bottle Mass After (g)	Wash Water Mass (g)	Water Mass (g)	Cum Flot Time (min)	Cum Quartz Rec (%)	Cum Water (g)
1	365.60	579.04	75.82	485.73	478.76	6.97	130.65	0.25	84.24	130.65
2	367.72	559.03	8.73			0.00	182.58	0.5	93.94	313.23
3	367.93	543.57	2.67			0.00	172.97	0.75	96.91	486.20
4	354.87	508.87	0.40			0.00	153.60	1	97.36	639.80
5	374.72	709.98	1.06			0.00	334.20	2	98.53	974.00

Cumulative Quartz Recovery	**98.53**	%	Conditioning Time	**5**	min
Cumulative Water (g)	**974.00**				

Run #13

Air Flow Rate	4 l/min	Water pH	8
Measured Froth Depth	20 mm	Adjusted pH	7

Sampl No	Pan Mass (g)	Froth + Pan Mass (g)	Quartz Dry Mass (g)	Bottle Mass Before (g)	Bottle Mass After (g)	Wash Water Mass (g)	Water Mass (g)	Cum Flot Time (min)	Cum Quartz Rec (%)	Cum Water (g)
1	363.90	630.80	64.87			0.00	202.03	0.5	72.08	202.03
2	374.06	611.30	9.12			0.00	228.12	1	82.21	430.15
3	354.87	570.10	7.97			0.00	207.26	1.5	91.07	637.41
4	374.84	505.00	2.55			0.00	127.61	2	93.90	765.02
5	370.30	486.65	1.35			0.00	115.00	3	95.40	880.02

Cumulative Quartz Recovery	**95.40**	%	Conditioning Time	**5**	min
Cumulative Water (g)	**880.02**				

Run #9

Air Flow Rate	6 l/min	Water pH	8
Measured Froth Depth	20 mm	Adjusted pH	7

Sampl No	Pan Mass (g)	Froth + Pan Mass (g)	Quartz Dry Mass (g)	Bottle Mass Before (g)	Bottle Mass After (g)	Wash Water Mass (g)	Water Mass (g)	Cum Flot Time (min)	Cum Quartz Rec (%)	Cum Water (g)
1	368.10	885.20	82.81			0.00	434.29	0.5	92.01	434.29
2	346.20	768.20	4.14			0.00	417.86	1	96.61	852.15
3	345.70	592.40	0.80			0.00	245.90	1.5	97.50	1098.05
4	374.84	557.60	0.05			0.00	182.71	2	97.56	1280.76
5	354.87	549.10	0.00			0.00	194.23	3	97.56	1474.99

Cumulative Quartz Recovery	**97.56**	%	Conditioning Time	**5**	min
Cumulative Water (g)	**1474.99**				

APPENDIX B

LABORATORY DATA COLLECTED USING THE NOMONALLY 75% PASSING 106 MICRONS FEED MATERIAL

B-1: Batch data

B-2: Continuous data

B-3: Batch with wash water

APPENDIX B: LABORATORY DATA COLLECTED USING THE NOMINALLY 75% PASSING 106 MICRONS FRACTION FEED MATERIAL

B-1: Batch data

Masses

Run #9

Air Flow Rate			3 l/min			Water pH		8		
Measured Froth Depth			5 mm			Adjusted pH		7		
Sampl No	Pan Mass (g)	Froth + Pan Mass (g)	Quartz Dry Mass (g)	Bottle Mass Before (g)	Bottle Mass After (g)	Wash Water Mass (g)	Water Mass (g)	Flot Time (min)	Cum Quartz Rec (%)	Cum Water (g)
1	351.52	714.60	170.06	567.21	563.17	4.04	188.98	0.5	56.69	188.98
2	367.85	566.01	78.13	565.33	547.45	17.88	102.15	1	82.73	291.13
3	365.70	583.96	34.77	530.74	530.59	0.15	183.34	2	94.32	474.47
4	355.70	449.32	6.26	558.36	554.63	3.73	83.63	3	96.41	558.10
5	370.44	433.79	2.09	570.74	543.98	26.76	34.50	5	97.10	592.60
Cumulative Quartz Recovery			**97.10**	%		Conditioning Time		**5**	min	
Cumulative Water (g)			**592.60**							

Run #10

Air Flow Rate			4 l/min			Water pH		8		
Measured Froth Depth			5 mm			Adjusted pH		7		
Sampl No	Pan Mass (g)	Froth + Pan Mass (g)	Quartz Dry Mass (g)	Bottle Mass Before (g)	Bottle Mass After (g)	Wash Water Mass (g)	Water Mass (g)	Flot Time (min)	Cum Quartz Rec (%)	Cum Water (g)
1	345.57	737.04	162.10	563.17	560.68	2.49	226.88	0.5	54.03	226.88
2	361.93	574.83	17.80	547.45	513.09	34.36	160.74	1	59.97	387.62
3	378.13	606.44	39.60	530.59	498.97	31.62	157.09	2	73.17	544.71
4	378.77	609.14	9.98	554.63	523.31	31.32	189.07	3	76.49	733.78
5	221.61	467.48	4.58	543.98	435.63	108.35	132.94	5	78.02	866.72
Cumulative Quartz Recovery			**78.02**	%		Conditioning Time		**5**	min	
Cumulative Water (g)			**866.72**							

Run #11

Air Flow Rate			5 l/min			Water pH		8		
Measured Froth Depth			5 mm			Adjusted pH		7		
Sampl No	Pan Mass (g)	Froth + Pan Mass (g)	Quartz Dry Mass (g)	Bottle Mass Before (g)	Bottle Mass After (g)	Wash Water Mass (g)	Water Mass (g)	Flot Time (min)	Cum Quartz Rec (%)	Cum Water (g)
1	355.70	837.48	170.03	560.68	507.26	53.42	258.33	0.5	56.68	258.33
2	345.57	568.97	64.18	513.09	464.53	48.56	110.66	1	78.07	368.99
3	378.13	593.91	35.03	498.97	471.57	27.40	153.35	2	89.75	522.34
4	378.77	574.78	10.53	523.31	513.05	10.26	175.22	3	93.26	697.56
5	370.44	704.32	5.35	435.63	405.03	30.60	297.93	5	95.04	995.49
Cumulative Quartz Recovery			**95.04**	%		Conditioning Time		**5**	min	
Cumulative Water (g)			**995.49**							

Run #12

Air Flow Rate			6	l/min		Water pH		8		
Measured Froth Depth			5	mm		Adjusted pH		7		
Sampl No	Pan Mass	Froth + Pan Mass	Quartz Dry Mass	Bottle Mass Before	Bottle Mass After	Wash Water Mass	Water Mass	Flot Time	Cum Quartz Rec	Cum Water
	(g)	(g)	(g)	(g)	(g)	(g)	(g)	(min)	(%)	(g)
1	351.52	952.68	186.03	507.26	422.19	85.07	330.06	0.5	62.01	330.06
2	367.85	602.42	68.14	464.53	454.05	10.48	155.95	1	84.72	486.01
3	365.70	660.38	26.54	471.57	405.96	65.61	202.53	2	93.57	688.54
4	358.36	587.72	5.17	513.05	467.91	45.14	179.05	3	95.29	867.59
5	221.61	687.12	3.06	405.03	356.29	48.74	413.71	5	96.31	1281.30
Cumulative Quartz Recovery			**96.31**	%		Conditioning		5	min	
Cumulative Water (g)			**1281.30**			Time				

Run #5

Air Flow Rate			3	l/min		Water pH		8		
Measured Froth Depth			25	mm		Adjusted pH		7		
Sampl No	Pan Mass	Froth + Pan Mass	Quartz Dry Mass	Bottle Mass Before	Bottle Mass After	Wash Water Mass	Water Mass	Flot Time	Cum Quartz Rec	Cum Water
	(g)	(g)	(g)	(g)	(g)	(g)	(g)	(min)	(%)	(g)
1	369.28	675.32	128.39	581.13	572.38	8.75	168.90	0.5	42.80	168.90
2	365.29	542.96	53.29	577.52	563.92	13.60	110.78	1	60.56	279.68
3	367.83	505.23	23.08	548.37	466.91	81.46	32.86	2	68.25	312.54
4	370.00	425.72	17.23	569.14	556.72	12.42	26.07	3	74.00	338.61
5	370.46	575.98	22.26	569.59	416.79	152.80	30.46	5	81.42	369.07
Cumulative Quartz Recovery			**81.42**	%		Conditioning		5	min	
Cumulative Water (g)			**369.07**			Time				

Run #6

Air Flow Rate			4	l/min		Water pH		8		
Measured Froth Depth			25	mm		Adjusted pH		7		
Sampl No	Pan Mass	Froth + Pan Mass	Quartz Dry Mass	Bottle Mass Before	Bottle Mass After	Wash Water Mass	Water Mass	Flot Time	Cum Quartz Rec	Cum Water
	(g)	(g)	(g)	(g)	(g)	(g)	(g)	(min)	(%)	(g)
1	355.70	634.06	127.28	572.38	562.69	9.69	141.39	0.5	42.43	141.39
2	354.84	542.34	62.05	563.92	514.84	49.08	76.37	1	63.11	217.76
3	351.52	446.69	17.23	466.91	418.93	47.98	29.96	2	68.85	247.72
4	367.64	445.65	10.17	556.72	509.76	46.96	20.88	3	72.24	268.60
5	367.85	438.02	8.29	416.79	373.86	42.93	18.95	5	75.01	287.55
Cumulative Quartz Recovery			**75.01**	%		Conditioning		5	min	
Cumulative Water (g)			**287.55**			Time				

Run #7

Air Flow Rate			5	l/min		Water pH		8		
Measured Froth Depth			25	mm		Adjusted pH		7		
Sampl No	Pan Mass (g)	Froth + Pan Mass (g)	Quartz Dry Mass (g)	Bottle Mass Before (g)	Bottle Mass After (g)	Wash Water Mass (g)	Water Mass (g)	Flot Time (min)	Cum Quartz Rec (%)	Cum Water (g)
1	371.39	650.82	115.75	562.69	546.13	16.56	147.12	0.5	38.58	147.12
2	244.41	435.48	74.59	514.84	492.27	22.57	93.91	1	63.45	241.03
3	370.34	469.39	24.98	418.93	384.51	34.42	39.65	2	71.77	280.68
4	221.61	288.97	10.00	509.76	475.53	34.23	23.13	3	75.11	303.81
5	382.61	518.29	11.27	373.86	270.19	103.67	20.74	5	78.86	324.55
Cumulative Quartz Recovery			**78.86**	%		Conditioning Time		**5**	min	
Cumulative Water (g)			**324.55**							

Run #8

Air Flow Rate			6	l/min		Water pH		8		
Measured Froth Depth			25	mm		Adjusted pH		7		
Sampl No	Pan Mass (g)	Froth + Pan Mass (g)	Quartz Dry Mass (g)	Bottle Mass Before (g)	Bottle Mass After (g)	Wash Water Mass (g)	Water Mass (g)	Flot Time (min)	Cum Quartz Rec (%)	Cum Water (g)
1	358.36	570.70	140.94	546.13	528.22	17.91	53.49	0.5	46.98	53.49
2	360.14	563.55	63.52	492.27	459.66	32.61	107.28	1	68.15	160.77
3	378.13	496.12	22.33	384.51	330.78	53.73	41.93	2	75.60	202.70
4	364.30	442.90	8.42	475.53	417.99	57.54	12.64	3	78.40	215.34
5	370.44	513.15	8.71	270.19	148.30	121.89	12.11	5	81.31	227.45
Cumulative Quartz Recovery			**81.31**	%		Conditioning Time		**5**	min	
Cumulative Water (g)			**227.45**							

Run #1

Air Flow Rate			3	l/min		Water pH		8		
Measured Froth Depth			45	mm		Adjusted pH		7		
Sampl No	Pan Mass (g)	Froth + Pan Mass (g)	Quartz Dry Mass (g)	Bottle Mass Before (g)	Bottle Mass After (g)	Wash Water Mass (g)	Water Mass (g)	Flot Time (min)	Cum Quartz Rec (%)	Cum Water (g)
1	355.70	656.34	144.57	467.38	444.75	22.63	133.44	1	48.19	133.44
2	354.84	472.18	26.00	484.42	419.58	64.84	26.50	2	56.86	159.94
3	370.34	441.23	8.02	527.12	464.53	62.59	0.28	3	59.53	160.22
4	370.44	461.23	4.23	443.05	360.63	82.42	4.14	4	60.94	164.36
5	382.61	446.40	1.40	470.82	409.49	61.33	1.06	5	61.41	165.42
Cumulative Quartz Recovery			**61.41**	%		Conditioning Time		**5**	min	
Cumulative Water (g)			**165.42**							

Run #2

Air Flow Rate			4	l/min		Water pH		8		
Measured Froth Depth			45	mm		Adjusted pH		7		
Sampl No	Pan Mass (g)	Froth + Pan Mass (g)	Quartz Dry Mass (g)	Bottle Mass Before (g)	Bottle Mass After (g)	Wash Water Mass (g)	Water Mass (g)	Flot Time (min)	Cum Quartz Rec (%)	Cum Water (g)
1	369.2	792.5	178.42	444.75	437.28	7.47	237.41	1	59.47	237.41
2	365.11	431.8	10.67	419.58	378.88	40.70	15.32	2	63.03	252.73
3	367.76	470.84	7.22	464.53	360.64	103.89	-8.03	3	65.44	244.70
4	367.64	479.56	3.9	360.63	258.63	102.00	6.02	4	66.74	250.72
5	370.44	458.84	1.87	409.49	323.34	86.15	0.38	5	67.36	251.10
Cumulative Quartz Recovery			**67.36**	%		Conditioning		5	min	
Cumulative Water (g)			**251.10**			Time				

Run #3

Air Flow Rate			5	l/min		Water pH		8		
Measured Froth Depth			45	mm		Adjusted pH		7		
Sampl No	Pan Mass (g)	Froth + Pan Mass (g)	Quartz Dry Mass (g)	Bottle Mass Before (g)	Bottle Mass After (g)	Wash Water Mass (g)	Water Mass (g)	Flot Time (min)	Cum Quartz Rec (%)	Cum Water (g)
1	358.36	780.58	172.75	437.28	341.53	95.75	153.72	1	57.58	153.72
2	244.41	341.83	7.67	378.88	348.26	30.62	59.13	2	60.14	212.85
3	351.52	441.71	3.83	360.64	273.04	87.60	-1.24	3	61.42	211.61
4	369.92	457.89	2.72	258.63	178.71	79.92	5.33	4	62.32	216.94
5	367.85	480.07	2.71	323.34	217.44	105.90	3.61	5	63.23	220.55
Cumulative Quartz Recovery			**63.23**	%		Conditioning		5	min	
Cumulative Water (g)			**220.55**			Time				

Run #4

Air Flow Rate			6	l/min		Water pH		8		
Measured Froth Depth			45	mm		Adjusted pH		7		
Sampl No	Pan Mass (g)	Froth + Pan Mass (g)	Quartz Dry Mass (g)	Bottle Mass Before (g)	Bottle Mass After (g)	Wash Water Mass (g)	Water Mass (g)	Flot Time (min)	Cum Quartz Rec (%)	Cum Water (g)
1	370.37	626.12	102.04	341.53	294.66	46.87	106.84	1	34.01	106.84
2	360.14	535.64	25.73	348.26	225.74	122.52	27.25	2	42.59	134.09
3	378.77	513.65	10.94	273.04	161.91	111.13	12.81	3	46.24	146.90
4	221.61	303.98	6.01	178.71	110.57	68.14	8.22	4	48.24	155.12
5	239.41	347.44	3.53	217.44	115.12	102.32	2.18	5	49.42	157.30
Cumulative Quartz Recovery			**49.42**	%		Conditioning		5	min	
Cumulative Water (g)			**157.30**			Time				

Particle Sizes

#1		Sizes					
	Sample	sub 10	10 to 25	25 to 45	45 to 75	75 to 106	plus 106
	C1	4.94	12.08	18.42	21.55	24.32	18.66
	C2	7.93	17.7	22.15	21.71	19.81	10.72
	C3	6.32	14.91	18.46	20.36	22.92	17.02
	C4	8.21	17.33	20.07	20.11	20.51	13.8
	C5	5.89	13.18	18.73	22.05	24.37	15.78
	Head	5.76	12.6	17.35	20.13	23.53	20.64

#2		Sizes					
	Sample	sub 10	10 to 25	25 to 45	45 to 75	75 to 106	plus 106
	C1	5.78	11.7	16.68	20.81	25.15	19.87
	C2	10.62	22.16	23.7	20.49	16.5	6.52
	C3	7.82	15.93	19.4	20.84	22.35	13.65
	C4	4.81	12.02	17.83	21.25	24.63	19.43
	C5	4.68	11	17.61	22.04	25.65	19.05
	Head	6.64	13.66	17.69	20.37	23.6	18.05

#3		Sizes					
	Sample	sub 10	10 to 25	25 to 45	45 to 75	75 to 106	plus 106
	C1	5.13	10.69	16.51	20.84	25.11	21.7
	C2	7.84	18.02	23.09	21.35	19.24	10.46
	C3	7.52	18.43	22.39	21.11	19.08	11.48
	C4	7.16	15.94	21.27	21.8	20.73	13.11
	C5	6.66	15.73	20.95	21.51	21.37	13.78
	Head	6.99	14.35	18.44	19.92	21.92	18.36

#4		Sizes				
Sample	sub 10	10 to 25	25 to 45	45 to 75	75 to 106	plus 106
C1	5.82	12.1	17.18	19.86	23.29	21.74
C2	6.8	14.83	20.07	21.04	21.64	15.64
C3	6.77	15.48	20.42	21.02	21.4	14.9
C4	4.9	14.58	22.83	23.71	21.6	12.36
C5	6.07	14.39	20.22	21.63	22.31	15.35
Head	6.25	12.76	17.45	20.01	22.95	20.56

#5		Sizes				
Sample	sub 10	10 to 25	25 to 45	45 to 75	75 to 106	plus 106
C1	4.42	9.18	15.03	20.92	26.89	23.56
C2	7.5	15.83	21.54	22.2	20.52	12.38
C3	7.27	13.2	15.75	18.45	22.84	22.5
C4	5.5	10.27	14.75	19.7	25.6	24.21
C5	4.34	8.37	12.88	19.22	27.29	27.91
Head	5.28	10.01	15.3	20.35	25.83	23.25

#6		Sizes				
Sample	sub 10	10 to 25	25 to 45	45 to 75	75 to 106	plus 106
C1	3.16	6.49	11.61	19.02	28.3	31.42
C2	4.58	9.16	15.56	21.76	27.32	21.62
C3	7.93	15.75	19.74	19.92	20.17	13.84
C4	7.59	15.5	19.11	19.98	21.48	16.31
C5	7.48	14.39	18.22	20.04	22.26	17.58
Head	4.99	9.66	14.71	20.25	26.4	24

#7			Sizes				
	Sample	sub 10	10 to 25	25 to 45	45 to 75	75 to 106	plus 106
	C1	3.16	6.53	11.76	19.27	28.69	30.59
	C2	4.42	9.28	16.27	22.07	26.86	21.08
	C3	6.06	12.51	18.1	21.5	24.23	17.6
	C4	6.56	13	16.91	19.69	23.31	20.54
	C5	6.86	13.64	17.57	19.93	22.74	19.25
	Head	4.84	9.07	14.16	19.94	26.55	25.45

#8			Sizes				
	Sample	sub 10	10 to 25	25 to 45	45 to 75	75 to 106	plus 106
	C1	4.1	8.04	13.56	19.97	27.47	26.83
	C2	5.69	11.75	18.38	22.12	24.57	17.5
	C3	7.87	16.63	20.77	20.43	20.19	14.1
	C4	6.46	13.6	17.36	19.36	22.49	20.72
	C5	7.16	14.22	17.59	19.63	22.54	18.83
	Head	5.23	10.63	15.66	20.09	25.13	23.24

#9			Sizes				
	Sample	sub 10	10 to 25	25 to 45	45 to 75	75 to 106	plus 106
	C1	2.51	4.7	9.25	17.81	29.98	35.76
	C2	4.16	8.33	15.64	22.45	27.86	21.54
	C3	6.5	12.72	18.22	20.71	22.89	18.95
	C4	10.7	20.14	21.94	19.32	16.95	10.96
	C5	13.66	25.48	23.6	17.56	12.67	7.01
	Head	4.81	9.08	14.2	19.75	26.24	25.91

#10			Sizes				
	Sample	sub 10	10 to 25	25 to 45	45 to 75	75 to 106	plus 106
	C1	2.95	6.18	11.74	19.27	28.3	31.54
	C2	4.67	9.86	16.97	22.25	26.35	19.89
	C3	7.26	15.03	20.06	20.99	21.54	15.12
	C4	10.27	19.38	20.6	18.85	17.93	12.94
	C5	14.42	26.08	22.97	16.83	12.59	7.12
	Head	4.74	9.17	14.15	19.53	26.02	26.39

#11			Sizes				
	Sample	sub 10	10 to 25	25 to 45	45 to 75	75 to 106	plus 106
	C1	3.04	6.23	11.95	19.55	28.48	30.74
	C2	4.85	10.31	17.41	22.29	25.9	19.25
	C3	7.2	14.35	19.35	20.9	22.11	16.05
	C4	9.21	17.27	19.8	19.47	19.85	14.41
	C5	14.9	23.75	21.33	17.23	14.15	8.64
	Head	5.26	10.1	15.11	19.88	25.39	24.25

#12			Sizes				
	Sample	sub 10	10 to 25	25 to 45	45 to 75	75 to 106	plus 106
	C1	3.14	6.32	11.86	19.6	28.77	30.32
	C2	5.33	11.14	18.13	22.38	25.2	17.82
	C3	8.82	17.21	20.69	20.31	19.52	13.45
	C4	12.3	22.46	21.77	17.92	15.43	10.11
	C5	18.57	29.22	22.73	14.72	9.79	4.97
	Head	5.07	9.79	15.07	19.98	25.53	24.57

B-2: Continuous data

Masses

OPERATING CONDITIONS				FEED					CONCENTRATE					TAILS			
Test	roth heigh (cm)	Airflow (L/min)		% Solids (g/g)	Water flow (g/min)	olids Flo (g/min)	Total (g/min)		% Solids (g/g)	Water flow (g/min)	olids Flo (g/min)	Total (g/min)		% Solids (g/g)	Water flow (g/min)	olids Flo (g/min)	Total (g/min)
23	0.5	4		6.02	830.6	61.6	892.2		19.31	207.7	49.7	257.4		1.88	623.5	11.9	635.4
8	0.8	4		2.56	1075.9	68.9	1144.8		13.09	344.2	51.8	396.0		2.29	731.7	17.1	748.8
42	1	4		6.76	1207.3	31.7	1239.0		11.10	196.3	24.5	220.8		0.71	1011.0	7.2	1018.2
24	1.5	4		3.26	807.8	58.6	866.4		12.18	215.0	29.8	244.8		4.63	592.8	28.8	621.6
43	2	4		6.75	977.5	32.9	1010.4		13.12	88.1	13.3	101.4		2.16	888.8	19.6	908.4
4	0.5	5		6.53	1044.6	75.6	1120.2		15.24	286.8	51.6	338.4		3.08	757.7	24.1	781.8
22	0.5	5		3.83	701.6	49.0	750.6		11.90	192.4	26.0	218.4		4.33	508.6	23.0	531.6
35	0.5	5		7.11	948.6	37.8	986.4		8.60	361.4	34.0	395.4		0.64	587.8	3.8	591.6
9	0.8	5		7.31	1069.0	81.8	1150.8		13.20	405.2	61.6	466.8		2.95	663.2	20.2	683.4
25	1	5		2.33	830.3	65.5	895.8		10.82	305.5	37.1	342.6		5.14	524.8	28.4	553.2
41	1	5		6.60	1133.4	27.0	1160.4		8.43	245.0	22.6	267.6		0.50	888.3	4.5	892.8
40	1	5		2.42	1247.7	30.9	1278.6		12.55	174.2	25.0	199.2		0.55	1073.5	5.9	1079.4
15	2	5		6.60	583.9	41.3	625.2		10.34	344.3	39.7	384.0		0.63	239.7	1.5	241.2
3	0.5	6		7.42	1139.8	91.4	1231.2		16.07	436.6	83.6	520.2		1.09	703.3	7.7	711.0
26	1	6		5.70	534.1	32.3	566.4		12.80	148.6	21.8	170.4		2.64	385.5	10.5	396.0
11	2	6		3.24	1135.0	38.0	1173.0		4.87	395.0	20.2	415.2		2.35	740.6	17.8	758.4
16	2	6		7.43	1026.4	82.4	1108.8		11.16	449.4	56.4	505.8		4.30	577.1	25.9	603.0
36	2.5	6		2.34	1036.0	24.8	1060.8		8.66	118.9	11.3	130.2		1.46	917.0	13.6	930.6
27	1	7		3.30	493.2	16.8	510.0		12.00	52.8	7.2	60.0		0.94	445.8	4.2	450.0
30	1	7		3.83	820.5	32.7	853.2		11.20	207.3	26.1	233.4		1.05	613.3	6.5	619.8
13	2	7		1.83	1326.5	24.7	1351.2		7.61	113.1	9.3	122.4		1.25	1213.4	15.4	1228.8
2	0.5	8		7.20	564.0	43.8	607.8		11.95	291.6	39.6	331.2		1.50	272.5	4.1	276.6
19	0.5	8		6.34	504.6	34.2	538.8		14.83	158.4	27.6	186.0		1.86	346.2	6.6	352.8
32	0.5	8		3.24	780.3	26.1	806.4		5.40	444.4	25.4	469.8		0.23	336.4	0.8	337.2
31	1.5	8		3.30	779.2	26.6	805.8		10.92	177.4	21.8	199.2		0.80	601.7	4.9	606.6
18	2	8		6.41	498.6	34.2	532.8		24.00	84.4	26.6	111.0		1.77	414.3	7.5	421.8

Particle Sizes

Feed Distribution						
Run	sub 10	10 to 25	25 to 45	45 to 75	75 to 106	plus 106
1	7.79	9.44	14.68	18.93	24.61	24.56
2	8.43	10.28	13.59	15.7	21.74	30.25
3	7.65	8.88	13.43	17.7	24.23	28.07
4	8.19	10.17	14.67	17.58	22.43	26.97
5	7.57	9.31	13.16	16.37	22.9	30.72
6	8.58	10.26	14.62	17.61	22.6	26.35
7	8.85	10.38	14.58	17.45	22.34	26.39
8	8.53	9.67	13.24	16.41	22.75	29.4
9	7.8	9.92	14.84	18.03	23.05	26.36
10	9.38	12.03	18.41	20.63	22.44	17.09
11	13.64	17.53	23.08	20.79	16.03	8.94
12	18.01	22.1	25.13	18.87	11.46	4.44
13	18.12	23.22	26.59	18.21	9.84	4.04
14	10.66	11.7	13.52	14.69	19.31	30.14
15	11.95	13.16	14.73	14.42	17.74	27.96
16	10.61	11.25	13.13	14.48	18.98	31.55
17	11.31	11.71	13.3	14.16	18.49	31.04
18	11.67	12.66	14.57	14.99	18.63	27.46
19	11.48	12.64	14.28	14.99	19.24	27.39
20	10.95	12.22	14.22	15.39	19.84	27.38
21	11.13	12.24	14.03	14.79	19.04	28.79
22	11.04	12.15	13.66	14.25	18.39	30.48
23	11.01	11.44	12.84	13.93	18.76	31.98
24	11.25	12.48	14.23	14.39	18.01	29.62
25	11.36	11.97	13.4	14.32	18.93	30
26	13.58	14.11	15.84	16.42	19.52	20.47
27	18.45	19.47	20.84	17.44	14.3	9.47
28	7.63	8.05	11.81	14.95	20.23	37.35
29	13.73	11.25	12.87	12.21	12.89	37.04
30	6.78	7.62	11.74	15.58	22.03	36.25
31	7.42	8.21	11.34	14.55	20.92	37.53
32	7.05	8.75	12.54	15.17	20.99	35.52
33	7.48	8.03	10.45	13.44	20.36	40.22
34	7.87	8.45	11.16	14.11	20.27	38.11
35	8.1	8.97	12.25	15.13	21.38	34.18
36	10.67	12.25	18.29	19.55	20.55	18.65
37	7.96	8.89	13.22	16.39	21.13	32.45
38	7.81	9.14	13.81	17.33	22.52	29.39
39	7.61	8.76	14.33	17.67	21.77	29.82
40	7.65	8.23	12.55	16.38	21.77	33.42
41	6.63	6.97	11.76	16.73	22.46	35.46
42	7.15	7.89	11.97	16.1	21.72	35.19
43	7.55	9.67	12.59	15.81	21.71	32.64

Conc Particle Size Distribution						
Run	sub 10	10 to 25	25 to 45	45 to 75	75 to 106	plus 106
1	6.66	7.82	12.85	17.32	23.6	31.76
2	8.05	10.33	13.88	15.77	21.2	30.73
3	7.81	9.8	14.67	17.74	22.86	27.14
4	7.32	9.28	13.77	17.16	23.11	29.35
5	8.18	10.03	15.06	17.5	21.34	27.9
6	7.72	9.5	13.8	16.91	22.82	29.25
7	7.65	9.14	13.78	17.43	22.96	29.06
8	8.82	10.51	14.89	17.61	22.23	25.94
9	7.17	8.37	12.27	16.1	23.3	32.78
10	7.5	9.65	15.03	18.49	23.27	26.1
11	13.29	16.68	22.13	20.61	17.37	9.91
12	15.48	20.35	24.77	19.97	13.55	5.88
13	19.59	24.74	26.03	17.13	9.24	3.23
14	10.31	11.6	13.85	14.96	19.22	30.04
15	11.28	12.55	14.3	14.83	18.62	28.42
16	11.26	12.31	13.74	14.44	18.33	29.32
17	9.22	10.71	12.7	14.11	19.18	34.05
18	9.99	11.48	13.54	14.94	19.99	30.04
19	10.48	12.49	14.64	15.53	20.05	26.82
20	10.97	12.74	14.95	15.53	19.44	26.38
21	9.97	10.66	12.65	14.37	19.11	33.27
22	11.38	12.61	13.82	14.02	17.89	30.27
23	10.04	11.34	13.3	14.44	19.08	31.78
24	10.47	11.49	13	13.91	18.28	32.87
25	10.7	12.06	13.98	14.92	19.38	28.96
26	12.86	14.06	15.22	15.15	18.66	24.05
27	14.13	16.82	19.5	18.07	17.97	13.45
28	5.9	6.6	9.77	13.16	19.86	44.72
29	5.64	6.63	9.5	12.77	20.03	45.4
30	7.08	8.68	12.19	15.4	21.67	35
31	6.99	8.54	12.09	15.57	21.92	34.86
32	7.6	8.97	12.59	15.6	21.65	33.6
33	6.85	7.95	11.34	15.03	21.64	37.21
34	6.73	7.71	11.05	14.47	20.77	39.27
35	7.15	8.63	12.32	15.34	21.04	35.55
36	10.91	12.63	17.38	18.77	20.73	19.55
37	7.04	8.49	13.04	16.82	22.78	31.82
38	8.08	9.92	15.49	18.56	22.62	25.31
39	7.57	8.71	13.27	16.87	22.19	31.39
40	7.79	9.28	14.39	17.83	22.27	28.43
41	8.05	9.26	13.61	16.88	21.69	30.54
42	6.65	7.87	12.43	16.74	22.8	33.52
43	7.16	8.57	12.52	16.33	22.19	33.2

B-3 Batch with wash water

Masses

Run #30

Air Flow Rate			4 l/min			Water pH		8		
Measured Froth Depth			Varied b/w 30 & 5		mm	Adjusted pH		7		
Sampl No	Pan Mass (g)	Froth + Pan Mass (g)	Quartz Dry Mass (g)	Bottle Mass Before (g)	Bottle Mass After (g)	Wash Water Mass (g)	Water Mass (g)	Flot Time (min)	Cum Quartz Rec (%)	Cum Water Rec (%)
1	360.70	742.48	92.67	566.10	563.43	2.67	286.44	0.17	30.89	10.61
2	367.30	582.30	52.44	560.40	540.35	20.05	142.51	0.5	48.37	15.89
3	363.10	529.90	40.58	555.58	514.19	41.39	84.83	1	61.90	19.03
4	358.70	519.26	25.87	547.17	513.94	33.23	101.46	1.5	70.52	22.79
5	351.30	605.47	10.13	554.83	527.43	27.40	216.64	2	73.90	30.81
6	368.10	628.63	5.21				255.32	2.5	75.63	40.27
7	361.43	622.71	3.15				258.13	3	76.68	49.83
Cumulative Quartz Recovery			**76.68**	%		Conditioning Time		**5**	min	
Cumulative Water (g)			**1345.33**							

Run #31

Air Flow Rate			5 l/min			Water pH		8		
Measured Froth Depth			Varied b/w 30 & 5		mm	Adjusted pH		7		
Sampl No	Pan Mass (g)	Froth + Pan Mass (g)	Quartz Dry Mass (g)	Bottle Mass Before (g)	Bottle Mass After (g)	Wash Water Mass (g)	Water Mass (g)	Flot Time (min)	Cum Quartz Rec (%)	Cum Water Rec (%)
1	375.95	639.33	96.36	563.43	552.76	10.67	156.35	0.17	32.12	5.79
2	363.27	588.29	59.88	540.35	509.46	30.89	134.25	0.5	52.08	10.76
3	350.80	572.30	41.58	514.19	431.60	82.59	97.33	1	65.94	14.37
4	376.30	524.67	20.23	513.94	479.65	34.29	93.85	1.5	72.68	17.84
5	370.16	583.51	12.17	527.43	465.90	61.53	139.65	2	76.74	23.02
6	369.70	595.63	6.47				219.46	2.5	78.90	31.14
7	357.40	583.50	3.99				222.11	3	80.23	39.37
Cumulative Quartz Recovery			**80.23**	%		Conditioning Time		**5**	min	
Cumulative Water (g)			**1063.00**							

Run #32

Air Flow Rate			6 l/min			Water pH		8		
Measured Froth Depth			Varied b/w 30 & 5		mm	Adjusted pH		7		
Sampl No	Pan Mass (g)	Froth + Pan Mass (g)	Quartz Dry Mass (g)	Bottle Mass Before (g)	Bottle Mass After (g)	Wash Water Mass (g)	Water Mass (g)	Flot Time (min)	Cum Quartz Rec (%)	Cum Water Rec (%)
1	361.54	701.49	107.95	552.76	541.51	11.25	220.75	0.17	35.98	8.18
2	368.52	639.46	62.48	509.46	488.54	20.92	187.54	0.5	56.81	15.12
3	351.30	607.40	36.28	595.95	509.11	86.84	132.98	1	68.90	20.05
4	358.70	516.89	14.59	479.65	443.17	36.48	107.12	1.5	73.77	24.01
5	363.10	582.34	13.78	465.90	374.39	91.51	113.95	2	78.36	28.23
6	367.30	532.32	8.96				156.06	2.5	81.35	34.01
7	366.70	568.62	5.13				196.79	3	83.06	41.30
Cumulative Quartz Recovery			**83.06**	%		Conditioning Time		**5**	min	
Cumulative Water (g)			**1115.19**							

Run #33

Air Flow Rate			7 l/min			Water pH		8		
Measured Froth Depth			Varied b/w 30 & 5		mm	Adjusted pH		7		
Sampl No	Pan Mass (g)	Froth + Pan Mass (g)	Quartz Dry Mass (g)	Bottle Mass Before (g)	Bottle Mass After (g)	Wash Water Mass (g)	Water Mass (g)	Flot Time (min)	Cum Quartz Rec (%)	Cum Water Rec (%)
1	345.60	683.19	113.15	541.51	538.17	3.34	221.10	0.17	37.72	8.19
2	377.50	627.70	60.70	488.54	459.03	29.51	159.99	0.5	57.95	14.11
3	355.00	589.39	38.07	509.11	408.61	100.50	95.82	1	70.64	17.66
4	367.40	509.49	19.98	443.17	401.95	41.22	80.89	1.5	77.30	20.66
5	377.10	612.14	12.07	374.39	298.76	75.63	147.34	2	81.32	26.12
6	351.63	533.06	4.99				176.44	2.5	82.99	32.65
7	365.53	583.25	3.16				214.56	3	84.04	40.60
Cumulative Quartz Recovery			**84.04**	%		Conditioning Time		**5**	min	
Cumulative Water (g)			**1096.14**							

Run #34

Air Flow Rate	8 l/min	Water pH	8
Measured Froth Depth	Varied b/w 30 & 5 mm	Adjusted pH	7

Sampl No	Pan Mass (g)	Froth + Pan Mass (g)	Quartz Dry Mass (g)	Bottle Mass Before (g)	Bottle Mass After (g)	Wash Water Mass (g)	Water Mass (g)	Flot Time (min)	Cum Quartz Rec (%)	Cum Water Rec (%)
1	366.70	754.15	127.95	538.17	527.84	10.33	249.17	0.17	42.65	9.23
2	365.53	628.14	65.60	459.03	439.02	20.01	177.00	0.5	64.52	15.78
3	351.63	577.09	20.57	408.61	324.63	83.98	120.91	1	71.37	20.26
4	377.10	517.07	8.07	401.95	371.02	30.93	100.97	1.5	74.06	24.00
5	368.40	572.48	10.11	298.76	224.74	74.02	119.95	2	77.43	28.44
6	355.00	511.90	7.48				149.42	2.5	79.93	33.98
7	377.50	542.68	4.41				160.77	3	81.40	39.93

Cumulative Quartz Recovery	**81.40**	%	Conditioning Time	**5**	min
Cumulative Water (g)	**1078.19**				

Run #35

Air Flow Rate	3 l/min	Water pH	8
Measured Froth Depth	Varied b/w 30 & 5 mm	Adjusted pH	7

Sampl No	Pan Mass (g)	Froth + Pan Mass (g)	Quartz Dry Mass (g)	Bottle Mass Before (g)	Bottle Mass After (g)	Wash Water Mass (g)	Water Mass (g)	Flot Time (min)	Cum Quartz Rec (%)	Cum Water Rec (%)
1	367.30	580.56	68.60	527.84	517.47	10.37	134.29	0.17	22.87	4.97
2	363.10	606.81	71.78	439.02	424.43	14.59	157.34	0.5	46.79	10.80
3	358.70	569.20	41.60	324.63	260.58	64.05	104.85	1	60.66	14.68
4	351.30	464.07	21.16	371.02	341.31	29.71	61.90	1.5	67.71	16.98
5	361.41	514.99	21.74	436.31	368.58	67.73	64.11	2	74.96	19.35
6	357.40	504.03	10.52				136.11	2.5	78.47	24.39
7	369.70	553.97	5.28				178.99	3	80.23	31.02

Cumulative Quartz Recovery	**80.23**	%	Conditioning Time	**5**	min
Cumulative Water (g)	**837.59**				

Particle Sizes

#30			Sizes				
	Sample	sub 10	10 to 25	25 to 45	45 to 75	75 to 106	plus 106
	C1	6.83	7.55	11.41	15.75	22.72	35.75
	C2	10.28	11.83	15.77	17.39	20.95	23.73
	C3	11.93	13.04	16.04	17.18	20.29	21.53
	C4	9.08	9.04	11.31	14.52	20.7	35.35
	C5	8.67	8.97	12.37	16.24	22.76	30.98
	C6	7.39	7.37	10.73	15.49	23.52	35.5
	C7	6.94	7.08	10.41	15.31	23.19	37.02
	Head	9.40	9.90	12.91	15.73	20.95	31.13

#31			Sizes				
	Sample	sub 10	10 to 25	25 to 45	45 to 75	75 to 106	plus 106
	C1	8.2	9.35	14.23	17.9	23.11	27.19
	C2	11.1	12.95	16.9	17.71	20	21.35
	C3	10.56	11.22	12.99	14.77	20.06	30.41
	C4	9.4	9.54	11.63	14.66	21.12	33.66
	C5	8.84	9.24	12.73	16.47	22.54	30.19
	C6	6.22	6.2	9.72	15.36	24.37	38.17
	C7	7.37	7.32	11.44	16.26	23.77	33.83
	Head	9.40	9.90	12.91	15.73	20.95	31.13

#32			Sizes				
	Sample	sub 10	10 to 25	25 to 45	45 to 75	75 to 106	plus 106
	C1	9.17	10.32	15.2	18.28	22.71	24.3
	C2	12.22	13.5	16.63	16.94	19.16	21.56
	C3	11.11	11.55	13.83	15.99	20.8	26.7
	C4	10.19	10.2	12.79	15.73	21.45	29.66
	C5	7.64	8.05	11.43	15.59	23.01	34.29
	C6	6.55	6.93	10.54	15.38	23.29	37.32
	C7	7.06	7.3	11.18	15.82	23.53	35.08
	Head	9.40	9.90	12.91	15.73	20.95	31.13

#33			Sizes				
	Sample	sub 10	10 to 25	25 to 45	45 to 75	75 to 106	plus 106
	C1	7.26	7.96	12.4	16.74	23.39	32.21
	C2	11.73	12.65	15.55	16.2	19.24	24.66
	C3	9.12	9.49	10.89	13.42	19.8	37.25
	C4	9.29	9.6	12.17	15.36	21.48	32.11
	C5	7.31	7.76	10.54	14.99	23.03	36.39
	C6	6.39	6.57	10.04	15.41	24.09	37.52
	C7	5.92	5.87	9.41	14.8	24.33	39.64
	Head	9.40	9.90	12.91	15.73	20.95	31.13

#34			Sizes				
	Sample	sub 10	10 to 25	25 to 45	45 to 75	75 to 106	plus 106
	C1	7.37	8	12.24	16.47	23.12	32.79
	C2	11.59	13.46	16.73	17.04	18.81	22.37
	C3	11.65	12.95	12.76	13.25	17.87	31.53
	C4	10.53	10.79	12.58	15.36	20.83	29.91
	C5	6.82	6.9	10.06	14.75	22.46	39.01
	C6	5.89	6.12	10	15.5	23.83	38.65
	C7	5.46	5.59	9.43	15.19	24.52	39.8
	Head	9.40	9.90	12.91	15.73	20.95	31.13

#35			Sizes				
	Sample	sub 10	10 to 25	25 to 45	45 to 75	75 to 106	plus 106
	C1	7.17	8.22	12.21	16.34	22.99	33.06
	C2	9.56	11.02	15.02	17.46	21.14	25.77
	C3	10.07	10.73	12.92	15.34	20.76	30.2
	C4	8.37	8.39	10.78	14.29	20.97	37.21
	C5	7.92	8.53	11.49	15.26	21.97	34.81
	C6	6.64	7.2	10.46	14.94	23.12	37.61
	C7	7.22	7.68	11.46	16.06	23.45	34.12
	Head	9.40	9.90	12.91	15.73	20.95	31.13

APPENDIX C

CALCULATION OF THE SAUTER MEAN BUBBLE DIAMETER

APPENDIX C: CALCULATION OF THE SAUTER MEAN BUBBLE DIAMETER

According to Tucker *et al* (1994), the Sauter Mean diameter is calculated as follows:

$d_{32} = 6\ V_b / A_b$

where V_b is the total volume of bubbles collected in burette (ml) and A_b is the total bubble surface area measured by the bubble sizer (mm^2).

Alternatively, the Sauter Mean diameter can be determined from the following expression (Barigou and Greaves, 1992):

$$d_{32} = \frac{\sum_{i=1}^{i=n} d^3_i}{\sum_{i=1}^{i=n} d^2_i}$$

where d_i is the equivalent spherical bubble diameter and n is the sample size (i.e. number of bubbles).

APPENDIX D

SAMPLE CALCULATION FOR EXTRACTING MODEL PARAMETERS FROM BATCH DATA

APPENDIX D: SAMPLE CALCULATION FOR EXTRACTING MODEL PARAMETERS FROM BATCH DATA

(I) Mass Balancing

Particle size classification chosen is indicated in Table D.1. Feed and concentrate samples were analysed by size. Three batch tests conducted at various froth heights and at an air flowrate of 6 litres/min are chosen to illustrate how mass distributions for the batch tests were calculated (Table D.2). To illustrate how mass balance for each batch test was conducted, Run#8 is used below to calculate masses, on sized basis, per flotation time interval (Figure D-1).

Table D-1 Particle size classification

Class	Size range (μm)
Size 1	Sub 10
Size 2	10 to 25
Size 3	25 to 45
Size 4	45 to 75
Size 5	75 to 106
Size 6	plus 106

Table D-2 Batch data

Run number	Froth collection time interval (min)	Concentrate Masses						
		Size 1	Size 2	Size 3	Size 4	Size 5	Size 6	Water (g)
#12	0.5	5.84	11.76	22.06	36.46	53.52	56.40	330.06
	0.5	3.63	7.59	12.35	15.25	17.17	12.14	155.95
	1	2.34	4.57	5.49	5.39	5.18	3.57	202.53
	1	0.64	1.16	1.13	0.93	0.8	0.52	179.05
	2	0.57	0.89	0.7	0.45	0.3	0.15	413.71
	Head	15.21	29.37	45.21	59.94	76.59	73.71	
#8	0.5	5.78	11.33	19.11	28.15	38.72	37.81	153.49
	0.5	3.61	7.46	11.67	14.05	15.61	11.12	107.28
	1	1.76	3.71	4.64	4.56	4.51	3.15	41.93
	1	0.54	1.15	1.46	1.63	1.89	1.74	12.64
	2	0.62	1.24	1.53	1.71	1.96	1.64	12.11
	Head	15.69	31.89	46.98	60.27	75.39	69.72	
#4	1	5.94	12.35	17.53	20.27	23.77	22.18	106.84
	1	1.75	3.82	5.16	5.41	5.57	4.02	27.25
	1	0.74	1.69	2.23	2.30	2.34	1.63	12.81
	1	0.29	0.88	1.37	1.42	1.3	0.74	8.22
	1	0.21	0.51	0.71	0.76	0.79	0.54	2.18
	Head	18.75	38.28	52.35	60.03	68.85	61.68	

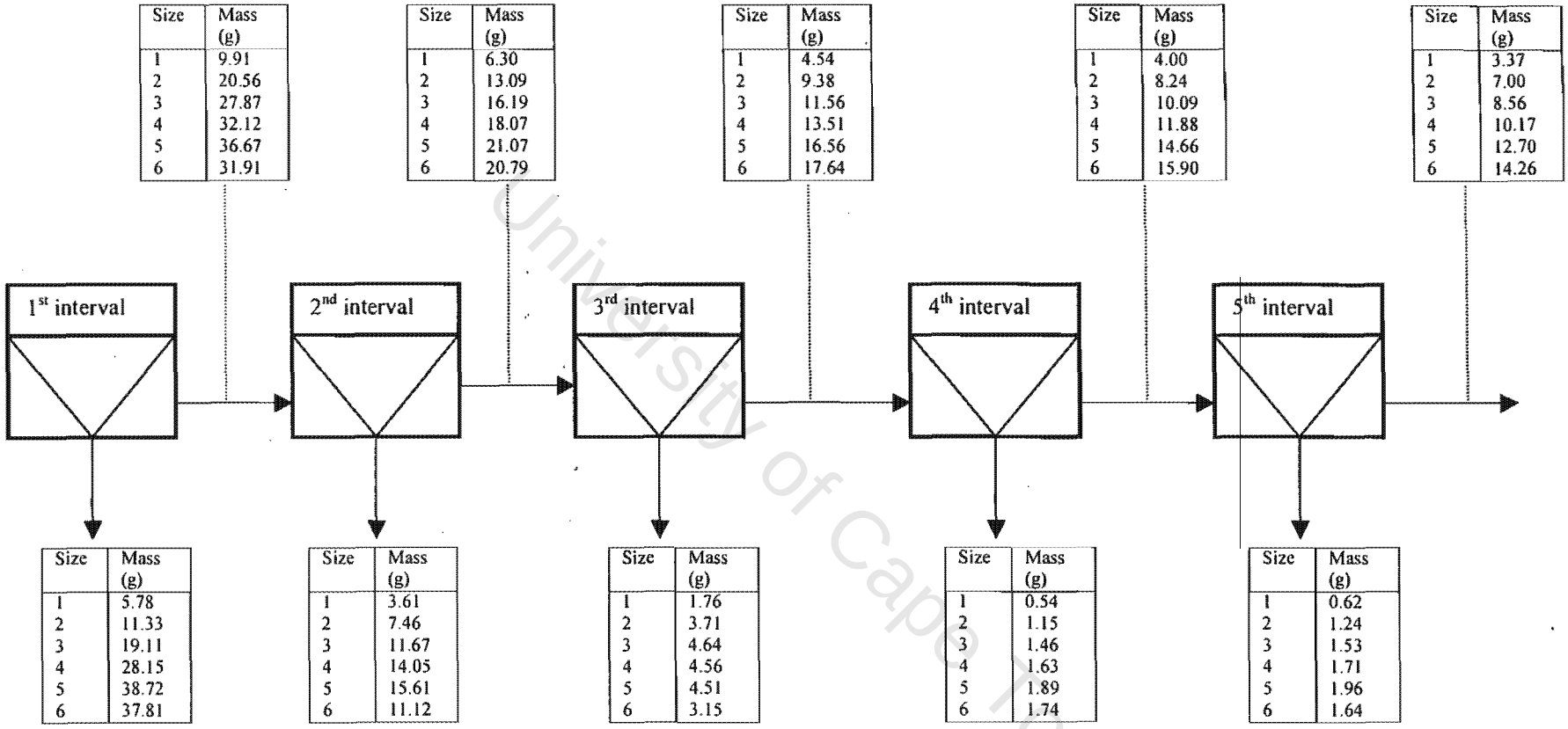

Figure D-1 Typical Mass Balance of a batch test data (Run #8)

(II) Measured Parameters

In addition to the mass distributions per flotation intervals, the parameters reported in Table D.3 were either measured or calculated using measurable variables. Again, data from Run#8 is used as an example.

Table D-3 Measured parameters

Cell No. "Interval"	τ (min)	d_b (cm)	J_g (cm/min)	S_b (1/min)	h (cm)	V_f (cm^3)	Q_{conc} (cm3/min)	FRT (min)	R_w (%)
1	0.5	1.49	32.40	1313.10	2.5	50.50	411.38	0.12	12.22
2	0.5	1.49	32.40	1313.10	2.5	50.50	261.61	0.19	5.78
3	1	1.49	32.40	1313.10	2.5	50.50	50.20	1.00	7.50
4	1	1.49	32.40	1313.10	2.5	50.50	15.76	3.20	6.63
5	2	1.49	32.40	1313.10	2.5	50.50	7.67	6.58	15.32

Comments:

τ is approximated by the flotation time interval. d_b, J_g, S_b, h and V_f were assumed to be constant. The mean bubble size was measured using the UCT bubble sizer in the presence of water and frother only. It was assumed that the bubble size does not change significantly with flotation time. S_b is described by the following equation:

$$S_b = 6*J_g/d_b$$

where J_g, the superficial gas velocity, was calculated by diving the cross-sectional area of the cell with the air flowrate.

Effective froth volume, V_f, was calculated using the following equation:

$$V_f = A_c \times h \ (1-\varepsilon_g)$$

where A_c is the effective cross-sectional area of the flotation cell (184 cm^2), h is the operating froth height and ε_g is the gas hold-up, calculated to be 90%, (estimated using data from Goodall, 1992).

Concentrate slurry volumetric flowrate, Q_{conc}, was calculated by dividing the measured concentrate slurry volume with the collection time period. Water recovery, R_w, was calculated using the amount of water collected in the concentrate divided by the amount of water inside the cell, 3000 litres x ε_p. ε_p, the fraction of water in the pulp phase, was calculated from the measurements of the volume of pulp with and without air addition.

(III) Setting-up performance equations

To illustrate this, particle size class 3 is chosen (Table D-4).

Table D-4 An example of how performance equations were set-up

Cell No.	Overall	Floatable		Entrained
		Pulp phase	Froth phase	
1	$Ro_1 = f(Rc_{1,\,size\,3}, Rf_{1,\,size\,3}, Ent_{1,\,size\,3}, Rw_1)$	$Rc_{1,\,size\,3} = f(\tau_1, P_{size\,3}, Sb_g)$	$Rf_{1,\,size\,3} = f(FRT_1, \beta, \omega_{size\,3})$	$Ent_1 = f(Rw_1, FRT_1, \beta, \omega_{size\,3})$
2	$Ro_2 = f(Rc_{2,\,size\,3}, Rf_{2,\,size\,3}, Ent_{2,\,size\,3}, Rw_2)$	$Rc_{2,\,size\,3} = f(\tau_2, P_{size\,3}, Sb_g)$	$Rf_{2,\,size\,3} = f(FRT_2, \beta, \omega_{size\,3})$	$Ent_2 = f(Rw_2, FRT_2, \beta, \omega_{size\,3})$
3	$Ro_3 = f(Rc_{3,\,size\,3}, Rf_{3,\,size\,3}, Ent_{3,\,size\,3}, Rw_3)$	$Rc_{3,\,size\,3} = f(\tau_3, P_{size\,3}, Sb_g)$	$Rf_{3,\,size\,3} = f(FRT_3, \beta, \omega_{size\,3})$	$Ent_3 = f(Rw_3, FRT_3, \beta, \omega_{size\,3})$
4	$Ro_4 = f(Rc_{4,\,size\,3}, Rf_{4,\,size\,3}, Ent_{4,\,size\,3}, Rw_4)$	$Rc_{4,\,size\,3} = f(\tau_4, P_{size\,3}, Sb_g)$	$Rf_{4,\,size\,3} = f(FRT_4, \beta, \omega_{size\,3})$	$Ent_4 = f(Rw_4, FRT_4, \beta, \omega_{size\,3})$
5	$Ro_5 = f(Rc_{5,\,size\,3}, Rf_{5,\,size\,3}, Ent_{5,\,size\,3}, Rw_5)$	$Rc_{5,\,size\,3} = f(\tau_5, P_{size\,3}, Sb_g)$	$Rf_{5,\,size\,3} = f(FRT_5, \beta, \omega_{size\,3})$	$Ent_5 = f(Rw_5, FRT_5, \beta, \omega_{size\,3})$

where, for example, the recovery equations for cell number 1 are as follows:

$$Ro_{1,size3} = \frac{Rc_{1,size3}\,Rf_{1,size3}\,(1-Rw_1)+Ent_{1,size3}\,Rw_1\,(1-Rc_{1,size3})}{(1-Rw_1)(1-Rc_{1,size3}+Rc_{1,size3}\,Rf_{1,size3})+Ent_{1,size3}\,Rw_1\,(1-Rc_{1,size3})}$$

$$Rc_{1,size3} = 1-\exp(-P_{size3}\,Sb_g\,\tau_1)$$

$$Rf_{1,size3} = \exp(-\beta\,FRT_1)+\left(1-\exp(-\beta\,FRT_1)\right)*\frac{1}{1+\omega_{size3}\,FRT_1}$$

$$Ent_{1,size3} = \left(\frac{1}{1+\omega_{size3}\,FRT_1}\right)/\,Rw_1$$

Comments:

P, the floatability parameter, varies only with size in the quartz system. This will vary by size and mineral in real system, and liberation may also need to be included for some ores.

S_b was also assumed not to vary with cell number, only varied with air flowrate.

ω, the drainage parameter, was assumed to vary only with size

τ and FRT values for all cell numbers were measured.

(IV) Initial Model Parameters

The method of determining model parameters used here, the linear least-square technique, usually requires reasonable initial estimates of the parameters to be fitted. The initial parameters for the floatability parameter, P, for various particle size classes were based on calculated flotation rate constants. This is illustrated below using particle size class 3.

$P_{size\,3} = k_{size\,3} / Sb_g$

where $k_{size\,3}$ is the flotation rate constant for particle size class 3 (obtained by fitting size 3 batch data to Klimpel's model). Sb_g was measured directly (see Table D-3).

e.g. for particle size class 3, $k_{size\ 3}$ was 0.288 (1/min), and $Sb_{at\ 4\ L/min}$ was 840 (1/min). The initial estimation of $P_{size\ 3}$ was therefore 0.000343.

The same procedure was followed for other P values for the chosen particle size classes (all values are shown in Table D-5). The β and ω parameters were initially set to unity. All parameters were constrained to be above zero.

Table D-5 Initial P values

Size	P
1	0.000277
2	0.000243
3	0.000343
4	0.000649
5	0.001270
6	0.002286

(V) Minimising the difference between measured concentrate masses and concentrate masses based on fitted parameters

Particle size class 3 is used in Table D-6 below to illustrate how the minimisation procedure was carried out. For example,

Fitted mass of size class 3 in Cell #1 = Feed of size class 3 to Cell #1 x Overall Recovery of Size class 3 ($Ro_{1,\ size\ 3}$)
Based on chosen initial parameters,

Fitted mass of size class 3 in Cell #1 = 46.98 x 0.53 = 24.90 g.

The corresponding measured concentrate mass was 19.11 g.

Error Squared for mass of size class 3 in cell #1:

$Error_{1,\ size\ 3}$ = (Measured - Fitted)/(σ x Measured), where σ, the data standard deviation based on reproducibility tests (discussed below), was 8%.

Total Error Squared$_1$ = $Error_{1,\ size\ 1}$ + $Error_{1,\ size\ 2+}$ $Error_{1,\ size\ 3+}$ $Error_{1,\ size\ 4+}$ $Error_{1,\ size\ 5+}$ $Error_{1,\ size\ 6}$

Total error squared for all cells and size classes, S:

$$S = \sum_{i=1}^{5}\sum_{k=1}^{6}\left(\frac{M_{i,k}-F_{i,k}}{\sigma_{i,k}M_{i,k}}\right)^2$$

where i is the cell number, k is the particle size class, M is the measured mass in concentrate, F is the fitted concentrate mass and σ is the data standard deviation.

The objective, therefore, was to minimise the above error by changing the unknown model parameters until the adjusted concentrate masses for various particle sizes equal the measured concentrate masses. Typical values of error squared obtained are shown in Table D-7.

Table D-7 Measured versus fitted masses in concentrate for size class 3 in Run #8

Cell No.	Measured Conc Mass (g)	Fitted Conc Mass (g)	Error Squared
1	22.06	25.42	9.27
2	12.35	10.68	7.31
3	5.49	5.24	0.20
4	1.13	2.20	91.95
5	0.70	1.10	33.93

(VI) Choosing standard deviation, σ

When extracting model parameters by fitting equations to existing plant or laboratory data, the best-fit estimate of the adjusted value is usually biased towards the values which are relatively high (Wills, 1997). This occurs when the absolute error is assumed to be distributed equally to each adjusted value, which is highly unlikely in practice. The amount of concentrate masses obtained from the batch tests vary with particle size class, increasing as the particle size class increases. As such, the standard deviation of each data point in a batch test was chosen to start at 10% for the fine particle size class (i.e. sub 10 microns), decreasing by unity toward the coarse particle size classes (i.e. plus 106 microns). A starting point of 10% was obtained by averaging the absolute errors obtained from the reproducibility tests (see Table D-8). From this table, the average error was approximately 9%. To be on the safe side, a value of 10% was chosen.

Table D-8 Error estimates calculated from reproducibility tests

Cell Number	Standard Deviation (%)
1	2.3
2	9.3
3	5.6
4	14.2
5	12.7
	8.8

In addition to the above variation of the standard deviation with mass, it is expected that the error is maximum at the start of a batch test. This is due to the initial build-up process of the froth phase and the non-steady state nature of froth removal. This error is expected to decrease during flotation as the froth and the froth height become more stable. To account for this, the standard deviations were also chosen such that they decrease with flotation time. An example of the set of standard deviation values used for each test are shown in Table D-9.

Table D-9 Standard Deviation values chosen for use in modelling

Cell Number	Standard Deviation (%)					
	Particle Size Class					
	1	2	3	4	5	6
1	10	9	8	7	6	5
2	9	8	7	6	5	4
3	8	7	6	5	4	3
4	7	6	5	4	3	2
5	6	5	4	3	2	1

APPENDIX E

MONTE CARLO PROGRAM

APPENDIX E: MONTE CARLO PROGRAM

```
Sub Macro1()
'
'Macro1 Macro
'
Dim i As Integer
Dim iset As Integer
Dim fac, gset, rsq, v1, v2

Application.StatusBar = "Calculating 1000 trials ..."
'Application.Calculation = x1Manual  'turn off calculation
Application.ScreenUpdating = True

iset = 0

'Set up loop to perform 1000 different parameter estimation from data set
'changed each time by a deviation normally distributed with a standard
'deviation based on the standard deviation of each experimental value

For i = 1 To 1000

'Determine a deviation (gasdev) normally distributed about zero with a
'variance of 1

For j = 1 To 270

If iset = 0 Then
   v1 = 2 * Rnd - 1
   v2 = 2 * Rnd - 1
   rsq = v1 ^ 2 + v2 ^ 2
   If (rsq >= 1 Or rsq = 0) Then
      j = j - 1
      GoTo 10
   End If
   fac = (-2 * Log(rsq) / rsq) ^ 0.5
   gset = v1 * fac
   gasdev = v2 * fac
   iset = 1
Else
   gasdev = gset
   iset = 0
End If

'Assign a new set of values of recovery for solving by
'taking the actual recovery measured and adding or subtracting
'the deviation calculated above multiplied by the standard deviation
'of the measured point

Range("Transformed").Item(j) = Range("Measured").Item(j).Value + gasdev *
Range("Stdev").Item(j).Value

10
```

```
Next

'Set up starting values of the parameters to be used in the
'solving procedure

Range("$ek$7").Value = 1
Range("$ek$8").Value = 1
Range("$ek$9").Value = 1
Range("$ek$10").Value = 1
Range("$ek$11").Value = 1
Range("$ek$12").Value = 1
Range("$ek$13").Value = 1
Range("$ek$14").Value = 1
Range("$ek$15").Value = 1
Range("$ek$16").Value = 1

'Solve to find the optimum set of parameters

For k = 1 To 5
Worksheets("Model Sheet").Activate

SolverOK setCell:="$ei$25", MaxMinVal:=2, ValueOf:="0", ByChange:="$ek$7:$ek$16"
   SolverSolve userFinish:=True
SolverFinish keepFinal:=1

Next

Application.StatusBar = "Iteration No: " + Str(i + 1)

'Record the values of each of the parameters and the total SSE in an array

Range("Results").Cells(i, 5) = Range("a").Value
Range("Results").Cells(i, 6) = Range("Vis").Value
Range("Results").Cells(i, 7) = Range("p1_").Value
Range("Results").Cells(i, 8) = Range("p2_").Value
Range("Results").Cells(i, 9) = Range("p3_").Value
Range("Results").Cells(i, 10) = Range("p4_").Value
Range("Results").Cells(i, 11) = Range("p5_").Value
Range("Results").Cells(i, 12) = Range("p6_").Value
Range("Results").Cells(i, 13) = Range("Kc_4").Value
Range("Results").Cells(i, 14) = Range("Kc_5").Value

If (i / 5) = Int(i / 5) Then
ActiveWorkbook.Save
End If

Next

Application.ScreenUpdating = True
'Application.Calculation = x1Automatic
Application.StatusBar = True

End Sub
```

APPENDIX F

MEASURING MASS DISTRIBUTIONS FOR THE MERENSKY DATA

APPENDIX F: MEASURED MASS DISTRIBUTIONS

Batch

Test	Sample	Cum Time (min)	Conc Mass (g)	Conc Water (g)	% Solids
1N	Head	0	29145.60	50054.40	36.80
	C1	2	258.82	1482.18	14.87
	C2	6	139.78	1708.22	7.56
	C3	12	106.45	1542.55	6.46
	C4	25	70.79	1123.21	5.93
2N	Head	0	33773.84	46176.69	42.24
	C1	3	215.17	562.50	27.67
	C2	10	210.50	1121.83	15.80
	C3	20	232.67	861.50	21.26
3N	Head	0	31457.12	47742.88	39.72
	C1	3	212.50	281.00	43.06
	C2	10	186.50	475.75	28.16
	C3	20	239.25	630.25	27.52
4N	Head	0	30085.48	49114.52	37.99
	C1	3	600.00	3276.00	15.48
	C2	10	374.00	2430.00	13.34
	C3	20	320.00	2598.00	10.97

Continuous

Test	Head			CONC			TAILS		
	Tot Dry Mass (g/min)	Water flow (g/min)	% Solids	Tot Dry Mass (g/min)	Water flow (g/min)	% Solids	Tot Dry Mass (g/min)	Water flow (g/min)	% Solids
R1S	4257.00	8805.14	32.59	33.00	119.14	21.69	4224.00	8686.00	32.72
R2S	3482.04	6724.88	34.11	24.54	40.88	37.51	3457.50	6684.00	34.09
1S	4411.60	7092.73	38.35	22.00	31.93	40.80	4389.60	7060.80	38.34
2S	5094.73	7260.99	41.23	60.44	246.72	19.68	5034.29	7014.27	41.78
3S	4092.84	5778.36	41.46	78.20	236.87	24.82	4014.64	5641.47	41.58
4S	5648.79	7827.01	41.92	41.79	108.01	27.90	5607.00	7719.00	42.08
5S	6449.10	10248.70	38.82	17.85	26.20	40.53	6431.25	10222.50	38.62
6S	5279.86	11152.31	32.13	36.95	53.41	40.89	5242.91	11098.91	32.08
7S	7011.20	10717.62	39.55	35.20	89.82	28.20	6976.00	10628.00	39.63
8S	11297.58	21305.97	34.65	130.72	885.40	12.86	11166.86	20420.57	35.35
9S	3556.25	6066.40	36.96	50.00	153.58	24.56	3506.25	5912.81	37.23
10S	11161.42	10939.04	50.50	193.42	878.04	22.19	10968.00	10261.00	51.67
11S	11122.09	8873.84	55.62	272.09	925.84	22.71	10850.00	7948.00	57.72
12S	10212.06	9711.01	51.26	108.06	198.01	35.31	10104.00	9513.00	51.51
13S	10595.76	12495.01	45.89	365.30	1134.70	24.35	10230.46	11360.31	47.38
14S	7548.25	6694.25	53.00	1514.25	2390.25	38.78	6034.00	4304.00	58.37
15S	6356.22	6534.67	49.31	410.22	906.67	31.15	5946.00	5628.00	51.37

APPENDIX G

ELEMENTAL ANALYSIS FOR THE MERENSKY DATA

APPENDIX G ELEMENTAL ANALYSIS

Continuous Tests

	Head					Conc					Tails				
Test	pgm (%)	Cu (%)	Ni (%)	Cr2O3 (%)	S (%)	pgm (%)	Cu (%)	Ni (%)	Cr2O3 (%)	S (%)	pgm (%)	Cu (%)	Ni (%)	Cr2O3 (%)	S (%)
R1S		0.083	0.120	1.25	0.410		5.37	8.16	0.52	22.83		0.062	0.093	2.37	0.220
R2S		0.099	0.135	1.25	0.410		6.98	8.26	0.52	22.83		0.058	0.082	2.37	0.220
1S		0.071	0.139	0.99	0.368	379.1	6.38	8.28	0.23	23.75	2.4	0.038	0.118	0.94	0.212
2S	4.3	0.074	0.142	0.91	0.378	196.9	2.84	5.07	0.42	16.25	3.1	0.055	0.103	2.25	0.037
3S	3.3	0.054	0.113	2.41	0.220	103.3	1.47	2.75	1.43	8.12	1.4	0.020	0.059	2.54	0.040
4S	4.3	0.081	0.162	2.46	0.261	116.6	4.63	7.30	0.52	18.50	1.7	0.023	0.060	2.37	0.128
5S	4.5	0.085	0.184	1.38	0.380	149.2	13.55	15.00	0.30	27.50	3.0	0.023	0.130	1.30	0.214
6S		0.078	0.123	1.00	0.309		4.49	7.57	0.15	19.10		0.052	0.078	0.80	0.130
7S	3.7	0.073	0.137	2.14	0.242	262.3	4.33	8.13	0.47	17.40	1.1	0.021	0.052	2.14	0.141
8S	3.0	0.063	0.119	1.88	0.330	65.3	1.20	2.22	0.90	6.60	0.6	0.014	0.032	2.00	0.016
9S	3.2	0.059	0.105	1.13	0.296	160.2	3.13	5.93	0.37	12.70	0.8	0.017	0.041	1.10	0.022
10S	3.9	0.061	0.104	0.82	0.308	114.8	2.45	4.54	0.37	10.00	0.8	0.020	0.043	0.88	0.022
11S	3.7	0.070	0.129	1.04	0.308	100.2	1.47	2.62	0.60	8.60	1.1	0.020	0.045	1.01	0.016
12S	4.1	0.066	0.125	1.06	0.308	101.0	3.73	7.23	0.31	17.30	1.2	0.024	0.055	1.04	0.127
13S	3.6	0.059	0.110	1.08	0.380	4.7	0.06	0.10	1.17	0.42	1.0	0.021	0.044	1.13	0.080
14S	4.5	0.065	0.120	1.42	0.348	7.1	0.04	0.10	1.25	0.45	1.0	0.017	0.033	1.23	0.015
15S	4.8	0.071	0.129	1.40	0.338	6.3	0.07	0.02	1.32	0.36	1.0	0.020	0.039	1.26	0.021

Batch Tests

Test	Conc	Cu (% mass)	Ni (% mass)	Fe (% mass)	Tot S (% mass)	Cr2O3 (% mass)	pgm (ppm)
1N	Head	0.09	0.13	8.25	0.30	1.25	-
	C1	2.55	4.70	20.21	13.10	0.38	-
	C2	1.00	1.85	14.42	6.29	0.40	-
	C3	0.80	1.19	12.07	4.49	0.42	-
	C4	0.76	1.00	11.10	3.83	0.40	-
2N	Head	0.07	0.14	-	0.35	1.28	3.80
	C1	3.48	6.75	-	17.77	0.40	252.40
	C2	1.85	3.25	-	10.30	0.50	70.60
	C3	0.88	1.51	-	5.24	0.55	46.10
3N	Head	0.07	0.13	-	0.31	1.89	3.60
	C1	2.98	5.62	-	16.95	0.55	215.90
	C2	1.90	3.23	-	11.35	0.54	110.30
	C3	0.95	1.61	-	6.36	0.58	59.10
4N	Head	0.06	0.11	-	0.33	1.07	3.80
	C1	1.96	3.24	-	10.65	0.70	106.60
	C2	0.93	1.86	-	5.34	0.66	50.90
	C3	0.27	0.40	-	1.94	0.68	18.50

APPENDIX H

MINERALOGY FOR THE MERENSKY DATA

APPENDIX H MINERALOGY

Size by Size Modal Abundance Data (wt%)

	10 S Head						10 S Conc			
MINERAL	plus 106	plus 53	plus 25	plus 10	plus 2	Head	plus 25	plus 10	plus 2	Head
Sulphides										
Fe-Sulphides	0.16	0.26	0.65	0.72	0.78	0.42	11.66	7.51	9.73	9.49
Pentlandite	0.12	0.16	0.45	0.70	0.57	0.30	11.60	8.95	7.84	8.09
Chalcopyrite	0.15	0.18	0.20	0.26	0.23	0.19	6.22	5.37	4.67	4.81
Other-Sulphides	0.01	0.02	0.06	0.03	0.02	0.02	0.33	0.24	0.06	0.09
Silicates										
Feldspar	55.62	45.61	42.02	44.19	44.54	47.74	9.58	7.45	12.82	12.03
Orthopyroxene	32.32	40.40	39.79	36.55	31.90	36.21	39.25	51.17	42.00	43.13
Clinopyroxene	6.14	6.97	8.28	8.54	10.18	7.57	6.51	7.31	7.40	7.37
Olivine	0.37	0.53	0.54	0.56	0.24	0.44	0.43	0.23	0.12	0.15
Mica	0.71	0.57	0.70	0.73	0.83	0.69	1.49	0.50	0.38	0.43
Quartz	1.13	1.18	1.79	1.06	2.64	1.50	3.23	3.04	5.34	4.98
Other-Silicates	1.04	0.95	0.99	1.21	1.64	1.11	3.24	3.65	5.00	4.77
Altered Silicates										
Talc	0.16	0.17	0.15	0.19	0.16	0.16	4.57	3.04	1.99	2.20
Serpentine	0.08	0.07	0.05	0.07	0.06	0.07	0.12	0.07	0.06	0.07
Chlorite	0.70	0.53	0.56	0.77	0.90	0.66	1.00	0.78	0.68	0.71
Oxides										
Chromite	1.12	2.11	3.16	3.66	4.01	2.41	0.17	0.34	1.23	1.08
Oxides	0.06	0.14	0.37	0.45	0.70	0.27	0.27	0.24	0.55	0.50
Others										
Carbonates	0.12	0.14	0.24	0.31	0.60	0.24	0.33	0.13	0.12	0.12
Others	0.00	0.00	0.00	0.00	0.00	0.00	0.00	0.00	0.00	0.00

	11 S Conc						12 S Conc					
MINERAL	plus 106	plus 53	plus 25	plus 10	plus 2	Head	plus 106	plus 53	plus 25	plus 10	plus 2	Head
Sulphides												
Fe-Sulphides	9.00	24.53	14.70	9.57	6.94	9.63	15.72	28.52	22.89	17.66	15.84	18.69
Pentlandite	4.72	19.89	13.78	10.17	5.47	8.04	7.72	25.81	28.64	24.78	12.54	18.27
Chalcopyrite	9.87	11.76	5.80	4.75	2.88	4.72	16.84	17.79	13.14	11.67	7.10	10.85
Other-Sulphides	0.22	0.47	0.29	0.26	0.05	0.15	0.44	0.55	0.46	0.39	0.15	0.31
Silicates												
Feldspar	48.22	18.23	16.34	15.82	23.79	23.58	41.51	11.60	5.46	2.68	4.63	8.30
Orthopyroxene	18.26	15.44	35.17	43.19	37.74	34.92	9.59	8.41	19.67	31.40	39.66	29.05
Clinopyroxene	4.99	4.04	6.05	7.37	8.75	7.58	3.18	2.49	2.71	3.43	4.56	3.73
Olivine	0.04	0.11	0.24	0.28	0.18	0.19	0.04	0.09	0.13	0.27	0.15	0.15
Mica	0.70	0.32	0.56	0.49	0.53	0.53	0.63	0.25	0.20	0.21	0.21	0.25
Quartz	1.41	1.70	1.97	1.89	4.37	3.29	1.81	1.25	1.79	1.91	5.44	3.49
Other-Silicates	1.12	1.47	1.91	2.16	3.55	2.80	1.36	1.55	1.88	2.38	5.83	3.76
Altered Silicates												
Talc	0.18	0.78	1.54	1.35	1.18	1.13	0.29	0.92	2.05	2.11	1.81	1.67
Serpentine	0.02	0.03	0.04	0.07	0.04	0.04	0.05	0.03	0.04	0.04	0.04	0.04
Chlorite	0.53	0.49	0.63	0.56	0.79	0.70	0.45	0.27	0.37	0.38	0.40	0.38
Oxides												
Chromite	0.57	0.47	0.59	1.24	2.50	1.78	0.27	0.27	0.20	0.28	0.81	0.52
Oxides	0.01	0.09	0.18	0.56	0.91	0.64	0.02	0.13	0.29	0.37	0.79	0.50
Others												
Carbonates	0.15	0.16	0.22	0.26	0.32	0.27	0.06	0.06	0.10	0.05	0.03	0.05
Others	0.00	0.00	0.00	0.00	0.00	0.00	0.00	0.00	0.00	0.00	0.00	0.00

APPENDIX H (continued)

	2 N Conc 1						2 N Conc 2					
MINERAL	plus 106	plus 53	plus 25	plus 10	plus 2	Head	plus 106	plus 53	plus 25	plus 10	plus 2	Head
Sulphides												
Fe-Sulphides	13.50	32.75	30.64	22.87	18.68	23.33	8.95	24.67	21.25	13.41	15.17	16.32
Pentlandite	4.31	18.80	25.41	22.90	13.74	17.77	2.91	9.83	13.52	10.24	7.01	8.48
Chalcopyrite	13.95	13.44	9.91	9.55	6.67	9.20	7.77	9.76	5.96	4.57	3.62	5.10
Other-Sulphides	0.35	0.64	0.42	0.27	0.13	0.29	0.43	0.45	0.30	0.20	0.09	0.20
Silicates												
Feldspar	44.28	13.65	5.99	2.97	5.97	8.85	55.66	18.79	6.09	3.24	4.18	10.00
Orthopyroxene	13.12	12.13	18.22	30.35	35.70	26.75	12.86	21.24	37.21	51.26	49.54	42.00
Clinopyroxene	3.65	3.04	2.74	3.24	4.12	3.52	4.90	5.77	5.86	6.37	6.27	6.06
Olivine	0.02	0.03	0.10	0.19	0.10	0.10	0.08	0.16	0.22	0.25	0.10	0.15
Mica	0.80	0.25	0.36	0.20	0.20	0.27	0.97	0.62	0.53	0.32	0.18	0.36
Quartz	2.65	1.31	1.41	1.75	4.83	2.99	2.36	2.45	2.12	2.79	3.44	2.95
Other-Silicates	1.76	1.72	1.51	2.42	4.93	3.17	1.64	1.84	2.26	3.21	6.42	4.42
Altered Silicates												
Talc	0.50	1.03	2.02	2.02	1.79	1.69	0.40	2.18	2.84	2.08	0.82	1.44
Serpentine	0.02	0.04	0.05	0.06	0.05	0.05	0.12	0.18	0.07	0.10	0.05	0.08
Chlorite	0.72	0.39	0.43	0.37	0.39	0.42	0.68	1.05	0.65	0.77	0.34	0.56
Oxides												
Chromite	0.23	0.57	0.28	0.39	1.44	0.83	0.11	0.54	0.36	0.44	1.48	0.94
Oxides	0.02	0.10	0.38	0.42	1.22	0.68	0.04	0.20	0.51	0.63	1.14	0.78
Others												
Carbonates	0.12	0.13	0.13	0.05	0.03	0.07	0.12	0.28	0.27	0.14	0.15	0.17
Others	0.00	0.00	0.00	0.00	0.00	0.00	0.00	0.00	0.00	0.00	0.00	0.00

	2 N Conc 3						2 N Head					
MINERAL	plus 106	plus 53	plus 25	plus 10	plus 2	Head	plus 106	plus 53	plus 25	plus 10	plus 2	Head
Sulphides												
Fe-Sulphides	3.05	17.78	13.74	6.64	8.07	8.78	0.09	0.31	0.60	0.62	0.96	0.47
Pentlandite	1.18	6.06	6.27	4.71	2.57	3.49	0.03	0.16	0.37	0.62	0.63	0.30
Chalcopyrite	2.64	5.52	3.36	2.26	1.35	2.48	0.09	0.11	0.13	0.28	0.28	0.16
Other-Sulphides	0.11	0.32	0.20	0.10	0.06	0.12	0.01	0.02	0.03	0.02	0.01	0.02
Silicates												
Feldspar	69.56	21.26	6.98	4.22	6.97	20.51	57.58	39.92	41.79	42.55	42.10	45.26
Orthopyroxene	13.21	31.96	51.20	63.37	58.17	46.09	32.98	45.18	40.16	38.17	33.32	38.18
Clinopyroxene	3.95	7.49	7.75	8.27	8.46	7.34	4.95	6.64	6.97	7.74	8.90	6.85
Olivine	0.03	0.09	0.25	0.41	0.06	0.13	0.18	0.35	0.30	0.22	0.06	0.23
Mica	1.58	0.85	0.79	0.41	0.24	0.67	0.65	0.54	0.77	0.75	0.93	0.71
Quartz	1.57	2.48	2.62	2.76	4.39	3.16	1.13	1.20	1.93	1.34	3.64	1.85
Other-Silicates	1.43	2.32	2.15	2.34	5.19	3.33	0.73	0.88	1.08	1.14	1.67	1.07
Altered Silicates												
Talc	0.46	2.01	2.64	1.96	0.67	1.22	0.22	0.18	0.19	0.21	0.15	0.19
Serpentine	0.21	0.14	0.11	0.11	0.03	0.10	0.10	0.07	0.08	0.07	0.06	0.08
Chlorite	0.64	0.84	0.77	0.83	0.39	0.60	0.52	0.04	0.46	0.57	0.72	0.52
Oxides												
Chromite	0.24	0.54	0.50	0.65	2.01	1.11	0.53	3.75	4.66	5.12	5.54	3.62
Oxides	0.04	0.12	0.46	0.74	1.24	0.70	0.06	0.14	0.31	0.32	0.47	0.24
Others												
Carbonates	0.10	0.22	0.21	0.21	0.15	0.17	0.15	0.15	0.17	0.30	0.55	0.25
Others	0.00	0.00	0.00	0.00	0.00	0.00	0.00	0.00	0.00	0.00	0.00	0.00

APPENDIX H (continued)

	12 S Head					
MINERAL	plus 106	plus 53	plus 25	plus 10	plus 2	Head
Sulphides						
Fe-Sulphides	0.16	0.41	0.64	0.67	0.85	0.45
Pentlandite	0.09	0.25	0.50	0.65	0.63	0.33
Chalcopyrite	0.14	0.16	0.23	0.28	0.29	0.19
Other-Sulphides	0.01	0.02	0.03	0.02	0.01	0.02
Silicates						
Feldspar	54.32	42.18	42.11	44.13	44.05	46.52
Orthopyroxene	33.62	42.53	39.22	35.89	31.94	37.04
Clinopyroxene	6.12	7.01	7.90	8.46	10.36	7.47
Olivine	0.36	0.57	0.51	0.48	0.21	0.43
Mica	0.69	0.49	0.64	0.57	0.65	0.61
Quartz	1.13	1.24	1.86	1.29	2.39	1.48
Other-Silicates	0.95	0.89	1.00	1.26	1.76	1.08
Altered Silicates						
Talc	0.15	0.18	0.17	0.14	0.11	0.16
Serpentine	0.06	0.07	0.07	0.07	0.05	0.06
Chlorite	0.53	0.59	0.60	0.67	0.70	0.60
Oxides						
Chromite	1.43	3.13	4.06	4.73	4.87	3.11
Oxides	0.09	0.15	0.30	0.44	0.72	0.26
Others						
Carbonates	0.15	0.14	0.16	0.26	0.39	0.19
Others	0.00	0.00	0.00	0.00	0.00	0.00

APPENDIX I

CALCULATION OF THE 100% LIBERATED MASSES

APPENDIX I CALCULATION OF THE 100% LIBERATED MASSES

Sample 2N Head was chosen to illustrate how the fraction of the liberated chalcopyrite, pentladite and iron-sulphides were calculated. The locking associations for sample 2N Head, from Appendix J, is shown in Table 1 below.

Table 1 Locking associations of sample 2N Head

Locking Class	+106	+53	+25	+10	-10
Monomineralic					
Fe-Sulphides	18.1	31.4	34.4	48.8	75
Pentlandite	0	2.7	1.8	3.7	30
Chalcopyrite	0	0	2.4	16.7	40

Note: QEM-SEM data supplied by Billiton Laboratory did not have the locking association information for particle size class below 10μm. Although particles in this size range are expected to be well liberated, the liberation curves (Figures 1, 2 and 3) showed that there is a strong chance that the particles in this size range were not 100% liberated. Subsequently locking associations of minerals in the sub 10 μm size range were estimated by extrapolation on these curves.

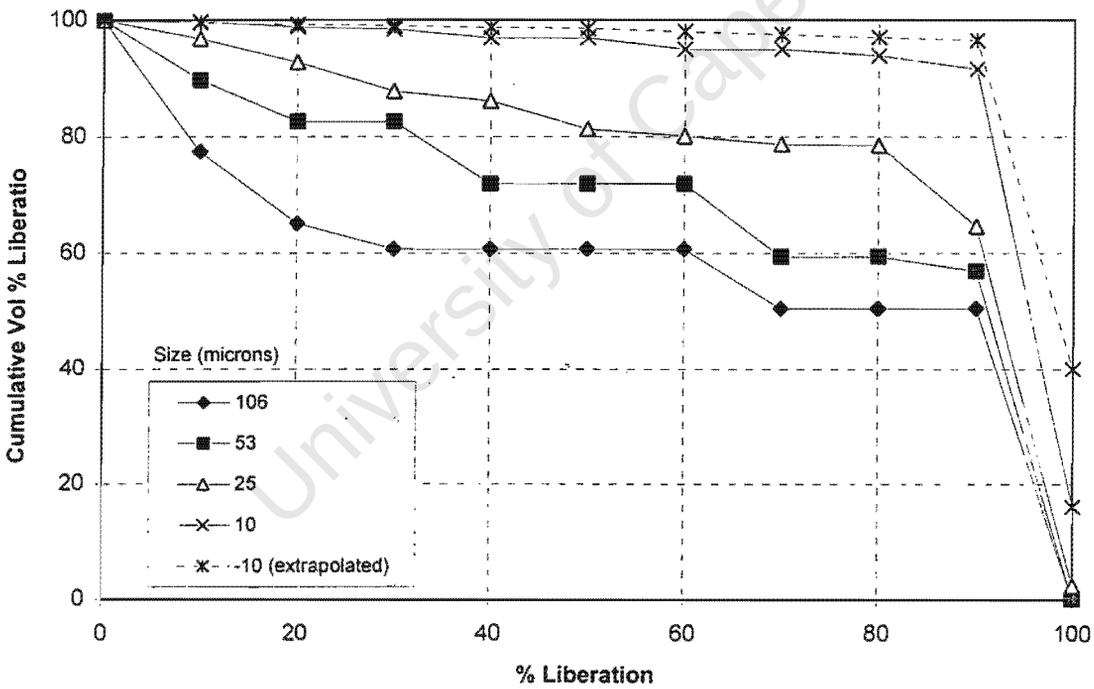

Figure 1 Chalcopyrite liberation curve

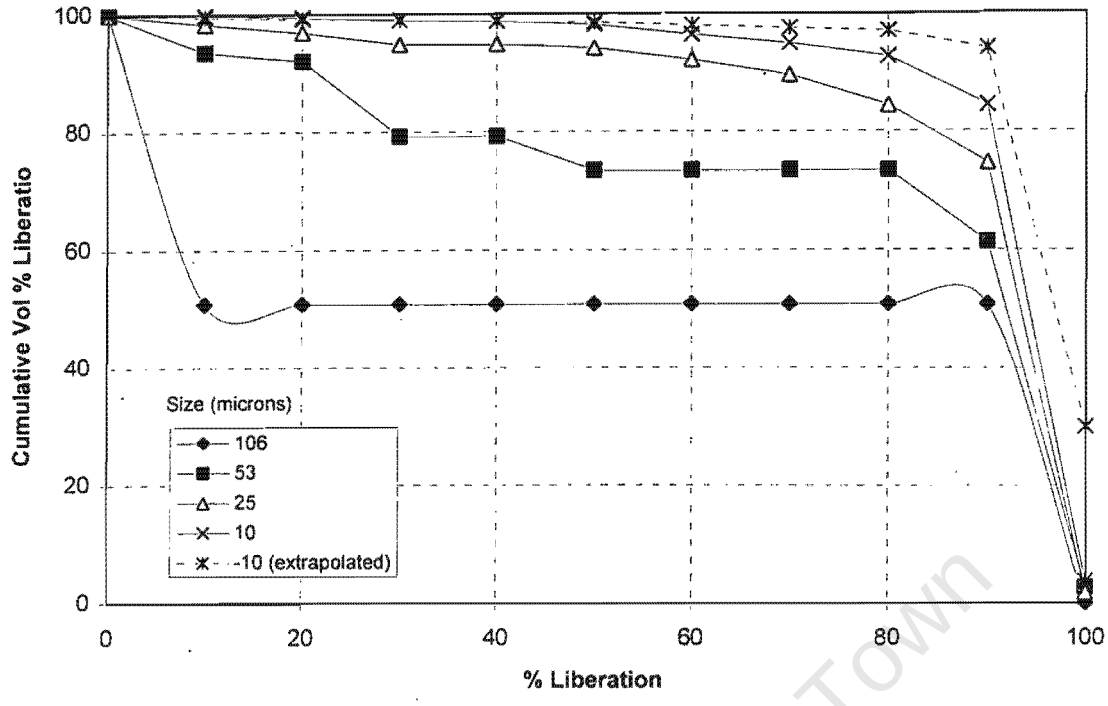

Figure 2 Pentlandite liberation curve

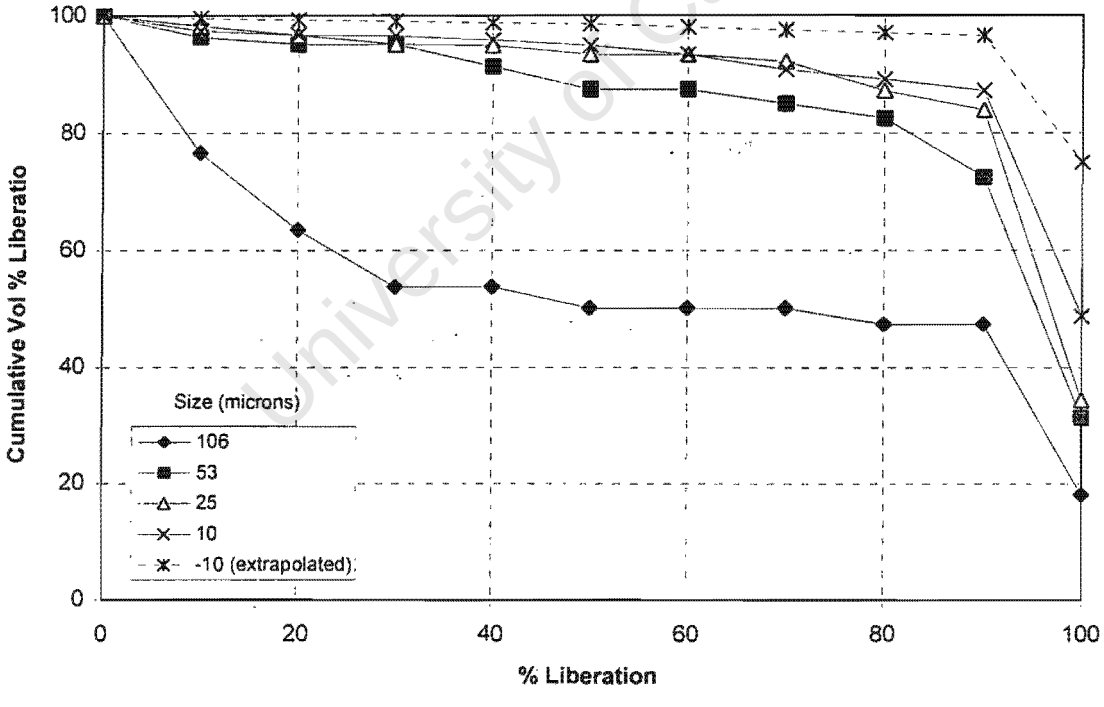

Figure 3 Iron-Sulphides liberation curve

The total mass of the dry sample (from Appendix F) and the measured particle size distribution (Appendix I) were then used to calculate the mass distribution by size for this sample (Table 2).

Table 2 Mass distribution in Sample 2N Head

Size	Mass	% of Total Sample
+106	8240.816	24.4
+53	9254.03	27.4
+25	6417.03	19.0
+10	2668.13	7.9
-10	7160.05	21.2
Total	33740.06	99.9

From the modal analysis (Appendix H) the compositions of sample 2N Head are shown in Table 3.

Table 3 Sulphide mineral compositions in Sample 2N Head

Mineral Type	+106	+53	+25	+10	-10
Fe-Sulphide	0.09	0.31	0.6	0.62	0.96
Pentlandite	0.03	0.16	0.37	0.62	0.68
Chalcopyrite	0.09	0.11	0.13	0.28	0.28

Using the mineral compositions in Table 3 above and the mass distributions in Table 2, the masses of sulphide minerals were calculated (Table 4).

Table 4 Masses of sulphide minerals in Sample 2N Head

Mineral Type	+106	+53	+25	+10	-10	Total
Fe-Sulphides	7.42	28.69	38.50	16.54	68.74	159.89
Pentlandite	2.47	14.81	23.74	16.54	45.11	102.67
Chalcopyrite	7.42	10.18	8.34	7.47	20.05	53.46

Using the locking associations in Table 1 and the masses of sulphide minerals in Table 4, the masses of the 100% liberated fractions were calculated (Table 5).

Table 5 Fully liberated masses in Sampple 2N Head

Mineral Type	+106	+53	+25	+10	-10	Total
Fe-Sulphides	1.34	9.0	13.24	8.07	54.99	86.65
Pentlandite	0.00	0.4	0.43	0.61	6.77	8.21
Chalcopyrite	0.00	0.0	0.20	1.20	6.00	7.40

Fraction of liberated masses for different sulphide minerals is reported in Table 6 below.

Table 6 Fraction of fully liberated sulphide minerals in Sample 2N Head

Mineral Type	Ratio	Liberated Fraction
Fe-Sulphides	86.65 / 9.89	0.54
Pentlandite	8.21 / 2.67	0.08
Chalcopyrite	7.4 / 46	0.14

Exactly the same procedure was followed to calculate the liberated fractions for the other Head and Concentrate samples. A summary of the final results is shown in Table 7. For the continuous tests an average of the three head samples was calculated for use in the samples not analysed for mineral liberation. Similarly this was done for the concentrate samples except for 10S Conc sample. This sample had an unusual high percentage of fines. As such it was treated as is. The results are shown in Table 8.

Table 7 Calculated fractions of fully liberated sulphide masses

Mineral Type	2S Head	2S C1	2S C2	2S C3
Fe-sulphides	0.46	0.51	0.56	0.48
Pentlandite	0.08	0.06	0.04	0.03
Chalcopyrite	0.12	0.14	0.15	0.09

Table 8 Calculated fractions of fully liberated sulphide masses for the continuous tests

Mineral Type	Head	Conc	10S Head	10S Conc
Fe-Sulphides	0.43	0.51	0.50	0.76
Pentlandite	0.08	0.07	0.07	0.09
Chalcopyrite	0.11	0.15	0.18	0.23

Average fractions calculated by adding fraction from tests 11S and 12S for the head, and by adding 11S and 12S for the concentrate. Tables 9a and 9b below show the estimated liberated mass distributions for all tests

Table 9a Calculated liberated mass distributions in batch tests

Test	Sample	Time (min)	Liberated Masses (g)		
			Chalco	Pent	Fe-S
1N	Head	0	9.30	5.76	52.09
	C1	2	2.75	2.09	20.48
	C2	6	0.59	0.31	6.90
	C3	12	0.23	0.12	3.30
	C4	25	0.14	0.07	1.86
2N	Head	0	8.19	7.30	79.56
	C1	3	3.07	2.48	24.32
	C2	10	1.65	0.84	17.11
	C3	20	0.54	0.33	7.82
3N	Head	0	7.41	6.21	63.29
	C1	3	2.60	2.04	23.61
	C2	10	1.50	0.74	16.74
	C3	20	0.60	0.36	11.03
4N	Head	0	5.98	5.14	72.24
	C1	3	4.08	2.49	50.18
	C2	10	1.31	0.64	16.37
	C3	20	0.17	0.09	5.26

Table 9b Calculated liberated mass distributions in continuous tests

Test	Liberated Masses (g/min)								
	Head			Conc			Tails		
	Chalco	Pent	Fe-S	Chalco	Pent	Fe-S	Chalco	Pent	Fe-S
R1S									
R1S (R)									
6S	1.00	1.29	10.13	0.74	0.63	3.80	0.26	0.66	6.33
1S	0.84	1.08	8.46	0.63	0.41	3.04	0.21	0.67	5.43
2S	0.97	1.24	9.77	0.77	0.69	6.74	0.20	0.56	3.04
3S	0.78	1.00	7.85	0.51	0.48	4.11	0.26	0.52	3.74
4S	1.07	1.38	10.84	0.86	0.68	4.11	0.21	0.70	6.72
5S	1.22	1.57	12.37	1.08	0.60	0.92	0.15	0.97	11.45
7S	1.33	1.71	13.45	0.68	0.64	2.68	0.65	1.07	10.77
8S	2.14	2.10	19.32	0.70	0.65	6.03	1.45	1.45	13.29
9S	0.77	0.87	6.82	0.70	0.66	2.79	0.07	0.20	4.03
12S	1.94	2.49	19.59	1.80	1.75	9.76	0.14	0.74	9.83
10S	3.62	2.39	25.11	3.15	2.17	12.87	0.47	0.22	12.24
11S	2.11	2.72	21.33	1.78	1.60	9.80	0.33	1.12	11.53
14S	1.43	1.84	14.48	0.35	0.30	7.08	1.08	1.54	7.40
13S	2.01	2.59	20.32	0.10	0.06	1.40	1.91	2.53	18.92
15S	1.21	1.55	12.19	0.13	0.02	1.59	1.07	1.53	10.61

APPENDIX J

LOCKING ASSOCIATIONS FOR SELECTED HEAD AND CONC SAMPLES

APPENDIX J LOCKING ASSOCIATIONS

LOCKING CLASS	New 10S Head +106	+53	+25	+10	New 10S Conc +25	+10	New 11S Conc +106	+53	+25	+10
Fe-Sulphides										
Monomimerallic	8.4	13.4	32.3	60.9	20.8	58.4	6.8	15.9	35.2	58.3
Binary										
Pentlandite	1.1	2.6	11.5	8	11.4	10.2	11.4	9.8	14.3	7.3
Chalcopyrite	1.1	3.8	3	3.7	5.8	3.3	4	7.2	3.5	3.2
Other Sulphides	0	0	4.4	4.3	9	2.9	2.3	1.3	6.1	3.8
Gangue	51.1	17.4	15.7	14.5	22.9	16.4	4	10.6	10.3	18.5
Composite										
Composite (Sulph)	21.6	24.1	5.1	0.8	8.7	1.3	10.9	17.5	6.7	1.7
Composite	16.7	38.7	27.9	7.8	21.3	7.6	60.6	37.6	24	7.2
Pentlandite										
Monomimerallic	0	0	5.2	6	1.1	5.3	0	1.3	2.8	6.5
Binary										
Chalcopyrite	0.5	0.3	0	0.4	0.5	0	0.3	1.1	0	0
Fe-Sulphides	0	12	30.5	37.5	30.3	49.8	10	17.9	41	53.6
Other Sulphides	0	0	0.5	0	0	0	0	0	0.5	0
Gangue	12	2.6	3.4	2	2.7	2.1	8.5	5.6	1.7	3.2
Composite										
Composite (Sulph)	0.3	34.4	23.5	28.6	14.4	18.8	16	14.9	16.6	22.7
Composite	87.1	50.7	37	25.5	50.9	24	65.3	59.2	37.4	13.9
Chalcopyrite										
Monomimerallic	0	0	4.8	16.2	7.4	21.4	3.3	5.7	1.3	26.3
Binary										
Fe-Sulphides	0.8	1.9	14.6	22.7	20.6	1.6	3.2	10.1	20.2	17.3
Pentlandite	0	0	0.1	0	0.6	0.2	0	2.4	0	0
Other Sulphides	0	4.1	0	0	2.6	0	0	0	0	0.8
Gangue	26.5	17.4	5.4	3.2	15.7	16	15.1	10.1	13.5	2.6
Composite										
Composite (Sulph)	0	9.2	30.7	32	18.1	17.7	15.1	19.6	23.6	25.8
Composite	72.8	67.5	44.4	25.9	35	23.1	63.3	52	41.3	27.3
BMS										
Monomimerallic	7.8	28	48.1	68.6	42	68.5	14.4	30.5	53.2	72.6
Binary										
Pyroxene/Olivine	0.2	0	0	0.2	0	0.4	0.1	0.8	0.3	0
Feldspar	10.2	6.1	4	8.3	1.5	1.4	5.6	3	1.6	2.9
Altered Silicates	1.5	4.4	3.3	3.2	6.1	4.7	4.1	3	4.3	10.3
Chromite	0	0	0	0.6	0	0.5	0	0	0	0.1
Other Gangue	20.5	32.3	28.5	4.8	24.9	4.2	36	32	23.5	4
Composite	59.9	29.2	16.1	14.3	25.4	20.2	39.7	30.7	17.2	10

APPENDIX J (Continued)

LOCKING	New 12S Conc				New 2N Conc1				New 2N Conc2			
CLASS	+106	+53	+25	+10	+106	+53	+25	+10	+106	+53	+25	+10
Fe-Sulphides												
Monomineralic	3.3	18.6	33	54.2	4	13.1	38.8	61.3	10.7	12.6	38.8	61.3
Binary												
Pentlandite	6.5	10.5	12.1	14.4	6.8	10.1	15	10.1	3.6	8.4	10.5	6.6
Chalcopyrite	5.8	6.3	5.7	5.5	5.8	6.1	5.8	1.9	4.1	5	3.5	3.1
Other Sulphides	3.8	1.7	13.8	7.7	4.3	3	9.1	10.1	3	6	6.6	2
Gangue	10.1	11.1	10.5	11.5	13.7	16.5	12.1	8.9	17.8	17.4	20	20.9
Composite												
Composite (Sulph)	12.5	14.6	5.5	2	13	9.3	2.7	1	12.2	11	4.6	1.2
Composite	58	37.3	19.3	4.8	52.5	41.9	16.5	6.7	48.7	39.7	16.5	4.9
Pentlandite												
Monomineralic	0	2.5	2	4.6	0.3	1.7	2.4	5.9	0	1.7	5.6	1.8
Binary												
Chalcopyrite	0.8	0	0.6	0.1	1.1	0	0.1	0	0.4	0	0	0
Fe-Sulphides	15.2	19	27.3	58.3	8.4	24.3	39.1	54.8	9.2	22.2	36.6	67.1
Other Sulphides	0	0	0	0	0	0	0	0	0	0	0	0
Gangue	9.4	1.5	0.3	0.3	15.7	3.9	0.6	0.9	18.1	7.7	1.5	2.1
Composite												
Composite (Sulph)	16.6	20.6	21.8	22.1	17.5	16.5	24.5	20.1	16.3	15.8	15.9	7.4
Composite	58	56.4	47.8	14.6	56.9	53.6	33.3	18.2	56	52.5	40.3	21.6
Chalcopyrite												
Monomineralic	0.3	4	9.6	15.3	2.7	1.6	11.8	18	4.2	5	10.3	16.6
Binary												
Fe-Sulphides	6.3	10.6	17.9	33.6	6	21.4	25.9	27.8	5.5	14.6	19.7	36.3
Pentlandite	0	0.7	1.5	0.1	0.2	0.4	0.2	0	0	0	0.6	0
Other Sulphides	0	0.2	1.3	0.3	0.2	0.8	0	0.3	0	0	0.5	0
Gangue	13.3	9.3	4	4.7	24.7	9.4	5.6	1.3	28.4	15.8	7.8	9.4
Composite												
Composite (Sulph)	9.2	23.5	27.4	30.3	12.7	15.1	21.8	33.7	6.8	9.5	17.6	13.3
Composite	71	51.7	38.4	15.7	53.7	51.4	34.7	19	55.1	55.2	43.5	24.4
BMS												
Monomineralic	11.7	31.2	50	76.6	13.4	29	57.7	77.5	12.2	27.7	51.8	70.8
Binary												
Pyroxene/olivine	0	0	0	0.2	0.3	0.4	0	0.2	0.4	0.4	0	0
Feldspar	5.7	2.5	0.8	0.9	9.1	3.6	1.6	0.5	8.8	3.7	1	0.7
Altered Silicates	2.4	3.9	2	5.4	2.8	2.3	1.5	5.2	0.8	4.5	3.1	10
chromite	0.2	0.5	0.5	0.9	0.5	0.4	0.7	0.2	0.6	0.1	0.4	0.6
Other Gangue	31.6	34.5	32.8	7	23.7	33.9	26.4	8.3	28	30.5	30	1.1
Composite	48.3	27.3	13.9	9	50.2	30.5	12.2	7.9	49.3	33.1	13.6	16.8

APPENDIX J (Continued)

LOCKING	New 2N Conc3				New 2N Head				New 12S Head			
CLASS	+106	+53	+25	+10	+106	+53	+25	+10	+106	+53	+25	+10
Fe-Sulphides												
Monomineralic	3.5	20.2	28	57.3	18.1	31.4	34.4	48.8	0	19.4	30.2	59.7
Binary												
Pentlandite	1.2	8.8	5.3	5.5	0.3	14.9	7.1	8.2	11.3	17.6	6.3	8.6
Chalcopyrite	1.1	0.6	2.1	1.8	0.3	2.8	3.2	1.6	0	2.7	2	0.6
Other Sulphides	4.6	6.4	10.8	2.6	12.6	4.3	9.9	11.4	0	17.1	12.4	3.4
Gangue	23.5	17.4	27	27.6	51.3	6.1	15.2	20.8	43.3	10.3	15.9	19.7
Composite												
Composite (Sulph)	8.6	2.7	2.3	0.3	0	4.7	4.6	0.4	0	6.9	5.3	0
Composite	57.5	44	24	4.9	17.5	35.7	25.5	8.8	45.3	26	28	8
Pentlandite												
Monomineralic	0	1	3.3		0	2.7	1.8	3.7	0	13.7	4	3.3
Binary												
Chalcopyrite	0	0	0		0	0	0.2	0	0	0.2	0.2	0
Fe-Sulphides	4.3	11.8	73		0	42.1	33.5	41.2	0.9	27.6	32.8	39
Other Sulphides	0	0	0		0	0	0	0	0	0	0.9	0
Gangue	37.1	13.5	0.8		34.2	6.2	3.4	1	31	3.6	4.1	0
Composite												
Composite (Sulph)	4.4	17.9	7		0	3	14.9	27.8	0	20	20.2	29.5
Composite	54.2	55.7	15.9		65.8	46	46.2	26.3	68.1	34.8	37.7	28.2
Chalcopyrite												
Monomineralic	2.1	5.3	14.1		0	0	2.4	16.1	0	0	22.4	15.5
Binary												
Fe-Sulphides	1.4	8	33.3		0	16.4	17.1	23.7	3.5	10.4	21.8	35.4
Pentlandite	0	0	0		0	0	0	0	0	0	0	0
Other Sulphides	0	0	0		0	0	1.1	0	0	0	0	0
Gangue	45.7	20.3	10.7		34.4	16.9	14.2	6.6	88.9	22.9	9.1	7.7
Composite												
Composite (Sulph)	10	21	15.5		50.5	0.8	27.9	28	0	24.1	11.4	16.7
Composite	40.8	45.4	26.3		15.1	65.9	37.2	25.6	7.6	42.6	35.4	24.8
BMS												
Monomineralic	8.4	31.6	68.2		10.8	39.4	47.9	64.1	7.1	38.2	49.5	66.2
Binary												
Pyroxene/Olivine	0.7	0.3	0		0.1	1.8	0.1	0.3	0.7	0.3	0.8	0.4
Feldspar	18.5	4.8	2.9		20.9	3.8	3.1	7.8	28.7	3.7	1.9	9.5
Altered Silicates	2.4	2.8	10.5		0	5	3.6	5.5	0.9	2.7	2.5	5.9
Chromite	0	0.5	1.3		0	1.5	0.6	1.6	2	0	0.8	2.2
Other Gangue	16.7	23.8	2.4		33.4	26.5	26.1	9.6	16.7	31.2	27.4	2.7
Composite	53.3	36.2	14.7		34.7	22.1	19	11.1	44	23.9	17	13.2

APPENDIX K

CONVERSION OF ELEMENTAL ASSAYS TO MINERAL COMPOSITIONS

APPENDIX K CONVERSION OF ELEMENTAL ASSAYS TO MINERAL COMPOSITIONS (Buswell, 1998)

Mineral	Grade (%)	Element / (mole ratio)			
		S	Cu	Ni	Fe
Chalcopyrite	0.18	2	1		1
Pentlandite	0.34	1		0.5	0.5
Pyrrhotite	0.39	1.13			1
Pyrite	0.09	2			1
PGM	0.1				
Other sulphides	0.03				
Pyrite/Pyrrhotite	0.48	1.29			1

Steps involved in converting elemental assay into mineral data

- All copper is associated with chalcopyrite
- Sulphur associated with chalcopyrite, based on stoichiometric coefficients, is subtracted from total sulphur
- Nickel associated with pentlandite is determined by assuming that 30% of nickel in the feed is associated with gangue
- Sulphur associated with pentlandite, based on stoichiometric coefficients, is subtracted from the remaining sulphur
- The residual suphur was assumed to be associated with iron-sulphide (pyrrhotite and pyrite)
- The gangue is then calculated from the total mass of solids minus total mass of sulphide minerals